Development and Functions of Patrolling Monocytes and Kidney Resident Macrophages

Bohm, Mathieu

Awarding institution:
King's College London

KING'S College LONDON

Development and functions of patrolling monocytes and kidney resident macrophages

By Mathieu Bohm

This thesis is submitted to King's College London for the degree of Doctor of Philosophy

September 2017

Abstract

Mononuclear phagocytes are crucial arms of the innate immune system, performing various fonctions, from clearance of pathogenic microorganisms, to maintenance of tissue homeostasis. Two cell types have been studied; first, monocytes, bone marrow-derived cells, of which two main subsets have been described. Ly6C^{+} monocytes are short-lived circulating cells that have the ability to quickly migrate into tissues, and produce a range of molecules, or differentiate into inflammatory cells. Ly6C$^{\mathbf{low}}$ monocytes are a patrolling cell type, which crawls on the luminal side of vessels where they perform a monitoring of the vasculature. In a collaborative effort, using nucleoside analogs and experimentally parameterised, computer-assisted modeling, the dynamics of these two subsets has been re-examined, in the light of genetic data obtained previously in the laboratory. The results suggest that the transition between a Ly6C^{+} to a Ly6C$^{\mathbf{low}}$ phenotype occurs more prominently in the bone marrow, rather than the blood as suggested by the literature.

Second, macrophages in the kidney were investigated in the context of circulating small immune complexes. Macrophages are large, resident cells which develop during embryonic life, maintaining their numbers locally and independently from bone marrow-derived cells in most tissues. Kidney resident macrophages perform a constant monitoring of the circulation, in collaboration with the endothelial cells they underlie. The experimental model for the study of their response to immune complexes was studied, and the results provide insight into the unique character of this function for kidney resident macrophages, as well as clarifying the means of access of the immune complexes to the macrophages.

Together, the work presented in this thesis sheds light on particular aspects of the biology of myeloid populations, in steady state and inflammatory settings.

Acknowledgements

I would first like to extend my thanks to Frederic Geissmann for his mentorship throughout my PhD, and for all that I have learned from him. I am very grateful to have been able to work in such tremendous environments both at King's College London and the the Memorial Sloan Kettering Cancer Center in New York, among such wonderful people. I have been honored and humbled to work alongside such brilliant people. I also thank my second supervisor Ajay Shah for his support.

I thank all the lab members, past and present, that have been a great support, and have welcomed me into the lab, or that I have had the pleasure to welcome, and who all participated to a great atmosphere and a tight group. First and foremost to Stathis and Hannah ; you both have taught me so much and have been wonderfully patient. I do mean that literally, as I am not only a slow learner but also a slow experimentalist ! I owe you immensely.

Next I need to thank everyone else in the lab, Christian, Lucile, Nehemiah, Ivan, Tomi, Stéphanie, Carolina, Simao (when the niiight !), Katie, Elvira, Katrin, Daniel, Elisa, Paula, Ysé, Xi, Zihou and Werner. You would all deserve a whole page of thanks, you have all made these four years a wonderful experience.

I also want to extend special thanks to the two lab managers I had the pleasure to work with, Céline in London, and Anne in New York. Céline,

thank you for taking care of everything that didn’t make sense to me in both the lab and the office, and patching me up on several occasions (people should know better than to let me be near anything sharp). Anne, it was so great to have you on board, and it is thanks to you that we managed to set up such a cool lab in New York. You know Memorial and the city so well, thank you (and Peter !) for making us discover both.

I want to thank our collaborators. First Jayanta Chaudhuri and his postdoc William (Teddy) Yewdell, with whom I have learned FPLC and had very interesting discussions. Also, I want to thank Grégoire Altan-Bonnet and Amir Erez for the collaboration we have engaged, and that has prompted very interesting discussions and helped move the project forward for the last two years.

I would also like to give a shout to Giorgio Anselmi, who has been a great company for the last few months, during the writing phase which he went through at the same time as I did. I wish him the best for his PhD and beyond.

I also want to thank the two members of my thesis committee, Elisabeth Ehler, who was always available for discussion, and Christian Schulz, who helped a lot understanding the platelet-related aspects of my project.

Finally I want to thank the people that took care of our mice, the BSU in London and the RARC in New York. Representing them, I thank Michelle and Antonio, respectively.

Last but not least, I want to thank my family who has supported me through this PhD (well, for quite a lot more, but let's stay focused), and notably my mother Nathalie, who had the kindness to read my whole introduction, and thanks to whom the English in there is made better.

Declaration

I declare that I have personally prepared this thesis and that results presented are my own, unless otherwise stated. All information sources included in this thesis are referenced accordingly.

Mathieu Bohm

September 2017

Table of contents

Table of Figures

Table of Tables

Abbreviations

Aβ : Amyloid beta

ADCC : Antibody Dependent Cellular Cytotoxicity

AF : Alexa Fluor

AGM : Aorta-Gonad Mesonephros

APC : Allophycocyanin

ApoE : Apolipoprotein E

A.U. : Arbitrary Units

BBB : Blood-Brain Barrier

BFU : Burst Forming Units

BM : Bone Marrow

bp : base pair

BSA : Bovine Serum Albumin

BrdU : 5-Bromo-2'-desoxyUridin

BV : Brilliant Violet

CCR/CCL : C-C Chemokine Receptor / C-C Chemokine Ligand

CD : Cluster of Differentiation

cDC : conventional Dendritic Cell

CDP : Common Dendritic cell Progenitor

C/EBP : CCAAT/Enhancer Binding Protein

CFC : Colony-Forming Cell

CFU-S: Colony-Forming Unit - Spleen

CLP : Common Lymphoid Progenitor

cMoP : common Monocyte Progenitor

CMP : Common Myeloid Progenitor

CR : Complement Receptor

CSF1 / CSF1R : Colony Stimulating Factor 1/ Colony Stimulating Factor 1 Receptor

CXCR : C-X-C Chemokine Receptor

CX_3CR1 : C-X3-C Chemokine Receptor

CyTOF : Cytometry by Time Of Flight

Da : Dalton

DAPI : 4',6-diamidino-2-phenylindol

DC : Dendritic Cell

DNA : Desoxyribonucleic Acid

dpc : days post-coïtum

DT : Diphteria Toxin

DTR : Diphteria Toxin Receptor

DVT : Deep Vein Thrombosis

E : Embryonic day

EDTA : Ethylenediaminetetraacetic acid

EdU : 5-Ethynyl-2'-deoxyUridine

EMP : Erythro-Myeloid Progenitor

F(ab')$_2$: antigen-binding Fragment

FACS : Fluorescence-Activated Cell Sorting

FBS : Fetal Bovine Serum

Fc : Fragment crystallizable region

FcγR : Fc gamma Receptor

FITC : Fluorecein isothiocyanate

FL : Fetal Liver

FPLC : Fast Protein Liquid Chromatography

FSC : Forward Scatter

GFP : Green Fluorescent Protein

gMFI : geometric Mean Fluorescence Intensity

GMP : Granulocyte Macrophage Progenitor

GP : GlycoProtein

HEV : High Endothelial Venule

HFD : High Fat Diet

HIV : Human Immunodeficiency Virus

HSC : Hematopoietic Stem Cells

IC : Immune Complex

ICAM : InterCellular Adhesion Molecule

ICSBP : Interferon Consensus Sequence Binding Protein

IEC : Intestinal Epithelial Cells

IFN : Interferon

IgG : Immunoglobulin G

IL : Interleukin

Il2rg : gamma chain of the IL-2 Receptor

iNOS : inducible Nitric Oxide Synthase

i.p. : intraperitoneal

IRF : Interferon Regulatory Factor

i.v. : intravenous

KLF : Krüppel-Like Factor

KO : Knock-Out

LFA-1 : Lymphocyte Function-associated Antigen 1

LMPP : Lymphoid-primed Multipotent Progenitor

LN : Lymph Node

LP : Long-Pass (filter)

LPS : Lipopolysaccharide

LSK : Lineage-negative Sca-1^+ c-Kit^+

LT-HSC : Long-Term HSC

MCMV : Mouse Cytomegalovirus

MCP-1 : Monocyte Chemoattractant Protein

MDP : Monocyte/Macrophage Dendritic cell Progenitor

MEP : Megakaryocyte/Erythrocyte lineage-restricted Progenitors

MFI : Mean Fluorescence Intensity

MHC : Major Histocompatibility Complex

MKP : Megakaryocyte-committed Progenitor

MPP : Multipotent Progenitor

MPS : Mononuclear Phagocyte System

NK : Natural Killer

OVA : Ovalbumin

PBMC : Peripheral Blood Mononuclear Cells

PBS : Phosphate Buffered Saline

PCR : Polymerase Chain Reaction

pDC : plasmacytoid Dendritic Cell

PE : Phycoerythrin

RA : Rheumatoid Arthritis

RAG : Recombinase Activating Gene

RBC : Red Blood Cells

RES : Reticulo-Endothelial System

RNA : Ribonucleic Acid

ROS : Reactive Oxygen Species

RPMΦ : Red Pulp Macrophages

S1PR5 : Sphingosine-1 Phosphate Receptor 5

SFFV : Spleen Focus Forming Virus

SLE : Systemic Lupus Erythematosus

SSC : Side Scatter

ST-HSC : Short-Term HSC

t-SNE : t-distributed Stochastic Neighbor Embedding

TAM : Tumor-Associated Macrophages

TBE : Tris/Borate/EDTA

TCR : T Cell Receptor

Th : T helper

Tip-DC : TNFα and iNOS-producing Dendritic Cell

TLR : Toll Like Receptor

TNF : Tumor Necrosis Factor

TRITC : Tetramethyl Rhodamine Iso-Thiocyanate

vWF : von Willebrand Factor

WNV : West-Nile Virus

WT : Wild-Type

YFP : Yellow Fluorescent Protein

YS : Yolk Sac

1 - Introduction

1.1 Historical perspective

This work describes an attempt to further the understanding of the biology of myeloid populations in mice. The study of immune cells has been a focus of research for well over a century, and this thesis will start by going over a few of the main steps leading to the current understanding of mononuclear phagocyte development and function. Immunity is a concept that has been known for a surprisingly long time, and explanations provided over the centuries much varied. Here, this thesis will briefly try to cover the main aspects of earlier views on immunity, before moving to the late 19th to 20th century works that lead to our current understanding of monocyte and macrophage biology.

1.1.1 Immunity to disease as a passive phenomenon

Although the Latin words "immunitas" and "immunis" were first used for legal concepts (in ancient Rome, the exemption from duty or service, during the Middle Ages the exemption of the Church's properties and personnel from civil control), the concept of immunity to disease has been known for over two millenia. Thucydides already mentions this phenomenon in his desciption of a plague that struck Athens in the 5th century B.C. (in *The History of the Peloponnesian War, 431 B.C.*). There, acquired immunity, although not explained nor theorized, was a phenomenon known well enough to influence people's behaviour when facing disease, as described by Arthur Silverstein in *A history of Immunology*: "Yet it was with those who had recovered from the disease that the sick and the dying found most compassion. These knew what it was from experience, and had now no fear for themselves ; for the same man was never attacked twice – never at least fatally" (Silverstein A.M. *A History of Immunology, 2nd Edition, 2009*).

The Hippocratic school of medicine explained the occurrence of diseases by the imbalance of what they belived were the main bodily fluids, termed the four humours (blood, phlegm, yellow and black bile). Galen (129 – 216 AD) added qualitative aspects to that dogma, saying that temperature, consistency, fermentation state would influence disease appearance and progression (Silvertein A.M. *A History of Immunology*, 2nd Edition). It is based on this premise that the first theory of acquired immunity was developed, by Islamic physician Abu Bekr Mohammed Ibn Zakariya al-Razi (880-932, also known as Rhazes), in his *Treatise on the Smallpox and Measles*. It was principally concerned with smallpox, which he said affects blood in a *drying* fashion: blood would lose some moisture quality, which was expelled from the body via the formation of pustules on the skin. However, it was believed that this drying of blood was a natural process, occurring slowly throughout the life of every healthy individual. Therefore, the disease merely accelerated this process. Hence, the fact that no patient would be affected a second time was because the excess moisture had already been expelled, leaving the blood too dry to be affected another time.

This is only the first of a long series of theories that aimed at explaining the long lasting observation of acquired immunity. After the Scientific Revolution of the 16th and 17th centuries (lead by Galileo, Descartes, Kepler and Newton, notably), physics left its mark in the fields of biology (Silverstein A.M.), and the schools of iatrophysics and iatrochemistry emerged, each with its set of theories on immunity. As a representative of the school of Iatrophysics, James Drake (1707, *Anthropologia Nova : Or, a New System of Anatomy*) proposed that smallpox induced a concoction of the blood, which could only be expelled from the blood by forcing its way through the skin, thereby forming the pustules. Because the symptoms and disease were not disjointed, his view of acquired immunity would make sense. The expulsion of the blood concoctions induced by the disease would alter the skin « tone » in such a way that after

the first forcing of the concoction, the altered skin would not "be able any more to arrest the Matter [*the blood concoction*] in its course outward long enough, or in such quantity" to create new pustules. Therefore, one could be infected again but not suffer the symptoms any more, because of the altered anatomy of the injured tissue (cited in Siverstein A.M.).

The practice of "variolation", an early form of vaccination for smallpox where the content of skin pustules would be introduced into healthy patients via various techniques as a preventive measure, has been reported from very early times, and was introduced into Western medicine with increasing success around the 17th century. This also prompted several theories of immunity trying to explain its efficacy. One concept emerged, that of the Innate Seed, defended notably by Thomas Fuller in 1730 (*Exanthematologia : or, an attempt to give a rational account of eruptive fevers*, pp175 ff. London, 1730), postulated that individuals possess specific, and single, "ovulae" for each disease, which were fertilized by the disease agent, which could therefore only occur once in a lifetime.

All the theories discussed above involved either changes in quality of humours, anatomical changes or exhaustion of inner seeds, would impact the state of mind when the scientific debate saw the rise of cellular theories.

1.1.2 The emergence of a cellular immune system

Although earlier scientists and physicians had already challenged the idea of an all humoral view of immunity, it was in 1858 that Rudolph Virchow claimed that pathology is due to the malfunction of cells rather than a disproportion or alteration of the humors. It is also important to note that for a comprehensive view of immunity, there had to be an acceptance that diseases are specific and reproducible. This view could only prevail if the idea of spontaneous generation was disproven which, after

centuries of dispute, came about largely due to the experimentations and argumentation of Louis Pasteur. Another important aspect for the understanding of a specific and reproducible disease has been the germ theory, which stemmed from Girolamo Fracastoro (1546) and gained acceptance with the works of Pasteur and Robert Koch in the late 1870s. Therefore, the work of Elie Metchnikoff (1845 – 1916) constituted an important component of a new view of pathology, rather than a step further within an established conceptual framework (Silverstein A.M.).

Metchnikoff's contribution came in the context of understanding the pathology of the inflammatory reaction, which had been a matter of intense debate for decades. Cells at inflammatory sites had been observed, although they were believed to be, with the inflammatory reaction as a whole, detrimental for the patient. As his colleague Varchow (*Life of Elie Metchnikoff*, O. Metchnikoff, 1921) pointed out to him in a letter: "Most pathologists [did] not believe in the protective role of inflammation". Phagocytosis had also previously been observed before, but inflammatory cells were viewed by most, though not all (Ambrose, 2006), as a means of transportation of disease vectors throughout the body.

Metchnikoff made experiments in various organisms. As a zoologist, he was influenced by the Theory of Evolution by Darwin, still fairly new at the time (*Origin of Species*, Darwin, 1859). This had an impact on Metchnikoff's experimental methods, following the premise that observations in simple animals would be relevant to more complex organisms. In Invertebrates, he described phagocytes as being cells that have "the power of ingesting and sometimes absorbing food particles" (Metchnikoff, 1883), and recalled the observation that the process of digestion in invertebrates is seemingly carried out by phagocytic activity of amoeboid corpuscles. He therefore put forward the idea that this was to be seen as a "true act of feeding". He then moved on to saying that there must be examples of such activity in Vertebrates. He then studied the development

of Bombinator toads : the tail of the larvae is digested during the metamorphosis stage of development. At that time, Metchnikoff observed amoeboid cells accumulating around the muscle tissue, before seeing muscle tissue remains inside these amoeboid cells. The now-intracellular components were observed to maintain their characteristic striation for a certain time, before losing this characteristic as the process of phagocytosis went on. Metchnikoff carried out a number of experiments inducing damage to different anatomical locations of various vertebrates and invertebrates, and during different developmental stages. These experiments led to the observation that phagocytic cells undergo morphological changes from “a superficial resemblance to an Actinophrys” (i.e. with filopodia), to round, amoeboid and motile cells (Metchnikoff, 1883). He summarizes his findings as follows : “My whole series of observations, on Vertebrates and Invertebrates together, is hardly compatible with the current theory, which regards inflammation as primarily due to a morbid condition of the walls of the blood-vessels. I rather believe that the essence of the whole process is a struggle between the phagocytes and the septic material, whether the latter be a dead or dying cell, or a fungus, or other foreign body”. The work of Metchnikoff prompted the birth of cellular immunology, and research that continues to this day on the biology of phagocytes. Metchnikoff understood that macrophages not only constituted the first line of defence against infectious agents (rather than being deleterious to the individual during inflammatory responses), but were critical for maintaining tissue homeostasis as well : two aspects of macrophage biology that have only been confirmed since their discovery in the late 19th century.

Figure 1.1: Metchnikoff's representation of phagocytosis (Metchnikoff, E. *Lectures on the Comparative Pathology of Inflammation*.) Observed in the caudal fin of a Triton embryo

1.1.3 Classification of phagocytes into unified systems : from the Reticulo-Endothelial System, to the Mononuclear Phagocyte System

Although Metchnikoff is widely regarded as the father of cellular immunity, many investigators of the 19th and 20th century contributed to the study of phagocytes and our understanding of the immune system. Paul Ehrlich, co-recipient with Metchnikoff of the 1908 Nobel Prize « in recognition of their work on immunity » (Nobel Prize official statement), had a critical impact on the understanding of humoral biology, with his side-chain theory of anti-toxins. Metchnikoff and Ehrlich were the respective

epicentres of a vivid debate during the late 19th century about the nature of the inflammatory response, opposing the cellular and humoral views on the matter (Silverstein A.M. *A History of Immunology*). However, Ehrlich also made crucial contributions to the understanding of phagocytes, developing staining methods that would allow him to distinguish mononuclear and different subsets of polymorphonuclear phagocytes – neutrophils, basophils and eosinophils (Ehrlich, P. 1956, *Collected papers of Paul Ehrlich*). Other investigators found phagocytes in various organs, such as in the liver by Kupffer in 1876 (Yona and Gordon, 2015), and interstitial cells in the brain discovered by Virchow in 1846, some of which were later coined "microglia" by the Spanish pathologist Pio Del Rio-Hortega in 1919 (Rezaie and Male, 2002). As data accumulated showing the existence of phagocytes throughout the tissues (brain, liver, lungs, bones, germinal centre of the spleen) of several species, the need for a unified nomenclature of all these cells became important. To this end, Karl Albert Ludwig Aschoff and his colleague Kiyono, performing a systematic study of tissues stainings in 1913, coined the term "Reticulo-Endoplasmic System" (RES) to describe the cells whose function was to clear particulate matter from the blood and lymph (Yona and Gordon, 2015 ; Halpern, 1959), and that could take up staining dyes form the circulation. The cells of the reticulo-endothelial system were extensively studied for their phagocytic activity for several decades, and were divided into "wandering" and "sessile" cells (Halpern, 1959). At the time, these phagocytic cells were believed to emerge from their organ of residence.

This unified system however became less and less in touch with accumulating *in vitro* and *in vivo* data showing particular developmental and functional relationships between the cells it was describing as one whole.

In vitro studies as early as 1926 started to investigate the behaviour of monocytes from circulation, amoeboid cells with small filipodiae, and macrophages from tissues,

large (several tens of microns) cells with long processes, in the context of various culture conditions. Monocytes and macrophages were seen "as functional variations of a single type" (Carrel and Ebeling, 1926), based on the similarity in morphological structure when in culture for long enough, with the same conditions.

Several groups performed *in vivo* investigations on the dynamics of mononuclear phagocytes. In 1939, Ebert and colleagues used intravital microscopy in the ears of rabbits to show that circulating monocytes could give rise to inflammatory macrophages in the skin and subcutaneous region (Ebert and Florey, 1939). Similar results were found in the skin of rats (Volkman and Gowans, 1965), or in mouse lungs (Pinkett et al., 1966) and liver (Howard et al., 1965) in various inflammatory conditions. Although it was postulated for some years that lymphocytic cells (small round cells with round nuclei and small cytosol/nucleus size ratio) may be a precursors of monocytes in the circulation, before turning into macrophages in the tissues (a model reminiscent of Metchnikoff's hypothesis as described in his *Lectures on the Comparative Pathology of Inflammation*, 1892), this hypothesis was dismissed and the following paradigm was put forth by van Furth and Cohn in a 1968 study on peritoneal macrophages: promonocytes in the bone marrow gave rise to monocytes in the circulation, which would differentiate into the macrophages observed in the tissues. After a Conference on Mononuclear Phagocytes in Leiden in September 1969, Van Furth and colleagues published a Memorandum describing the Mononuclear Phagocyte System in a version taking into account the discussion with numerous researchers of the field (van Furth et al., 1972).

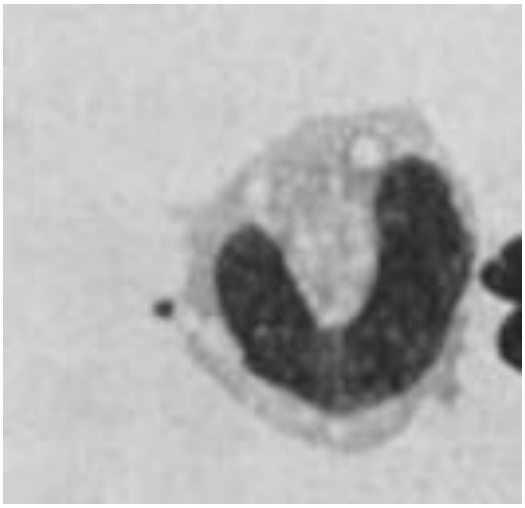

Figure 1.2. A monocyte, form Rebuck and Crowley, 1955

During the following years, Steinman and colleagues carried out seminal work that resulted in the identification of a new type of mononuclear phagocyte, depicted in a series of papers in the Journal of Experimental Medicine from 1973 to 1975 : the Dendritic Cell (DC). These papers described the morphology, quantification and local distribution, as well as their functional properties *in vitro* and *in vivo* (Steinman and Cohn, 1974, 1973; Steinman et al., 1974). It also provided a description of the cells in the spleen and tools to study these cells (Steinman et al., 1975, 1979). As a newly described mononuclear phagocyte, it was incoporated in the MPS. Thanks notably to seminal work carried out in the early 80s by Steinman and his colleagues at the Rockefeller, DCs were characterized during the following years as the (until then) elusive “accessory” cell type that linked innate and adaptive immunity, by presenting antigens to lymphocytes (Nussenzweig and Steinman, 1980; Steinman et al., 1983).

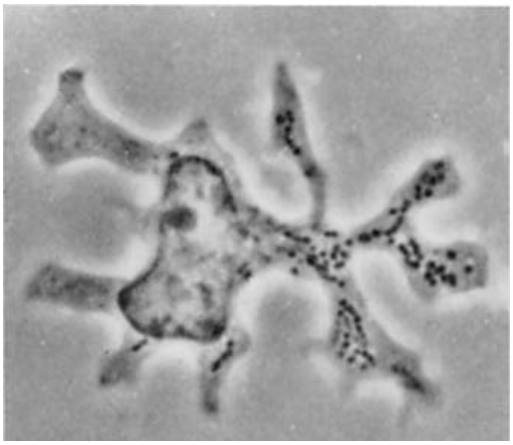

Figure 1.3. A dendritic cell. From Steinman and Cohn, 1973

1.1.4. New paradigm and the contribution of studies on fetal hematopoiesis

As pointed out above, the construction of the MPS was based on knowledge acquired mostly thanks to studies of inflammatory situations, and this formed the basis for the understanding of macrophage ontogeny. However, this paradigm was challenged as studies in adults and embryos of several species were performed. Many studies found that macrophages were still present in tissues of monocytopenic mice (Morahan et al., 1986; Sawyer, 1986; Yamada et al., 1990). Furthermore, tissue macrophages do not exchange between parabiotic mice (Ajami et al., 2007; Merad et al., 2002). This points to macrophages being less dependent on monocytes than suggested by the MPS model.

The development of hematopoietic cells during embryogenesis has been a subject of study for over a century (Sabin, 1917). The first myeloid potential was discovered in the yolk-sac (YS) by seminal work carried out by Moore and Metcalf (Moore and Metcalf, 1970). In 1992, Sorokin and colleagues described the appearance in the embryo of macrophages before hematopoietic stem cells (HSC) emerge (Sorokin et al., 1992). In the zebrafish, development of macrophages was shown to by-pass the monocyte stage (Herbomel et al., 1999). Over the last two decades, many studies have firmly established that most tissue macrophages emerge during embryogenesis before, and

independently of HSCs (Ginhoux et al., 2010; Schulz et al., 2012; Yona et al., 2013), and emerge from a progenitor with myeloid and erythroid potential, therefore termed erythro-myeloid progenitor, or EMP (Bertrand et al., 2005; Gomez Perdiguero et al., 2014; Palis et al., 1999; Schulz et al., 2012).

The work presented in this thesis focuses on two aspects of phagocyte biology : one relates to the development of monocytes from the bone marrow, and the other participated in the description of the function of monocytes and tissue resident macrophages in the kidney. Therefore an overview of the current knowledge on monocytes and on macrophages will now be presented, separately.

1.2. Monocyte Subsets and Functions

1.2.1. Human subsets

Monocytes are part of the three main types of mononuclear phagocytes of the innate arm of the immune system (the others being macrophages and dendritic cells), and represent 4 to 11% of blood circulating cells (Sluss et al., 2004). The heterogeneity of this cell type has been recognized since the late 1980s. It had been known for a long time that these cells were able to migrate into inflamed tissues to give rise to inflammatory macrophages, and it was suspected at the time that the heterogeneity of macrophages in tissues may be a result of monocyte heterogeneity. This prompted the examination of monocytes by various techniques, and flow cytometry uncovered a new human monocyte subset. Monocytes in human were stained with an antibody generated against myelo-monocytic leukemia cells, My4 (CD14) ; it was found that their expression of CD14 was not homogeneously high (Ziegler-Heitbrock et al., 1988), nor was their size and granularity profile. A year later, the staining of human Peripheral

Blood Mononuclear Cells (PBMC) with an antibody against CD16 (already used in the 1988 paper by Ziegler-Heitbrock et al.) uncovered that monocytes in human peripheral blood consisted of two main subsets, $CD14^{hi}$ $CD16^{-}$ and $CD14^{dim}$ $CD16^{+}$ monocytes (Passlick et al., 1989); although it was unclear then whether the latter was a bona fide subset of monocyte or rather just a distinct maturation state of $CD16^{-}$ monocytes, these cells were shown to have monocyte characteristic: morphology, esterase reactivity and Reactive Oxygen Species (ROS) production capacity (Ziegler-Heitbrock et al., 1988). Many studies have since then found specific functions of this subset, identifying it as such. The two subsets can be distinguished based on several surface markers, including the Fc-Receptor gamma 1 (FcγRI, or CD64, Grage-Griebenow et al., 2001a, 2001b). Given the wide range of CD14 expression by $CD16^{+}$ cells and functional studies, a later nomenclature has been developed to categorise human blood monocytes : the "classical" $CD14^{+}$ $CD16^{-}$ monocytes; the "intermediate" $CD14^{+}$ $CD16^{+}$ and the "non-classical" $CD14^{dim}$ $CD16^{+}$, (Ancuta et al., 2006; Heron et al., 2008; Ziegler-Heitbrock et al., 2010). The intermediate subset of monocytes has been shown to be specifically increased and show an anti-inflammatory phenotype (CD163 expression) in severe asthmatic patients (Moniuszko et al., 2009), and to produce large quantity of the interleukin (IL) -10 upon lipopolysaccharide (LPS) stimulation (Skrzeczynska-Moncznik et al., 2008), compared to the other subsets. Recently, it has even been proposed that this intermediate population may be heterogeneous itself, based on single cell RNA-sequencing analysis, leading to four subsets of monocytes in human blood rather than the known three (Villani et al., 2017).

Heterogeneity in monocyte populations is recognized across several species (Ziegler-Heitbrock, 2014). In non-human primates, the anti-human CD16 antibody was used to detect intermediate and non-classical monocytes in proportions similar to human blood subsets (Munn et al., 1990), with similar chemokine receptor expression patterns,

response to M-CSF (Munn et al., 1990; Munn et al., 1996), and expansion after infection with immunodeficiency virus than observed in humans (Jaworowski et al., 2006; Kim et al., 2010). In pigs (Fairbairn et al., 2013; Ziegler-Heitbrock et al., 1994), cows (Hussen et al., 2013), and horses (Kabithe et al., 2010; Noronha et al., 2012), classical and non classical subsets of monocytes have been described, either with the anti-human antibodies to CD14 and CD16, or with species-specific ones, and there seems to be a comparable distribution of these subsets. They have also been described in rodents, notably in rats (Scriba et al., 1997). The study of monocytes in mice has been a very active field of research and these animals also present heterogeneity in their monocyte compartment, which will be presented in the next section.

1.2.2. Mouse subsets

In mice, the first hint at monocyte heterogeneity in mice may be found in a 2001 article where the authors were studying the recruitment of monocytes to draining lymph nodes (LN) of the skin (Palframan et al., 2001). The authors were analysing the role of the C-C chemokine Monocyte Chemoattractant Protein-1 (MCP-1, or CCL2), in their recruitment to skin draining LN via High Endothelial Venules (HEV). They found, using the recently generated *Cx3cr1*$^{gfp/+}$ mice (Jung et al., 2000) that monocytes of various intensities of Green Fluorescent Protein (GFP) expression under the control of the C-X3-C chemokine receptor 1 (CX_3CR1) gene expression, were infiltrating the LN in an MCP-1 dependent manner.

However, the proper description of two phenotypically and functionally distinct subsets of monocytes was published two years later (Geissmann et al., 2003). Because CX_3CR1 is expressed not only by myeloid but also lymphoid populations of cells, the authors generated *Cx3cr1*$^{gfp/+}$ *Rag2*$^{-/-}$ mice, which also had the advantage that monocytes constituted 45-50% of circulating cells, instead of the usual 2% of mouse

blood (Mouse Phenome Database, Jackson Laboratories). Subsets of circulating monocytes were identified based on the level of CX_3CR1 as well as Ly6C, CCR2, L-selectin (CD62L) and various other markers : one subset expressed high levels of Ly6C (stained with a Gr-1 antibody), intermediate levels of CX_3CR1, high levels of CCR2 and was positive for CD62L. The other subset was found to be $Ly6C^{low}$ CX_3CR1^{high} $CCR2^-$ $CD62L^-$. Upon adoptive transfer into non-irradiated hosts, these cells had also different half lives in the circulation and tissue homing properties *in vivo* : while transferred $Ly6C^{low}$ monocytes were observed in the host's blood for 4 days, the $Ly6C^+$ subset was only observed in the host's blood for 24h, not after. Upon transfer into an inflamed host (after intraperitoneal – *i.p.* – injection of thioglycollate), the two subsets showed different responses, with the $Ly6C^{low}$ staying mainly in the blood and homing to non-inflamed tissues, while the $Ly6C^+$ subset invaded the peritoneum, acquired DC markers (MHC-II and CD11c) and could induce T cell proliferation *in vivo*, suggesting these cells could differentiate into functional DC in the context of inflammation (Geissmann et al., 2003).

Based on these observations, the $Ly6C^+$ CX_3CR1^{int} monocytes were termed 'inflammatory' monocytes, while the $Ly6C^{low}$ CX_3CR1^{hi} subset was termed 'resident'. Other terms have been used since then to designate these cells, such as 'classical' and 'non-classical' ; this thesis will mainly refer to them as $Ly6C^+$ and $Ly6C^{low}$ monocytes. Gene expression patterns were found to be very similar between, on one hand the mouse $Ly6C^+$ monocytes and the human $CD14^+$ $CD16^-$ monocytes, and on the other hand between the $Ly6C^{low}$ and $CD14^{dim}$ $CD16^+$ subsets (Cros et al., 2010; Ingersoll et al., 2010).

Monocytes have been further characterized thanks to the use of flow cytometry, and the two main subsets can be distinguished based on the differential expression of Ly6C,

CX_3CR1, CCR2 and CD43, while they express similarly high levels of CD115, the M-CSF receptor (Sunderkotter et al., 2004).

Monocytes have been further characterised over the years, with regards to their development, phenotype, function, and fate *in vivo*, of which an overview will now be given.

1.2.3. Ly6C$^+$ monocytes functions

During microbial tissue invasion, Ly6C$^+$ monocytes are mobilized form the bone marrow, circulate in the blood until they extravasate at the site of infection, where they play critical roles in pathogen phagocytosis, cross-talk with other innate cells and eventually may participate in the activation of adaptive immunity. Here a summary of these different roles in the context of various microbial threats, as well as sterile inflammation and cancer, will be given.

1.2.3.1. In bacterial infections

In response to bacterial infections, Ly6C$^+$ monocytes have most notably been studied in the context of *Listeria monocytogenes* infection. They first exit the bone marrow via CCR2-dependent mechanisms, and mice deficient for CCR2 have a markedly increased susceptibility to *L. monocytogenes* infection (Serbina and Pamer, 2006 ; see also section ***1.3.4.2***). Once in the circulation, chemokine signalling via G-coupled proteins seems dispensable for their localisation into sites of infection (Shi et al., 2010) as pertussis toxin pre-treatment of monocytes before their transfer into infected host does not disturb their recruitment; they rather rely on the integrin CD11b, also known as Mac-1 or Complement Receptor 3 (CR3), CD44 and the adhesion molecule ICAM-1 (Intercellular Adhesion Molecule -1) (Rosen et al., 1989; Shi et al., 2010). Once at the site of *L. monocytogenes* infection, Ly6C$^+$ monocytes were shown to differentiate into

Tumor Necrosis Factor alpha- (TNFα) and inducible-Nitric Oxide Synthase (iNOS) – producing cells, which prompted the term "Tip-DCs" to designate them (Serbina et al., 2003b).

The detection of bacterial products via Toll-Like Receptors (TLR) is crucial for host defence and mice lacking the intracellular signalling MyD88 downstream of many TLRs leads to a worsen survival of infected mice (Serbina et al., 2003a). However, MyD88 is not required in $Ly6C^+$ monocytes for their recruitment to sites of infection, nor for their differentiation into Tip-DCs. However, it is necessary in other cell types (possibly classical DCs) for the proper function of Tip-DCs (Serbina et al., 2003a ; Arnold-Schrauf et al., 2014). During a secondary encounter with *L. monocytogenes*, memory CD8+ T cells produce CCL-3, which induces the production by $Ly6C^+$ monocytes of TNFα, and eventually of Reactive Oxygen Species (ROS), thus mediating crucial bacterial clearance (Narni-Mancinelli et al., 2007, 2011).

The role of CCR2-expressing $Ly6C^+$ monocytes was also shown in the clearance of *Klebsiella pneumoniae* (Xiong et al., 2015), as well as during *Brucella melitensis* infection, where cells with similar phenotypical and functional features as Tip-DCs were found during the first days post infection (Copin et al., 2007). The response to *Mycobacterium tuberculosis* also requires CCR2 for monocytes to leave the bone marrow (Peters et al., 2001), and although the injection of poly I:C, leading to an increased recruitment of $Ly6C^+$ monocytes during infection, has shown to worsen the *M. tuberculosis* bacterial load (Antonelli et al., 2010), $Ly6C^+$ monocytes participate positively to the decrease in bacterial load at specific times after infection, through the delivery of the pathogen to the draining lymph nodes, but not the priming of T-cells (Samstein et al., 2013). In addition, it is also important to mention *Legionella pneumophila* infection in the lungs, during which monocyte-derived cells seem to play a

critical role in cooperation with other cell types during various stages of infection (Brown et al., 2016; Casson et al., 2017).

1.2.3.2. In parasitic infections

Toxoplasma gondii is a protozoan parasite that invades the intestinal epithelium and can reside in a variety of hosts, including humans, in muscle and neural tissues without causing symptoms to immune-competent hosts. However immuno-deficient individuals, such as AIDS patients, can develop toxoplasmosis, which can lead to major brain damage. Initial reports pointed to neutrophils as the principal early responders by rapid production of IL-12p40 (Bliss et al., 2000), although the use of Gr-1 (clone RB6-8C5, targets both Ly6C and Ly6G) to deplete innate immune cells lead to some confusion as to which cell type was most influential during the early phases of infection. Later, reports showed the critical role of $Ly6C^+$ monocytes in the control of infection (Dunay et al., 2010; Neal and Knoll, 2014; Robben et al., 2005).

$Ly6C^+$ monocytes have also been shown to be involved in the response to many other parasites, such as strains of *Leishmania* : *Leishmania mexicana* was shown to target the recruitment of inflammatory monocytes, which resulted in a lessen Th1 induction by monocyte-derived dendritic cells on the sites of infection (Petritus et al., 2012). During the blood stage of malaria infection (*Plasmodium chabaudi*), $Ly6C^+$ monocytes were shown to be critical to the control of the parasite through production of iNOS, Reactive Oxygen Intermediates (ROI) and phagocytic activity, all without any sign of differentiation into DC (Sponaas et al., 2009), and the role of monocytes in this pathology is a matter of investigation at many stages of the disease in several organs of the infected patients (Chua et al., 2013). Infection by the helminth *Schistosoma mansoni* induces an increased production of $Ly6C^+$ monocytes in the bone marrow that are found

in the circulation and then in the liver (together with other phagocytes), where they seem to differentiate into macrophages (Girgis et al., 2014; Nascimento et al., 2014).

1.2.3.3. In fungal infections

Inhalation of fungal spores (conidia) happens daily, and it has been measured for *Aspergillus fumigatus* that 0.2 to 15 spores were present in each cubic meter of air (VandenBergh et al., 1999). Once deposited in the upper and lower airways, the epithelial cells of the lung usually clear these spores, and most invaded hosts never develop any symptoms. However, immuno-deficient or critically ill patients are susceptible to disease form *A. fumigatus* (Stevens and Melikian, 2011). The early response to this fungus is mediated by a number of innate cells such as neutrophils (Bonnett et al., 2006), plasmacytoid DCs (Ramirez-Ortiz et al., 2011), and Natural Killer cells (Park et al., 2009). In this context too, the CCR2-dependent exit of $Ly6C^+$ monocytes from the bone marrow and their recruitment on the infection site is critical for the host protection (Espinosa et al., 2014). $Ly6C^+$ monocytes have a direct role in taking up the spores and differentiation in monocyte-derived DCs, as deciphered with the use of fluorescent conidia (Espinosa et al., 2014; Jhingran et al., 2012), as well as an indirect role, as promoters of neutrophil-mediated killing and mounting of $CD4^+$ T cell responses.

The importance of $Ly6C^+$ monocytes has also been well established in the context of infection by *Candida albicans*, a fungus that mostly targets the kidney (although its presence can be detected in most organs upon infection), and can cause sepsis (Spellberg et al., 2005). In response to infection, $Ly6C^+$ monocytes accumulate in most organs (Lionakis et al., 2011), and become the predominant inflammatory cell type in the kidney during early infection (Ngo et al., 2014), where they are crucial for the killing of *C. albicans* and the control of its growth. $Ly6C^+$ monocytes were also found

to upregulate MHC-II, CD11c and down-regulate Ly6C, migrate into draining lymph nodes and gain the ability to prime CD4 T cells *ex vivo*, suggesting they could also have an antigen-presenting role in the context of this infection (Trautwein-Weidner et al., 2015). Finally, it was recently shown that Ly6C$^+$ monocytes were the primary source of IL-15 during *C. albicans* infection, which results in the activation of the NK cell/neutrophil axis in the liver and spleen, which in turn is critical for the fungus killing (Domínguez-Andrés et al., 2017).

1.2.3.4. In viral infections

Ly6C$^+$ monocytes also participate to the anti-viral response, such as studied in the context of influenza virus. It was shown in a 2009 study that several strains of Influenza A virus could induce the CCR2-dependent monopoiesis and subsequent recruitment to the lung of, among other cell types, Ly6C$^+$ CD11b$^+$ cells, producing TNFα and iNOS (Aldridge et al., 2009). These cells were shown to be important players in the response to influenza, although the dose used in models of influenza can impact the outcome of *Ccr2*-deficiency (Aldridge et al., 2009; Dawson et al., 2000; Lin et al., 2008). It seems "Tip-DCs" recruited to the lungs can act as local antigen-presenting cells to induce a stronger CD8 T cell response (Aldridge et al., 2009), which impacts the outcome of disease, as CD8 T cells are thought to be the main mediators of virus-producing epithelial cells killing (Doherty et al., 1997).

Additionally, Ly6C$^+$ have been shown to have a detrimental impact during early phases of West-Nile Virus infection, which infects the brain. Within the first week of infection, Ly6C$^+$ monocytes have been shown to be recruited from the BM and to cross the Blood-Brain Barrier (BBB), and infiltrate the brain, with both these steps CCR2-dependent (Getts et al., 2008), based on a CCL-2 blockade strategy, while competitive

transfer experiments of CCR2-potent and CCR2-deficient monocytes argue for a CCR2-independent infiltration of monocytes from blood to brain (Lim et al., 2011).

Finally, it can be mentioned that $CD14^+$ monocytes (of which the mouse $Ly6C^+$ monocytes are analogues) circulating in humans were found to be reservoirs for the Human Immunodeficiency Virus (HIV) -1 (McElrath et al., 1991; Quiros et al., 1995), and these cells, as well as $CD14^{dim}$ $CD16^+$, are involved in the virus latency, even in patient under anti-retroviral therapy (Zhu et al., 2002).

1.2.3.5. During cancer

Cancer progression occurs as a succession of events. First, cells autonomously acquire and accumulate mutations that lead to their transformation, then these transformed cells perform clonal expansion in their organ of origin, which becomes the primary cancer site; finally, some cancer cells can circulate and engraft other organs, and proliferate *in situ* to constitute metastasis. During these developments, tumour cells acquire various properties that can be designated as hallmarks of cancer, that allow their growth and escape from various defence mechanisms (Hanahan and Weinberg, 2011). There is a tremendous variability regarding whether a particular immune cell type is associated with a good or bad prognosis, and this depends on the immune cell type, cancer primary site and stage of disease. Consistent with this general observation, monocyte responses to cancer have been shown to be variable.

Adding a layer of complexity, myeloid populations of different origins (see ***section 1.4.1*** about macrophage development) can populate tumours at various stages (Perdiguero and Geissmann, 2014). This issue has notably been tackled in a study on myeloid cell response in a mouse model of spontaneous mammary gland cancer, where *Ccr2*-deficient mice, gene expression profiling and transfer techniques were used to decipher the identity and origin of tumor-infiltrating cells. The authors found that upon

tumor growth, Ly6C$^+$ monocytes exited the BM in a CCR2-dependent manner, and contributed to myeloid populations found in the tumor, where they differentiated into tumor associated macrophages (TAM), in a Notch-dependent manner (Franklin et al., 2014). Several studies have suggested a role for extramedullary haematopoiesis in the spleen, and this organ considered a potential reservoir for inflammatory monocytes in the context of cancer (Cortez-Retamozo et al., 2012). The use of photo-convertible protein-bearing mice revealed that spleen monocytes made only a marginal contribution to tumour-infiltrating monocytes, and that their origin was mainly in the bone marrow (Shand et al., 2014).

1.2.3.6. During sterile inflammation or injury

Beyond pathogenic stimuli or cancer, monocytes are involved in a number of other inflammatory settings. For example, although graft rejection is typically associated with T cell responses, it has long been recognized that the infiltration of myeloid cells in renal transplant had a strong impact as well (Girlanda et al., 2008; Hancock et al., 1983). Swirski and colleagues found that Ly6C$^+$ monocytes were the predominant myeloid infiltrating cells present in rejected grafts in a mouse model of heart transplantation (Swirski et al., 2010).

Atherosclerosis is a complex progressive disease characterised by the formation, on large and medium-sized arteries, of plaques with a defined structure of lipid-rich necrotic core, covered by a fibrous cap, which contains inflamed smooth-muscle cells, and collagen fibres (Usman et al., 2015). These plaques have the capacity to block blood flow leading to ischemia of the heart, brain or extremities. It has long been recognized that atherosclerosis is an inflammatory disease (Ross, 1999), and the lesions are also populated with cells referred to as ‘foam cells’, the origin of which is still a matter of research (Woollard and Geissmann, 2010). The infiltration of monocytes,

among other immune cells, has been observed as early as 1979 by Gerrity and colleagues, who found mononuclear cells in the plaques by light microscopy, and monocytes extending microvilli into endothelial cells, by electron microscopy (Gerrity et al., 1979).

Apolipoprotein E (ApoE) is critical for lipid transport and metabolism, and is the primary ligand for low-density lipoprotein receptor-mediated removal of circulating lipoproteins. *ApoE*$^{-/-}$ mice (Nakashima et al., 1994) have been instrumental in the study of the initiation and progression of atherosclerosis, as they develop similar lesions as humans, which occur faster when fed a lipid-rich, Western-type diet (Nakashima et al., 1994; Plump and Breslow, 1995). Monocytes are found inside the plaques thus formed, and although other cells have been proposed as precursors for the foam cells (Paulson et al., 2010), Ly6C^{+} monocytes in *ApoE*$^{-/-}$ mice were found to be produced in greater number in the bone marrow, adhere to the arterial wall and infiltrated the lesions, where they differentiated into plaque macrophages (Swirski et al., 2007).

Finally, recent reports have used intravital microscopy to try unravel the *in situ* behaviour of Ly6C^{+} monocytes after sterile injury in the liver, showing they are rapidly recruited (within hours) to the focal point of injury, together with, but independently of, neutrophils (Dal-Secco et al., 2015), where they upregulate CX$_3$CR1 and down-regulate Ly6C. Some studies, as in the context of heart ischemia, have proposed that the different subsets of monocytes were recruited sequentially to the necrotic tissue and started with a wave of Ly6C^{+} monocytes that would participate to the inflammatory milieu, followed by a second wave of pro-repair Ly6C$^{\mathbf{low}}$ monocytes (Nahrendorf et al., 2007), recruited separately, rather than the product of an *in situ* conversion of Ly6C^{+} monocytes into Ly6C$^{\mathbf{low}}$ monocytes. However, this view has been challenged some years later by the same group (Hilgendorf et al., 2014), showing that Ly6C^{+} monocytes

were involved in both inflammatory and reparative phases or myocardial infarction progression.

1.2.4. Ly6C^{low} monocyte functions

1.2.4.1. Patrolling activity

When they were first described, Ly6C^{low} monocytes were found to have a longer life span in the circulation than their Ly6C^{+} counterparts (Geissmann et al., 2003) ; however, their function remained unclear. These cells develop independently of the lymphoid lineage, as they are present in normal numbers in Recombination Activated Gene 2 (*Rag2*) -deficient, *Il2rg* (gamma chain of the IL-2 receptor) –deficient mice (Auffray et al., 2007a; Geissmann et al., 2003), as well as *Il2rg*$^{-/-}$ patients (Cros et al., 2010). In 2007, Frederic Geissmann's laboratory published work that characterised their behaviour *in vivo* (Auffray et al., 2007). Utilising *Cx3cr1*$^{gfp/+}$ crossed to a *Rag2*$^{-/-}$ *Il2rg*$^{-/-}$ background mice allowed the visualisation of monocytes as the only GFP expressing cells, the authors found that Ly6C^{low} monocytes crawl on the luminal side of the endothelium in different organs (skin, mesenteric vessels). This crawling is relatively slow (about 12μm/min in average), compared to other cells rolling on endothelium (Springer, 1994), and does not depend on the direction of the blood flow, with their track showing various patterns, including loops, hairpins and waves. Their confinement ratio was found to be low, 0.5 in average, meaning that the distance travelled by individual cells was only half the total length of their tracks. These characteristics of their crawling was suggestive that these cells may be surveying the endothelium, which coined the term 'patrolling' to describe their behaviour. It also implied a firm attachment of the crawling monocytes to the endothelium, which was found to be LFA-1 (Lymphocyte Function-associated Antigen 1) -dependent and partially CX_3CR1-dependent. Patrolling monocytes seem to extravasate rarely in the steady state, although

they can do so rapidly in response to tissue damage with tissue irritants, sterile injury and infection with *L. monocytogeneses*, after which the authors measured a strong TNFα production by these cells, 2h post infection, which is before the full recruitment of either neutrophils or Ly6C^{+} monocytes (Auffray et al., 2007).

A few years later, human CD14$^{\mathbf{dim}}$ CD16^{+} monocytes were also found to have a patrolling activity, as pre-labelled transferred monocytes of that phenotype were found crawling on the luminal side of blood vessel of mice alongside mouse *Cx3cr1-gfp*$^{+}$ Ly6C$^{\mathbf{low}}$ monocytes (Cros et al., 2010).

This Ly6C$^{\mathbf{low}}$ patrolling monocyte subset was found crawling in the capillaries of the kidney, in an ICAM-1 (InterCellular Adhesion Molecule -1) -dependent manner, where these cells are able to phagocytose microbeads injected intravenously (Carlin et al., 2013). The interaction between patrolling monocytes with the endothelium is dynamic at steady state, where it was estimated that at any time, one third of Ly6C$^{\mathbf{low}}$ monocytes are crawling on the luminal side of vessel, from which they attach and detach constantly. Upon topical application, or 'painting', of a TLR7 agonist on the kidney, Ly6C$^{\mathbf{low}}$ monocytes were found to be retained by the endothelium via a CX$_{\mathbf{3}}$CR1-CX$_{\mathbf{3}}$CL1 dependent mechanism, with a decreased instantaneous velocity, lower confinement ratio and increased track length and duration, leading to their accumulation over a few hours in the kidney. This leads to the recruitment, by the retained monocytes, of neutrophils, whose numbers are greatly increased following TLR7 agonist painting of the kidney. In turn, these recruited neutrophils induce the endothelial cells to necrose (Carlin et al., 2013). A set of experiments presented in **Chapter 4** focused on a certain aspect of this inflammatory response of Ly6C$^{\mathbf{low}}$ monocytes. Of note, in this study by Carlin and colleagues, the authors stained MHC-II on monocytes in order to separate the steady state MHCII^{+} and MHC-II^{-} within the CD11b^{+} CD115^{+} blood monocytes, identifying an MHC-II^{+} fraction that expresses a range of levels of Ly6C. The

'patrolling' subset of monocytes was hence defined as CD11b^{+} CD115^{+} Ly6C^{low} MHC-II^{-} (Carlin et al., 2013). This separation is not performed in most articles published to date (to our knowledge), so is not accounted for in the studies we will mention from here.

These studies demonstrated a role of Ly6C^{low} monocytes as « housekeepers » of the vasculature, which has been confirmed by several other groups, who have described patrolling monocytes in other settings. Ly6C^{low} monocytes have also been observed in larger vessels than kidney capillaries, such as in the carotid arteries, crawling at higher velocities during steady state (average of 36µm/min, versus an average of 8µm/min in the kidney – Carlin et al., 2013 - or 12µm/min in the skin – Auffray et al., 2007), where they are increased by TLR7 agonist application (Quintar et al., 2017). In the brain, Ly6C^{low} CX$_3$CR1^{hi} monocytes have been found patrolling in the cerebral vasculature where small aggregates of amyloid β (Aβ) deposited in mouse models of Alzheimer disease, but not during steady state or in arteries where Aβ is surrounding the vessels (Michaud et al., 2013). Development of endoscopic imaging techniques of the heart allow the longitudinal analysis of this organ over several days, and allowed the observation of steady state crawling of CX$_3$CR1^{hi} Ly6C^{low} monocytes (Jung et al., 2013), where they were found to crawl at similar velocities than in the kidney capillaries (Li et al., 2012a). Finally, LFA-1 mediated crawling of Ly6C^{low} monocytes has been described in the mouse cremaster muscle (Sumagin et al., 2010). Taken together these observations suggest that the patrolling behaviour of Ly6C^{low} CX$_3$CR1^{hi} monocytes is a feature that seems universally found in the vasculature, which allows this subset to perform specific functions in the circulation.

1.2.4.2. Ly6C^{low} monocytes in infectious diseases and cancer

Ly6C^{low} monocytes have been implicated in the response to infection in some cases, although it has not yet been as much studied as in the case of Ly6C^{+} monocytes. First, as mentioned above, they extravasate rapidly after intraperitoneal infection with *Listeria monocytogenes* (Auffray et al., 2007). Following infection, they are found in great numbers in the peritoneal cavity, where they produce TNFα, and upregulate genes associated with a differentiation program towards macrophage-like phenotype, such as *cMaf* and *MafB*, but not *RelB* nor *Pu.1* (Auffray et al., 2007) ; this is in contrast to Ly6C^{+} monocytes, which upregulate genes associated with DC differentiation (Auffray et al., 2007), consistent with their described extravasation and differentiation to TNFα and iNOS producing Tip-DCs, as described by the group of Eric Pamer (Serbina et al., 2006).

Recently, the mouse cytomegalovirus (MCMV) was found to 'hijack' patrolling Ly6C^{low} monocytes to use them has Trojan horses to disseminate to the salivary glands, in an experimental model of infection of the footpad (Daley-Bauer et al., 2014). Consistent with the CX$_3$CR1-dependent steady-state crawling and retention of Ly6C^{low} monocytes (Auffray et al., 2007 ; Carlin et al., 2013), this dissemination was impaired in *Cx3cr1$^{gfp/gfp}$* mice, which are Knock-Out (KO) for *Cx3cr1*. Studies on the response to virus by human CD14^{dim} CD16^{+} monocytes revealed they can respond to nucleic acids from Herpes Simplex Virus 1 and measles via TLR7/TLR8, which signal through the MYD88-MEK pathway, to produce IL-1β, TNFα and CCL3 (Cros et al., 2010).

In models of cancer development, a fraction of Ly6C^{low} monocytes have been shown to express Tie-2, and promote angiogenesis in the tumor microenvironment (De Palma et al., 2005). Equivalents of these Tie-2 expressing monocytes have been characterised in human among the CD14^{dim} CD16^{+} (Murdoch et al., 2007; Venneri et al., 2007).

Angiogenesis is one of the hallmarks of cancer (Hanahan and Weinberg, 2011), and participates to tumor progression, which points to a detrimental role of patrolling monocytes in certain cancers or cancer models. However, a fraction of Ly6C^{low} monocytes expressing neuropilin-1 has been shown to hinder tumor growth when injected by intratumoral route, by promoting a certain pathway of vessel maturation, thereby increasing tumor perfusion ; this limited hypoxia, which is a factor that can promote tumoral growth (Carrer et al., 2012). In a recent report, Ly6C^{low} monocytes were found patrolling the vasculature of lung tumors, and several models of *Nr4a1* deficiency, in which the Ly6C^{low} subset of monocytes is lacking (Hanna et al., 2011 ; see *section 1.3.4.1*), showed enhanced metastasis to the lung in a model of spontaneous mammary tumors (Guy et al., 1992) ; together with the observation of fluorescently labeled cancer cells being ingested by Ly6C^{low} monocytes, these results suggested they participate in the clearing of metastasizing cancer cells (Hanna et al., 2015).

1.2.4.3. Role of Ly6C^{low} monocytes in other immunological disorders

Ly6C^{low} monocytes have also been shown to be part of the response to various non-pathogenic nor cancerous diseases, such as atherosclerosis, Systemic Lupus Erythematosus (SLE) or Rheumatoid Arthritis (RA).

As mentioned above, *ApoE*$^{-/-}$ mice rapidly develop atherosclerotic plaques in their arteries when fed a high fat diet (HFD, Nakashima et al., 1994). During this process, Ly6C^{low} also enter the lesions, though less frequently than Ly6C^{+} monocytes, in a CX_3CR1-independent, but CCR5-dependent manner (Tacke et al., 2007). Consistently, using this same model of *ApoE*$^{-/-}$ mice fed a HFD, Combadière and colleagues found that combined deficiency in CCL2, CX_3CR1 and blocking of CCR5 was enough to almost completely abrogate atherosclerotic plaque formation (Combadière et al., 2008), suggestive of an overall deleterious effect of monocyte influx into lesions. However,

other reports suggest otherwise, in mice lacking Ly6C^{low} monocytes, in the context of *ApoE*$^{-/-}$ mice fed a HFD, Chao and colleagues found no correlation with outcome in terms of arterial lesion formation (Chao et al., 2013). Finally, a number of studies from different groups suggest that Ly6C^{low} monocytes have a protective effect in the context of atherosclerosis. Combined deficiency in *Nr4a1* (on which Ly6C^{low} depend for their development, see Hanna et al., 2011 and *section 1.3.4.1*) and *ApoE* (Nakashima et al., 1994) resulted in an increase of atherosclerosis (Hamers et al., 2012; Hanna et al., 2012). Intravital imaging of the steady state and atherosclerotic arteries also suggested a protective role of Ly6C^{low} monocytes, which patrolled the endothelium of large arteries as mentioned before, and improved the proper disposal of dying endothelial cells during lesion formation (Quintar et al., 2017).

Systemic Lupus Erythematosus is a chronic, systemic autoimmune disorder involving multiple organs, and the diagnostic of which can call to many different clinical signs, and during which autoantibodies are produced against double-stranded DNA (Rahman and Isenberg, 2008). Increase in production of monocytes has long been recognised in genetic mouse models of spontaneous development of this disease (Wofsy et al., 1984). In certain murine models of lupus, Ly6C^{low} monocytes seem to expand more than their Ly6C^{+} counterparts (Amano et al., 2005). A study where the authors developed an antagonist of CX_3CR1 found it delayed and ameliorated lupus (Inoue et al., 2005). Consistently, Nakatani and colleagues found that CX_3CR1 ligand and the accumulation of CD16^{+} monocytes were associated with the severity of lupus (Nakatani et al., 2010). Finally, increased generation of Ly6C^{low} monocytes with an activated phenotype was observed in lupus-prone mice, which was associated with the dysregulation of auto-reactive B cells (Santiago-Raber et al., 2009). The 'hyperactive' phenotype of these monocytes was based notably on their pattern of expression of Fc-gamma receptors, which will be discussed in the next section.

Of note, Ly6C^{low} monocytes have also been found to play an important role in rheumatoid arthritis (RA), which is one of the most prevalent chronic autoimmune diseases (Helmick et al., 2008). Misharin and colleagues obtained results suggesting that Ly6C^{low} monocytes were a driving force for the initiation of RA, by being recruited to the joints, where they upregulate genes associated with pro-inflammatory activity, before 'switching' to a more 'healing' transcriptional profile (Misharin et al., 2014). However, a recent study shows that initiation of arthritis was not massively impacted in *Cx3cr1*-deficient mice, despite the fact that these mice have significantly lower Ly6C^{low} monocytes patrolling the vasculature (Auffray et al., 2007), suggesting that Ly6C^{low} monocytes, or at least their patrolling activity, was not critical to the onset of disease (Brunet et al., 2016). Furthermore, the authors conducted experiments suggesting that *Nr4a1*-dependent Ly6C^{low} monocytes participated to the activation of regulatory T cells (T-reg) in the joint, therefore promoting a reduction of disease severity (Brunet et al., 2016). Therefore, further study will be needed to decipher the precise role of Ly6C^{low} monocytes at various stages of RA in different disease models.

1.2.4.4. Ly6C^{low} monocytes as mediators of IgG-dependent functions

Receptors recognizing the Fc (fragment crystallisable) of the constant fraction of immunoglobulins, and notably the Fc receptors (FcR) to IgG (FcγR) play a major role in immune responses (Nimmerjahn and Ravetch, 2011). They constitute a critical link between the specific response mediated by adaptive immune cells (B cells) and the innate arm of the immune system. To date, four FcγR have been characterised in mice : the activating FcγRI, FcγRIII and FcγRIV, and the inhibitory FcγRIIB (Nimmerjahn et al., 2005). Co-expression of activating and inhibitory FcγRs and their variable engagements sets a threshold of activation and determines the strength of the response by innate immune cells such as ADCC (Antibody Dependent Cellular Cytotoxicity).

Ly6C^{low} monocytes were found to express the broadest range of FcγRs, as they express both all the activating (FcγRI, FcγRIII and FcγRIV) and inhibitory (FcγRIIB) ones (Biburger et al., 2011). In a series of experiments designed to address the FcγR-mediated functions of different immune cell populations, the authors found that Ly6C^{low} monocytes had the highest capacity to perform ADCC-mediated killing of B cells in vitro, as well as efficient uptake of fluorescent liposomal vesicles and platelet depletion in vivo (Biburger et al., 2011). This suggested Ly6C^{low} may be of general importance in IgG-mediated functions in various settings. This is consistent with their involvement in several autoimmune disorders such as SLE, as mentioned above (Santiago-Raber et al., 2009).

1.3. Monocyte development

1.3.1. Hematopoiesis, overview

Hematopoiesis, the production of all blood cells, of the innate and adaptive arms of the immune system, as well as red blood cells and platelets, takes place mainly in the bone marrow of adult vertebrates. This production is a sequential process, during which cells progress from multipotent to mature, differentiated states, progressively losing this multilineage potential. At the top of this hierarchy reside hematopoietic stem cells (HSC), which are characterised by two major properties: multipotency, the ability to give rise to all blood lineages, and self-renewability. Indeed, these cells are generated once in the lifetime during the embryonic and fetal life, and then undergo asymetric mitotic divisions : one daughter cell differentiates while the other retains its HSC identity and properties. The founding work of Till and McCulloch (Till and McCulloch, 1961; Till et al., 1964) demonstrated that cells present in the BM have the potential to form clonal expansion of progenitors giving rise to Colony-Forming Units – Spleen

(CFU-S), in irradiated hosts. The founding clone could give rise to several blood lineages, hence was a multipotent progenitor. Their self-renewability was evidenced by experiments showing that these CFU-S could form not only mature cells, but also other CFU-S with the same functionality as the original CFU-S (Worton et al., 1969; Wu et al., 1968). These were the first observations of what would thereafter be termed Hematopoietic Stem Cells.

HSC have been mainly defined functionally by their ability to reconstitute the hematopoietic compartments of fully irradiated hosts (mice have been instrumental as a model for these studies, Weissman and Shizuru, 2008), giving rise to all blood lineages over a long period of time. The identification of HSCs using surface phenotypic markers was critical for their functional study; the laboratory of Irving Weissman, among others, has been carrying out seminal work in this direction. In 1986, it was found that B cell producing progenitor did not express B220 (Muller-Sieburg et al., 1986), a marker identified as specific for B cells (Coffman and Weissman, 1981). This was the basis from which a Lineage negative gating strategy was adopted (Weissman and Shizuru, 2008), and lead to the finding that all identified clonal lineage progenitors were contained in Lin^- cells, which were enriched for reconstituting cells (Muller-Sieburg et al., 1986). A little later, Thy-1 and Sca-1 (Spangrude et al., 1988), and finally c-Kit, the receptor for Stem Cell Factor (Ikuta and Weissman, 1992) were shown to be expressed by a mixture of cells enriched for cells with repopulation capacity (Morrison et al., 1994). This was then termed the LSK compartment, for Lin^- $Sca\text{-}1^+$ $c\text{-}Kit^+$. It contained Long-Term HSCs (LT-HSC), Short Term HSCs (ST-HSC) as defined by the extent of their self-renewal capacity, as well as the multipotent progenitors (MPP), identified in 1997 as having the potential to reconstitute all blood lineages but with no self-renewal capacity (Morrison et al., 1997). The use of the SLAM family receptors

CD48, CD150 and CD244 allowed an easier identification of these hierarchical stages (Kiel et al., 2005).

Beyond cells that can give rise to all blood lineages with various levels of self-renewal capacity, several other more restricted progenitors were discovered during the 1990s and 2000s. The separation of progenitors from the LSK cells, based on their expression of the alpha chain of the IL-7 receptor (IL-7Rα), allowed the identification of a clonogenic Common Lymphoid Progenitor (CLP), restricted to lymphoid cells, i.e. T cells, B cells and NK cells (Kondo et al., 1997). Within cells negative for IL-7Rα, the differential expression of Fcγ Receptors (FcγR) II / III (stained with a single 2.4G2 antibody clone) and CD34 identified a IL-7Rα^{-} FcγR$^{\mathbf{lo}}$ CD34^{+} cell population able to give rise to myeloid and erythroid cells, termed the Common Myeloid Progenitor, or CMP (Akashi et al., 2000). This CMP could differentiate into either FcγR$^{\mathbf{hi}}$ CD34$^{\mathbf{hi}}$ cells that gave rise to granulocyte and macrophage colonies upon culture with various growth factors, and therefore termed Granulocyte/Macrophage lineage-restricted Progenitors (GMP), or into FcγR$^{\mathbf{lo}}$ CD34$^{\mathbf{lo}}$ Megakaryocyte/Erythrocyte lineage-restricted Progenitors – MEP (Akashi et al., 2000). The work of Nakorn in 2003 identified a CD9^{+} progenitor population in the mouse bone marrow, more restricted than the MEP, as they could selectively give rise to megakaryocytes, the precursor giant cells to platelets, that was termed MKP, for Megakaryocyte-committed Progenitor (Nakorn et al., 2003).

The view that, after losing self-renewability from LT-HSC to MPP stages, progenitors would directly engage in well segregated myeloid/erythroid or lymphoid differentiation pathways through CMP or CLP respectively (Miyamoto et al., 2002), has since then been challenged. First, the identification of a new cell population termed the LMPP (Adolfsson et al., 2005; Månsson et al., 2007), for Lymphoid-primed Multipotent Progenitor, which expressed Flt3 and had both myeloid and lymphoid potential but little to no megakaryocytic/erythroid potential. But beyond the identification of cell

populations that would constitute a step within the differentiation tree, heterogeneity has been shown for other aspects of hematopoiesis. For example, the SLAM family markers allow the distinction within the LSK cells of potentially seven subsets of HSCs, MPPs and more restricted progenitor cells (Oguro et al., 2013). Additionally, the potential of these various progenitor cells can vary depending on the experimental conditions, and the irradiation of mice has been shown to greatly influence the outcome of progenitor cell differentiation compared to steady state (Pietras et al., 2015). The ability to self-renew was found to not be restricted to the most undifferentiated HSCs, but also in early myeloid-restricted repopulating progenitors that can by-pass the usual stepwise process of hematopoiesis (Yamamoto et al., 2013). The development of genetic barcoding techniques has allowed investigators to revisit lineage potential of individual cells *in vivo* in mice; a group showed that individual CMP tended to selectively give rise to either myeloid or megakaryocytic/erythroid progeny, which argued against its MEP/GMP pluripotency, and suggested a more pluripotent progenitor population may actually reside upstream, within the MPPs (Perié et al., 2015). Finally, analysis of the transcription profiles of individual cells sorted based on small phenotypic variations (i.e. intensities of expression of markers) suggested a vast heterogeneity of known progenitor populations (Paul et al., 2015). Therefore, the classical road map identifying distinct progenitor populations with fixed lineage potential and self-renewal capacity is to be considered with caution.

Monocyte development has been unveiled over the years and a brief summary of the knowledge gathered about the known monocyte progenitors will now be given.

1.3.2. MDP and cMoP are steps towards differentiated monocytes

Further downstream from the GMP, a progenitor restricted to mononuclear phagocytes was identified in 2006 and was termed the MDP, for Macrophage/Dendritic

cell Progenitor (Fogg et al., 2006). Until then, results from various laboratories over many years had suggested different hypothesis. Some results suggested that macrophages and dendritic cells were derived from a common progenitor (Inaba et al., 1993). However a number of studies pointed toward separated pathways of differentiation, for example the fact that while macrophages rely of M-CSF (Macrophage-Colony Stimulating Factor) for their development, DCs don't (Witmer-Pack et al., 1993), and are rather Flt3-dependent (McKenna et al., 2000). Progenitor populations identified until then did not allow a clear pathway for DC lineage, as dendritic cells could be generated both from the CMP (Akashi et al., 2000) and CLP (Karsunky et al., 2008; Kondo et al., 1997).

Based on the knowledge that CX_3CR1 is expressed widely by monocytes, DCs and macrophages (Jung et al., 2000 ; Geissmann et al., 2003), the study of Fogg and colleagues (Fogg et al., 2006) identified a c-Kit^+ population that expressed CX_3CR1-GFP in the *Cx3cr1*$^{gfp/+}$ mouse. These cells were also negative for CD11b and markers of lineage, did not express IL-7Rα (associated with lymphoid restricted progenitors, Kondo et al., 1997), and expressed CD34 and FcγR, as do GMP (Akashi et al., 2000), from which they were still distinct due to their expression of CSF-1R and CX_3CR1 (GMPs don't express these). They were small cells with a progenitor morphology, i.e. large nucleus to cytoplasm ratio, and proliferated rapidly in culture, though stromal cell lines supporting their growth would efficiently sustain them if they expressed M-CSF, unlike OP9 cells. Single MDP cells would give rise to colonies with macrophage and DC morphology, but not granulocytes, and were devoid of lymphoid potential. Cultivating these cells without stroma but with M-CSF would give rise to $CD11b^+$ $CD11c^+$ macrophage-morphology cells that could engulf heat-killed bacteria, while culture with GM-CSF would give rise to $CD11b^{int}$ $CD11c^+$ DC-morphology cells with the ability to process and present antigens. Upon transfer into irradiated hosts, MDPs

gave rise to monocytes, DC subsets and macrophages in the spleen. Interestingly, donor-derived DCs were present in the host even when the host was not irradiated, which argued against the generation of monocyte-derived DCs because of the inflammation that irradiation may cause. This gave way to the hypothesis of the MDP being a progenitor for steady-state DCs (Fogg et al., 2006). Given its phenotypical features of Lin^- IL-7Rα^- CSF-1R^+ CX_3CR1^+ $CD34^+$ FcγR^+ and lineage restriction to myeloid, mononuclear phagocytes (but not polymorphonuclear granulocytes), the MDP was defined as a downstream population of the CMP, and GMP.

Further analysis of the MDP revealed that they were the precursors of both monocyte subsets in the blood and bone marrow, as well as conventional DC subsets without a monocyte intermediate (Auffray et al., 2009; Varol et al., 2007). Transfer experiments and the study of inflammatory situations showed that the MDP could give rise to $Ly6C^+$ monocytes that could respond to *L. monocytogenes* by migrating to infected spleens and produce TNFα and iNOS, thus differentiating into Tip-DCs as observed previously (Serbina et al., 2003), and also give rise to conventional DCs (cDCs) as well as plasmacytoid DCs (pDCs) (Auffray et al., 2009). Therefore, it showed a broader lineage potential than the then recently described CDP (Common Dendritic cell Progenitor), which could give rise to cDCs and pDCs but not monocytes (Onai et al., 2007). Consequently, it was suggested that MDPs are slightly upstream the CDPs, though their phenotypes are very similar (Auffray et al., 2009).

A population downstream of the MDP was recently identified, termed the cMoP, for common Monocyte Progenitor (Hettinger et al., 2013). Prospective analysis of the bone marrow revealed the presence of an actively proliferating population similar in phenotype to MDPs, with the exception of Ly6C and Flt3, and in morphology. *In vitro*, a single cMoP cell only had the ability to generate clonal colonies of macrophages but not DCs. *In vivo*, following MDP transfer into non-irradiated hosts, the authors

observed the successive appearance of donor-derived cMoP, then Ly6C^{+} monocytes and finally Ly6C$^{\mathbf{low}}$ monocytes, but not DCs or macrophages. The generation of the two populations of monocytes in that order in time, together with transfer experiments and kinetic studies (Hettinger et al., 2013; Tamura et al., 2017; Yona et al., 2013), are part of the body of work that suggests Ly6C^{+} monocytes, beyond their ability to respond to inflammatory situations and extravasate, also constitute a precursor population to Ly6C$^{\mathbf{low}}$ monocytes (such as, recently, Mildner et al., 2017). This monocyte 'conversion' has also been suggested recently for the human monocyte populations, where CD14^{+} monocytes gave rise to CD14$^{\mathbf{dim}}$ CD16^{+} monocytes, through the CD14^{+} CD16^{+} intermediate stage (Patel et al., 2017). We will see later in this section that, although this conversion has been observed in several conditions, the distinct genetic requirements and mechanisms of bone marrow egress for the two main populations of monocytes are also consistent with potentially distinct pathways of differentiation in mice (see ***section 1.3.4***). Actually, testing various possibilities, whether monocytes convert from one population to the other, or whether another hypothesis is possible, is the point of the strategy we have followed, and will be presented in **section 3**.

The use of co-culture systems (Lee et al., 2015a) has recently allowed the identification of the human equivalents to GMP, MDP and CDP in the cord blood and bone marrow (Lee et al., 2015b). A human equivalent to the cMoP has also been recently proposed (Kawamura et al., 2017).

1.3.3. Relationship of monocytes with dendritic cells and macrophages

Monocytes have long been considered solely as circulating precursors for macrophages and dendritic cells (van Furth et al., 1972). This view has been slowly altered by accumulating evidence that, although there are links between monocytes and macrophages and DCs, it is not a simple precursor / progeny relationship.

In steady state, monocytes and dendritic cells share a common bone marrow progenitor as presented above, termed the MDP (Fogg et al., 2006 ; Auffray et al., 2009), which has also been reported in human bone marrow and cord blood, termed human MDP (hMDP, Lee et al., 2015b). However, monocyte and dendritic cell lineages downstream branch out to, on the one hand, the cMoP (Hettinger et al., 2013 ; Kawamura et al., 2017), and the CDP (Naik et al., 2007 ; Onai et al., 2007), supporting further the idea that the production of dendritic cells from the MDP does not go through a monocyte stage (Varol et al., 2007).

Of note, in a number of studies on response to pathogens (see ***Section 1.2.3***), $Ly6C^+$ monocytes are shown to extravasate and upregulate DC-like markers (such as MHC-II and CD11c) and/or produce TNFα and iNOS. This is the base on which some articles have used the term "Tip-DCs" to name these cells. However, it is important to remember that dendritic cells are in essence antigen-presenting cells that kick-start the adaptive immune response. Therefore, when this function is not performed by extravasated monocytes, it is not entirely justified to term these cells "dendritic cells".

Furthermore, accumulating evidence over the past two decades has firmly established that most tissue-resident macrophages arise from embryonic origin, as will be further discussed later (see ***section 1.4.1***, Bertrand et al., 2005; Ginhoux et al., 2010; Gomez Perdiguero et al., 2014; Kierdorf et al., 2013; Palis et al., 1999; Schulz et al., 2012). Steady state contribution from monocytes to tissue macrophages is minimal for many tissues, in which their numbers are maintained locally, through proliferation (Chorro et al., 2009; Merad et al., 2002; Perdiguero and Geissmann, 2015). As we will discuss, the intestine is a counter example to that trend, for monocyte influx into this tissue overcomes the embryonic-derived resident macrophages throughout adult life (Bain et al., 2014).

Monocytes have been known to differentiate into macrophages in *in vitro* culture for many years (Carrel and Ebeling, 1926). *In vivo*, in the context of inflammation caused by pathogens or sterile insults, to extravasate from vessels, and for example to engage in a DC-like transcriptional program, produce TNFα and iNOS after infection with *L. monocytogenes* (Auffray et al., 2007b; Serbina and Pamer, 2006; Serbina et al., 2009). Recently, heterogeneity among $Ly6C^+$ monocytes has been recognised in mice; separating $Ly6C^+$ monocytes with Flt3, CD11c, MHC-II and PU.1 levels of expression, the authors were able to identify committed subsets, which were direct precursors to iNOS-producing macrophages on the one hand, and to Granulocyte-Macrophage Colony Stimulating Factor (GM–CSF) -induced dendritic cells on the other (Menezes et al., 2016).

It is therefore important to keep in mind the different situations that drive the production of either steady state populations or inflammation-driven ones, as well as ontogeny, i.e. generation of cells during adulthood or embryonic development.

1.3.4. Molecular control of monocyte development and exit from the bone marrow

1.3.4.1 Molecular control of monocytes development

- *CSF-1/CSF-1R axis*

In the 1970's a spontaneous mutation occurred at the Jackson laboratory, in two mice of a transgenic C57BL/6 strain, which resulted in shorten limbs and an absence of teeth. The description of mice bearing only this mutation was first done by Marks and Lane, estimating they may carry it on Chromosome 12, leading to osteopetrosis, a skeletal condition in which the bone is excessively mineralized because of a lack in bone resorption, due to a reduced number of osteoclasts (Marks and Lane, 1976). Osteoclasts are the professional bone-resorbing cells, that are thought to be of myeloid-monocytic

origin (Jacome-Galarza et al., 2013). These mutated mice, termed *op/op* mice, have a retarded growth, and lack a proper bone marrow cavity (Marks and Lane, 1976). A few years later, *op/op* mice were analysed for their hematological features, and were found to have vastly decreased numbers of monocytes and macrophages *in vivo*, as well as a hindered capacity to generate macrophages *in vitro* upon culture of their splenocytes (Wiktor-Jedrzejczak et al., 1982). Later genetic studies found that these mice carry a mutation on the proto-ocongene *c-fms* in Chromosome 3 (Yoshida et al., 1990), which codes for the Macrophage Colony Stimulating Factor (M-CSF), also called CSF-1, which is absent in these mice (Wiktor-Jedrzejczak et al., 1990; Yoshida et al., 1990). The study of both $Csf1^{op/op}$ mice and mice deficient for the receptor for CSF-1, CSF-1R ($Csf1r^{-/-}$ mice), showed they both lack circulating monocytes and tissue macrophages in many tissues, showing the fundamental role for the growth factor in the development and function of blood monocytes and tissue macrophages ; introduction of CSF-1 via a transgene into *op/op* mice resulted in a rescued phenotype (Cecchini et al., 1994; Dai et al., 2002; Witmer-Pack et al., 1993).

Studies of the expression patterns of CSF-1R gene *c-fms*, using both whole mount *in situ* hybridization (Hume et al., 1995) and in *c-fms*-eGFP mice (Sasmono et al., 2003), revealed its expression very early during murine embryogenesis, and in adults throughout myeloid populations of the blood and bone marrow, and tissue macrophages. CSF-1R is notably expressed by the MDP (Fogg et al., 2006). CSF-1 was shown to instruct the GMP (Granulocyte/Macrophage Progenitor) towards the monocytic lineage (Rieger et al., 2009). It was more recently shown that this lineage "instruction" toward myeloid fate can be induced as early during hematopoiesis as the HSC stage (Mossadegh-Keller et al., 2013). This allowed to give credit to the hypothesis that cytokines can influence lineage specification in HSCs, something that had been debated for a long time (Cross and Enver, 1997; Enver et al., 1998), and has

been conforted since then (Endele et al., 2014). The instruction of HSCs by CSF-1 towards a myeloid fate is induced through the activation of the master regulator PU.1 (Mossadegh-Keller et al., 2013), which is the focus of the next section.

- *PU.1*

PU.1 is a transcription factor involved in the development of all hematopoietic lineages except erythroid. Its coding gene was first identified as an oncogene, as it was induced by the acute leukaemogenic retrovirus spleen focus forming virus (SFFV), and was therefore termed *Spi-1*, for SFFV proviral integration 1 (Moreau-Gachelin et al., 1988). Mice deficient for PU.1 died at late embryonic stages (E18 at latest), due to severe anemia, and showed severe lack of T and B cells, monocytes and granulocytes (Scott et al., 1994). Mice with a defective PU.1 DNA binding domain were generated and, although they were born, died within 48 hours after birth and showed important defects again in T cells, B cells, granulocytes and monocytes (McKercher et al., 1996). PU.1 deficient myeloid progenitors do not form colonies in response to CSF-1, and this absence of responsiveness could be reversed by transgenic re-introduction of *c-fms* (DeKoter et al., 1998). To allow the study of PU.1 role in adult hematopoiesis, a system was developed in which PU.1 could be inactivated in adults, which also resulted in loss of responsiveness to CSF-1, and dramatic increase in the production of granulocytes (Dakic et al., 2005).

PU.1 is a master regulator of lineage commitment through its interactions with other transcription factors. For example, PU.1 and GATA-1, another transcription factor, can inhibit each other's activity (Nerlov et al., 2000; Zhang et al., 2000), and are both expressed early during hematopoiesis (Miyamoto et al., 2002). A recently developed mouse model, in which PU.1 and GATA-1 levels of expression are monitored through the level of expression of fluorescent proteins, shows that the balanced expression of

these two proteins, rather than influencing the lineage commitment, enforced lineage decisions already adopted by differentiating hematopoietic progenitors (Hoppe et al., 2016).

Beyond myeloid cell development, many other roles have been found for PU.1 throughout the hematopoietic system, notably in the development of T cells (Champhekar et al., 2015).

- *Role of the IRF8 / KLF4 cascade in the lineage specification towards monocytes*

Interferon regulatory factor 8 (IRF8) is a part of the IRF transcripton factor family, which comprises 9 members in mammals (Tamura et al., 2008). It was originally cloned in 1990 by Driggers and colleagues (Driggers et al., 1990) as an Interferon gamma (IFNγ)-inducible nuclear protein (and at the time was termed Interferon Consensus Sequence-Binding Protein – ICSBP). It is expressed exclusively in hematopoietic cells of both myeloid (monocytes, macrophages and dendritic cells) and lymphoid (B cells and activated T cells) lineages (Kantakamalakul et al., 1999; Nelson et al., 1996). The analysis of the *Irf8*$^{-/-}$ mice, generated in 1996, revealed its role in myeloid populations development, as these animals spontaneously develop chronic myelogenous leukemia-like syndrome (Holtschke et al., 1996). Using cell lines derived from the bone marrow of *Irf8*$^{-/-}$ mice, Tamura and colleagues show that reintroduction of *Irf8* using retroviral vectors into *Irf8*$^{-/-}$ myeloid progenitors (Lineage-negative cells), induced the stimulation of genes critical for monocyte production *in vitro*, as well as a restored macrophage colony forming potential, while suppressing genes involved in neutrophil development and correcting the abnormal overgrowth of granulocyte colonies from *Irf8*$^{-/-}$ cells, suggesting a role for *Irf8* in monocyte/macrophage lineage specification *in vitro* (Tamura et al., 2000; Tsujimura et al., 2002).

IRF8 can function as either transcriptional activator or repressor, depending on the heterodimer it forms with various molecules and the DNA region it binds to (Tamura and Ozato, 2002 ; Kanno et al., 2005), with an impact on myeloid cell development. IRF8 was shown to form a heterodimer with PU.1 to promote the expression of *Klf4* (Kurotaki et al., 2013), a gene critical for Ly6C^{+} monocyte differentiation (Alder et al., 2008) *in vivo*. Hence, *Irf8*$^{-/-}$ mice almost completely lack Ly6C^{+} monocytes while their Ly6C^{low} population is partially reduced (Kurotaki et al., 2013). At the level of myeloid progenitors, the MDP and cMoP express high levels of IRF8 (Hettinger et al., 2013), and they accumulate in *Irf8*$^{-/-}$ mice (Schönheit et al., 2013). These data suggest the developmental arrest of Ly6C^{+} monocytes in *Irf8*$^{-/-}$ mice may be between the cMoP and the monocytes. In these cells, IRF8 functions as an inhibitor of C/EBPα, thereby blocking neutrophil differentiation ; in turn, *Irf8*$^{-/-}$ MDP and cMoP express high levels of C/EBPα, and aberrantly give rise to a large number of neutrophils (Kurotaki et al., 2014). This also occurs in dendritic cell-restricted progenitor, and it was shown that even lymphoid progenitors in *Irf8*$^{-/-}$ mice could give rise to neutrophils (Becker et al., 2012). These all participate to the important neutrophilia in *Irf8*$^{-/-}$ mice. One example showing the importance of *Irf8* for Ly6C^{+} monocytes is a study showing that *Irf8*$^{-/-}$ mice have a defective response to West Nile Virus (WNV), after which the few remaining *Irf8*$^{-/-}$ monocytes were not recruited to the brain, and did not participate to the inflammatory myeloid population increase usually observed after WNV infection (Terry et al., 2015).

In humans, it has been reported that mutations affecting IRF8 binding to DNA resulted in a lack of circulating monocytes and either all or some subsets of dendritic cells (Hambleton et al., 2011), consequently, patients carrying such a mutation had increased susceptibility to mycobacterial infection during infancy.

- *NR4A1 controls Ly6C^{low} monocyte differentiation*

NR4A1 belongs to the NR4A subfamily of nuclear receptors that comprises NR4A1 (also known as Nur77), NR4A2 (Nurr1) and NR4A3 (NOR-1), within the steroid/thryroid receptor family (Martínez-González and Badimon, 2005). These nuclear receptors have a very similar structure and all have a Ligand-Binding Domain (LBD); however, a study found that NR4A2, although having such a LBD, did not require the binging of a ligand for its function. Together with their similar genomic structure, this observation prompted the suggestion that the NR4A family members do not need ligand binding for their function (Wang et al., 2003). NR4A1 is coded in the mouse by *Nr4a1*, but was the first of this subfamily to be discovered, in 1988, as NGFI-B (Nerve Growth Factor Induced gene – clone B), a gene rapidly and transiently induced in a rat cell line of differentiating neurons, that responded to NGF (Milbrandt, 1988), and was therefore proposed as potentially involved in the differentiation of neurons at the time. The human NR4A1 (called TR3) was later found to translocate to the mitochondria upon apoptotic stimuli and induce the release of cytochrome c and apoptosis, independently of its binding to DNA (Li et al., 2000). This role in apoptosis has also been shown in the mouse for the selection of T cells, this time independently of mitochondria or cytochrome c, but through the induction of transcription of pro-apoptotic genes such as Fas ligand (Rajpal et al., 2003). This role in apoptosis was found to be important in T cell negative selection in the thymus (Zhou et al., 1996). Recently, the thymic myeloid cells were studied in *Nr4a1*-deficient mice, and a population of CD11b^{-} F4/80^{+} thymic macrophages was found to be reduced by two-third in *Nr4a1*$^{-/-}$ compared to *wt* littermates, a population of cells implicated in the clearance of apoptotic thymocytes; however the other thymic myeloid populations were unaltered (Tacke et al., 2015). The three members of the NR4A family have been shown to be very rapidly induced by inflammatory stimuli such as Lipopolysaccharide (LPS)

or oxydized lipids on macrophages *in vitro*, and NR4A1 was found to be expressed in macrophages in atherosclerotic lesions (Pei et al., 2005).

In 2011, analysis of the expression of the different NR4A family members in monocytes revealed that *Nr4a1* was expressed at high levels in Ly6C^{low} monocytes, although also present in Ly6C^{+} monocytes (Hanna et al., 2011). Higher expression of *Nr4a1* in Ly6C^{low} monocytes than in the Ly6C^{+} subset in the bone marrow was also confirmed using flow cytometry, both by antibody staining (anti-NR4A1) and GFP expression in *Nr4a1*^{GFP} mice (Hanna et al., 2011). In mice lacking *Nr4a1* (Lee et al., 1995), Ly6C^{low} monocytes, defined by flow cytometry as CD11b^{+} CD115^{+} and low side scatter, are almost absent from the bone marrow, spleen and blood; the remaining cells have lost the bean shape of their nuclei, are arrested in S-phase of the cell cycle and undergo apoptosis in the bone marrow (Hanna et al., 2011). Ly6C^{low} monocytes in these mice also showed downregulated effector molecules such as adhesion (LFA-1) and chemokine receptors (CCR2 and CX$_3$CR1) at their surface. In contrast, *Nr4a1* expression is low in the MDP and progenitor populations including HSC, CMP and MDP, which were unaffected in numbers by *Nr4a1*-deficiency, an observation also applicable to Ly6C^{+} monocytes of the bone marrow and blood (Hanna et al., 2011). This suggested that although the MDP was known to give rise to both subsets of monocytes, they then had different genetic requirements and differentiated independently in the bone marrow downstream of the MDP.

Recently, CCAAT/Enhancer Binding Protein β (C/EBPβ) has been characterised as a critical actor in monopoiesis. A study by Mildner and colleagues found that C/EBPβ bound to the *Nr4a1* promoter and regulated its expression (Mildner et al., 2017). This is consistent with other articles published over the last few years establishing a role for C/EBPβ in monocyte survival in the periphery, and in particular for Ly6C^{low} monocytes (Tamura et al., 2015, 2017). Mice lacking C/EBPβ were found to lack Ly6C^{low}

monocytes in the blood (and to a lesser extent blood Ly6C^{+} monocytes); Ly6C$^{\mathbf{low}}$ monocytes of the bone marrow were specifically missing, while all upstream monocyte progenitors examined remained unaffected (Tamura et al., 2017). The decreased numbers of monocytes in these mice were attributable to increased apoptosis, which is consistent with the apoptosis observed in *Nr4a1*$^{-/-}$ mice (Hanna et al., 2011).

1.3.4.2. Control of monocyte exit from the bone marrow

- *CCR2 and the egress of Ly6C^{+} monocytes from the bone marrow*

When the mice lacking the C-C chemokine Receptor 2 (CCR2) were generated in 1997, impaired myeloid leukocyte recruitment to the peritoneum following thioglycollate intraperitoneal injection was observed, as well as a decreased recruitment of monocytes following injection of beads coated with protein derivative of *Mycobacterium bovis* (Boring et al., 1997). Seminal work by Serbina and colleagues characterised further monocyte responses in *Ccr2*$^{-/-}$ mice (Serbina and Pamer, 2006). They observed fewer Ly6C^{+} monocytes in their circulation at steady state, while more numerous in the bone marrow, suggesting a control by CCR2 of Ly6C^{+} monocyte homeostasis. They then show that their response to *Listeria monocytogenes*, which is to migrate to infected tissues and produce TNFα and iNOS (Serbina et al., 2003b), was impaired in *Ccr2*$^{-/-}$ mice, and that TNFα-producing cells accumulated in the bone marrow, but blood monocytes numbers did not increase. Thus, this work showed that CCR2 was crucial for the egress of Ly6C^{+} monocytes upon infection with *L. monocytogenes*, though not for their migration from blood to tissues (Serbina and Pamer, 2006). This phenotype was not as marked in mice lacking one of the CCR2 ligands, CCL2 (Lu et al., 1998), suggesting other ligands might be involved (Serbina and Pamer, 2006).

A year later, a report by Tsou et al provided further insight into the role of CCR2 and its ligands for monocyte homeostasis and inflammatory response (Tsou et al., 2007). In this study, the lower levels of Ly6C^{+} monocytes in the blood in steady state was confirmed (Ly6C^{+} monocytes are identified as 7/4^{+} in this study, a marker known to be expressed by Ly6C^{+} monocytes, but not Ly6C$^{\mathbf{low}}$, see Henderson et al., 2003). These low levels of circulating Ly6C^{+} monocytes in *Ccr2*$^{-/-}$ mice did not increase upon high fat diet feeding, like observed in the WT littermates and were retained in the bone marrow, similar to the response observed by Serbina and colleague after *L. monocytogenes* (Serbina and Pamer, 2006). Finally, the work of Tsou et al. suggested a role for MCP-1 and MCP-3, but not MCP-2 nor MCP-5, as the major ligands of CCR2 for the homeostasis and responses of Ly6C^{+} monocytes (Tsou et al., 2007). This was confirmed in the context of *L. monocytogenes* by Jia and colleagues a year later (Jia et al., 2008). Using KO mice and various strains of *L. monocytogenes*, the authors found that sensing of cytosol invasion of the bacteria promoted the production of MCP-1and MCP-3, but also found that increased suceptibility of mice lacking these chemokines was due to reduced recruitment of Ly6C^{+} monocytes in the spleen rather than a defect in their production of TNFα and iNOS (Jia et al., 2008).

- *S1PR5 controls the exit of Ly6C$^{\mathbf{low}}$ monocytes from the bone marrow*

S1PR5 (Sphingosine-1 Phosphate Receptor 5) is one of the five known S1P receptors, which are heterodimeric G protein-coupled receptors with high affinity for S1P (Chun et al., 2010). The role of these receptors in leukocyte trafficking was first suggested by the finding that a compound that binds four of these receptors inhibited the exit of T and B cells from thymus and secondary lymphoid organs (Cyster and Schwab, 2012). It was later found that NK cells express S1PR5 and that this receptor is involved in their

recirculation in the blood, from the bone marrow and lymph nodes (Jenne et al., 2009; Walzer et al., 2007).

In 2013, Debien, Mayol and colleagues found that *S1pr5*$^{-/-}$ mice lack Ly6C^{low} monocytes in the blood and periphery organs such as the spleen, lung and kidney, while showing normal numbers in the bone marrow (Debien et al., 2013). Ly6C^{low} monocytes express 30 times more *S1pr5* than Ly6C^{+} monocytes, which remain at normal numbers in all organs studied by Debien, Mayol and co-workers (Debien, Mayol et al., 2013). Therefore, similarly to CCR2 for Ly6C^{+} monocytes, S1PR5 controls the egress of Ly6C^{low} monocytes from the bone marrow to the periphery.

1.4 Tissue Macrophages

1.4.1. Macrophage development and maintenance

1.4.1.1. Embryonic Hematopoiesis, overview

The production of hematopoietic cells, whether it be red blood cells, platelets or leukocytes, starts very early on, before birth, and the production of HSCs occurs during this period, once for the whole life, as in adults they only self-maintain (see ***section 1.3.1***). The establishment of hematopoiesis during embryonic and fetal life is a vast field of study ; once in place, embryonic hamatopoiesis is a complex process with unique features that distinguish it from its adult counterpart. Because, as mentioned in the historical perspective, most tissue-resident macrophages arise during embryonic life (see ***section 1.1.4***), it is important to understand these processes, which we will overview in this section. Many years of research in several animal models (mice, Xenopus, zebrafish and avian models notably) have uncovered a complex

spatiotemporal sequence leading to different waves of hematopoietic progenitors, which we will overview here.

The origin of the first HSC has been a matter of discussion for a long time, and early reports suggested their origin may be in the YS, based notably on the observation, made by Weissman and colleagues in the late 1970s, that injection of YS cells into the embryo circulation gave rise to T-cells of donor origin in the thymus of the recipients (Golub and Cumano, 2013). However, critical experimentations carried out in the 1970s by Françoise Dieterlen-Lievre and colleagues in chicken - quail chimeras showed an intra-embryonic origin of HSC ; these experiments were conclusive because of the distinctive shape of the nuclei of the cells of these two species. When quail embryos were grafted to the yolk-sacs of chicks of similar development stages (before or after the establishment of circulation), cells populating the hematopoietic organs of the quail embryos only contained quail cells, meaning these cells had to originate from the (quail) embryo proper, not the (chick) YS (Dieterlen-Lievre, 1975). Current understanding suggests that the hematopoietic system develops in two main distinct, but partially overlapping, waves: an HSC-independent production of cells that starts around embryonic day (E) 7.25 in the YS, and an HSC-dependent wave that starts with the first pre-HSC arising around E8 in the arterial vessels of the embryo.

The first wave consists of two heterogeneous sets of cells that arise in the YS as blood islands. These islands contain primitive erythrocytes, large nucleated cells containing haemoglobin produced only at this stage, for the transport of oxygen (Palis, 2016) and phagocyte progenitors, which will be the focus of the next section, and a mongst which the progenitors of adult tissue resident macrophages can be found from E8.5.

Several studies in the 1990s have established that the dorsal aorta is the site at which definitive hematopoietic stem cells first emerge, more precisely in the Aorta Gonad-

Mesonephros (AGM). One approach consisted in the dissection of embryonic structures and their engraftment to adult, immuno-deficient mice : these experiments pointed to the anlage of the aorta, gonads and mesonephros, as containing cells with the capacity to generate not only lymphoid cells in the host, but also long term reconstitution (Godin et al., 1993; Medvinsky et al., 1993; Müller et al., 1994). In order to set aside the hypothesis that the isolated anlages may contain circulating precursors generated elsewhere, an organ culture system was used to more firmly test the organ of origin of definitive HSCs, which was confirmed to be the AGM at E8 (Cumano et al., 1996, 2001). The study of inducible models of lineage tracing seem to indicate that HSCs found in the mouse adult are generated during a narrow window of time. Following the fate of cells expressing Cre under the control of the *Runx1* or *VE-Cadherin* (Samokhvalov et al., 2007; Zovein et al., 2008) promoters between E8.5 and E9.5 showed this was sufficient to label almost all HSCs of the adult, while pulses done before or after that window had a very poor efficiency of HSC labelling. Other sites for the generation of definitive HSCs have been proposed, such as the head (Li et al., 2012c) or the placenta (Gekas et al., 2005; Robin et al., 2009), although they are still debated (Golub and Cumano, 2013).

Once generated in the AGM region, HSCs undergo steps of maturation (notably the acquisition of CD45 and MHC-I expression, allowing them to reconstitute NK-competent mice upon transplantation, Kieusseian et al., 2012), and then migrate to the fetal liver between E10 and E11.5 (Houssaint, 1981), where they undergo proliferation and differentiation. The fetal liver then becomes the main site of hematopoiesis during embryogenesis ; it is notably from the fetal liver that two distinct waves of progenitors sucessively colonise the thymus, thus establishing T cell development progressively and in an orderly fashion, with distinct features of lymphopoiesis for each wave (Ramond et al., 2014). It is also from fetal liver HSCs that other embryonic-specific progenitors give

rise to cells that are generated during pre-natal life, such as populations of B cells (termed B1a lymphocytes, Hardy and Hayakawa, 1991), and of γδ T cells (which become the skin resident Dendritic Epidermal T Cells, or DETCs, (Ikuta et al., 1990). The production of embryo-specific immune populations is in part controlled by the micro-RNAs Lin28b and let-7, which are expressed in fetal but not adult HSCs (Yuan et al., 2012). Their ectopic expression in adult progenitors is sufficient to give them the potential to generate fetal immune cells (Yuan et al., 2012), and also allow, through one of their targets (*Hmga2*), the fetal HSCs to have a higher self-renewal capacity (Copley et al., 2013). Finally, HSCs start to migrate to the bone anlages around E15, where the marrow is formed and where they reside throughout the entire life.

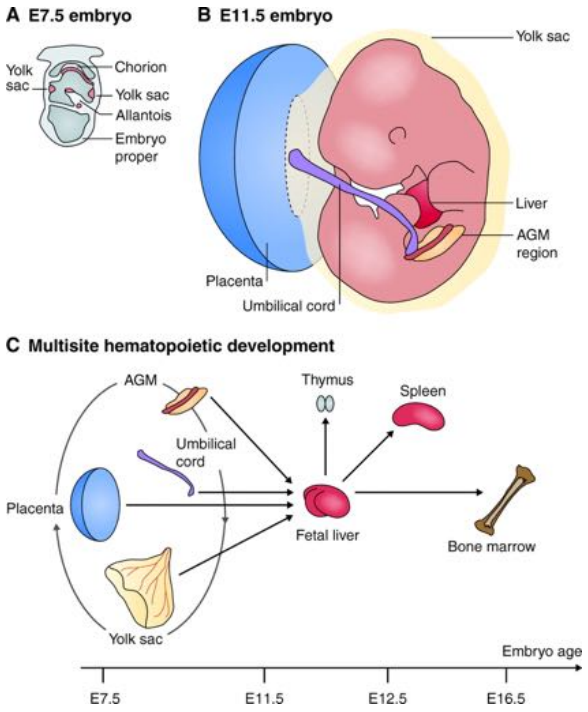

Figure 1.4. Overview of hematopoiesis sites during embryonic development. Adapted from (Medvinsky et al., 2011)

As mentioned in the historical perspective, deciphering the precise spacio-temporal development of hematopoietic progenitors has been critical to understanding the development of macrophages that are generated early in embryos.

1.4.1.2. Development of tissue resident macrophages from an Erythro-Myeloid Progenitor (EMP)

As pointed out earlier, it has for a number of years now become well established that macrophages that reside in many organs are not primarily the product of a differentiation process of bone marrow HSC-derived monocytes in the steady state. Rather, they are generated in the embryo at very early stages while the hematopoietic system is developing, and at E10.5, while the definitive HSCs are still being generated and maturing in the AGM, macrophages have already seeded the entire embryo (Schulz et al., 2012).

As mentioned above, blood islands in the YS are the first sign of hematopoietic cells in the embryo. Blood islands notably contain large nucleated erythroid cells, which arise from Primitive erythroid colony-forming cells (EryP-CFC) at E7.5 (Palis et al., 1999; Wong et al., 1986). These EryP-CFC proliferate, and start to circulate after the onset of the first heartbeats at E8.25 (Ji et al., 2003; McGrath et al., 2003), before eventually enucleate between E12.5 and E16.5, and remain detectable up until a few days after birth (Kingsley et al., 2004, 2006). A transient wave of erythroid progenitors Burst Forming Units- Erythroid (BFU-E), which emerge at E8.25 in the YS (Wong 1986 ; Palis 1999), proliferate in the YS, enter the bloodstream and seed the FL before the AGM-derived HSCs, and generate the first definitive erythrocytes (McGrath et al., 2011). *Ncx-1* null embryos lack circulation and heartbeat; they have normal amounts of BFU-E in the YS but lack hematopoietic progenitors in the embryo proper, which suggests BFU-E may be part of the necessary elements to jump-start the production of blood cells before the establishment of an HSC-derived hematopoiesis (Lux et al.,

2008). Myb is critical for definitive erythropoiesis, as *Myb*$^{-/-}$ embryos die of severe anemia at E15.5 (Mucenski et al., 1991).

Megakaryocyte Colony-Forming Cells (Meg-CFC), able to generate colonies of Megakaryocytes in vitro are first detected at E7.25 in the YS blood island, same time and place as EryP-CFC (Xu M et al., 2001). In fact, embryonic equivalent of MEP were detected at E7.25 in the YS (Tober et al., 2007). A subsequent wave of MEP was found in YS between 9.5 and 10.5. Meg-CFC proliferate between E8.5 and E10.5 and end up in the circulation and FL.

The first myeloid potential was detected at E7.25 in the YS (Moore and Metcalf, 1970) as Macrophage Colony-Forming Cells (Mac-CFC), which expand in number in the YS (Palis et al.,1999). By E10.5, Mac-CFC are found in the circulation and FL. Beginning at 8.25, other myeloid lineage progenitor arise in the YS (Palis et al., 1999 ; Palis et al., 2001): neutrophil progenitors, granulocyte-macrophages bipotent progenitors (GM-CFC), mast cell progenitors, and high proliferative potential-CFC (HPP-CFC). HPP-CFC give rise in culture to macrophages, mast cells and basophils (Palis et al., 2001). These myeloid progenitors expand in the YS between E8.25 and E10.5, enter the bloodstream and seed the fetal liver (McGrath et al., 2015; Palis et al., 2001). Thus the first maturing macrophages were found between E9 and E9.5 in the YS, before they seed the head of the embryo, and disseminate the entire embryo (Hume et al., 1995; Morris et al., 1991; Takahashi, 1989). *Ex vivo* culture of the macrophage progenitors found that these embryonic macrophages differentiated directly from progenitors, without going through a monocytic stage (Naito et al., 1989).

Spatiotemporal study of the emergence and lineage potential of these different waves of progenitors found that the E8.25 cells were ‘definitive’ progenitors of the YS, had erythroid and myeloid potential (Bertrand et al., 2005, 2013; Palis et al., 1999), and were therefore termed Erythro-Myeloid Progenitors (EMPs), phenotypically defined as

Kit^{+} AA4.1^{+} CD45^{lo} CD41^{+}, VE-Cadherin^{+} and FcγRII^{+} and FcγRIII^{+} (Bertrand et al., 2005b ; McGarth et al., 2015). These cells were found to be distinct from the AGM-derived HSCs, not only in regards to their tissue origin (YS vs AGM), but also by the fact that EMPs did not have lymphoid potential (Bertrand et al., 2005b), nor did they have long-term reconstitution potential or express Sca-1 (McGarth et al., 2015). Furthermore, although both the EMP (Frame et al., 2016; Miller et al., 2002; North et al., 1999) and HSCs (Bertrand et al., 2010; Boisset et al., 2010; Kissa and Herbomel, 2010; Lam et al., 2010) arise via endothelial-to-hematopoietic transition, they do so via distinct hemogenic endothelial cells (Chen et al., 2011).

Both adult and fetal HSCs rely on the transcription factor c-Myb for their development (Mucenski et al., 1991; Mukouyama et al., 1999; Sumner et al., 2000), however a study by Schulz, Gomez Perdiguero and colleagues found that the F4/80^{hi} CD11b^{low} populations of macrophages in several tissues (E10.5 YS, E14.5 and E16.5 liver, skin, spleen, pancreas, kidney and lung) developed in normal numbers in *Myb*$^{-/-}$ embryos (Schulz et al., 2012). Conversely, at these developmental stages in these organs, the F4/80^{low} CD11b^{hi} myeloid cells were strongly impaired in *Myb*$^{-/-}$ animals, suggesting they develop from HSC-derived progenitors. Additionally, gene expression profile analyses revealed similarities between E10.5 YS F4/80^{hi} macrophages and E16.5 F4/80^{hi} macrophages from various tissues, which did not show alteration in *Myb*$^{-/-}$ F4/80^{hi} macrophages, suggesting a developmental relationship, and was consistent with the maintained presence of F4/80^{hi} macrophages in *Myb*$^{-/-}$ embryos (Schulz et al., 2012). Taking advantage of the early expression of CSF-1R in F4/80^{hi} macrophages during development, the authors were able to pulse label these cells by injection of 4-OH tamoxifen to *Csf1r*$^{Mer\text{-}iCre\text{-}Mer}$ *Rosa26*$^{LSL\text{-}YFP}$ at E8.5 (inducing Cre-mediated deletion of the STOP sequence on the *Rosa26* locus and YFP expression in cells expressing CSF-1R between E8.5 and E9.5) ; this resulted in the specific labelling of F4/80^{hi} CD11b^{low}

macrophages residing in various adult tissues, but not of F4/80^{low} CD11b^{hi} cells. Altogether, this work indicated that YS-derived precursors give rise to resident macrophages, which develop independently from HSCs and persist in adults (Schulz et al., 2012).

Fate mapping analysis has allowed the identification of the EMPs at E8.5 as the YS progenitors expressing CSF-1R that give rise to tissue-resident macrophages (Gomez Perdiguero et al., 2014). Indeed, phenotypic analysis of cells positive for *Csf1r*^{iCre} and *Csf1r*$^{Mer\text{-}iCre\text{-}Mer}$ –mediated expression of YFP at E8.5 in the YS revealed a CD45^{lo} Kit^{+} AA4.1^{+} progenitor (EMP) that originates in the YS, while absent in the AGM, seeds the fetal liver where it expanded, and differentiated into myeloid cells (macrophages, monocytes, granulocytes) and erythrocytes. To trace the progeny of AGM-derived HSCs, the authors analysed the *Flt3*^{Cre} –mediated expression of YFP in different myeloid populations in parallel to the progeny of YS-derived *Csf1r*$^{Mer\text{-}iCre\text{-}Mer}$ YFP^{+} cells. They found that while F4/80^{hi} CD11b^{low} cells such as brain microglia, lung alveolar macrophages, skin Langerhans cells or liver Kupffer cells were YS, EMP-derived, increasing amounts from E14.5 to E18.5 and in adults of F4/80^{low} CD11b^{hi} cells were of HSC origin (Gomez Perdiguero et al., 2014). Finally, the use of *Tie2*$^{Mer\text{-}iCre\text{-}Mer}$ mice (Busch et al., 2015) pulsed at various embryonic time points allowed to demonstrate that, although HSC-derived cells can be traced back to Tie2-expressing progenitors, adult tissue resident macrophages also originate from a Tie2-expressing progenitor, which arises earlier and therefore is temporally and locally distinct from the AGM HSCs.

Recent studies from various teams including Frederic Geissmann's have deciphered how cells that reside in such a variety of tissues can possess tissue-specific identities, while originating from a common progenitor. There was speculation that tissues of the developing embryo were seeded by already committed subsets of macrophages or

EMPs. Rather, Mass, Ballesteros and colleagues have found that the EMPs generated in the YS colonize the fetal liver, where they acquire a core transcriptional program while differentiating into a cell type termed pre-macrophage, before seeding tissues in a CX_3CR1-dependent manner; only once they are in their tissue of residence, do macrophages acquire specific gene signatures in response to tissue-restricted cues (Mass et al., 2016). Furthermore, different tissue environments determine gene expression programs at the level of enhancers, impacting chromatin state and transcriptional programs in tissue-resident macrophages (Gosselin et al., 2014; Lavin et al., 2014). These studies have uncovered the crucial role the micro-environment plays in the establishment of macrophages tissue-specific identities.

In summary, tissue resident macrophages, typically identified phenotypically as F4/80^{hi} CD11b^{low}, develop independently from HSCs, from YS-derived, CSF-1R^{+} EMPs found at E8.5. Numerous studies of embryonic hematopoiesis and fate mapping analysis have allowed to show that the paradigm proposed in the early 1970s (van Furth et al. 1972), where tissue macrophages are the product of circulating monocyte differentiation, has shifted. Then, this sheds a new light on how myeloid dynamics are to be considered in the adult, during homeostasis and various other conditions such as pathogenic insult, sterile injury or cancer.

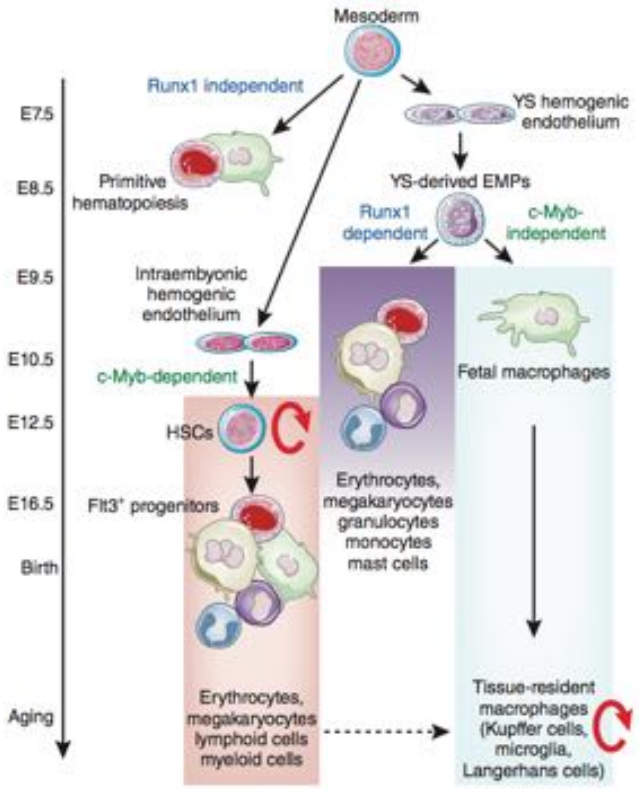

Figure 1.5. Myeloid development in the mouse embryo. From Gomez Perdiguero and Geissmann, 2016

1.4.1.3. Macrophage maintenance throughout adult life

The studies mentioned above established an embryonic origin for most tissue-resident macrophages. Although this is a clear step away from the paradigm of the MPS (van Furth et al., 1972), it does not mean the separation between monocytes and macrophages in steady state is perfectly sharp. The use of various tools (fate mapping, immunodeficient mice, parabiosis) have allowed the composition of myeloid populations residing in tissues to be deciphered more precisely in terms of ontogeny. Generally speaking, it would seem HSC-derived contribution to tissue resident macrophages varies between organs, and increases with age (Perdiguero and Geissmann, 2015).

Fate mapping analysis revealed that only a very small fraction of microglia were labelled by the *Flt3*^{Cre} –driven expression of YFP in the aging adult suggesting that microglia remain independent of bone marrow derived cells imput. Conversely in the lung the proportion of alveolar macrophages derived from Flt3-expressing, HSC-derived cells slowly increases over time (from 20% at 4 weeks to 40% at 1 year of age, Gomez Perdiguero et al., 2014).

The intestine is exceptional with regards to macrophage ontogeny: at birth the intestine is mainly populated by embryonic progenitor-derived F4/80^{hi} CD11b^{low} cells, but from the time of weaning, and driven by the settling of intestinal microbiota, these cells were found to be replaced gradually by Ly6C^{+} monocytes in a CCR2-dependent manner (Bain et al., 2014). A similar phenomenon was also observed in the peritoneum, where the resident F4/80^{+} GATA-6^{+} macrophages were of embryonic origin and renewed by local proliferation for the first 4 month of the mouse life, before being replaced by a constitutive CCR2-dependent influx of Ly6C^{+} monocytes, some of which eventually differentiate into F4/80^{+} GATA-6^{+} macrophages (Bain et al., 2016). A slow replacement of embryonic derived macrophages by monocytes has also been suggested for cardiac macrophages during the ageing process (Molawi et al., 2014). A recent study showed that in a model of experimentally induced lung fibrosis, monocyte-derived macrophages participated in the resolution of injury, and persisted in the lung afterwards, gaining a phenotype and gene expression profile similar to resident alveolar macrophages (Misharin et al., 2017).

Beside the varying fraction of tissue macrophages that are the result of replenishment by monocytes, for several years data has been accumulating to show that tissue-resident macrophages also maintain via local proliferation, such as in microglia (Bruttger et al., 2015; Lawson et al., 1992), or Kupffer cells (Yamada et al., 1990). Parabiosis and fate mapping showed maintenance through local proliferation in several tissues, including

lung, peritoneum, spleen, bone marrow and brain (Hashimoto et al., 2013). Skin Langerhans cells expand locally their numbers by over 10-fold during the first post-natal week, and can respond to tissue insult by local proliferation as well, driven by keratinocytes (Chorro et al., 2009). Peritoneal macrophages have also been shown to perform local proliferation to maintain their numbers, even after inflammation has induced the recruitment of leukocytes from the circulation (Davies et al., 2011). A recent study showed resident macrophages activate a program of self-renewal similar to that found in embryonic stem cells (Soucie et al., 2016). Recently, a study has examined the origin and maintenance of testicular macrophages, and found that while interstitial macrophages are embryonic-derived, BM progenitors contribute to this population later in life, and peritubular macrophages are only seeded post-natally by BM-derived progenitors during puberty (Mossadegh-Keller et al., 2017).

To summarize, it is now thought that most tissue-resident macrophages derive from embryonic progenitors distinct from HSCs, and maintain their steady state local numbers either by local proliferation, or via replenishment of various speed throughout adult life, and their response to inflammation may be mediated by one or the other mechanism depending on the organ. Importantly, critical periods of life also seem to impact the mechanisms of maintenance of macrophages in tissues, such as weaning and establishment of microbiota in the intestine (Bain et al., 2014) or puberty for the testis (Mossadegh-Keller et al., 2017).

1.4.2. Macrophage functions in various tissues and conditions

1.4.2.1 Macrophage function in homeostasis

As postulated well over a century ago by Metchnikoff (Metchnikoff, 1883), macrophages are not solely immune cells that perform their function during

inflammatory settings ; they have an impact in the development and function of their tissue of residence as well, which have been uncovered over the years.

Microglia are a well-studied myeloid population of the brain which develops during embryogenesis (Ginhoux et al., 2010; Gomez Perdiguero et al., 2014; Kierdorf et al., 2013). Recent imaging techniques have notably uncovered their behaviour in vivo during steady state (Tremblay, 2011) : they have highly motile processes (Davalos et al., 2005), continuously sampling their micro-environment. Beyond their surveillance function during steady state, microglia and their surrounding neural network reciprocally regulate their activities (Li et al., 2012b; Tremblay et al., 2010), and microglia are also involved in the formation and activity of synapses (Tremblay et al., 2010; Wake et al., 2009). Altogether, microglia have been found to be critical in the development of neurons, and to impact learning, memory and behaviour (Paolicelli et al., 2014; Tremblay, 2011; Tremblay et al., 2011).

While microglia provide a great example of macrophage importance in the homeostasis of its tissue of residence, it is not the only one. The intestine is a very large organ that is constantly renewed, and intestinal epithelial cells (IEC) are thought to have a life cycle of about 4 to 5 days, before undergoing apoptosis (Blander, 2016). Intestinal macrophages, together with the DC subsets that are found in this tissue, form a complex network (Gross et al., 2015) and these macrophages have been implicated in the homeostatic phagocytosis of apoptotic IEC (Cummings et al., 2016). They also participate in a molecular cross-talk with enteric neurons to regulate the pattern of intestinal smooth muscle contractions, therefore have a role in the gut motility (Muller et al., 2014).

To mention other examples, it was shown recently that embryonic derived macrophages in the T cell zone of lymph nodes (LN), which are slowly replaced

throughout life by monocyte-derived cells, are in charge of clearing apoptotic bodies, a role ascribed before to the resident DCs of the LN (Baratin et al., 2017). In the long bones and vertebrae, macrophages called osteoclasts are critiacal for the targeted digestion of mineral and matrix components of bone, to form microscopic trenches that allow bone marrow to fill the space, or osteoblasts to form new bone component (Boyce et al., 2009). In the adipose tissues, recruited macrophages have angiogenic roles crucial for the formation of the dense vascular network in this tissue (Cho et al., 2007), while resident cells regulate thermogenesis (Nguyen et al., 2011). Finally, the liver is one of the solid organs that is most densely populated by resident macrophages, as there are 1 to 2 macrophages for every 5 hepatocytes (Lopez et al., 2011), and some of these cells, called the Kupffer cells, are notably critical for the clearance of red blood cell derived vesicles (Willekens et al., 2005), as well as iron metabolism (Theurl et al., 2008).

Therefore, resident macrophages form networks in many tissues, that during homeostasis participate in a general monitoring of their microenvironment and may also participate to the organ development and function.

1.4.2.2. Macrophage function during various perturbations of steady state

Based notably on *in vitro* work, two ends of a spectrum of activation states for macrophages has been proposed : 'M1' and 'M2' macrophages (Gordon, 2003; Martinez et al., 2009). It had long been recognised that lymphocytes were major actors in macrophage activation and in 1986, interferon-γ (IFN-γ) was shown to be a key factor in this interaction leading to increase monocyte-derived macrophages phagocytic activity (Nathan et al., 1983). Since that was the first anti-microbicidal mechanism of macrophages activation to be recognised, it was thereafter termed 'classical activation of macrophages', or 'M1 macrophages' (Martinez et al., 2009). IFN-γ is produced mainly by $CD4^+$ T-helper 1 (Th1) cells and NK cells, while its immunological

counterpart, IL-4, is produced mainly by Th2 (Mosmann and Coffman, 1989), and was shown to inhibit the production of the respiratory burst and production of inflammatory cytokines such as IL-1β by macrophages (Abramson and Gallin, 1990), which correspond to another activation state. These observations set the basis for the 'M1' and 'M2', or 'classically' and 'alternatively' activated macrophages. Subsequently, a large portion of the work on *in situ* macrophage function has been included in this framework (such as Nguyen et al., 2011) ; , and several nomenclature systems have been proposed in that regard (Mantovani et al., 2004; Martinez et al., 2009).

Although these terms might be useful to designate a particular set of molecule secreted or expressed by macrophages in a given condition, they may not entirely reflect macrophage biology *in vivo*. Recent studies taking into account the ontogeny of the mononuclear phagocytes to study their response to various contexts have been performed. In the lungs, bone marrow derived monocytes have been shown to participate to the resolution of fibrosis, and then remain in the tissue with a phenotype similar to tissue resident alveolar macrophages (Misharin et al., 2017). In the intestine, studying the inflammatory bowel disease, Bain and colleagues have found that both the resident macrophages producing anti-inflammatory signals like IL-10, and the ones capable of highly inflammatory states, were derived from circulating $Ly6C^+$ monocytes that egress the bone marrow in a CCR2-dependent manner (Bain et al., 2013). In a model of pancreatic cancer, the macrophages found in the tumors were found to be heterogeneous and derived, some form $Ly6C^+$ monocyte recruitment, and some from embryonic progenitors, with distinct functions for each subset (Zhu et al., 2017).

A new nomenclature has been proposed to include the ontogeny of myeloid cells in their identification (Guilliams et al., 2014). Overall, the content of various 'activation' stages should be considered, at least in part, through the spectrum of developmental lineage, i.e. embryonic-derived and locally maintained resident populations, as well as

monocyte-derived, short-lived or long-lived cells (Geissmann and Mass, 2015). The terms ‘resident’ and ‘passenger’ subsets have been proposed.

1.4.3. Kidney macrophages in health and disease

1.4.3.1 Tissue localisation and definition of myeloid populations in the kidney

Kidney macrophages were first identified in 1983 (Hume and Gordon, 1983), as part of a seminal series of publications by Siamon Gordon, David Hume and colleagues, who studied the distribution of macrophages using the antibody to F4/80 to stain various adult and embryonic tissues (Hume et al., 1983, 1984a, 1984a, 1984b; Perry et al., 1985). They found F4/80^{+} cells non-randomly distributed throughout the whole thickness of the organ, from the proximity to small capillaries in the cortex, throughout the surroundings of the tubes inside the medulla, and to the proximity to arterioles near the glomeruli and Bowman’s capsules (Hume and Gordon, 1983). Because these cells were defined by F4/80 expression, they were termed macrophages. In the 1990s, however, some reports defined these tubulo-interstitial cells as DCs due to their morphology and MHC-II expression (Austyn et al., 1994; Kaissling and Le Hir, 1994). The ‘debate’ about the naming of mononuclear phagocytes of the kidney became more pronounced when the use of *Cx3cr1*$^{gfp/+}$ mice (Jung et al., 2000) allowed the identification of most of them are CX$_3$CR1^{+} F4/80^{+} CD11c^{+} CD11b^{+}, which can satisfy both the definition of DCs or macrophages (Kruger, 2004). Because the fields of DC biology and macrophage biology have evolved somewhat independent of each other (Gottschalk and Kurts, 2015), some confusion may arise when studying the literature of the past few decades regarding mononuclear phagocytes, notably of the kidney. In a recent study published by our laboratory, F4/80$^{\mathbf{bright}}$ cells of the kidney were analysed by intravital microscopy in the *Cx3cr1*$^{gfp/+}$ mice, flow cytometry analysis, RNA-sequencing, and in parabiotic of mice (Stamatiades et al., 2016). There, F4/80$^{\mathbf{bright}}$

phagocytes were defined as resident macrophages, and these are the cells that are part of the focus of **Chapter 4**, where the reader may find further information about these cells.

1.4.3.2. Kidney macrophage functions in different contexts

The presence of macrophages or monocytes in the kidney has been a known clinical observation for several decades in the context of kidney diseases, such as glomerular nephritis (Atkins et al., 1976), in which the amount of tubular damage of the kidney is correlated with the severity of clinical signs (Risdon et al., 1968). The presence of macrophages in biopsies during systemic lupus erythematosus (SLE) is even a predictive tool of the disease's outcome for patients (Hill et al., 2001). Therefore, the impact of macrophage populations and kidney phagocytes in general on the initiation, progression and resolution of kidney diseases has been extensively studied over the last few decades. The infiltration of cells described as macrophages has been a known feature of kidney diseases (Kluth et al., 2004; Rodríguez-Iturbe et al., 2001).

Cells expressing CX_3CR1, CD11c and MHC-II, therefore termed DCs (Kruger, 2004), have been shown to depend on CX_3CR1 and the expression of its ligand fractalkine (CX_3CL1) by kidney cells to populate the kidney and to infiltrate the organ during experimental nephritis, during which these cells exert local Th cell stimulation and chemokine production for the recruitment of neutrophils (Hochheiser et al., 2013). It has been known for some time that macrophages isolated from kidneys can produce iNOS and ROS, as shown in the rat (Cook et al., 1989; Erwig et al., 2000) and rabbit (Boyce et al., 1989), notably, either upon *in vitro* stimulation or during various stages of glomerular nephritis. However, whether or not this production of iNOS is detrimental remain unclear, as some reports suggest its inhibition is beneficial (Ogawa et al., 2002), while others suggest its inhibition increases the proteinuria observed during nephritis, which is a sign of kidney damage (Cattell et al., 1991; Waddington et al., 1996).

Cytokines such as TNFα (Lan et al., 1997) and IL-1β (Tipping et al., 1991) have also been implicated in kidney disease. Several studies have documented a positive effect on the progression of glomerulonephritis and a diminution of kidney damage signs such as proteinuria and kidney necrosis, when antagonists of the IL-1 receptor were administered during experimental glomerulonephritis (Lan et al., 1993, 1995). Inhibition of TNFα either before or during the induction of experimental glomerular nephritis allowed to prevent or reduce the clinical signs of kidney damage, and notably kidney levels of IL-1β (Karkar et al., 2001).

The implication of macrophages in kidney inflammation has been studied with various tools, which, while none are perfect to target a particular population, give weight to the hypothesis of their importance in the initiation and/or progression of disease. One technique is the administration of liposomal clodronate, which upon injection are phagocytosed by macrophages, which in turn will die (Van Rooijen and Sanders, 1997). When performed in the context of experimentally induced kidney ischemia, liposomal clodronate injection reduced signs of kidney damage such as levels of plasma creatinin (Day et al., 2005; Jo et al., 2006), kidney tubular cells apoptosis and whole kidney levels of TNFα and IL-1β (Jo et al., 2006). The use of an 'anti-macrophage serum', generally obtained by injecting pre-cultured mouse peritoneal macrophages to rabbits (Gallily, 1971; Hirsch et al., 1969), has suggested a role of macrophages and monocytes in the kidney damage observed after experimental kidney ischemia (Holdsworth et al., 1981). Finally, the development of mice that express the human receptor to diphteria toxin (Diphteria Toxin Receptor, DTR) under the control of particular gene promoters, allows the depletion of populations that selectively express these markers. CD11b-DTR mice (Duffield et al., 2005a) showed decreased tubular damage and improved kidney function upon DT injection during glomerulonephritis (Duffield et al., 2005b). The use of either clodronate liposomes or CD11b-DTR to affect

myeloid populations during renal ischemia models in mice have shown different results (Ferenbach et al., 2012). These techniques are not specific for a given population of resident or recruited population, not specific to the kidney, and it is therefore necessary to consider these results with great caution, not having certainty for the role of a given population, nor very good control of the effect of these depletion techniques on myeloid cells of other organs.

Our laboratory has taken advantage of intravital microscopy and flow cytometry analyses to try to decipher the identity and organ-specific functions of a population of *Cx3cr1-gfp* expressing resident macrophage population in the context of circulating small immune complexes (ICs). Although immune complexes containing self-antigens are a common feature of a group of reactions called 'type III hypersensitivity', which encompass diseases such as serum sickness, glomerulonephritis or SLE, our laboratory attempted, rather than to study a disease model, to identify basic behaviours of kidney resident macrophages in response to the presence of ICs (Stamatiades et al., 2016). The results shown in **Chapter 4** show some of the characterisation of this model of inflammation.

1.5. On mathematical modeling

The first part of the results presented in this work (**Chapter 3**) is showing the biological data that have been generated in order, not only to characterise the biological systems in question, but also to be analysed with a computer-assisted *in silico* mathematical model. Using mathematics to try understanding biological phenomena is

not new and we will briefly overview the use of mathematics in science in general, and in biology in particular.

1.5.1. On the efficiency of mathematics in science

Mathematics, often considered 'the queen of sciences', have been used as a tool to study the laws of Nature for centuries. The 'mathematization' of physics has been introduced by the Italian astronomer Galileo Galilei (1564 - 1642). In his book *The Assayer* (originally *Il Saggiatore*, 1623), he writes « [the book of Nature] *is written in the language of mathematics, and its characters are triangles, circles, and other geometrical figures, without which it is humanly impossible to understand a single word of it* ». This prompted the rise of modern physics. The use of mathematics to describe the laws of Nature meant that not only was the Universe governed by laws applicable for its entirety (unified Universe), but also that the laws of physics were now fully accessible to human intelligence, via this tool that had been developed for thousands of years. This constitutes what is now referred to as the Scientific Revolution of the 17th century (Koyré A., *Etudes d'Histoire de la Pensée Scientifique*).

The efficiency of mathematics in the description of the laws of physics has been proven and has allowed great discoveries. This efficiency can be described in several ways. Beyond their use in the description of phenomena within different theories, such as the description of motion in mechanics, they also have allowed to predict the very existence of new objects. This predictive power can be illustrated with two examples. First, let us consider the case of the 8th planet from the Sun, Neptune. Its existence was only postulated, in order to correct for the dicrepancies between the calculated and observed orbit of its neighbour Uranus. The French astronomer Urbain Le Verrier (1811-1877) calculated the position, mass and orbit of a planet that would correct for this dicrepancy, and in september 1864, the German Johann Goffried Galle turned his

telescope to where the planet should be according to calculations, and found it. There was Neptune. This is an impressive illustration of the predictive power of Mathematics, which allowed to predict the existence of a planet. Here is an example of Mathematics being used to discover, thanks to known laws of physics, a known type of physical object - a planet.

Another example seems even more striking. It is the discoveries made by the physicist Paul Dirac (1902 - 1984). He is one of the physicists who participated in the creation and development of particle physics, or quantum mechanics, in the first half of the 20th Century. And what he found, when calculating the Energy (E) of a particle, is that it varies in regards to its momentum « p » and its mass « m » such as $E^2=p^2+m^2$. This is a simplified version of the equation, but the important aspect of it is preserved : one can see that the solution of this equation can be positive or negative, i.e. $E= \sqrt{(p^2+m^2)}$ or $E= -\sqrt{(m^2+p^2)}$. Therefore, the rules of mathematics pointed Dirac to a solution of the equation that seemed irrelevant : a *negative* energy. Not accepting it at first, he was forced by his mathematician contemporaries to not discard this solution. This prompted him to understand the existence of *anti-matter*, consisting of particles with negative energies.

These two examples illustrate how mathematics have allowed Physics to describe a great number of new objects and phenomena. The discovery of Neptune is a spectacular example of maths' predictive power within a well-established theory (that of gravitation). However, our second example shows that the mathematic rules have yielded a *new type* of physical object.

The reason behind the efficiency of mathematics in Sciences has baffled scientists for a long time. Nobel-prize winning physicist Eugene Wigner in a 1960 article says « the enormous usefulness of mathematics in the natural sciences is something bordering on

the mysterious and there is no rational explanation for it » (Wigner, 1960). Indeed, there are important questions raised by this effectiveness, which have been the topic of reflection for the philosophers of science and the theories of knowledge : how can a formal system of logical thought process, of such abstract nature, and completely invented by humans, be so well adapted to the description of all the physical objects and phenomena ? Does it mean Nature is indeed mathematical in its essence somehow, or is it just that some of mathematics fit well with the phenomena described ? We will not deal with such complex issues, but they are worth having in mind.

1.5.2. Modeling Biology with Mathematics

If Mathematics are the language of Physics, it appears very different in Biology. Indeed, this area of science is not taught through equations. Aside from statistics, which are an essential (though sometimes potentially misleading) tool to discern « significant » differences and trends in experimental data, it appears mathematics are not the primary means to accessing knowledge in Biology. It is not necessarily clear exactly why (or indeed if) biological phenomena cannot in principle be described by mathematics. It may be due to the nature of the subject of study itself, i.e. living organisms, which are composed by many interconnected elements, that interact at different levels of organization (molecular, cellular, tissue, organ, organism, ecosystems). These organisms, in terms used by physicists, are open systems very far from thermodynamic equilibrium (Prigogine et al., 1974), which makes them very hard to pin down in a quantitative manner.

This does not mean that biology as a whole has been kept away from any mathematical approach. On the contrary, many phenomena can be at least partially described using more or less sophisticated mathematical models. These include a wide range throughout the study of biology : agronomic systems (Keurentjes et al., 2013),

development biology (Economou and Green, 2014; Yu and Fernandez-Gonzalez, 2016), tissue organisation (Molitoris et al., 2016), vaccinology (Pappalardo et al., 2015), virology (Bocharov et al., 2015; Huber et al., 2017), oncology (Powathil et al., 2015) and many other domains. Many levels of biological activity can be modelled, from molecular interactions between a receptor and a ligand, to populations dynamics.

As we said above, there is no mathematical theory of biology ; our understanding of this field is guided by experimental data. When attempting to produce a mathematical model that is relevant to Biology, it is important for experimental data to be an integral part of the modeling activity. The interaction between mathematical models and biological experimental data has notably been the focus of the laboratory of Grégoire Altan-Bonnet, with whom we have collaborated for the work presented in **Chapter 3**. His work on T cell responses is a perfect example of what the mathematical interrogation of biological data, as well as the predictive power of properly experimentally parameterised models, can be. This allowed a better understanding of early T cell activation upon T Cell Receptor (TCR) recognition of peptide-MHC : data gathered on the response of specific T cells to agonists and antagonists allowed the formulation of mathematical models which could yield predictions that were successfully tested (Altan-Bonnet and Germain, 2005). Further generation of mathematical models and the use of important computing power can allow the formulation of a wide range of predictions for the behaviour of T cells in response to various agonists and antigonists, and these predictions can then be tested in an experimental setting (François et al., 2013). The combination of increasingly complex, however tightly controlled, experimental conditions *in vitro* allowed Altan-Bonnet's group to shed light on the integration of different types of signals leading to various levels of T cell activation, and the precise regulation of intracellular signaling that allows their discrimination of antigens (Voisinne et al., 2015).

Although the topic of monocyte development is quite distinct from that of T cell activation, the process of mathematical modeling followed by experimental testing is applicable for potentially any biological system within a certain limit of parameters. We will now present some of the key proceedings that had been done before the work showed in this thesis started, and will explain our general aim and approach.

1.6. Preceeding work, general aims, and experimental approach

1.6.1. Study of monocyte dynamics in the steady state toward anin silico model

1.6.1.1. Previous results in the laboratory regarding monocytes in the steady state

Previous work carried out by Hannah Garner in our laboratory has focused on characterising the monocytes and their progenitors *in vivo*, and notably investigating the role of *Nr4a1* in the development of the patrolling Ly6C^{low} subset. Her results lead to the identification of a cell population in the bone marrow that may constitute a direct precursor for Ly6C^{low} monocytes. Indeed, these cells are phenotypically very similar to Ly6C^{low} monocytes, and have the same genetic requirements. In addition to the description of this population, her work has re-examined genetic models, and refining one, for the study of monocyte subsets. Her results confirm that the two main monocyte subsets have dinstinct genetic requirements, and are compatible with distinct pathways of differentiation. For more details on these preceeding results, see **Chapter 3, section 3.1**. Therefore, this thesis presents a collaborative approach that was undertaken in the laboratory to re-examine monocyte dynamics (see below).

1.6.1.2. Aim, and experimental approach

We first aimed at probing monocyte and monocyte progenitor dynamics in order to further understand monocyte differentiation from the bone marrow to the circulation.

To study monocyte dynamics, we took advantage of nucleoside analogues, mainly EdU (Limsirichaikul et al., 2009). This allows to stain dividing cells (progenitors) and follow over time how the incorporated EdU is distributed towards differentiated monocytes, which don't proliferate in the blood at steady state (Geissmann et al., 2003 ; Shand et al., 2014). This method has been used in the past on many occasions, and notably to study monocyte dynamics in the mouse (Yona et al., 2013). We sought to use the results from such methods to analyse in detail the quantitative information, in a way that would make use of more parameters and would be the least biased possible ; for this we collaborated with a laboratory specialised in generating experimentally parameterised, computer-assisted models (for a general presentation of this mathematical model, see **Materials and Methods**, **section 2.9**). Here the characterisation of our biological system, that is monocytes and progenitors in the bone marrow, blood and spleen, taking up EdU and analysed at various time points, will be presented. The process through which the analysis of that system was refined, in order to have the most predictive model possible, in the least biased way, though still in keeping with the results found in the literature and genetic data obtained in the laboratory, will be exposed.

1.6.2. Study of monocyte and macrophage functions in the kidney

1.6.2.1. Monocytes as housekeepers of the vasculature, and kidney macrophages as monitors of circulation

We aimed at understanding further monocyte and macrophages functions in the kidney. Previous work from the laboratory showed their capacity to be retained by the capillary endothelium upon TLR7 signals, and recruit neutrophils which induced endothelial necrosis, and monocyte probably involved in the scavenging of the resulting debris (Carlin et al., 2013). Work carried out by Efstathios Stamatiades in the laboratory has allowed a characterisation, by intravital microscopy and flow cytometry, of the kidney macrophages, as resident cells with highly motile processes that probe their microenvironment constantly (Stamatiades et al., 2016). They also displayed the ability to take up circulating fluorescently labeled Bovine Serum Albumin (BSA) or chicken Ovalbumin (OVA), within the first few minutes following intravenous (i.v.) injection, and to do so more efficiently for *in vitro* prepared immune complexes, in a FcγR-IV-dependent manner. This resulted in the recruitment of monocytes and neutrophils to the kidney within hours after inection.

1.6.2.2. Aim and experimental approach

We first interrogated the mechanism of patrolling and retention of monocytes by investigating a potential role of platelets, which have been increasingly recognised as active participants to the immune response, beyond their role in coagulation (Semple et al., 2011; Vieira-de-Abreu et al., 2012). We used the already characterised model of R848 (Resiquimode, a TLR7 agonist) 'painting' on the kidney, and intravital microscopy (Carlin et al., 2013), to probe for the role of platelet in the patrolling activity of monocytes, during steady state and inflammation. We also investigated the role of macrophages in the kidney, in the context of circulating immune complexes

(Stamatiades et al., 2016). We aimed at characterising some aspects of that model of inflammation, using Fast Protein Liquid Chromatography (FPLC), flow cytometry and intravital microscopy. These techniques allowed us to do a qualitative analysis of the immune complexes used in this model of study, to analyse uptake of immune complexes throughout several organs and to probe some mechanisms by which the immune complexes may access the macrophages of the kidney.

2. Materials and Methods

2.1. Mice

2.1.1. Animals used for this study

All animal procedures were performed in adherence to FG project license issued by the United Kingdom Home Office, under the Animals (Scientific Procedures) Act 1986,

and with the Institutional Review Board (IACUC 15-04-006) at Memorial Sloan Kettering Cancer Center (MSKCC), New York, NY, USA. Eight week-old male C57BL/6 mice were purchased form Charles River (strain 027). *Cx3cr1*$^{gfp/+}$ *Rag2*$^{-/-}$ *Il2rg*$^{-/-}$ (Auffray et al., 2007) and *Cx3cr1*$^{gfp/+}$ (Jung et al., 2000) were maintained in house. *Nr4a1*^{GFP} (Moran et al., 2011) were generated by Kristin A. Hogquist and provided by George Kassiotis (NIMR). *Nr4a1*$^{-/-}$ (Lee et al., 1995) (B6.129S2-Nr4a1$^{tm1Jmi/J}$) were purchased from Jackson Laboratories as frozen embryos, rederived in house, and then crossed to *Nr4a1*^{GFP} in order to generate *Nr4a1*^{GFP} ; *Nr4a1*$^{-/-}$ and littermates. *Csf1r*^{iCre} mice (Deng et al., 2010) were crossed to *Fcgr4*$^{f/f}$ mice (Nimmerjahn et al., 2010) in house to generate *Csf1r*^{iCre} *Fcgr4*$^{f/f}$ mice.

2.1.2. Genotyping

2.1.2.1. Nr4a1^{GFP}*; Nr4a1*$^{-/-}$

Nr4a1 knock-out was assessed by genotyping using the following primers (5' > 3'): CAC GAG ACT AGT GAG ACG TG (Mutant) and CCA CGT CTT CTT CCT CAT CC (Common). The Polymerase Chain Reaction (PCR) was then set up as follows: 95ºC for 5 min, followed by 35 cycles of 94ºC for 30sec, 62ºC for 1min, 72ºC for 1min, and finally 72ºC for 2min. Mutant band was detected at 350 base-pairs (bp) in a 1.5% agarose gel in TBE. This genotyping was coupled to a blood phenotyping of the mice (tail vein bleeding followed by flow cytometry analysis) for the presence of GFP and circulating Ly6C^{low} monocytes.

2.1.2.2. Cx3cr1$^{gfp/+}$

Cx3cr1 and/or *gfp* were detected with the following primers (5' > 3'): GTC TTC ACG TTC GGT CTG GT (Rev WT), CCC AGA CAC TCG TTG TCC TT (For), and CTC CCC CTG AAC CTG AAA C (Rev Mut). Then a PCR with the following

conditions was performed: 94ºC for 3min, followed by 35 cycles of 94ºC for 30sec, 60ºC for 30sec and 72ºC for 30sec, and finally 72ºC for 5min. A band at 450bp for the WT *Cx3cr1* and 550bp for the knock-in *gfp* were detected in a 1.5% agarose gel in TBE.

2.1.2.3. Rag2$^{-/-}$ Il2rg$^{-/-}$

Rag2 knock out was detected with the following primers (5' > 3'): GGG AGG ACA CTC ACT TGC CAG TA (R011), AGT CAG GAG TCT CCA TCT CAC TGA (R012), and CGG CCG GAG AAC CTG CGT GCA A (R013). A combination of R011 and R012 was used to detect a 263bp band for the WT, and a combination of R013 and R012 was used to detect a 350bp for the mutant, in a 1.5% agarose gel in TBE. For both PCR, the conditions were as follows: first 94ºC for 3min, then 35 cycles of 94ºC for 30sec, 60ºC for 30sec and 72ºC for 30sec and finally 72ºC for 7min.

Il2rg knock out was detected using the three following primers (5' > 3') in a single PCR reaction: CTT CTT AGT CCT TCA GCT GC (oIMR0301), AGG CTC AGA ACT GCT ATT CC (oIMR0302) and GTA TGG TAG TGT TCT CAC CG (oIMR0303). The following PCR reaction was then performed : 94ºC for 3min, followed by 35 cycles of 94ºC for 20sec, 55ºC for 20sec and 72ºC for 35sec, then 72ºC for 2min. A band at 400bp was detected for WT and 600bp for Mutant in a 1.5% agarose gel in TBE.

2.1.2.4. Csf1r^{iCre} Fcgr4$^{f/f}$

Csf1r^{iCre} : *Cre* was detected using the following primers (3' > 5'): TCT CTG CCC AGA GTC ATC CT (For) and CTC TGA CAG ATG CCA GGA CA (Rev). The following PCR reaction was then performed : 95ºC for 5min, followed by 30 cycles of 95ºC for 45sec, 60ºC for 45sec, 72ºC for 45sec, then 72ºC for min. A band at 400bp was detected for the presence of Cre in a 1.5% agarose gel in TBE.

Fcgr4$^{f/f}$: the following primers were used (5' > 3') : TAT ATG TGG TCA GAC CCT TGC CTG C (R4flox-5, For), GGA GTT GGC AGG TCC AAG ACA GCC (R4flox-3, For), and CTT ATC ACC TTG CCT CCT TAG ACA GAT CC (R4Flox-2, Rev). A PCR with all three primers was performed with the following conditions : 95ºC for 15 min, followed by 35 cycles of 94ºC for 30sec, 61ºC for 30sec, 72ºC for 30sec, then 72ºC for 10min. Bands were detected at 184bp for *wt* allele and 235bp for the floxed allele, in a 1.5% agarose gel in TBE.

2.2. Flow Cytometry

2.2.1. Tissue preparation for flow cytometry

*2.2.1.1. Blood pr*eparation

Mice were euthanized using CO_2 and blood was collected by cardiac puncture using a 1mL syringe (Beckon Dickinson [BD], Cat#309659) and a 26Gx1/2" hypodermic needle (Exel, Cat#26402) containing 50 μ 0 of 100mM EDTA. Volume of blood taken was measured directly with the syringe, before it was placed in 15mL conical tubes containing 50 μ L EDTA 100mM. Red blood cells (RBC) were lyzed by adding 5mL of RBC lysis buffer (0.5g $NaHCO_3$ + 4.15g NH_4Cl + 500µL EDTA 100mM in 500mL MilliQ H_2O total volume). After 5min incubation, 5mL of FACS buffer (PBS 1X 0.5% BSA 2mM EDTA) was added and the cells were spun. This was repeated with 3mL, then 1mL of RBC lysis buffer, then FACS buffer after incubation. After the final step of RBC lysis, cells were resuspended in 70 μ L of FcBlock (BD Cat#553141, clone 2.4G2). 50µL of cells were placed in 96-well U-bottom plates, and 50 μ L of antibody mix was added to the cells. See *Common protocol for all organs* for subsequent steps.

2.2.1.2. Spleen preparation for monocyte staining

Spleens were dissected and mechanically disrupted through a 100 μ m cell strainer (Falcon, Cat#352360) in 6mL FACS buffer, filtered through a 70 μ m cell strainer into a 15mL conical tube (BD, Cat#352070). After spinning the cells, red blood cells were lyzed with a resuspension in 3mL of RBC lysis buffer. 3mL of FACS buffer were added after a 5min incubation on ice, and cells were spun. Spleen cells were then resuspended in 500 μ L FcBlock (BD Cat#553141, clone 2.4G2). 50 μ L of cells were then plated in 96-well U-bottom plates, and stained with the antibody mix. See *Common protocol for all organs* for subsequent steps.

2.2.1.3. Bone marrow preparation

Hind limbs were excised, the legs were dissected into femur and tibia and each end of the bones cut with a razor blade to allow flushing of the bone marrow. Bones were held with forceps and flushed using a 27Gx1/2'' needle and 10mL syringe with RPMI into 15mL conical tubes, and centrifuged at 320*g* 4˚C for 5 minutes. Cell pellet was resuspended with 1mL of FACS buffer (PBS, 0.5% BSA, 2mM EDTA and filtered with Stericup 0.22µm [Fisher Scientific Cat#SCGVU05RE]). Cells were filtered through 70µm cell strainers (Fisher, Cat#08-771-2), tube and filter were washed with 2mL of FACS buffer. To deplete $Ly6G^+$ granulocytes and $Ter119^+$ red blood cells, the pellet was resuspended in the following antibodies: clone 1A8 (anti-Ly6G) at 10µg/ml (BioXcell, Cat#BE0075-1) and clone TER-119 (anti-Ter119) at 20µg/ml (BioXcell, Cat#BE0183) in a total volume of 500µL of RPMI 1640 (Life Technologies, Cat#11875-093) 10% FBS (Life Technologies, Cat#10438026), then incubated 15 min on ice and washed with 1mL of RPMI 1640 10% FBS. Dynabeads (Sheep anti-Rat IgG, Life Technologies Cat#11035), previously washed 2 times with RPMI 10% FBS, were added to the cells, before transfer into a polypropylene FACS tube. Tubes were capped

with FACS tube caps, sealed with Parafilm, and placed on roller for 45 minutes at 4°C. After incubation with beads, tube were placed in magnet (MPC-6 Magnet Life Technologies, Cat#12002D). 2 minutes after, the supernatant containing bone marrow cells depleted of $Ly6G^+$ and $Ter119^+$ cells was collected into 15mL conical tubes and centrifuged at 320 x g 4˚C for 7 minutes. Cells were resuspended in 200 μ L of Fc block (BD Cat#553141, clone 2.4G2). 50 μ L of cells were transferred into a 96-well U-bottom plate, and 50 μ L of antibody mix were added, and incubated for 20 minutes on ice.

2.2.1.4. Kidney, Liver, Spleen, Lungs, Brain for staining macrophages

All the organs were dissected out after the male C57BL/6 mice were sacrificed by cervical dislocation. Kidney capsules were removed manually. They were placed in 12-well plates containing 2mL of the following enzymatic digestion mix: Hank's Balanced Salt Solution (HBSS, no Ca^{2+}/Mg^{2+}, Gibco) containing 1mg/mL Collagenase D (Roche), 100U/mL DNAse I (Sigma), and FBS (Fetal Bovine Serum, Gibco). They were then cut into small (~ 1 - 5 mm^3) pieces with scissors and incubated at 37ºC for 30 min. They were then transferred into 6-well plates containing 6mL of FACS buffer on ice, and mashed through a 100µm cell strainer. Cells were spun at 320g for 7min at 4ºC and resuspended in 3mL RBC lysis buffer, incubated for 5min before rincing with 3mL FACS buffer and spun again. Cells were then incubated in FcBlock (clone 2.4G2) for 15min on ice, followed by 30min incubation with the antibody mix. Cells were rinsed once in FACS buffers, spun, resuspended in FACS buffer and acquired at the flow cytometer (BD Fortessa).

For the measure of intracellular TNFα production by kidney macrophages, all reagents and media contained Brefeldin A (1/1000 dilution, eBioscience, Cat#00-4506-51). After tissue isolation a reduction into a cell suspension, total kidney cells were

placed in 5mL of RPMI medium supplemented with 10% FBS, 1% Penicillin/Streptomycin (Sigma-Aldrich, Cat#P4458), and incubated for 5 hours at 37ºC. Cells were then stained for extracellular antigens with fluorescently labeled antibodies for flow cytometry, fixed and permeabilized with buffers from eBioscience (Cat#88-8823-88), and stained with anti-TNFα APC, or APC-labeled isotype control.

2.2.1.5. Skin preparation for epidermal Langerhans cell and dermal macrophages isolation

Ears from C57BL/6 males sacrificed by cervical dislocation were cut and placed in ice-cold PBS. Then the two skin sheets were separated using forceps, and placed, dermis down, on top of (floating on) 2mL of HBSS containing 3% FBS and dispase (2.4mg/ml, Invitrogen) at 37ºC for 1h. Then the dermis was separated from epidermis using forceps, and each skin layer was separately cut into small (~1 – 5 mm^3) pieces using scissors and incubated in 2mL of HBSS containing 3% FBS, 1mg/mL Collagenase D, 100U/mL DNAse I and 2.4mg/mL dispase at 37ºC for 45min. The suspensions were then transferred to a 6-well plate containing 6mL of FACS buffer, mashed through a 100μm cell strainer, and spun at 320g at 4ºC for 7min. Cells were then incubated with FcBlock (Clone 2.4G2) for 15min on ice and then in the antibody mix for another 30min. Cells were then rinsed once and resuspended in FACS buffer, before acquisition at the flow cytometer (BD Fortessa).

2.2.2 Flow cytometry acquisition

Cell acquisition was performed on a BD Fortessa (5 lasers: UV 355nm, Violet 405nm, Blue 488nm, Yellow-Green 561nm and Red 640nm). See **Table 2.1** for the detail of fluorochrome to laser and PMT filter correspondance. The machine was run with DIVA software (BD). The resulting .fcs files were analysed using FlowJo v9.9 (FlowJo LLC, TreeStar).

2.3. EdU incorporation Experiments.

2.3.1. EdU administration for single-pusle study

8 to 12 week old C57BL/6N mice (Charles River, strain 027) were injected intraperitoneally with 200 μ L of a solution of 2.5mg/mL of EdU (10mM, in PBS) per mouse (Fisher Cat#C10420, Click-iT EdU Alexa Fluor 488 Flow Cytometry Assay Kit). Blood, bone samples (femurs and tibiae) and spleens were collected at time points ranging from 15 minutes to 240 hours post injection, and prepared for FACS analysis. The organs were then prepared as for flow cytometry, and the manufacturer's instructions were followed to stain the cells and reveal the EdU content, which constitute the common protocol for all organs as follows.

2.3.2. Common protocol for all organs for EdU detection

Briefly, cells were washed with incubated with pre-click antibody mixes conatining all antibodies except those coupled to PE or PECy7 as indicated by the manufacturer's instruction. Then cells were fixed with 4% PFA (prepared from 16% in PBS [Thermo Scientific Cat#28908]), incubated for 15min at room temperature. Cells were then permeabilized with a resuspension in 200 μ L of the provided saponin-based Perm/Wash buffer 1X (diluted from 10X using FACS Buffer). Cells were then resuspended in 200 μ L of a Click-reaction mix prepared following the manufacturer's instructions (see content for 1mL below). After 30 min incubation at room temperature, cells were spun directly, then resuspended in 200 μ L of saponin-based Perm/Wash buffer 1X, then spun again, before resuspension in 100 μ L of antibody mix containing the PE and PECy7 coupled antibodies (prepared in FACS buffer), and incubated 20min on ice. Cells were then washed with 100µL of FACS buffer, spun and resuspended in 200 μ L of FACS buffer, before acquisition at a BD Fortessa.

Content of Click-reaction Mix, following manufacturer's instructions (Thermo Fisher, Cat#C10420 or C10419): 875µL PBS 1X + 20µL $CuSO_4$ + 5µL Azide-A488 (or A647) + 100µL Buffer Additive.

Table 2.1. Antibodies used for this study, for flow cytometry

Antibody name	**Clone**	**Laser for excitation**	**PMT filter**	**Company – Catalog #**
c-Kit BV605	2B8	Violet (405nm)	595LP →610/20	BD – 563146
CD115 APC	AFS98	Red (640nm)	670/30	eBiosciences - 17-1152-82
Ly6C BV421	HK1.4	Violet (405nm)	450/50	Biolegend – 128031
MHC-II AF700	M5/114.15.2	Red (640nm)	710LP →730/45	Biolegend – 107622
CD45.2 APCCy7	104	Red (640nm)	750LP →780/60	BD - 560694
F4/80 BV605	BM8	Violet (405nm)	595LP →610/20	BD
CD43 BV510	S7	Violet (405nm)	495LP →525/50	BD – 564398
CD3 PE	145-2C11	Yellow-Green (561nm)	586/15	eBioscience – 12-0031-82
CD19 PE	1D3	Yellow-Green (561nm)	586/15	eBioscience – 12-0193-83
NKp46 PE	29A1.4	Yellow-Green (561nm)	586/15	eBioscience – 12-3351-82
Sca-1 PE	D7	Yellow-Green (561nm)	586/15	Biolegend – 108108
Ly6G PE	1A8	Yellow-Green (561nm)	586/15	BD – 551461

CD11b PECy7	M1/70	Yellow-Green (561nm)	750LP →780/60	BD – 552850
F4/80 eFluor 450	BM8	Violet (405nm)	450/50	eBioscience - 48-4801-82
TNFα APC	MP6-XT22	Red (640nm)	670/30	BD – 554420
Gr-1 APC	RB6-8C5	Red (640nm)	670/30	BD – 553129
CD16/CD32, purified	2.4G2	N/A	N/A	BD – 553142
Siglec F PE	E50-2440	Yellow-Green (561nm)	586/15	BD – 552126

2.4 Cytospin

Bone marrow cells from 8 week old C57BL/6 male mice were isolated and processed for flow cytometry as described above. Cell sorting was performed on a BD ARIA II, using a 100μm nozzle, as a 4-way sort into 1.5mL Eppendorf tubes containing 250 μ L of FBS maintained at 4°C for the duration of the sort. The six "classical" bone marrow populations were sorted: MDP (5,000 cells), cMoP (2,000 cells), Ly6C^{+} pro-monocytes (10,000 cells), MHC-II^{+} monocytes (2,500 cells), Ly6C^{low} monocytes (1,500 cells), CD115^{low} cells (1,500 cells). Cells were transferred into single funnels (Fisher scientific #10-354), clipped to L-Lysin coated slides using Shandon Cytoclips (Thermo Scientific #59910052), and spun using the Cytospin 4 Cytocentrifuge (Thermo Fisher Scientific) at 800rpm for 8min. Then, a May-Grünwald-Giemsa staining was performed, as

described previously (Gomez Perdiguero et al., 2014). Briefly, slides were air dried for 30 minutes after the spin, followed by a 5min fixation with 100% Methanol (SIGMA). Then, the cytospin preparations were manually stained with a 50% May-Grünwald solution (Sigma-Aldrich Cat#MG500-500mL) for 10 minutes, rinced with Sorenson's buffered distilled water (pH=6.8, 43.75mL Na_2HPO_4 + 56.25mL KH_2PO_4, both from Sigma), then stained with a 14% Giemsa solution (SLS, Cat# SLS 48900-100ML-F) for 20 minutes. The stained slides were air dried before mouting in Entellan New mounting medium (Merck). Cells were observed and pictured with an Oil N-Achroplan 100x objective 1.25 N.A., mounted on an Axio Lab.A1 Bright Field microscope (Zeiss).

2.5. CyTOF

Blood and Bone Marrow cells were harvested from 8 week old C57BL/6 or *Cx3cr1*$^{gfp/+}$ *Rag2*$^{-/-}$ *Il2rg*$^{-/y}$ males as for Flow Cytometry. Red blood cell for blood samples, as well as Ly6G$^+$ and Ter119$^+$ cells depletion for bone marrow samples, were performed as described above. For some experiments, half the cells were used for flow cytometry analysis, while the other half was processed as follows for CyTOF analysis. Cells were incubated in a solution of 5 μ M Cell-ID Cisplatin in PBS (Fluidigm Cat #201064) for 10 minutes at room temperature, for staining of viable cells. After the blocking step with anti-CD16/32 (clone 2.4G2), cells were washed once in Maxpar Staining Buffer (Fluidigm, Cat #201068). The antibody mix (see **Table 2.2**) prepared in Maxpar Staining Buffer was added with a final volume of 50 μ a, and incubated with the cells for 30 minutes on ice. After two steps of wash with Marpar Staining Buffer, cells were incubated in 500 μ n of Marpax Fix and Perm Buffer (Fluidigm Cat #201067) containing DNA intercalator-Ir (Fluidigm Cat #201192A) at 125nM, for 1 hour at room temperature. After two steps of washing with Marpar Staining Buffer, cells were

resuspended of Maxpar Water (Fluidigm Cat #201069), counted manually using a Neubauer chamber, and the volume adjusted to $0.5x10^6$/mL cells. 500 μ 0 of cells were added to 50 μ e of EQ Four Element Calibration beads (Fluidigm Cat #201078), loaded to a 1mL syringe and introduced to a CyTOF 2 (Fluidigm) for acquisition.

When staining organs form *Cx3cr1*^{GFP} mice (*Rag2*$^{-/-}$ *Il2rg*$^{-/-}$ *or Rag2*$^{+/+}$ *Il2rg*$^{+/+}$), intracellular GFP was stained after extracellular antigens staining and fixation, using an anti-GFP antibody (see **Table 2.2**)

Table 2.2. Antibodies used in this study, for CyTOF

Antigen	**Tag**	**Clone**	**Fluidigm, Cat #**
CD11b	172 Yb	M1/70	3172012B
CD45	175 Lu	30-F11	3175010B
CD11c	162 Dy	N418	3162017B
B220	176 Yb	RA3-6B2	3176002B
F4/80	159 Tb	BM8	3159009B
cKit (CD117)	173 Yb	2B8	3173004B
CD64	151 Eu	X54-5/7.1	3151012B
Sca-1 (Ly6A/E)	169 Tm	D7	3169015B
Ly6C	150 Nd	HK1.4	3150010B

CD3e	165 Ho	145-2C11	3165020B
NKp46	153 Eu	29A1.4	3153006B
CD11b	143 Nd	M1/70	3143015B
CD43	146 Nd	S11	3146009B
Ly6G	151 Eu	1A8	3151010B
Sca-1 (Ly6A/E)	164 Dy	D7	3164005B
Ly6G	141 Pr	1A8	3141008B
CD11c	142 Nd	N418	3142003B
CD115	144 Nd	AFS98	3144012B
CD45.2	147 Sm	104	3147004B
CD11b	148Nd	M1/70	3148003B
CD3e	152 Sm	145-2C11	3152004B
Ly6C	162 Dy	HK1.4	3162014B
CD19	166 Er	6D5	3166015B
NKp46	167 Er	29A 1.4	3167008B
CD8a	168 Er	53-6.7	3168003B
NK1.1	170 Er	PK136	3170002B
CD4	172 Yb	RM4-5	3172003B
MHC-II (IA/IE)	174 Yb	M5/114.15.2	3174003B

GFP	169 Tm	5F12.4	3169009B

2.6. Absolute cell numbers

2.6.1. Cell preparation

Cells from each organ were isolated as indicated above for flow cytometry. Aliquots were taken once the cells were in Fc Blocking solution, as described below, and diluted to different extent:

2.6.1.1. Blood

An aliquot of cells was taken after the red blood cell lysis steps; 10 μ L of cells were placed in 90 μ L of FACS buffer (1/10 dilution), then 50 μ L of that suspension was placed in 50 μ L of Trypan Blue (1/2 dilution) before counting. Resulting dilution factor: 20

2.6.1.2. Bone Marrow

An aliquot of cells was taken after the $Ter119^+$ and $Ly6G^+$ cell depletion with Dynabeads and resuspension in Fc Block; 10 μ L were placed in 190 μ L FACS buffer (1/20 dilution); 50 μ L of this suspension was placed in 50 μ L Trypan Blue (1/2 dilution) before counting. Resulting dilution factor: 40

2.6.1.3. Spleen

An aliquot of cell was taken after the red blood cell lysis step; 10 μ L of cells were

placed in 190 μ L of FACS buffer (1/20 dilution), and 50 μ L of this suspension was placed in 150 μ L of Trypan Blue (1/4 dilution) before counting. Resulting dilution factor: 80.

2.6.2. Cell count using Neubauer Chambers

Cells processed for flow cytometry were counted once in Fc Blocking solution (see Tissue Preparation for Flow Cytometry). Cells were counted using Neubauer chamber. 10 μ L of diluted cells mixed with Trypan Blue (Invitrogen Cat# 15250-061) – see cell preparation above for each organ – was introduced to the chamber, which was then observed under an Air 20x N-Achroplan 0.45 N.A. objective, mounted on an Axio Lab.A1 Bright Field microscope (Zeiss). Live cells (Trypan Blue – negative) were counted in the four outer grids (excluding two edges for each grid). The number of cells per mL in the original cell suspension was calculated using the following formula:

Cells/mL = average cells/grid x dilution factor x 10,000

This number was then multiplied by the amount, in mL, of Fc Blocking solution, to reach the total number of cells being processed for flow cytometry (for 60 μ L of cell suspension in Fc Block, the total number of cells was then equal to Cells/mL x 0.06).

2.6.3. Whole body cells numbers per organ

For each organ, a certain estimations was used to obtain whole body cell count.

2.6.3.1. Blood

Blood volume has been estimated as recorded by Hakness and Wagner (Hackness and Wagner, 2005) to be 80mL/kg for C57BL/6 mice, and 8-week old males were considered to be 25g (Mitruka and Rawnsley, *Clinical biochemical and hematological*

reference values in normal experimental animals and normal humans, 1981); hence, total blood volume was estimated at 2mL per mouse. Therefore the total amount of cells in Fc Block suspension was divided by the volume (in μL) of blood withdrawn by cardiac puncture (usually between 500 μL and 1mL), and multiplied by 2,000 μL for the whole body blood cell count.

2.6.3.2 Bone Marrow

The study performed by Colvin and colleagues (Colvin et al., 2004) has shown (for Balb/c mice) that the two femurs constituted 10% of the whole body bone marrow, while the two tibiae constituted 4% of it. Therefore, we estimated that the two hind legs used for our flow cytometry studies represented 14% (10% + 4%) of the whole body bone marrow. Cells counted for the two hind legs using Neubauer chamber were therefore multiplied by 100/14, to reach the number of whole body bone marrow cells.

2.6.4. Absolute counts for each population of each organ and their representation

After acquisition and analysis, the frequency of each population among $CD45^+$ cells was multiplied by the total number of cells obtained as described above, to obtain the absolute number of each population in the whole body of the mouse. In order to help visualize the relative sizes of the populations, each was represented by a coloured circle, the area (A) of which was equal to the population's whole body count/10^6. To draw the circle, its diameter was deduced after remembering that the area of a circle (A) is calculated as $A = \pi . r^2$ where r is the radius of the circle, and r = D/2 where D is its diameter.

Therefore, knowing its Area, we can deduce its diameter D:

$A = \pi . r^2$

$A = \pi . (D/2)^2$

$A = \pi . D^2/4$

$D^2 = 4A / \pi$

$D = \sqrt{(4A/ \pi)}$, where A = whole body cell count/10^6

2.7. Intravital microscopy

2.7.1. Imaging of the renal cortex

Male *Cx3cr1*$^{gfp/+}$ *Rag2*$^{-/-}$ *Il2rg*$^{-/Y}$ mice (8 to 12 weeks old) were anesthetized by intra-peritoneal injection of about 300-350µL of a cocktail of Ketamine (50mg/kg), xylazine (10mg/kg) and acepromazine (1.7mg/kg). The mice were kept on a heating pad during surgery. They received oxygen (0.5 L/min) and anesthesia was maintained by continuous inhalation of 0.5% isoflurane (Merial, Harlow, United Kingdom). Deep anesthesia was confirmed by loss of reflex (pinching the toe and tail)

In order to image the kidney of either *Cx3cr1*$^{gfp/+}$ *Rag2*$^{-/-}$ *Il2rg*$^{-/-}$ or C57BL/6 mice, the fur from the left flank region was removed using a hair trimmer. The left kidney was surgically exposed after a small incision in the skin and body cavitiy was performed, without interrupting the blood flow or removing the capsule. The mouse was then placed in such a way the the kidney was positioned on a coverslip attached with high vacuum grease (VWR, Cat#DOWC636082B) to a custom-made aluminium tray stage (Life Imaging Services), coated with PBS-soaked strips of paper. The mice were further stabilized using two strips of adhesive tape gently applied on the front and back legs of the animal. The kidney was kept moist by applying pre-warmed (37ºC) PBS regularly. The whole microscope, mouse, stage and objectives were maintained at 37ºC for the

whole duration of the imaging sessions thanks to thermostat controlled heated chamber (Life Imaging Services).

2.7.2. Platelet study

Cx3cr1$^{gfp/+}$ *Rag2*$^{-/-}$ *Il2rg*$^{-/-}$ mice were prepared for intravital micrscopy of the kidney as described above ; after either 2h (steady state experiments) to measure the background number of monocytes, or 15 min of imaging ('R848 experiments') that allowed the stabilisation of the kidney in both YX plane and Z direction, 100µg of anti-GPIbα F(ab)$_2$ fragments (kind gift from Prof. Bernhard Nieswandt, University Clinic of Wuerzburg, Germany ; PBS as control) or full antibody (Emfret Analytics Cat#R300, non-immune rat IgG as controls, Emfret Analytics Cat#C301) were injected *i.v.* via the retro-orbital sinus while imaging, in order to block activation or deplete the platelets, respectively. For steady state experiments, the kidney was imaged for another 3h. For 'R848 experiments', 1h after injection, R848 (Invitrogen Cat# tlrl-r848-5) 400µL was applied at 0.5mg/mL in PBS, and the kidney was imaged for another 5h.

For platelet depletion experiments, at the end of the imaging session, the platelet count was obtained after tail vein bleeding, the blood was diluted 1/2 in warm (37ºC) PBS, and loaded into an automated cell counter (KX-21N from Sysmex Corporation).

2.7.3. Immune complex study

To measure the recruitment of monocytes and neutrophils induced by circulating immune complexes, *Cx3cr1*$^{gfp/+}$ *Rag2*$^{-/-}$ *Il2rg*$^{-/-}$ mice were injected *i.v.* at time 0 via tail vein with either BSA-TRITC (Invitrogen, Cat# A23016) or BSA-ICs at 1 : 1 molar ratio (50µg BSA + 125µg anti-BSA), obtained by incubating BSA and anti-BSA IgG for 1h at 4ºC. At time 2h, mice prepared for kidney intravital microscopy as indicated above, and imaged with channels for GFP and TRITC open. After 4h of imaging, neutrophils

were stained with a Gr-1 - APC antibody and the mice further imaged for 30 min.

2.7.4 Neutrophil and platelet staining during intravital imaging

For neutrophil quantification in the kidney of *Cx3cr1*$^{gfp/+}$ *Rag2*$^{-/-}$ *Il2rg*$^{-/-}$ mice, the fluorescence of the channel in which the staining was to be done was measured by imaging the kidney with the relevant channel open for 5min, then 10µg of either anti-Ly6G - PE (clone 1A8, BD Cat# 551461) or Gr-1 - APC (clone RB6 8C5, BD Cat# 553129) were injeted *i.v.* via the retro-orbital sinus while imaging. The kidney was then imaged for a further 30 minutes.

For platelet staining, an anti-CD49b – PE antibody was injected i.v. via retro-orbital sinus while imaging the renal cortex, and the organ was further imaged for 30 minutes.

2.7.5. Vascular permeability assay

C57BL/6 mice were prepared for imaging of the renal cortex as above. The vascular bed was visualized by *i.v.* injection of 100 µl 70 µM 70kDa Dextran-TRITC (Invitrogen, Cat#D1819) at t=0h. After 5 to 7 min, sterile PBS, low-endotoxin BSA (50 µg, Sigma #A8806), or BSA-ICs (50 µg BSA + 110 µg anti-BSA, prepared as described above) was administered intravenously, without interrupting the imaging. The kidney was imaged for a further 30 minutes to assess vascular leakage.

2.7.6. Intravital microscopy acquisition and analysis

Images were acquired using a 20x 0.5 NA PL Fluotar objective on a Leica TSC SP5 DM6000 confocal inverted microscope, with the Argon ion laser (488nm) for GFP excitation, DPSS 561nm laser for PE or TRITC excitation, and the HeNe laser (633nm) for APC excitation. The resolution was 512x512 pixels (or 1024x1024 for the vascular permeability assay, see below) and each image averaged from 2 scans (line average of

2). Images of the chosen field of view (XY plane) were taken every 4µm on the Z (depth) axis, until no signal was perceptible, and leaving 20-30µm below the surface of the kidney, in order to compensate for potential lowering of the position of the kidney with regards to the objective, for a total of ~80µm width of the volume, and a 40-50µm depth into the kidney. This volume was imaged sequentially, each volume consituting a time frame, of 50-60 seconds.

Quantification of leukocytes was done as follows. In *Cx3cr1*$^{gfp/+}$ *Rag2*$^{-/-}$ *Il2rg*$^{-/-}$, were counted as patrolling monocytes cells that were around 15µm in diameter, GFP^{+}, round, and mobile. This was in contrast to kidney resident macrophages, that were clearly larger (up to 100µm) cells with long, motile processes, though their cell bodies were still (Carlin et al., 2013; Stamatiades et al., 2016). Neutrophils were found as round, mobile PE^{+} cells when stained with Ly6G - PE, or GFP^{-} APC^{+} when stained with Gr-1 - APC. The quantification of neutrophils, cells were counted when the staining was maximal, generally within 10 minutes after staining antibody *i.v.* injection. Quantification of their numbers was done at specific times during the imaging session, typically every hour following an injection of kidney painting. At each time point, monocytes or neutrophils were counted throughout 5 time frames that spread around this time point. For example, for a count at '1h', the number of monocytes were counted at the time frames taken at 58min, 59min, 1h, 1h01 and 1h02. The numbers of cells for one mouse and one time point were the average of the counted cells during those 5 time frames.

2.8. Fast protein liquid chromatography (FPLC) analysis

BSA-ICs and OVA-ICs were generated as above (section ***2.7.3***) at Antigen:Antibody (Ag:IgG) ratios of 1:1, 5:1 or 10:1 (see **Table 2.3**). For controls, BSA, OVA, anti-BSA IgG or anti-OVA IgG were mixed with sterile PBS and incubated the same way,

keeping consistent volumes and concentrations. Using a 1 mL syringe the samples were then injected into a 100 µl loop linked to a Superose 6, 10/ 300 column placed in a ÄKTA FPLC system (GE Healthcare Life Sciences), where a constant flow rate of 0.5 mL/min was applied. Protein content was assessed by measurement of absorbance at 280 nm at the bottom of the column. The data was recorded and analyzed using the UNICORN software (GE Healthcare Life Sciences). The percentage of ICs was calculated by integrating the protein elution curve, and dividing the area under the black bars by the total area.

Table 2.3. *In vitro* preparation of immune complexes for FPLC

Antigen amount	**Antibody amount**	**Molar Ratio Ag:Ab**
BSA-TRITC 125µg	**Anti-BSA 312.5µg**	**1:1**
BSA-TRITC 625µg	**Anti-BSA 312.5µg**	**5:1**
BSA-TRITC 1,250µg	**Anti-BSA 312.5µg**	**10:1**
OVA 125µg	**Anti-OVA 437.5µg**	**1:1**
OVA 625µg	**Anti-OVA 437.5µg**	**5:1**
OVA 1,250µg	**Anti-OVA 437.5µg**	**10:1**
OVA 446.5µg	**Anti-BSA 312.5µg**	**5:1**

2.9. Mathematical model developed by our collaborators

Grégoire Altan-Bonnet and Amir Erez (NIH, Washington DC) generated an *in silico* model which, in general terms, describes the bone marrow, blood and spleen as a closed

system. A single pulse of EdU given to the mice allows to label a single wavw of proliferating progenitors and subsequently their progeny. Each cell population is considered in terms of its size (absolute numbers in whole body), proliferation rate (calculated based on experiments, see chapter 3), intensity of EdU signal (gMFI of EdU signal, informs on the number of divisions since the initial EdU pulse), and kinetics of EdU uptake and 'dilution' over time, i.e. the proportion of EdU^+ cells in each cell population over time (kinetics of EdU over 10 days, see chapter 3). A useful parallel, in our opinion, to understand the biological system as 'seen' by the mathematical model is that of communicating vessels. Each cell population constitutes a vessel, the size of which corresponds to the absolute number of cells for that population. The model aims at establishing communication between the various cell populations taking into account the speed at which content must flow from that cell type, determined by the proliferation rates. The flow between populations can be followed by using a single pulse of EdU: this not only informs on the proliferation rate, but also on the kinetic of dilution of EdU (gMFI of EdU signal) and its distribution throughout the different populations over time.

A major principle governing the model is that it must maintain the system 'homeostatic': this simply means that all cells that are produced (by proliferation) must 'disappear'. The rate of proliferation is established experimentally with early analysis of EdU uptake (see chapter 3). Because the pulse of EdU is very short, cells that become EdU^+ after ~1h post-injection must have acquired this proportion of EdU-labeled cells from cells upstream that have differentiated into them. The amount of time a cell remain EdU^+ informs on its life-span. Concerning the rate of disappearance of cells, it is difficult to measure experimentally; when a cell population sees a decrease in its proportion of EdU^+ cells it can correspond to four types of event: either the cell has divided enough times to bring the signal EdU below the threshold of detection by flow

cytometry; the EdU^+ cells may have differentiated into another cell population, therefore "pouring" into another cell population analysed by flow cytometry, or into another one not considered in the gating strategy; the 'disappearing' EdU^+ cell may also migrate into a tissue not isolated for flow cytometry analysis; finally, it may have died. Not all these events are measured experimentally, and therefore this parameter is allowed to vary.

Taking these elements into consideration, as well as many strictly statistical elements that can inform on the quality of the data set generated by flow cytometry (for example the stability of the measured sizes of populations during the various days of analysis), the mathematical model aims at establishing developmental relationships between the various cells. This way, it is hoped that the most mathematically relevant hypothesis will be most in line with the experimental EdU data. Once a hypothesis is yielded by the model, it has to be considered in light of data from the literature and the genetic data obtained previously in the laboratory.

3 – Studying monocyte development and dynamics towards an *in silico* model

3.1 Introduction and aims

As discussed above (***section 1.3.4***), the two main subsets of monocytes rely on distinct transcription factors for their development in the bone marrow. They also depend on different chemokine receptors for their migratory properties. *Nr4a1* has been shown to be necessary for Ly6C^{low} monocyte development and survival using the *Nr4a1*$^{-/-}$ mice and transfer experiments into irradiated hosts (Hanna et al., 2011). However, although transfer experiments have shown a cell-intrinsic role of *Nr4a1* in the

development and survival of Ly6C^{low} monocytes, the ubiquitous expression of *Nr4a1* throughout the organism raises the worry of side effects of knocking out *Nr4a1* outside of the hematopoietic system.

With this in mind, *Csf1r*^{iCre} mice were crossed with *Nr4a1*$^{f/f}$ mice, to generate *Csf1r*^{iCre} *; Nr4a1*$^{f/f}$ and littermate controls, which are deficient for *Nr4a1* in hemotopoietic cells only, in all lineages studied (Hannah Garner's data, not shown). Analysis of the bone marrow of these mice revealed a population that was c-Kit^{-} CD11b^{+} Ly6C^{low} MHC-II^{-} similarly to BM Ly6C^{low} monocytes, but was CD115^{low} at the surface protein level, while expressing similar levels of the CD115 transcript to that of Ly6C^{low} BM monocytes (Hannah Garner's data, not shown). This BM CD115^{low} population was critically *Nr4a1*-dependent, as lacking one allele of *Nr4a1* was sufficient to reduce this population by almost 40%. The remaining cells of this population, similarly BM Ly6C^{low} monocytes, in conditional *Csf1r*$^{iCre+}$ *Nr4a1*$^{\Delta/\Delta}$ mice, proliferated intensively compared to their *wt* littermates, as seen by BrdU incorporation and Ki67/DAPI staining. Lack of *Nr4a1* also induced a higher apoptosis rate of the remaining BM CD115^{low} population. Finally, the BM CD115^{low} population was found to express *Nr4a1* at similarly high levels as Ly6C^{low} monocytes, and they specifically lack, in a haplo-deficient manner, in *Nr4a1*$^{-/-}$ mice. Together, these data obtained by Hannah Garner suggested that this BM CD115^{low} population may represent a direct precursor to Ly6C^{low} monocytes in the bone marrow. Therefore, it was taken into account in the analyses presented in this work

The analysis during steady state of the blood, spleen and bone marrow of *Csf1r*$^{iCre+}$ *; Nr4a1*$^{\Delta/\Delta}$ mice revealed, consistent with the results obtained in *Nr4a1*$^{-/-}$ mice (Hanna et al., 2011), that Ly6C^{low} MHC-II^{-} monocytes were specifically missing, compared to *Csf1r*$^{iCre-}$ *; Nr4a1*$^{f/f}$ littermate controls, in all three organs. Interestingly, MHC-II^{+} monocytes, expressing various levels of Ly6C, including cells that are Ly6C^{low} MHC-

II$^+$, were not affected by hematopoietic-specific KO of *Nr4a1*. These cells may account for the remaining Ly6C^{low} monocytes seen in the full *Nr4a1*$^{-/-}$ mice as shown by Richard Hanna and colleagues (Hanna et al., 2011). Ly6C$^+$ MHC-II$^-$ monocytes were unaffected by the conditional knock-out of *Nr4a1*. Finally, the BM CD115^{low} population was also strongly reduced by *Nr4a1* deficiency as presented above.

Conversely, when analysing the bone marrow, blood, and spleen of mice lacking *Irf8* (*Irf8*$^{-/-}$), Ly6C$^+$ MHC-II$^-$ monocytes in all organs were strongly decreased, as well as Ly6C^{int} MHC-II$^+$ cells. Ly6C^{low} MHC-II$^-$ monocytes from bone marrow, blood and spleen were unaffected in terms of numbers. This lack of MHC-II$^+$ monocytes, among which some cells are Ly6C^{low}, may reflect the slightly decreased numbers of total Ly6C^{low} monocytes observed previously. Also, bone marrow Ly6C$^+$ monocytes were strongly reduced, while cMoP were strongly increased in number, seemingly accumulating, consistent with previous findings (Kurotaki et al., 2013 ; Kurotaki et al., 2014 ; Schonheit et al., 2013).

Finally, analysis of *Ccr2*$^{-/-}$ mice and littermates allowed to find similar results as previously in steady state (Serbina and Pamer, 2006) : Ly6C$^+$ MHC-II$^-$, although not lacking in the circulation, were strongly reduced in the blood, and spleen, and very small changes were observed in the bone marrow in the steady state. Similar observations can be made for the Ly6C^{int} MHC-II$^+$ cells ; however, Ly6C^{low} MHC-II$^-$ monocytes were unaffected in the *Ccr2*$^{-/-}$ mice compared to littermates.

Therefore, the separation of monocytes into MHC-II$^-$ and MHC-II$^+$ cells, in addition to Ly6C, seems to overall help delineate monocyte population more precisely. These genetic data are compatible with two distinct pathways of differentiation for monocytes : Ly6C$^+$ MHC-II$^-$ cells that are *Irf8*-dependent, *Nr4a1*-independent ; Ly6C^{int}

MHC-II^{+} monocytes that have the same genetic requirements, and Ly6C^{low} MHC-II^{-} monocytes, the patrolling subset, that are *Irf8*-independent *Nr4a1*-dependent.

This is not in line with the current model of monocytes development, which suggests that Ly6C^{low} monocytes are a product of Ly6C^{+} monocyte conversion in the circulation (Hettinger et al., 2013; Varol et al., 2007; Yona et al., 2013). However, the data presented so far may not be enough to fully support any hypothesis.

Therefore the aim of this thesis was to re-examine monocyte dynamics in hematopoietic compartments (bone marrow, blood and spleen) using experimentally parameterized and computer-assisted mathematical modeling, developed by Grégoire Altan-Bonnet and Amir Erez (National Institute of Health, Washington). Presented here are the results of some of the experiments that allowed to pin down some of the parameters of the model, as well as data that has been modeled. This was done with the intent to provide a hypothesis for monocyte dynamics, and notably the developmental origin of Ly6C^{low} monocytes, with the support of mathematical analysis of biological data (**Figure 3.0**).

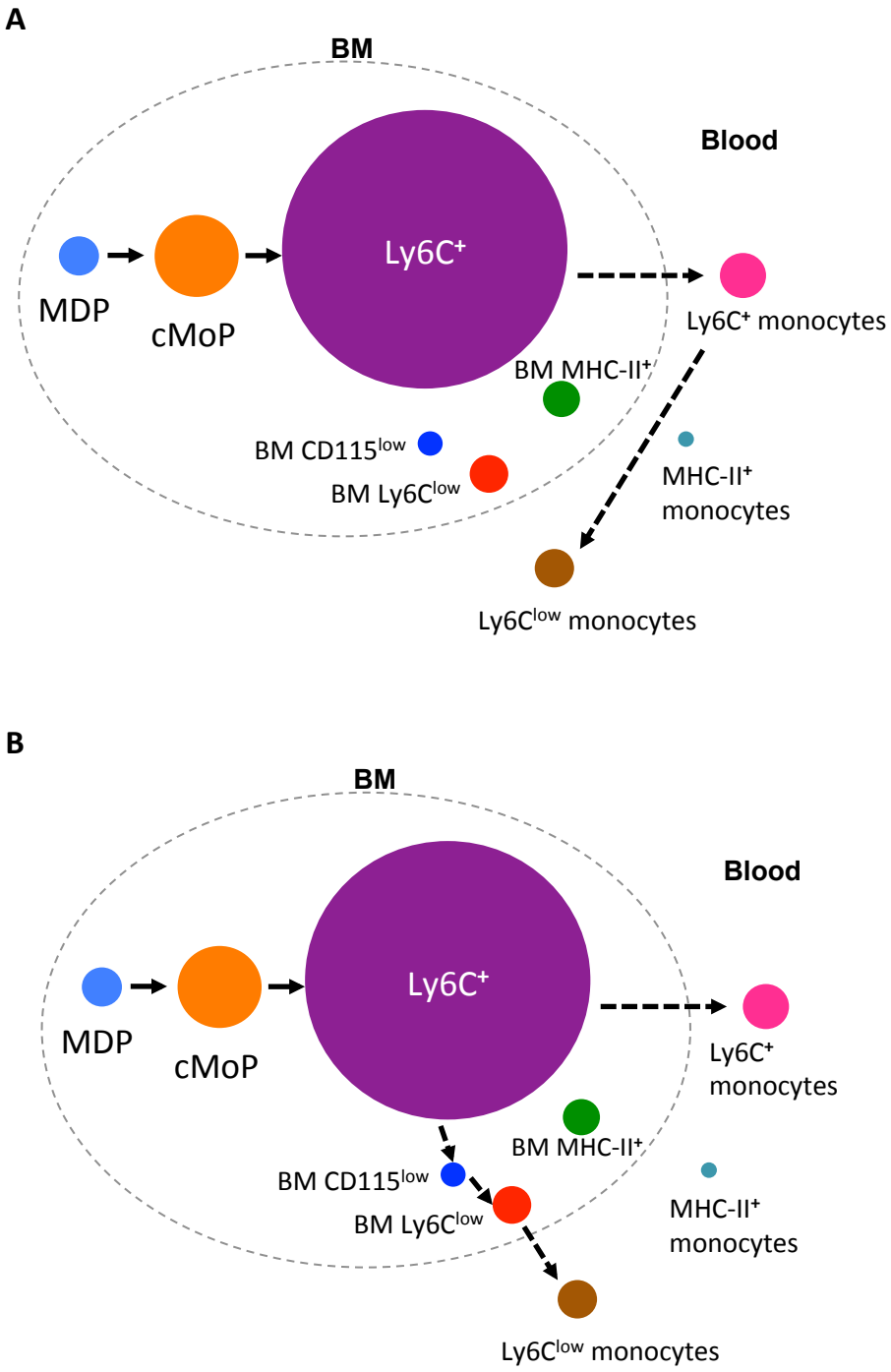

Figure 3.0. Different hypotheses for monocyte development.
(A) Several studies suggest that monocytes exit the bone marrow as Ly6C^{+} cells, that mature, or convert, into Ly6C^{low} monocytes, in the periphery under the control of homeostatic and inflammatory cues (Yona et al., 2013).
(B) Alternatively monocyte heterogeneity may result from a differentiation process in the bone marrow under the control of specific transcription factors and growth factors (Hanna et al., 2011).
The area of each circle represents the population size *in vivo* (see Methods)

3.2. Characterisation of the biological system and of the methodology for study of monocyte dynamics

3.2.1. Gating strategy and morphology of the studied cell populations

Blood and bone marrow were analysed in adult C57BL/6 male mice, by flow cytometry. Monocytes and their known late progenitors MDP (Fogg et al., 2006) and cMoP (Hettinger et al., 2013) were gated as classically done, with the use of c-Kit, CD115 (CSF-1R), CD11b and Ly6C expression, as well as MHC-II to distinguish three monocyte populations in the blood and bone marrow (**Figure 3.1**). MDP and cMoP were defined as Lineage negative (CD3, CD19, NKp46, Sca-1, Ly6G), c-Kit$^+$ CD115$^+$, CD11b$^-$, with MDP as Ly6C$^-$ and cMoP as Ly6C$^+$ (**Figure 3.1-A,** *top*). The BM CD115^{low} population was defined as Lineage negative, Ly6C^{low} CD11b$^+$ MHC-II$^-$ c-Kit$^-$ CD43$^+$ (**Figure 3.1-A**, *bottom*). Blood and bone marrow monocytes were defined as Lineage negative (CD3, CD19, NKp46, Ly6G), CD115$^+$ CD11b$^+$ and subdivided in Ly6C$^+$ MHC-II$^-$, Ly6C^{int} MHC-II$^+$ and Ly6C^{low} MHC-II$^-$ (**Figure 3.1-A, B**). The same gating strategy as for blood samples was adopted for spleen monocytes (data not shown).

Each of these population was FACS sorted and their morphology was analysed by cytospin followed by May-Grünwald Giemsa staining. MDP, cMoP and the BM CD115^{low} cells had a round shape, and small cytoplasm with a high nucleus/cytoplasm size ratio (**Figure 3.1-A**). BM Ly6C$^+$ monocytes appeared slightly heterogeneous in terms of morphology ; most cells had similar morphology as blood monocytes, with a bean-shaped nucleus and small filipodiae, but some had a rounder shape. Some were isolated as they were dividing, as seen by the shape of their nucleus (**Figure 3.1-A**), a feature also seen for some MDP and cMoP (data not shown). Because monocytes of the blood do not proliferate (Geissmann et al., 2003 ; Shand et al., 2014), and in line with

previous findings (Chong et al., 2016; Menezes et al., 2016; Shand et al., 2014), this heterogeneity in morphology might be representative of the fact that BM Ly6C^{+} cells may not be best termed 'monocytes'. They will from now on be referred to as 'BM Ly6C^{+} cells' to avoid confusion with blood or spleen monocytes. Ly6C$^{\mathbf{low}}$ monocytes of the BM had a classic monocyte morphology with a bean-shaped nucleus, and so did blood monocytes of both classical subsets. MHC-II^{+} monocytes of both bone marrow and blood had a similar morphology as classical monocytes, with small filipodiae, bean-shaped nuclei and vacuoles (although these might be due to the cells staying too long in FBS after the sort, before being spun onto the L-Lysine coated slides).

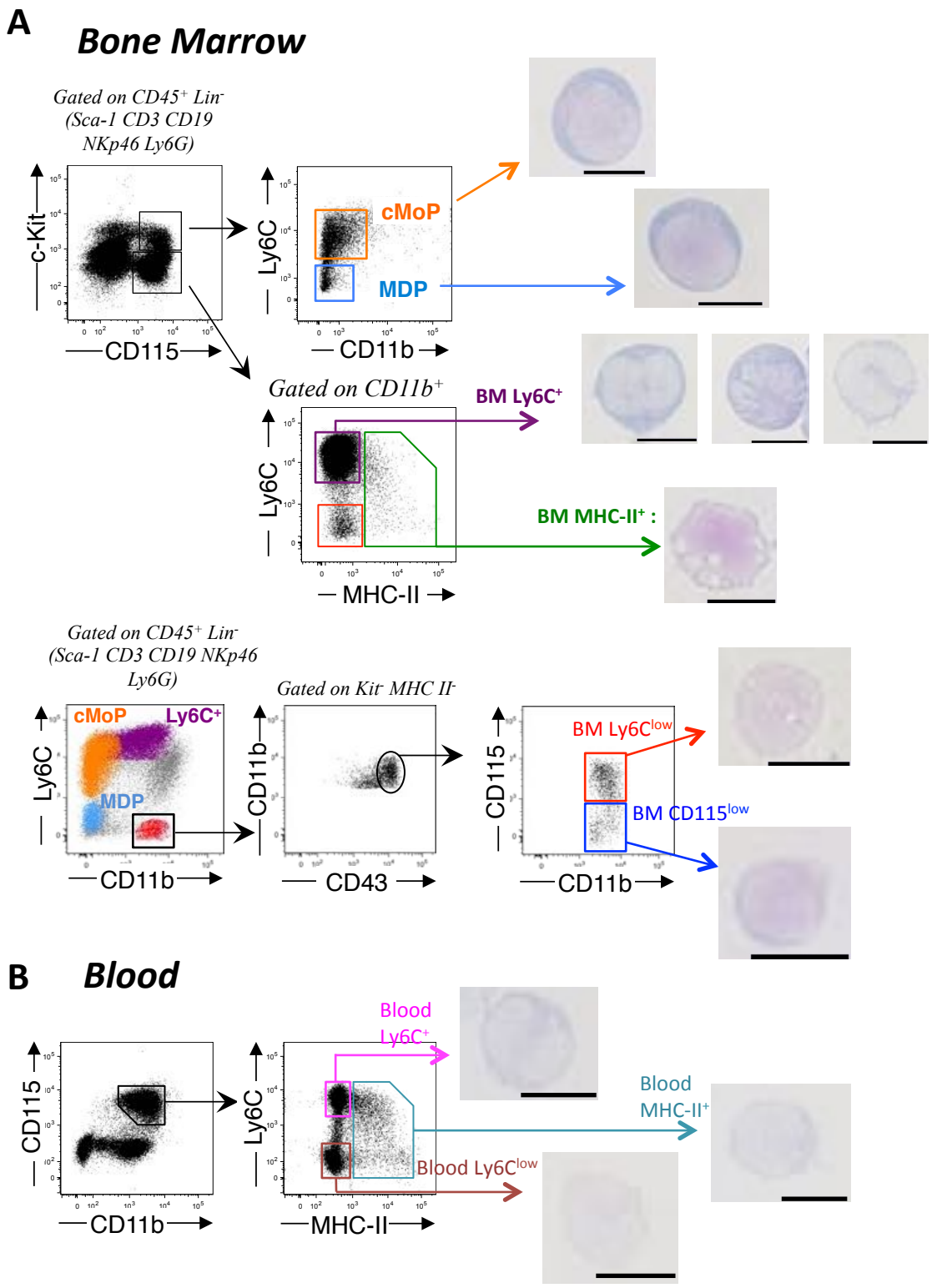

Figure 3.1: Gating strategy and morphology of the bone marrow and blood prospective populations. (A) Bone marrow from C57BL/6 was collected and the indicated populations were FACS sorted (2000 to 10,000 cells), cytospun on L-Lysin-coated slides, and a May-Grünwald-Giemsa staining was performed. Images are representative of at least 50 cells observed for each population, using a 100x oil objective. For the BM Kit$^-$ CD115$^+$ Ly6C$^+$ cells, representative images of the different morphologies observed are shown. **(B)** Blood from C57BL/6 mice was collected and the indicated monocyte populations were FACS sorted (5,000 to 10,000 cells) Scale bars = 10µm

3.2.2. Size of the populations, blood and bone marrow as separate compartments

Because the size of the cell populations is a critical parameter of the mathematical model, the various populations of cells in blood and bone marrow in the whole body had to be quantified. These quantifications have been made by others, and their results were used as estimates. First, for the bone marrow, Colvin and colleagues (Colvin et al., 2004) have estimated that femurs contain 10% of the bone marrow of the whole body, while tibiae contain 4% of whole bone marrow. Therefore, the sizes of the bone marrow cell populations for whole body BM were calculated considering that the absolute numbers obtained from two femurs and two tibiae constituted 14% of it.

For blood populations, estimations made previously were used: mice have 80mL of blood per kg of body weight, and weigh 25g on average (Hakness and Wagner, 1995; Mitruka and Rawnsley, 1981), therefore the estimation of 2mL of blood per adult mouse was used.

Finally, similar phenotypes are considered for blood monocytes and their apparent BM counterparts : these cells are gated as c-Kit$^-$ CD115$^+$ CD11b$^+$ in both organs, within which Ly6C$^+$ MHC-II$^-$, Ly6C^{int} MHC-II$^+$ and Ly6C^{low} MHC-II$^-$ cells are present and gated as such (**Figure 3.2-C**). It is therefore relevant to ask whether some cells analysed in the bone marrow may actually be blood cells that were circulating in the bone marrow at the time of the mouse sacrifice. Estimations of the amount of blood in the bone marrow have been made previously : Osmond and colleagues found that 2% of the circulating blood was to be found in the bone marrow ; conversely, 5% of the bone marrow volume is made out of blood (**Figure 3.2-B**). Using these estimations, the amount of blood cells among bone marrow populations were calculated (**Figure 3.2-C**). 'Contamination' of blood populations into BM cells was minimal, as 0.6 - 3% of cells found in the bone marrow cells are blood cells (**Figure 3.2-C**). Therefore the bone

marrow populations analysed were likely in the parenchyma of the bone marrow, and constitute a compartment distinct from the blood.

Finally, because modeling monocyte dynamics would be performed with long-term pulse-chase of nucleoside analog experiments, the identification of proliferating populations was first assessed by analysing EdU (5-ethynyl-2'-deoxyuridine) uptake at 1h post intraperitoneal injection to adult C57BL/6 males (**Figure 3.2-D**). This allowed the identification of the MDP, cMoP and BM Ly6C^{+} cells as the main proliferative cells within the analysed compartments, consistent with the literature (Fogg et al., 2006 ; Hettinger et al., 2013 ; Shand et al., 2014 ; Geissmann et al., 2003), and with previous results obtained by Hannah Garner in the laboratory, by BrdU (5-bromo 2-deoxyuridine) incorporation and Ki67/DAPI satining (data not shown). Therefore these populations were the focus of the next set of experiments.

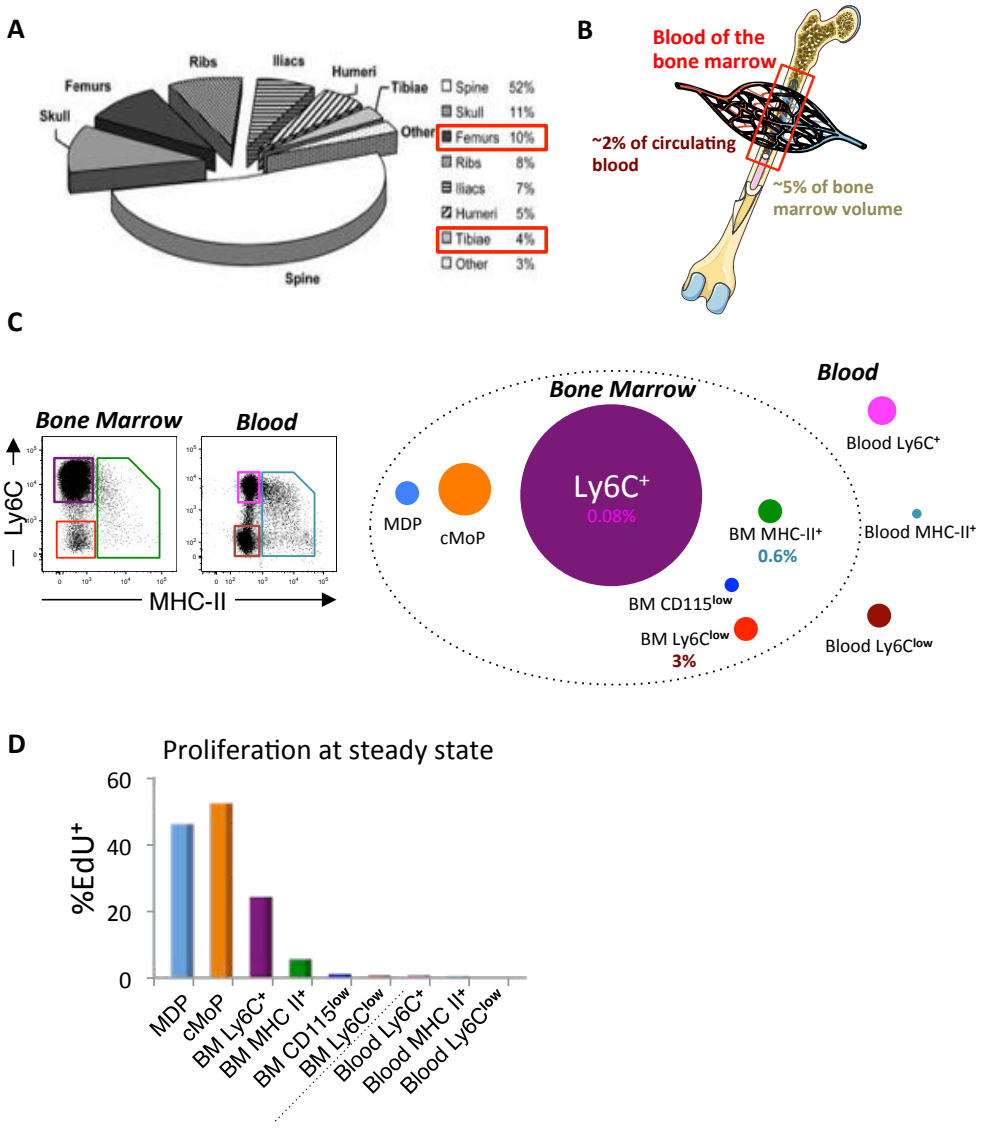

Figure 3.2. Cellularity of Bone Marrow and Blood, two separate compartments, and proliferation at steady state. **(A)** Cellularity of the bone marrow was quantified in the whole skeleton of a Balb/c mouse; together, femurs and tibiae amount to 14% of the total bone marrow. Adapted from Colvin et al., 2004. **(B)** The volume of blood found in the bone marrow (red rectangle) represents 2% of the whole circulating blood volume, and constitutes 5% of the bone marrow volume. Estimations from Osmond et al., 1965. **(C)** Similar phenotypes for blood monocytes and bone marrow monocytes or pro-monocytes, by flow cytometry (*left*). Bone Marrow and blood prospective populations as circles (*right*); the size of the circles reflects the size of the populations *in vivo*, for whole body bone marrow (in the estimation from (A)) and whole circulating blood (2mL, Hakness and Wagner, 1995; Mitruka and Rawnsley, 1981). Percentages represent the 'contamination' from blood cells within the bone marrow cell numbers, in the estimation from (B). **(D)** Proliferation of prospective populations, measured by EdU incorporation 1h after injection of 0.5mg EdU i.p. These data suggest that MDP, cMoP and BM Ly6C$^+$ cells are the main proliferative populations of the bone marrow, among the cells analysed.

3.2.3. Characterisation of the EdU pulse and of the first division of proliferating cells

Another parameter that the model requires, and that can be measured experimentally, is the proliferation rate of the different populations considered. For this, it was first necessary to know for how long the *i.p.* injected EdU is available for the cells in S-phase to take up. The intensity of the EdU signal in cells that did take it up was also an important measure, as it represents the amount of EdU contained in the cells. To investigate this issue, groups of three mice were injected with a single dose of 0.5mg of EdU *i.p.*, and the EdU content (both the proportion of cells from the proliferative populations, and the intensity of the signal) was measured, in the MDP, cMoP and BM Ly6C$^+$ cells, from 15min after injection, and every 15min until 2h (**Figure 3.3-A**). The results show that the percentage of EdU$^+$ cells within the analysed populations was already maximal at 15min post-injection (**Figure 3.3-B**). This suggests a bio-availability of EdU that is very short. Therefore the EdU pulse constitutes a very narrow window during which the cells are able to pick up EdU. Interestingly, however, the intensity of the EdU signal, measured by the geometric Mean Fluorescence Intensity (gMFI) in EdU$^+$ cells, increased from 15 min to 1h (**Figure 3.3-A, B**), after which the gMFI values plateaued (**Figure 3.3-B**). This suggests that, although the cells only take up EdU for no longer than 15min, it takes around 1h for the EdU to be fully incorporated into the DNA during the S-phase.

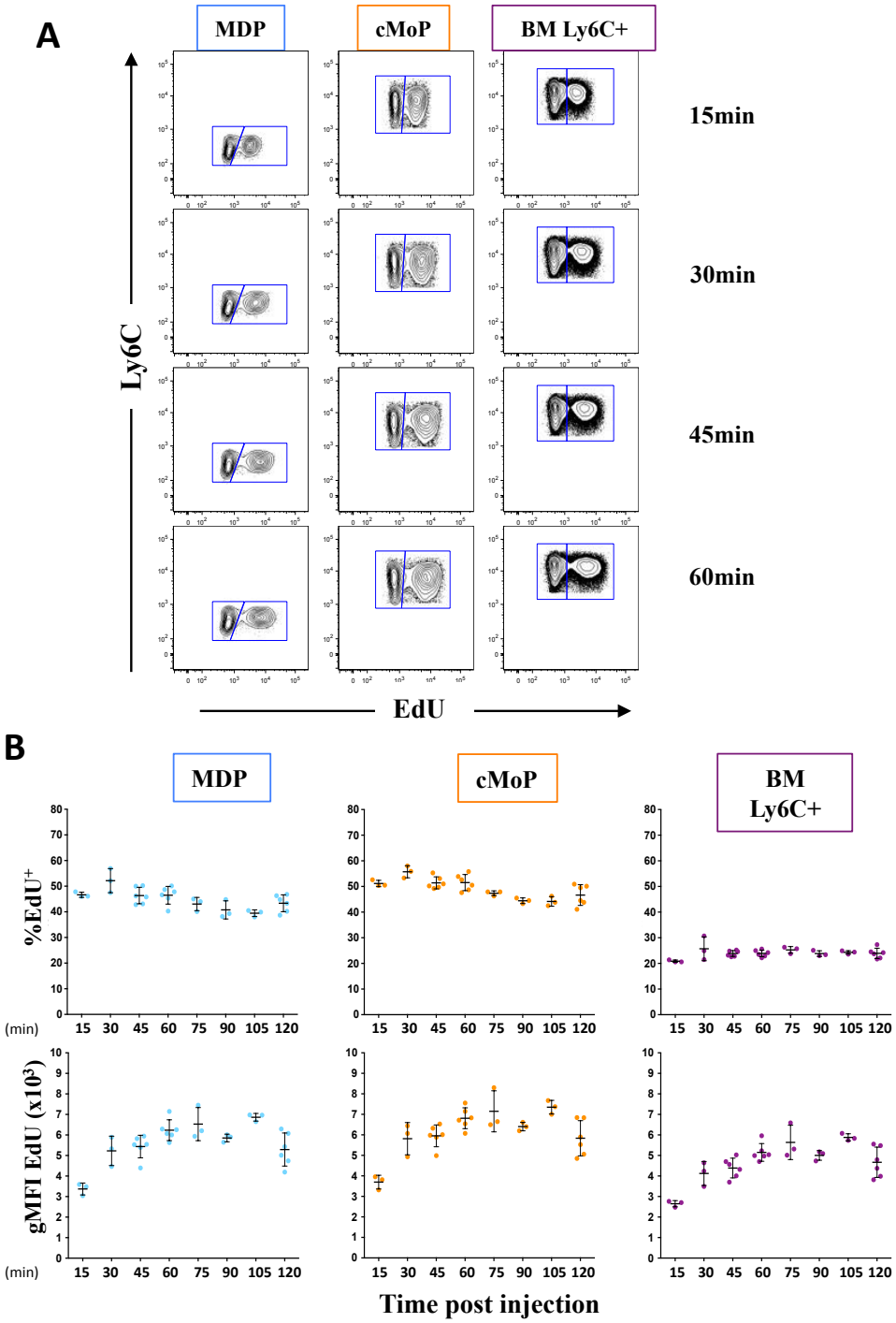

Figure 3.3. Characterisation of the EdU pulse. C57BL/6 mice were injected intraperitoneally with 0.5mg of EdU. At the indicated times after injection, their bone marrow was analysed by flow cytometry for EdU content in prospective populations **(A)** EdU content in prospective populations. Cells were gated as Lineage (CD3, CD19, NKp46, Sca-1, Ly6G) negative, $CD115^+$ $c\text{-}Kit^+$ (MDP and cMoP, $Ly6C^-$ and LyC^+ respectively) or $CD115^+$ $c\text{-}Kit^-$ (BM $Ly6C^+$). Contour plots representative of 3 – 6 mice per time point. **(B)** Percentage of EdU^+ cells in the MDP, cMoP and BM $Ly6C^+$ cells at the indicated times after EdU injection (top); geometric Mean Fluorescence Intensity (gMFI) of the EdU signal in the EdU^+ cells, among MDP, cMoP and BM $Ly6C^+$ cells (bottom). Each dot represents a mouse, 3-6 mice per time point, bars represent mean ± SD.

Therefore, these experiments characterise a short EdU pulse of 15 minutes, and the maximum intensity of the signal is reached after 1h. Based on these experiments, our collaborators were able to calculate the proliferation rates of the various populations of the bone marrow, using a method similar to that of Schittler and colleagues (Schittler et al., 2013).

Next, EdU incorporation was investigated for up to 12h post EdU injection (**Figure 3.4**). Following %EdU^+ cells within MDP, cMoP and BM $Ly6C^+$ cells, an increase in the proportion of EdU^+ cells was observed starting at 2h and up to 12h (**Figure 3.4**, *blue dots*). Parallel to this increase in %EdU^+ cells, a drop of around half in the intensity of EdU signal within the EdU^+ cells was observed starting at 2h post EdU injection (**Figure 3.4**, *red dots*). This suggested two things. First, that starting at 2h post EdU injection, the cells that were caught in S-phase during the EdU pulse were starting to perform mitosis, giving rise to daughter cells with half the EdU content of that of first-generation cells. Second, given the size of the populations (calculated in **Figure 3.2-C**), all cMoP that had taken up EdU during the pulse, had to each give rise to 2 daughter cells differentiating quickly to BM $Ly6C^+$ cells.

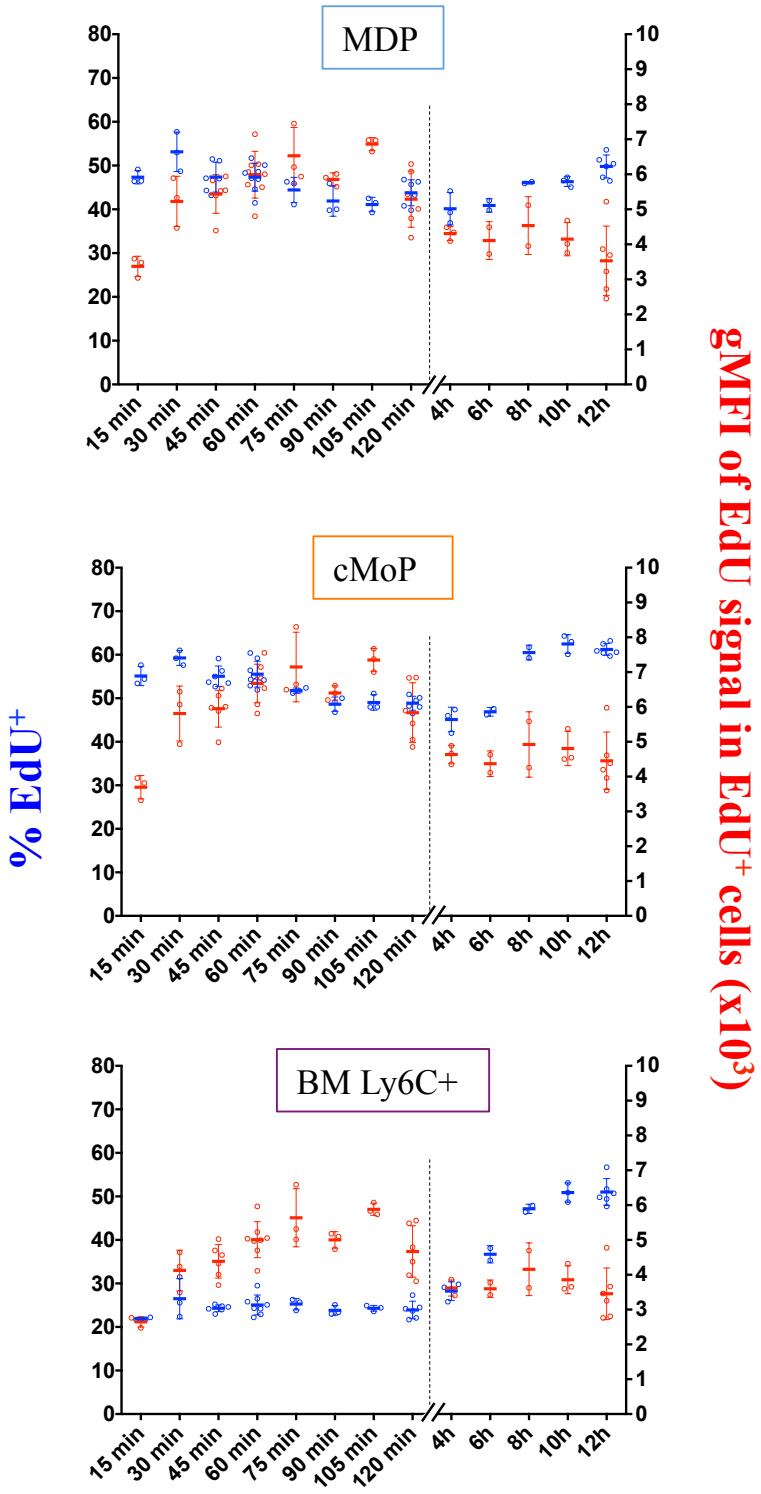

Figure 3.4. Kinetics of EdU incorporation and dilution over 12 hours. C57BL/6 mice were injected intraperitoneally with 0.5mg EdU. At the indicated times after injection (every 15min to the left of the dotted line – see also previous figure; every 2 hours to the right of the dotted line), their bone marrow was analysed for EdU content in the indicated populations (MDP, cMoP and BM Ly6C$^+$). Graphs show the proportion of EdU$^+$ cells within each population (blue, read on left axis) and the gMFI of the EdU signal of the EdU$^+$ cells (red, read on the right axis). Each dot represents an individual mouse. n=3 to 8 mice per time point. Bars represent mean ± SD.

In order to investigate further whether a step forward in cell cycle was happening around 2 to 4h after EdU injection, the size of the EdU^+ cells was analysed at the various time points between 1h and 12h (**Figure 3.5**). When analysing the Forward and Side Scattering of light (FSC/SSC), respectively informing on size and granularity of cells in flow cytometry, EdU^+ cells at 1h (just after the pulse) had high FSC/SSC intensities, suggesting their cell cycle was still in progress. Starting at 2h, but mainly visible at 4h, EdU^+ cells with lower FSC/SSC started to appear, showing they had completed cell division (**Figure 3.5**). This was consistent with the drop in gMFI of the EdU^+ cells observed at 2h and 4h as shown in **Figure 3.4**.

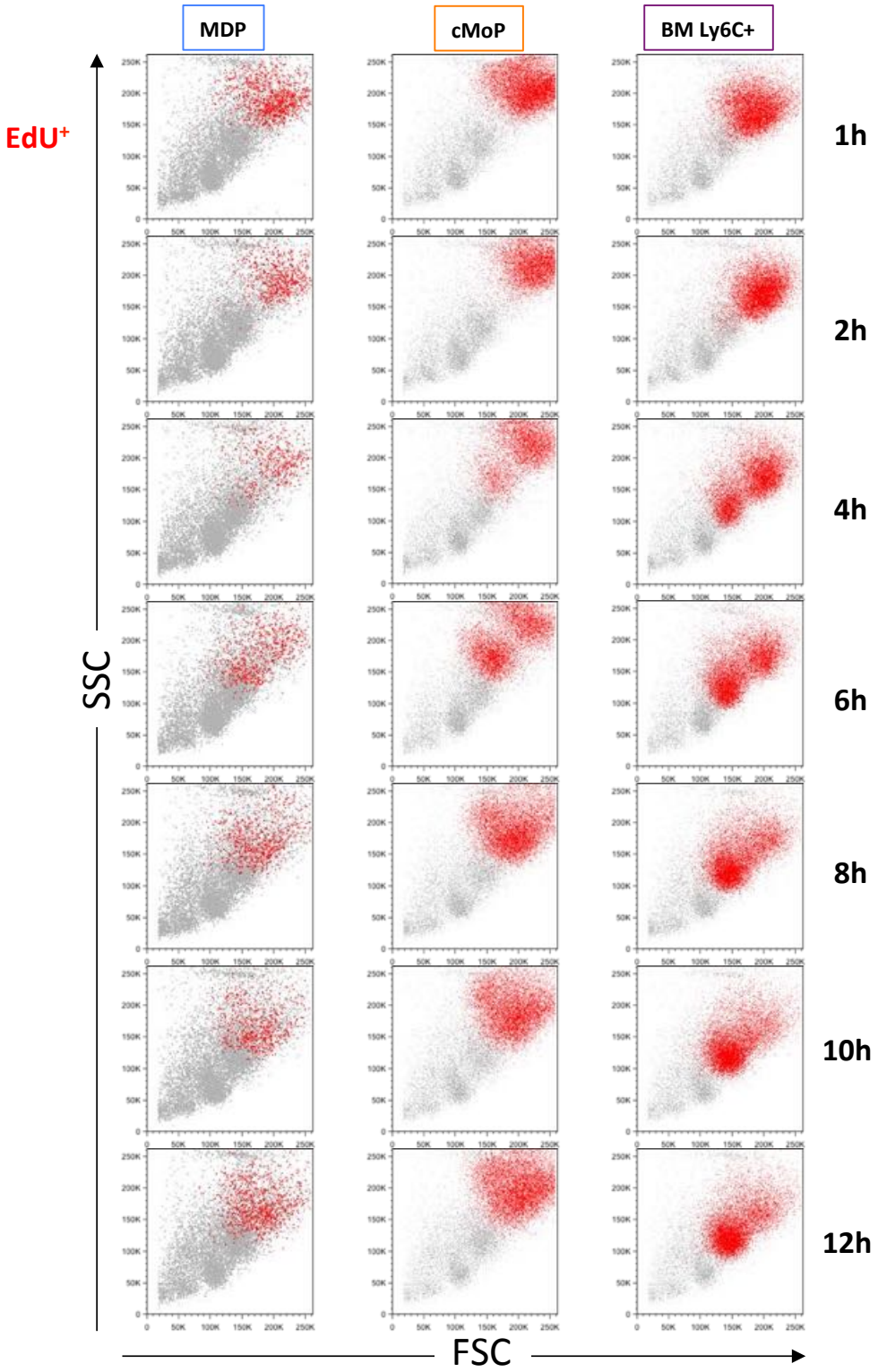

Figure 3.5. FSC/SSC profile of proliferating cells after a single pulse of EdU. C57BL/6 mice were injected i.p. with a single dose of EdU (0.5mg), and their bone marrow was analysed for EdU content at the time points indicated on the right. EdU^+ cells (*red*) from the populations indicated at the top (MDP, cMoP and BM $Ly6C^+$) were backgated to show their FSC/SSC profile against the total BM cells (*grey*). Representative of 3-6 mice per time point. Cells of lower FSC and SSC start clearly appearing at 4h after EdU injection.

Together, these data of EdU incorporation during the first 12h after injection showed that a single injection of EdU provided a very short pulse for cells to take up the nucleoside analog, and that cells started to undergo mitosis at 2 to 4h after injection, with the daughter cells seemingly differentiating very quickly from cMoP to Ly6C^{+} cells. In terms of information for the mathematical model, this informed the length of the labeling phase of EdU (15min), identified 1h post injection as the time for which the signal intensity was maximum and from which the proliferation rates could be calculated ; it also showed that both daughter cells from the late progenitors had to give rise to the next step of differentiation, as opposed to an 'asymetric' mitosis, where a progenitor would give rise to a daughter cell identical to the mother cell, and another daughter cell differentiating forward.

3.2.4. Kinetics of EdU incorporation and dilution over 10 days

After establishing some aspects of the biological system under study, a single pulse of EdU was given to groups of three male C57BL/6 mice and EdU content in the bone marrow, blood and spleen prospective populations of monocytes and late progenitors was analysed from 1h to 10 days after injection (**Figure 3.6**). For all populations in all organs, there was a phase during which the proportion of EdU content reached its maximum, followed by a decrease in %EdU^{+}. For MDP and cMoP, maximum %EdU^{+} was at the very start and only decreased over time. For BM Ly6C^{+} and BM MHC-II^{+} cells, some cells were proliferating as shown by their EdU content at 1h, and proportion of EdU^{+} cells increased during the next 48h, before starting to decrease. This suggest an imput of EdU^{+} from upstream cells before futher differentiation. Finally, BM CD115$^{\mathbf{low}}$ cells, BM Ly6C$^{\mathbf{low}}$ monocytes, as well as blood and spleen monocytes, started as EdU^{-}, showing they don't proliferate at steady state (consistent with the literature, Geissmann

et al., 2003 ; Shand et al., 2014). They only started to show a proportion of EdU^+ cells later on ; the analysis of the pulse (**Figure 3.3**) shows that this cannot be due to these cells entering cell cycle and taking up EdU (the second analysed time point was 12h post EdU injection, long after the EdU has stopped being available for cells in S-phase). This rather suggests an imput of EdU-labeled cells from upstream of the differentiation process. Interestingly, blood and spleen monocytes had overlapping kinetics of EdU incorporation and dilution, excluding the spleen as a site of production for blood monocytes in the steady state.

Searching for succession of EdU peaks over time between two populations is not sufficient to establish a precursor-progeny relashionship between them. Indeed, such an analysis could result in various different and overlapping differentiation pathways. This data set (including the population sizes as shown in **Figure 3.2-C**, taking into account the results of the early EdU time points shown in **Figures 3.3** and **3.4**, as well as the gMFI of the EdU signal for the data set shown in Figure 3.6 – see **Supplemental Figure 3.1**), was therefore analysed with the *in silico* model by our collaborators Grégoire Altan-Bonnet and Amir Erez. However, their analysis showed that the production of $Ly6C^{low}$ monocytes in the blood and bone marrow could not be explained by a mathematical analysis of the prospective populations as they were described in this experiment. Notably, it pointed to a potential population that would act as a 'missing link' in the bone marrow, between the actively proliferating populations (MDP, cMoP and BM $Ly6C^+$), and the $Ly6C^{low}$ monocytes of the blood and spleen. Therefore, a set of experiments was designed, aiming for the identification of such cells.

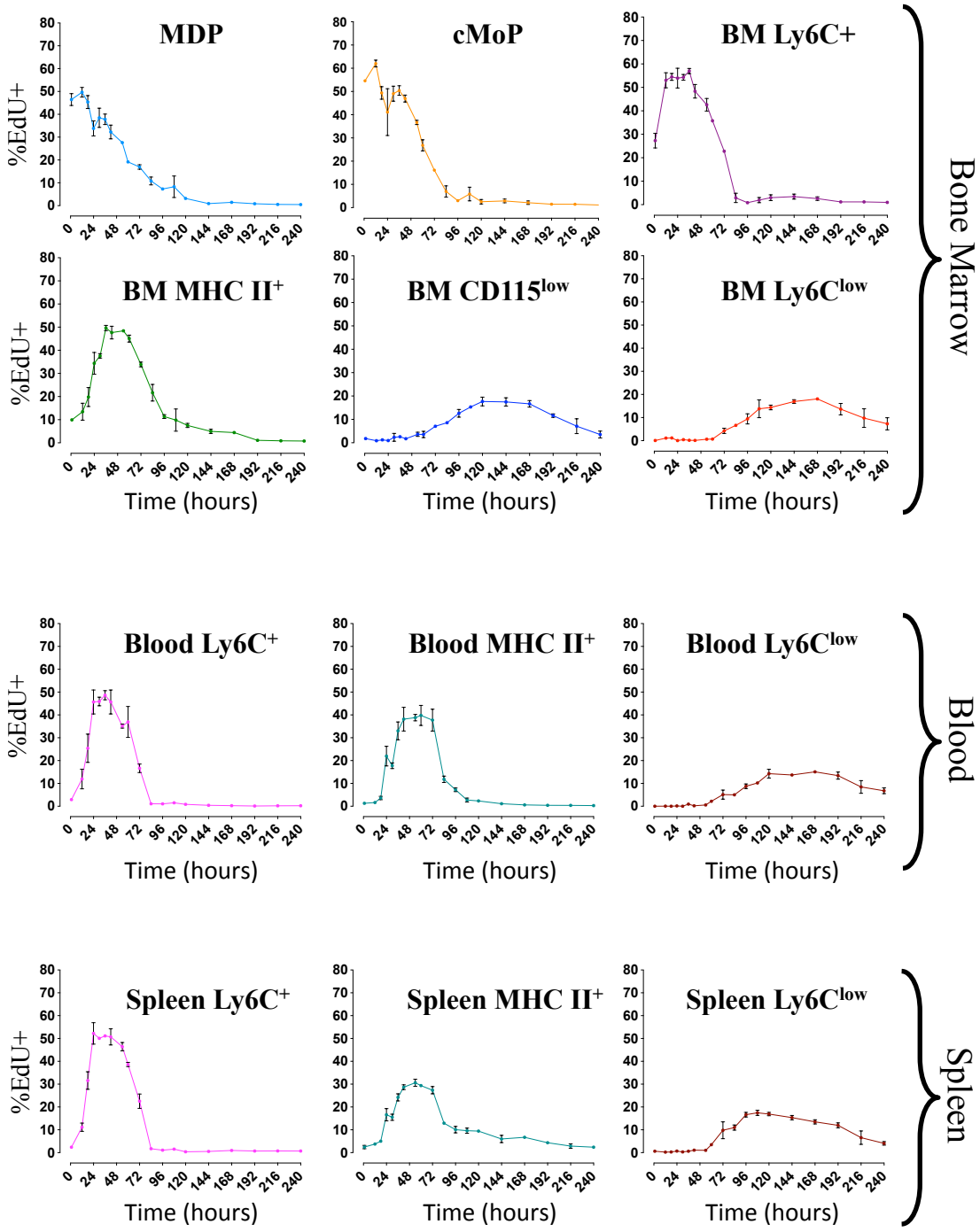

Figure 3.6. Kinetics of EdU incorporation and distribution over 10 days
C57BL/6 mice were injected with a single dose of 0.5mg of EdU intraperitoneally, and sacrificed at the indicated time points after injection for analysis of their BM (top), Blood (middle) and Spleen (bottom) for EdU content in the indicated populations. n=3 mice per time point. Bars represent mean ± SD

3.2.5. Search of a potential 'missing link' in the bone marrow, by CyTOF

In order to identify a population that could act as a 'missing link' in the differentiation process of Ly6C^{low} monocytes, two transgenic mouse models were used : first the *Cx3cr1*$^{gfp/+}$ knock-in mice (Jung et al., 2000), on a *Rag2*$^{-/-}$ *Il2rg*$^{-/-}$ background, in which monocytes are the only blood cells to express GFP under the control of the *Cx3cr1* promoter (Auffray et al., 2007). All prospective populations analysed express *Cx3cr1-gfp* (**Figure 3.7-A**), consistent with previous results from the lab and with the literature (Geissmann et al., 2003 ; Fogg et al., 2006 ; Hettinger et al., 2013, Yona et al., 2013). It was therefore expected that if there was a population of interest to be found, it would also express *Cx3cr1-gfp*. The second model was that of *Nr4a1*^{GFP} mice, because Ly6C^{low} monocytes express high levels of *Nr4a1*^{GFP} (**Figure 3.8-A**, consistent with previous results from the lab) and are dependent on *Nr4a1* for their development (Hanna et al., 2011). We took advantage of CyTOF (mass Cytometry by Time Of Flight), in which a large number of extracellular and intracellular markers can be detected with antibodies conjugated to heavy isotopes of various metals.

Staining the bone marrow of *Cx3cr1*$^{gfp/+}$ *Rag2*$^{-/-}$ *Il2rg*$^{-/-}$, and *Rag2*$^{-/-}$ *Il2rg*$^{-/-}$ as controls for the GFP staining, the bone marrow was analysed in two parallel ways. On one hand, the prospective populations were gated, within the GFP^{+} cells, with the same strategy as in **Figure 3.1**, which resulted in the isolation of the same populations as in the WT animals analysed by fluorescence flow cytometry (**Figure 3.7-B**). In addition, total Lineage negative GFP^{+} cells were subjected to a t-SNE (t-distributed Stochastic Neighbor Embedding) clustering analysis (Van Der Maaten and Hinton, 2008). This technique analyses each cell in a high dimensional space, where each marker measurement constitutes a dimension. Each cell is compared to all the other cells in

terms of all the markers it expresses, and cells that are phenotypically similar are clustered together, within this high dimensional space. The major interest of t-SNE is its ability to perform what is termed a dimension reduction, which means that the clustering of the cells in the high dimensional space is represented in a 2-dimensional dot plot, in which the relative distance between the cells, i.e. the clustering of cells, is conserved. Therefore, it allows to conserve the information gained in high dimensional space, that is taking into account all the cell markers, and to represent it in a dot-plot. This constitutes a tool for the clustering of cell populations that is less biased than classical gating. The result of the t-SNE performed on total lineage negative, *Cx3cr1-gfp*$^{+}$ cells is shown in **Figure 3.7-C**. Then, cells gated in **Figure 3.7-B** were overlayed on the t-SNE plot ; this shows that the populations gated in a 'classical' manner are mostly homogeneous, as they each correspond to one cluster of cells in t-SNE (**Figure 3.7-C**). Similar clusters were found when performing t-SNE multiple times with various parameters (**Supplemental Figure 3.2**). Interestingly, three clusters of GFP^{+} cells did not correspond to any of the gates, or in other words, these cluster of cells were not taken into consideration by classical gating.

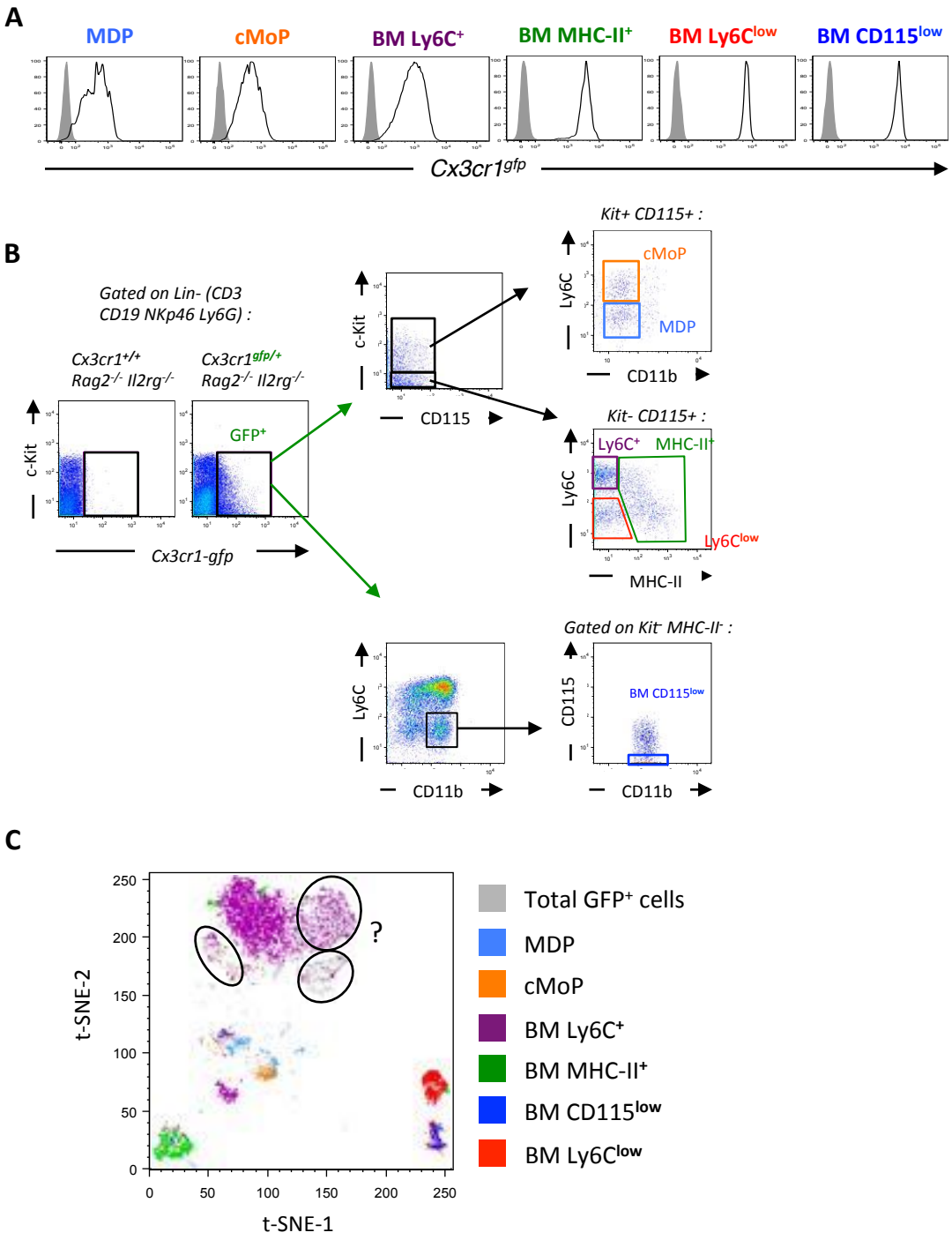

Figure 3.7. Analysis of *Cx3cr1-gfp* expressing bone marrow cells by CyTOF. *Cx3cr1*$^{gfp/+}$ *Rag2*$^{-/-}$ *Il2rg*$^{-/-}$ and *Cx3cr1*$^{+/+}$ *Rag2*$^{-/-}$ *Il2rg*$^{-/-}$ mice were sacrificed and their bone marrow analysed for either flow cytometry (A) or CyTOF (B and C). **(A)** The indicated populations were gated by flow cytometry as indicated in Figure 3.1, and the expression of GFP analysed in GFP mice (*black lines*) and C57BL/6 mice (*grey histograms*) **(B)** Same gating strategy of bone marrow prospective populations by CyTOF, as used by flow cytometry in Figure 3.1. **(C)** t-SNE was performed on the Lineage negative, *Cx3cr1-gfp*$^{+}$ bone marrow cells. The resulting clusters are shown, and total Lin^{-} GFP^{+} cells are shown in grey, while the populations gated in (B) are overlayed. The GFP^{+} clusters not taken into account by classical gating are circled and their phenotype will be shown in **Figure 3.9.**

A similar process was applied to total lineage negative, *Nr4a1-gfp*$^{+}$ cells (**Figure 3.8**). Because the MDP, cMoP and BM Ly6C^{+} cells express little to no *Nr4a1-gfp* (**Figure 3.8-A,** consistent with previous results from the lab), they were not recovered when gating on total lineage negative *Nr4a1-gfp*$^{+}$ cells. Only BM MHC-II^{+}, BM CD115$^{\mathbf{low}}$ and BM Ly6C$^{\mathbf{low}}$ cells, which express intermediate to high levels of *Nr4a1-gfp* (**Figure 3.8-A**), were found within the *Nr4a1-gfp*$^{+}$ gate (**Figure 3.8-B**). A t-SNE was performed on total lineage negative, *Nr4a1-gfp*$^{+}$ cells, and cells gated in parallel were overlayed on the t-SNE dot plot (**Figure 3.8-C**). The clusters thus generated were found even when performing t-SNE multiple time, with various parameters (**Supplemental Figure 3.3**). Similar to results obtained in *Cx3cr1*$^{\mathbf{gfp/+}}$ *Rag2*$^{\mathbf{-/-}}$ *Il2rg*$^{\mathbf{-/-}}$, not all GFP^{+} cells were taken into account by classical gating (**Figure 3.8-C**).

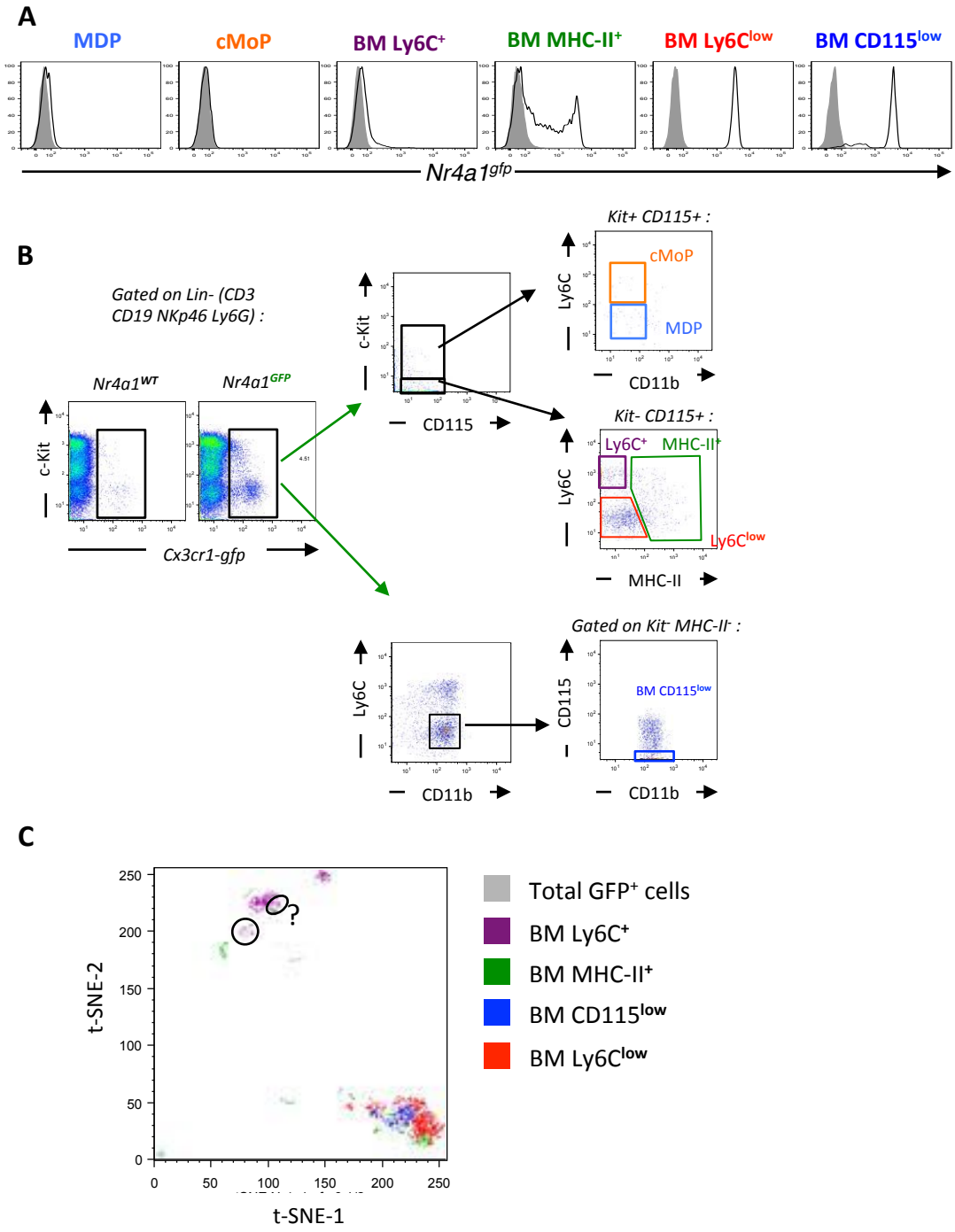

Figure 3.8. Analysis of *Nr4a1-gfp* expressing bone marrow cells by CyTOF. *Nr4a1*^{GFP} mice and *Nr4a1*^{WT} littermate controls were sacrificed and their bone marrow analysed for either flow cytometry (A) or CyTOF (B and C). **(A)** The indicated populations were gated by flow cytometry as indicated in Figure 3.1, and the expression of GFP analysed in *Nr4a1*^{GFP} mice (*black line*) and *Nr4a1*^{WT} littermates (*grey histograms*) **(B)** Same gating strategy of bone marrow prospective populations by CyTOF, as used by flow cytometry in Figure 3.1. **(C)** t-SNE was performed on the Lineage negative, GFP^{+} bone marrow cells of a *Nr4a1*^{GFP} mouse. The resulting clusters are shown, and total Lin^{-} GFP^{+} cells are shown in grey, while the populations gated in (B) are overlayed. The GFP^{+} clusters not taken into account by classical gating are circled and their phenotype will be shown in **Figure 3.9.**

The clusters of cells that were either *Cx3cr1-gfp*$^{+}$ (**Figure 3.7-C**) or *Nr4a1-gfp*$^{+}$ (**Figure 3.8-C**), but not taken into account by a 'classical' gating startegy, were gated directly on the t-SNE plots (**Figure 3.9**). Their expression for all markers used in the CyTOF staining was analysed (**Figure 3.9-A**, **B**). The three clusters identified in *Cx3cr1*$^{gfp/+}$ *Rag2*$^{-/-}$ *Il2rg*$^{-/-}$ mice were termed C1, C2 and C3, while the two clusters identified in *Nr4a1*^{GFP} mice were termed N1 and N2. All these cells were negative for CD11c, CD64, as well as lineage markers CD3, CD19, NKp46 and Ly6G (data not shown). Interestingly, two clusters of cells could be found in both GFP mice models : C2 had the same phenotype as N1, and C3 had the same phenotype as N2 (**Figure 3.9-A, B**).

These cells were all potentially interesting in the context of a search for a 'missing link', therefore they were analysed further by classical flow cytometry and EdU incorporation assays. Because the cells found in *Nr4a1*^{GFP} mice were similar in phenotype to two of the clusters found in *Cx3cr1*$^{gfp/+}$ *Rag2*$^{-/-}$ *Il2rg*$^{-/-}$, we will only refer to the populations as C1, C2 and C3 (since C2=N1 and C3=N2).

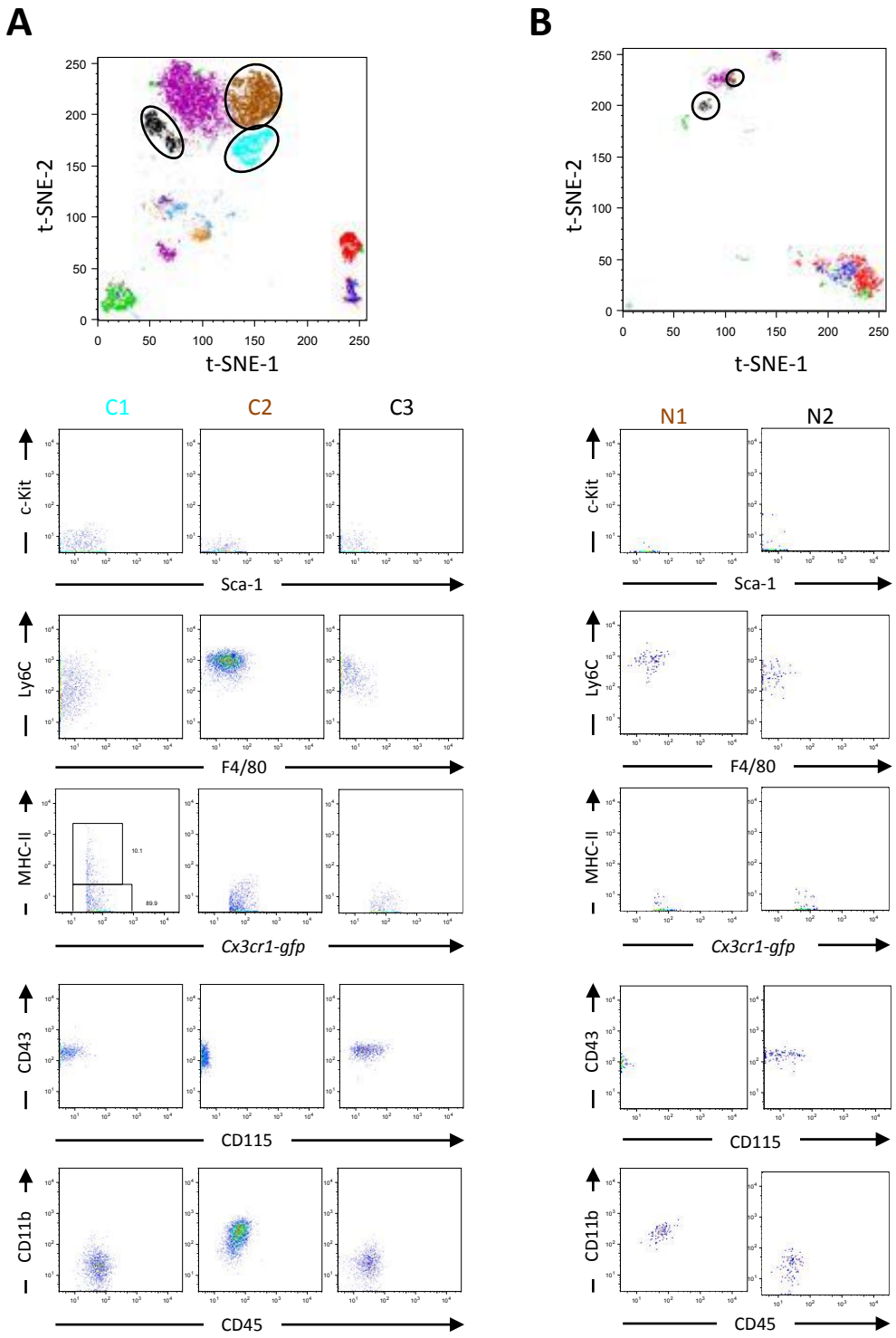

Figure 3.9. Phenotype of the identified GFP^{+} cells by CyTOF. Cells identified in the GFP fraction of *Cx3cr1*$^{gfp/+}$ *Rag2*$^{-/-}$ *Il2rg*$^{-/-}$ mice **(A)** and *Nr4a1*^{GFP} mice **(B)** in Figures 3.7 and 3.8 respectively, were phenotyped by CyTOF. Their phenotype is represented as a series of 2D dot plots. Of note, C2 and N1 as well as C3 and N2 have similar phenotype.

First, a gating strategy was designed in order to select these populations by fluorescence flow cytometry. C1 was gated as CD115^{low} CD11b^{low} Ly6C^{int} c-Kit^{low} MHC-II^{-} CD43^{+}, consistent with its phenotype found by CyTOF (**Figure 3.10-A**). C2 was gated as CD115^{low} CD11b^{+} Ly6C^{high} c-Kit^{-} MHC-II^{-} CD43^{+}, and C3 was gated as CD115^{+} CD11b^{low} Ly6C$^{high/int}$ MHC-II^{-} CD43^{+}, also according to their phenotype by CyTOF analysis (**Figure 3.10-B** and **C**, respectively). The expression of *Cx3cr1-gfp* by these cells was confirmed by conventional flow cytometry as well (**Figure 3.10-A, B** and **C**). Next, EdU incorporation at 60h was analysed in these cells, as a population that would 'peak' in EdU content at this time point could constitute an interesting target for a 'missing link' population. All three populations were found to have an important proportion of EdU^{+} cells at 60h (**Figure 3.10-A**, **B**, **C**).

Therefore, populations C1 to C3 were gated as indicated in **Figure 3.10** into the data set of EdU kinetics (10 days) presented in **Figure 3.6** (data not shown, analysis performed by Hannah Garner). However, incorporating these three population into the *in silico* modeling by our collaborators Grégoire Altan-Bonnet and Amir Erez, showed that the production of Ly6C^{low} monocytes was still not properly explained by a mathematical analysis (data not shown).

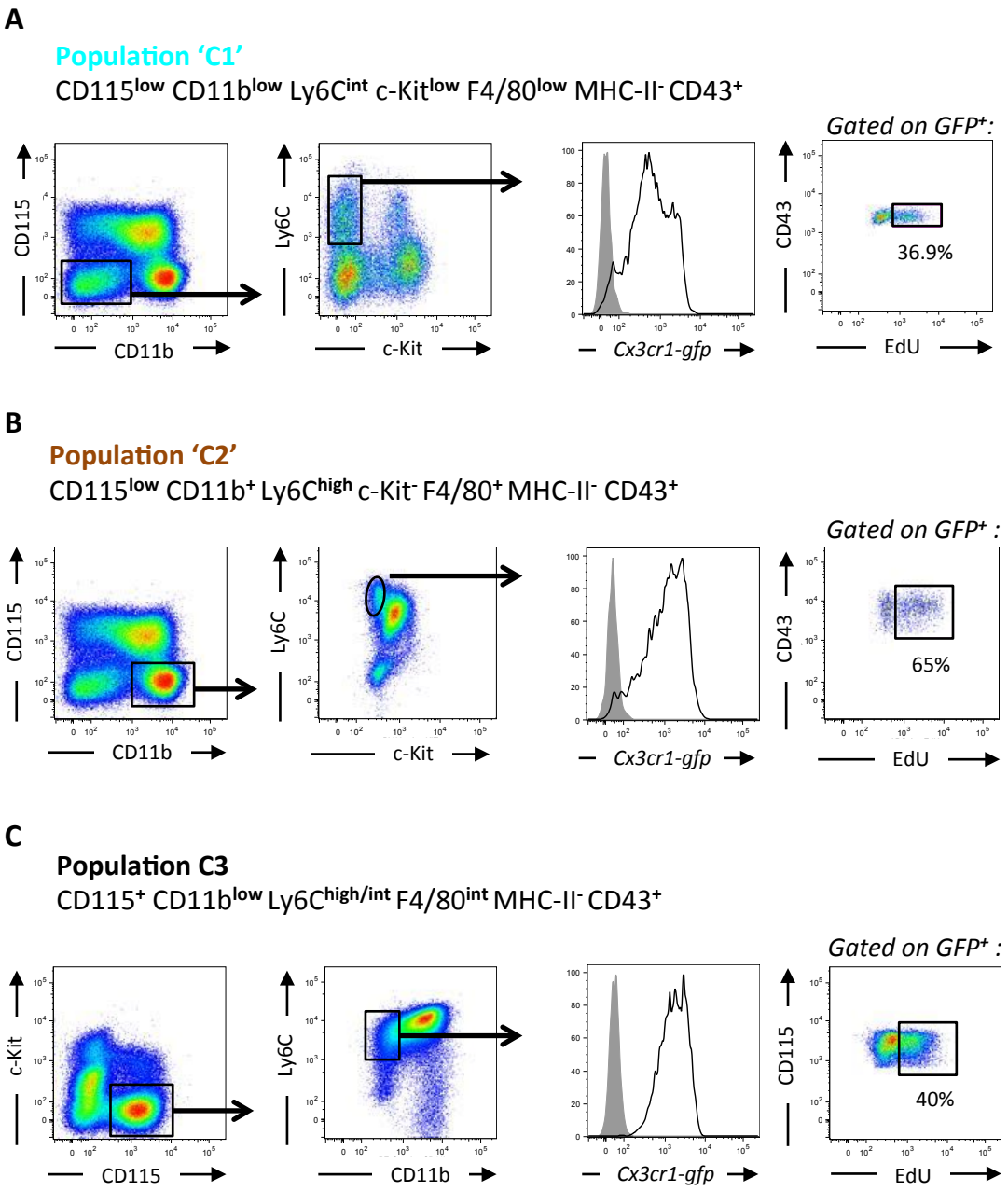

Figure 3.10. Gating in flow cytometry of the *Cx3cr1-gfp*$^{+}$ populations identified by CyTOF, EdU analysis at 60h. Bone marrow of *Cx3cr1*$^{gfp/+}$ *Rag2*$^{-/-}$ *Il2rg*$^{-/-}$ mice was analysed by flow cytometry. Populations identified in the CyTOF experiments presented in Figures 3.7, 3.8 and 3.9 were gated according to the phenotypes found in Figure 3.9, and as rewritten under each population name for C1 **(A)**, C2 **(B)** and C3 **(C)**. Their level of GFP expression was measured (*black lines*), and compared to *Cx3cr1*$^{+/+}$ control mice (*grey histograms*). Finally, *Cx3cr1*$^{gfp/+}$ *Rag2*$^{-/-}$ *Il2rg*$^{-/-}$ mice were injected with a single pulse of 0.5mg EdU and the EdU content of C1 **(A)**, C2 **(B)** and C3 **(C)** was measured at 60h post EdU injection (*right*).

3.2.6. Inclusion of CXCR4^{+} pre-monocytes and standardisation of the protocol for bone marrow preparation

In the search for a better way of analysing the various populations, staining for CXCR4 was included in the analysis of bone marrow, following the recent publication of the work by Chong and colleagues (Chong et al., 2016). In this article, the authors use CXCR4 staining to identify cells termed 'pre-monocytes' in the bone marrow, which are within the BM Ly6C^{+} cells, and are highly proliferative. CXCR4^{+} Ly6C^{+} pre-monocytes were suggested as a direct upstream population that gave rise to CXCR4^{-} Ly6C^{+} cells in the bone marrow (Chong et al., 2016). Consistent with these results, CXCR4^{+} cells within the BM Ly6C^{+} cell population identified its proliferative fraction, as the CXCR4^{+} cells corresponded to the EdU^{+} cells 1h after EdU injection (**Figure 3.11-A**).

In addition to the new staining of the bone marrow, the protocol for the preparation of the bone marrow was standardised with that of other organs. Up to this point, bone marrow cells were subjected to a magnetic beads-mediated depletion of Ly6G^{+} neutrophils and Ter119^{+} erythrocytes (see **Materials and Methods**, *section 2.2.1.3*). This was done in order to remove a large number of cells from the bone marrow, and help the identification of discrete populations, such as Ly6C$^{\mathbf{low}}$ monocytes or the BM CD115$^{\mathbf{low}}$ cells. However, comparing the bone marrow of mice with or without including this depletion step before staining with surface antibodies, revealed that depleting Ly6G^{+} and Ter119^{+} cells lead to a loss of Ly6C$^{\mathbf{low}}$ monocytes in the bone marrow (**Figure 3.11-B**).

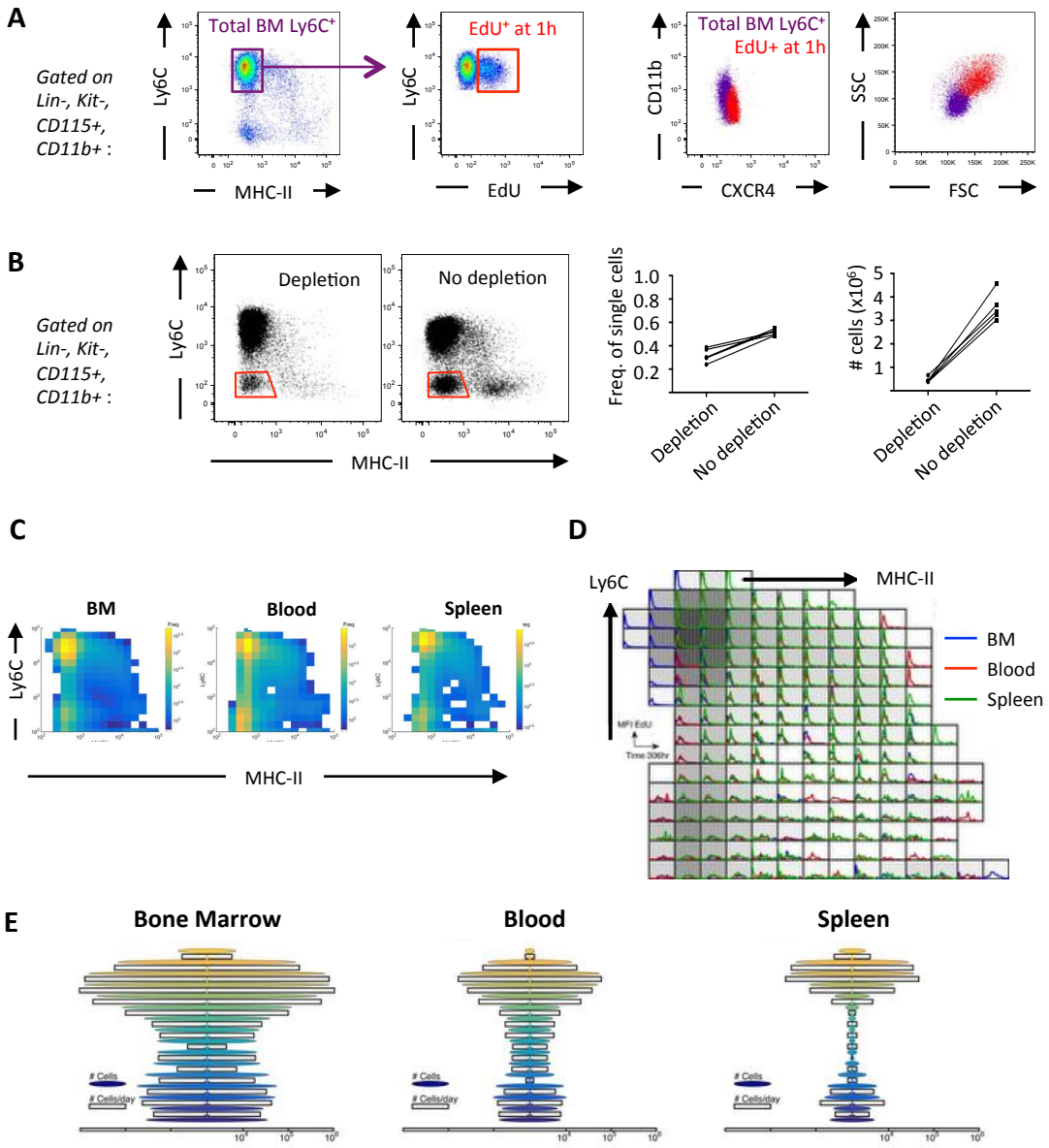

Figure 3.11. Latest analysis of Bone marrow, Blood and Spleen population as continuum on the Ly6C expression axis. (A) Consistent with results from Chong and colleagues (Chong et al., 2016) CXCR4 expression in the bone marrow identifies the proliferating fraction of BM Ly6C^{+} cells. **(B)** Preparing bone marrow cells for flow cytometry without magnetic depletion of Ly6G^{+} neutrophils and Ter119^{+} erythrocytes allows to yield more Ly6C^{low} monocytes. **(C)** Subdivision of monocytes in BM (*left*), blood (*middle*) and spleen (*right*) into small voxels along the Ly6C and MHC-II axis. Ly6C expression is colour-coded from yellow (high expression) to blue (low expression). Gated on Lin^{-} c-Kit^{-} CD115^{+} CD11b^{+} CXCR4^{-} **(D)** Kinetics of EdU incorporation and distribution over time for each voxel of Ly6C expression subdivided in (C). The EdU kinetic of bone marrow (*blue lines*), Blood (*red lines*) and spleen (*green lines*) are overlayed. **(E)** Flux of cells from Ly6C^{high} (yellow) to Ly6C^{low} (blue) in bone marrow (left), blood (*middle*) and spleen (*right*). The width of ellispes represents the number of cells with a given level of Ly6C expression (colour-coded in yellow to blue). The width of the white rectangles represents the number of cells which transition, per day, from one level of Ly6C to the next, from high (yellow) to low (blue). *Figures C, D and E generated by Amir Erez.*

A new time series of EdU kinetic analysis was performed by our collaborators on bone marrow, blood and spleen, this time staining the bone marrow with CXCR4, and without performing the depletion as mentioned above (data not shown). Groups of three mice were analysed from 1h to 180h (7.5 days) post EdU injection, and every 18h. Modeling of this new data set by our collaborators Grégoire Altan-Bonnet and Amir Erez, provided insight into monocyte dynamics in the different compartments. When considering bone marrow cells negative for CXCR4, hence excluding the proliferating fraction of BM Ly6C^{+} cells, the c-Kit^{-} CD115^{+} CD11b^{+} cells were divided into small fractions of cells along the Ly6C and MHC-II fluorescence axis, termed 'voxels'. This was performed in all three organs (**Figure 3.11-C**). Then, a computer assisted analysis of EdU content over time was performed for each of these voxels, in all three organs (**Figure 3.11-D**). Finally, modeling the kinetics of these voxels yielded the results presented in **Figure 3.11-E**. In this figure, Ly6C expression is represented by a colour-code from yellow (high expression) to blue (low expression). The width of the ellipses represents the number of cells with the corresponding Ly6C level of expression, in each organ. Below each ellipse is a rectangle whose width represents the number of cells, per day, that 'flow' from the level of Ly6C expression above the rectangle, to the level of Ly6C expression represented below the rectangle. Therefore, the larger the rectangle, that more cells flow from Ly6C$^{\mathbf{high}}$ expression to intermediate and then lower levels of Ly6C expression. Having more cells that express low levels of Ly6C in the bone marrow, and analysing in parallel all three organs using the same phenotypes (CXCR4^{-} c-Kit^{-} CD115^{+} CD11b^{+}) thanks to the absence of the depletion step, allows a flow of cells that is explained with a mathematical analysis. Given the relative size of the rectangles representing the transitions from Ly6C$^{\mathbf{high}}$ expression to Ly6C$^{\mathbf{low}}$ expression, these results suggest that this phenotypical transition occurs predominantly in the bone marrow (**Figure 3.11-E**). Additionally, analysis of CD115 expression in the voxels

along the Ly6C expression axis, shows that during Ly6C down-regulation, there is a transitory drop in CD115 expression, which is restored by the time cells reach a Ly6C^{low} phenotype (data not shown). This drop in CD115 expression was not observed in blood nor spleen. This suggests that cells that differentiate from a Ly6C^{high} to Ly6C^{low} phenotype in the bone marrow may transition through a state similar to the BM CD115^{low} population.

3.3. Discussion and future work

The work presented in this chapter aimed at a further understanding of monocyte dynamics. This issue was investigated with the support of a mathematical and computer assisted approach. Data from pulse-chase experiments were used. First, the biological system had to be established, as the modeling relies on several parameters, that could partially be fixed thanks to experiments. Therefore, the size of the populations were estimated for the wole body, and the EdU pulse was characterised in order to make sure the first, founding events that lauch the EdU incorporation was understood. A short or long labeling phase is not a trivial element, as a long labeling phase could potentially label many more cells at the start of the kinetics study, during the time following EdU injection. Indeed, there is no firm evidence that cells that are in the process of differentiating and proliferating in the bone marrow, do so in a staggered manner, where waves of progenitors undergo cell cycles together, and long breaks occur before another wave starts. However, the data showed in **Figures 3.4** and **3.5** suggest that such a phenomenon may occur at the level of the progenitors under study, as there was a surprising coordination of EdU^{+} cells to start appearing low in FSC/SSC and drop in gMFI of EdU signal. However, the time points studied were relatively far apart (2h between each time point), and there is no information (i) about how reproducible this type of wave-suggesting result may be, and (ii) what happens between the time points, notably between 2h and 4h. Additionally, EdU and other nucleoside analogs have been

shown to influence cell cycle (Pereira et al., 2017). This is a caveat for this entire study in a sense, as monocyte dynamics might be partially flawed, due to the experimental tool itself influencing the phenomenon to measure. However, Pereira and colleagues show minimal to no influence of EdU on the cell cycle at the 10mM dose that was used in this thesis.

The biological system that was under investigation was based on literature (known populations for the most part) and results obtained up to that point in the laboratory. However, no gating strategy is perfect, and no population gated in one specific way is surely completely homogeneous, or constitutes a biological unit. Techniques such as t-SNE allow to cluster the cells in an unbiased way – or at least in a less biased way : indeed, the high dimensional space, in which the algorithm calculates the phenotypical resemblance between cells, is constituted by the markers used in the antibody mix ; in other words, the experimentator still choses with which set of markers the cells are going to be placed in clusters. This is still a choice, hence partially biased (which does not mean necessarily wrong). Additionally, the method shown in **Figures 3.7** and **3.8** is not an optimal way of taking full advantage of the t-SNE algorithm. Classical gating was performed and overlapped with the t-SNE plot. This had the advantage to confirm that based on the markers used for the cell clustering, classically gated populations were mostly homogeneous. However, it was also minimising the use of cell clustering, as the only clusters discovered were those not included in the gating strategy. Another way of using t-SNE in an even less biased way, is to set aside any known gating strategy, perform t-SNE on a selected, wide population of cells, for example GFP^+ cells in a transgenic mouse model, and then gate directly on the clusters thus formed, and phenotype these cluster with either marker expression heat maps, or by a large selection of 2x2 dot plots showing expression of all markers selected for the staining. This latter method was used in the laboratory, and results generated by Hannah Garner (data not

shown). Some of the resulting populations were relatable to the known, more classical cells populations, but it was an entirely new look at the different compartments. Unfortunately, such analysis did not yield significant results from a mathematical analysis.

The last figure presents the latest analysis performed by our collaborators. This analysis took advantage of the newly discovered subdivision of BM Ly6C^{+} cells with CXCR4, published by Chong and colleagues last year (Chong et al., 2016), which allowed separating their proliferating fraction. The morphologies found in the BM Ly6C^{+} cells, as well as their very important size, and their constant proliferating fraction was indicative that this population was probably heterogeneous. It was only logical to follow up on the article by Chong et al. and stain the bone marrow with CXCR4. The protocol for the isolation of bone marrow cells was also an important improvement, allowing to recover more Ly6C^{low} monocytes. Up to that point, one of the issues faced when trying to model the cell dynamics in blood and bone marrow, was that the Ly6C^{low} monocytes of the bone marrow, as a 'destination', or 'end product' of the cells produced upstream, was too small a population to account for much of the cell production of bone marrow late progenitors. The proliferation rates, calculated based on the data shown in **Figure 3.3**, impose a form of 'pressure' of cell production, and in the closed system that was established as the prospective cell populations considered here, the output of this cell proliferation had to be found. When depleting the bone marrow of Ly6G^{+} and Ter119^{+} cells, the additional 1h15-1h30 of processing, as well as additional centrifugation steps, diminished significantly the amount of Ly6C^{low} monocytes retrived. Therefore the population appeared smaller than it actualy is, and the results proposed by the model were difficult to interpret. One example of hypothesis the model yielded when Ly6C^{low} monocytes were being decreased due to the protocol, was one where the Ly6C^{+} monocytes of the bone marrow would transit into the blood, give rise

to MHC-II^{+} monocytes before re-circulating into the bone marrow, where they would differentiate into MHC-II^{-} Ly6C^{low} monocytes. Recirculation of monocytes to the bone marrow for their differentiation into Ly6C^{low} monocytes has been proposed and was observed upon transplantation of Ly6C^{+} monocytes into irradiated hosts (Varol et al., 2007). However, this does not fit well with genetic data form *Nr4a1*, *Ccr2* and *Irf8*-deficient animals (MHC-II^{+} are *Nr4a1*-independent), and the regulation of MHC-II at the cell surface seems unlikely. But this hypothesis was put forth by the modeling analysis because the MHC-II^{+} cells of the blood seemed to constitute some form of output for the production of cells occurring in the bone marrow. With the increased number of Ly6C^{low} monocytes in the bone marrow when perfoming the isolation of cells without depleting Ly6G^{+} and Ter119^{+} cells by magnetic separation, the Ly6C^{low} monocytes of the bone marrow constituted a viable 'destination' for part of the cell production.

The modeling data support a flow of cells progressing from high Ly6C expression to Ly6C^{low} expression among c-Kit^{-} CD115^{+} CD11b^{+} CXCR4^{-}. Although this flow of cells seemingly occurs in parallel in the bone marrow, blood and spleen, the number of cells flowing per day (**Figure 3.11-E**, white rectangles below ellipses) suggests the most important flow occurs in the bone marrow. This seems to be distinct from the most prominent hypothesis described in the literature, which states that Ly6C^{+} monocytes give rise to Ly6C^{low} as a conversion in the *circulation* (see **Figure 3.0, A**), as one of the possible fates for Ly6C^{+} monocytes, the other being to migrate into tissues. Therefore, our data seem to point to a branching point for monocyte differentiation in the bone marrow (a hypothesis represented in **Figure 3.0, B**).

However, there are limits that should be considered, regarding this last analysis. The modeling focuses on a restricted number of cells, i.e. cells of a monocytic phenotype (c-Kit^{-} CD115^{+} CD11b^{+} CXCR4^{-}), rather than including all the other populations of the

bone marrow (MDP, cMoP, BM Ly6C^{+} CXCR4^{+}). Furthermore, even if these cells had been included to form a more general hypothesis, not all possibly relevant cells would be included ; the MDP also gives rise to dendritic cells through the CDP (Onai et al., 2007), independent from a monocyte intermediate : this constitutes one of the 'outputs' of the production of cells (Fogg et al., 2006). Upstream progenitor populations of the hematopoiesis differentiation tree could also be taken into account, from long-term HSCs to GMPs.

Similarly, the 'output' for monocyte fate would be interesting to include, considering that Ly6C^{+} monocytes have been shown to participate to the pool of macrophages in some tissues, such as the intestine (Bain et al., 2014). The intestine is a very large organ which is in constant renewal, which means the constant replenishment of macrophages from monocytes involves a large number of cells. Other organs may be concerned, such as the lungs, in which up to 40% of alveolar macrophages can be fate-mapped using the Flt3-Cre driver at 1 year of age (Gomez-Perdiguero et al., 2014). Osteoclasts in long bones are thought to have a monocytic origin in the adults, and some studies have shown that the MDP had the potential to give rise to osteoclasts *in vitro* (Jacome-Galarza et al., 2013; Jacquin et al., 2006) ; it would be therefore interesting to know how much Ly6C^{+} monocytes participate to the turnover of these cells *in vivo*. Of note, Ly6C$^{\mathbf{low}}$ monocytes do not seem to participate to the resident macrophage pool in any of the tissues studied, according to data from Hannah Garner in our laboratory. Overall, modeling a biological system as wide as possible would be an interesting though challenging aim.

4 – Monocyte and Macrophage functions in the kidney

4.1. Introduction and general aims

4.1.1. Ly6C^{low} monocytes as patrolling housekeepers of the vasculature

Ly6C^{low} monocytes have been characterised over the last decade as a patrolling cell population, found in various organs, crawling on the endothelium. Intravital microscopy studies have been instrumental for deciphering some of the functions of these cells. They were first observed crawling in the lumen of vessels of the skin (Auffray et al., 2007). The relative low speed of this crawling, its independence from the blood flow direction and other aspects have coined the term « patrolling » for their behaviour. Since then, several studies have uncovered functions for the Ly6C^{low} monocytes directly linked to their ability to patrol vessels of various sizes, in many organs (Sumajin et al., 2010 ; Li et al., 2012 ; Jung et al., 2013 ; Michaud et al., 2013 ; Daley-Bauer et al., 2014 ; Quintar et al., 2017). The study by Carlin, Stamatiades and colleagues (2013) has shown that Ly6C^{low} CX$_3$CR1^{hi} patrolling monocytes are retained by the vasculature of the kidney capillaries in a CX$_3$CR1-dependent manner upon stimulation with a TLR7 agonist. Following their retention, patrolling monocytes recruit neutrophils to the kidney, where these granulocytes induce necrosis of endothelial cells, the resulting debris of which Ly6C^{low} monocytes phagocytose. Some questions remained to be investigated about this model of inflammation.

One of these questions is the involvment of platelets in the vascular housekeeping functions of monocytes. Indeed, platelets have been increasingly well recognised over the last 20 years as fundamental actors of inflammation (Schulz et al., 2013; Semple et al., 2011), notably as they are part of a cross-talk with monocytes and neutrophils. Therefore, the first set of experiments presented in this chapter will tackle the issue of platelets in Ly6C^{low} monocyte patrolling activity.

4.1.2. Kidney macrophages as resident cells with motile filipodiae

Previous work carried out in the laboratory by Efstathios Stamatiades characterised kidney macrophages using intravital microscopy and flow cytometry. These cells represent ~50% of the total hematopoietic cells of the kidney (Stamatiades et al., 2016). Phenotypic analysis of F4/80$^{\mathbf{bright}}$ CD11b$^{\mathbf{low}}$ cells revealed they express *Cx3cr1-gfp*, as well as MHC-II, CD11c and FcγRI, IIb, III and IV. They do not exchange between parabionts and do not rely on CCR2, suggesting these cells do not rely on replenishment from circulating cells such as monocytes (Stamatiades et al., 2016). Furthermore, intravital microscopy of *Cx3cr1*$^{gfp/+}$ *Rag2*$^{-/-}$ *Il2rg*$^{-/-}$ mice showed that *Cx3cr1-gfp*$^{+}$ macrophages form a dense network of cells, located in the intertitium of the kidney cortex and around glomeruli, in close association with the capillaries. These cells are sessile, as little to no movement from their cell body could be observed during imaging sessions of up to 6 hours. However, they show long processes that are very motile, which suggests a survey activity during steady state (Stamatiades et al., 2016). Together, these data show that kidney F4/80$^{\mathbf{bright}}$ *Cx3cr1-gfp*$^{+}$ macrophages are tissue-resident cells.

Given the known implication of macrophages in various chronic inflammatory diseases (see **Introduction**, *section 1.4.3.2.*), as well as their privileged localisation within their tissue of residence, it appeared relevant to study basic mechanisms regarding their response to circulating immune complexes. In the context of these investigations, experiments were performed that will be presented in this chapter.

4.2. Results

4.2.1. Platelets are required for retention of patrolling monocytes but not steady state crawling

In order to asses the potential role of platelets in the function of Ly6C^{low} monocytes in the vasculature, the glycoprotein GPIbα was targeted, as it is a mediator of platelet activation present at their surface (Romo et al., 1999), which normally binds to von Willebrand Factor (vWF). First, anti-GPIbα F(ab')$_2$ fragments were injected during steady state and the superficial cortex of kidneys of *Cx3cr1*$^{gfp/+}$ *Rag2*$^{-/-}$ *Il2rg*$^{-/-}$ mice were imaged in live mice, as previously performed in the laboratory (Carlin et al., 2013 ; Stamatiades et al., 2016). In these mice, Ly6C^{low} CX$_3$CR1^{hi} monocytes appear to crawl on the endothelium of the small capillaries of the kidney cortex. Injection of the anti-GPIbα F(ab')$_2$ fragments did not alter the number of patrolling monocytes, when imaging the kidney for up to five hours at steady state (**Figure 4.1-A**, *top*). Next, the TLR7 agonist R848 (Resiquimod) was topically applied onto the exposed kidney during intravital microscopy sessions, as described previously (Carlin et al., 2013); this has been shown to induce the retention of patrolling monocytes, leading to their accumulation in the kidney, and the recruitment of neutrophils (Carlin et al., 2013). When injecting anti-GPIbα F(ab')$_2$ fragments before topically applying R848 to the kidney, no change in the retention of Ly6C^{low} monocytes, nor of the recruitment of neutrophils, was oberved (**Figure 4.1-A**, *bottom*). These results suggest that GPIbα-mediated activation is not necessary for either steady state crawling, nor TLR7-dependent retention of patrolling monocytes.

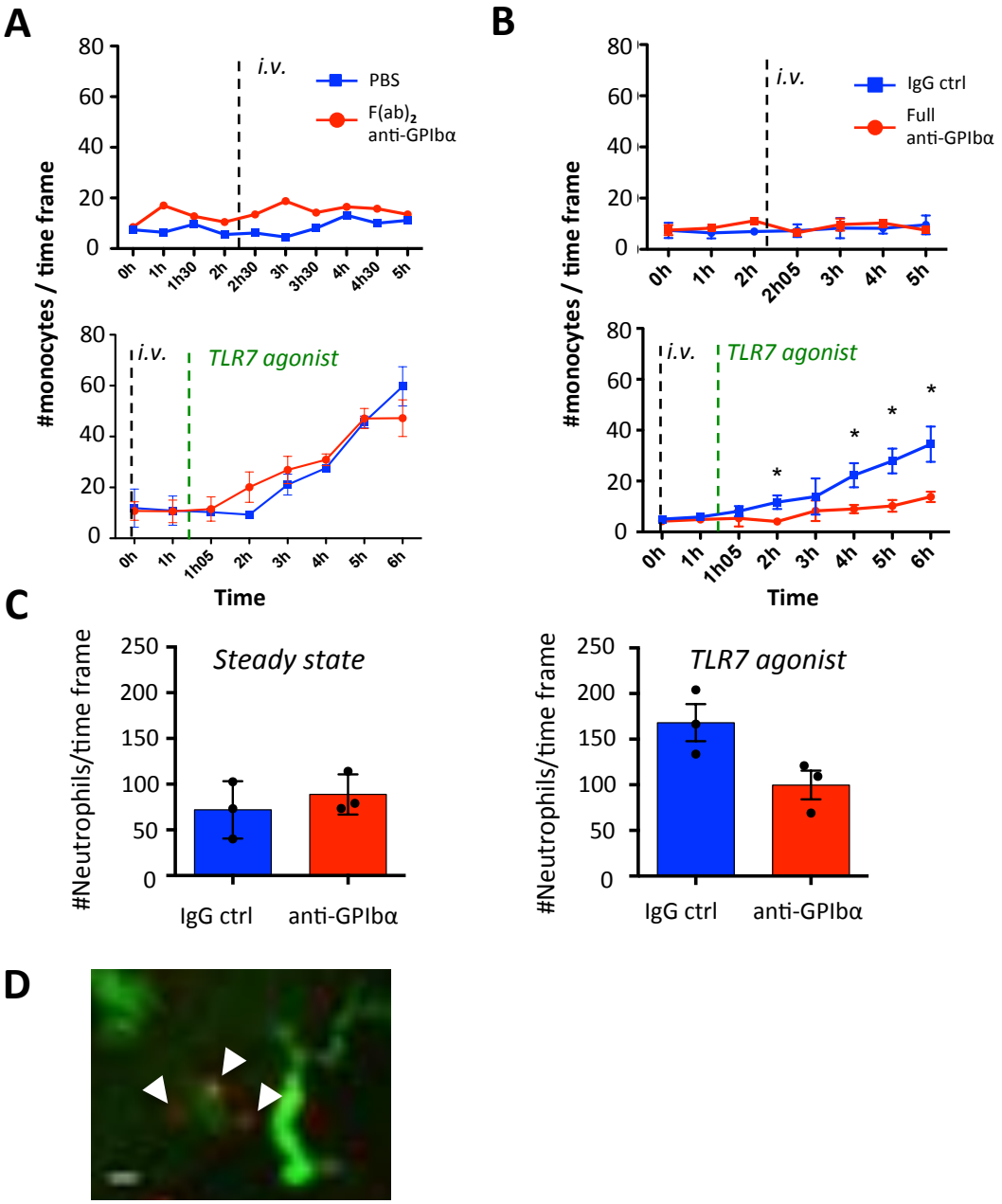

Figure 4.1. Patrolling monocytes depend on platelets for their TLR7 dependent retention in the renal capillaries. *Cx3cr1*$^{gfp/+}$ *Rag2*$^{-/-}$ *Il2rg*$^{-/-}$ mice were anesthesized and their renal cortex imaged by intravital microscopy. **(A)** Effect of platelet inactivation by anti-GPIbα F(ab')$_2$ fragments injection (black dotted line) on steady state patrolling (top) and TLR7 agonist-induced (bottom, green dotted line) retention of Ly6C^{low} monocytes. **(B)** Effect of platelet depletion by Full anti-GPIbα antibody injection (black dotted line) on steady state patrolling (top) and TLR7 agonist-induced (bottom, green dotted line) retention of Ly6C^{low} monocytes. 3 mice per condition, bars represent mean±SEM. * denotes $p<0.05$ in Two-way ANOVA. **(C)** Neutrophil numbers at the end of imaging sessions during steady state (left) and after TLR7 agonist painting, following full anti-GPIbα injection for platelet depletion. Neutrophil recruitment is impaired, consistent with impaired monocyte retention observed in (B). each dot represent a single mouse. **(D)** Monocyte-platelet aggregate following anti-CD49b-PE injection during steady state Platelets appear as very small round structures in red (arrowheads). Bar = 5µm.

Next, platelets were depleted, using a full antibody directed against GPIbα (Bergmeier et al., 2000). The depletion was controlled at the end of each experiment and systematically brought the number of platelets in the blood to below the detection threshold of the cell counter (data not shown). During steady state, platelet depletion did not alter the crawling of monocytes in the capillaries of the kidney, as their number remained stable over a 3-hour period after injection (**Figure 4.1-B**, *top*). Consistently, neutrophil numbers, as measured at the end of the imaging sessions, were not affected at steady state after platelet depletion (**Figure 4.1-C**, *left*). However, when applying the TLR7 agonist R848 topically on the kidney while imaging, patrolling monocytes did not accumulate in the kidneys of mice injected with the platelet depleting antibody (**Figure 4.1-B**, *bottom*). Furthermore, neutrophil recruitment was impaired (**Figure 4.1-C**, *right*).

Together, these results suggest that, while GPIbα-mediated activation of platelets is not necessary for Ly6C^{low} monocyte function, platelets are required for their TLR7-mediated retention and recruitment of neutrophils, but not steady state crawling.

Next, patrolling monocytes and macrophages were studied in another inflammatory setting : their early response to circulating small immune complexes.

4.2.2. Characterisation of immune complexes prepared in vitro

The next set of experiments presented in this thesis rely on the use of immune complexes prepared *in vitro*, by mixing albumin (either bovine serum Albumin – BSA – or chicken ovalbumin - OVA) with polyclonal immunoglobulins directed against these proteins (see Materials and Methods, section ***2.7.3*** and **Table 2.3**). As a quantification of the antigen : antibody (Ag : Ab) immune complexes generated with this method,

various Ag : Ab molar ratios of OVA + anti-OVA (**Figure 4.2-A**) or BSA-TRITC + anti-BSA (**Figure 4.2-B**) were loaded into a Fast Protein Liquid Chromatography (FPLC) column. In order to control for the weight of individual protein (OVA, BSA-TRITC, anti-OVA and anti-BSA), each of them were mixed with PBS using the same protocol as for the generation of immune complexes, and loaded separately into the column.

The results are shown in **Figure 4.2**. In this representation, the amount of protein detected at the bottom of the column is represented on the Y-axis as arbitrary units (A.U.) for the absorbtion of ultraviolet light of 280nm wavelength. The elution volume that passes through the chromatography column is indicated on the X-axis ; the higher the elution volume, the longer it takes for the constant pressure on the liquid (flow rate of 0.5 mL/min) to bring the protein down the column, therefore the lighter the protein. Conversely, the smaller the elution volume, the heavier the protein.

In order to set up the column and as a control for the consistency of sizes for various proteins, a mixture of known sized-proteins was injected to the column prior to the experimental samples, i.e. standards were run (**Figure 4.2-D**). Based on these values, the results presented in Figures 4.2-A, and B are consistent, with IgGs detected at elution values similar to the 158 kDa (kilo-Dalton) IgG from the standards (**Figure 4.2-D**, '2'). Similarly, the sizes observed for OVA (40k Da) and BSA (60 kDa) were consistent. Of note, samples containing only BSA showed two peaks, one corresponding to single BSA at 16.2 mL elution (i.e. 60 kDa), and another at 15 mL elution, most likely corresponding to BSA dimers, as observed before (De Frutos et al., 1998).

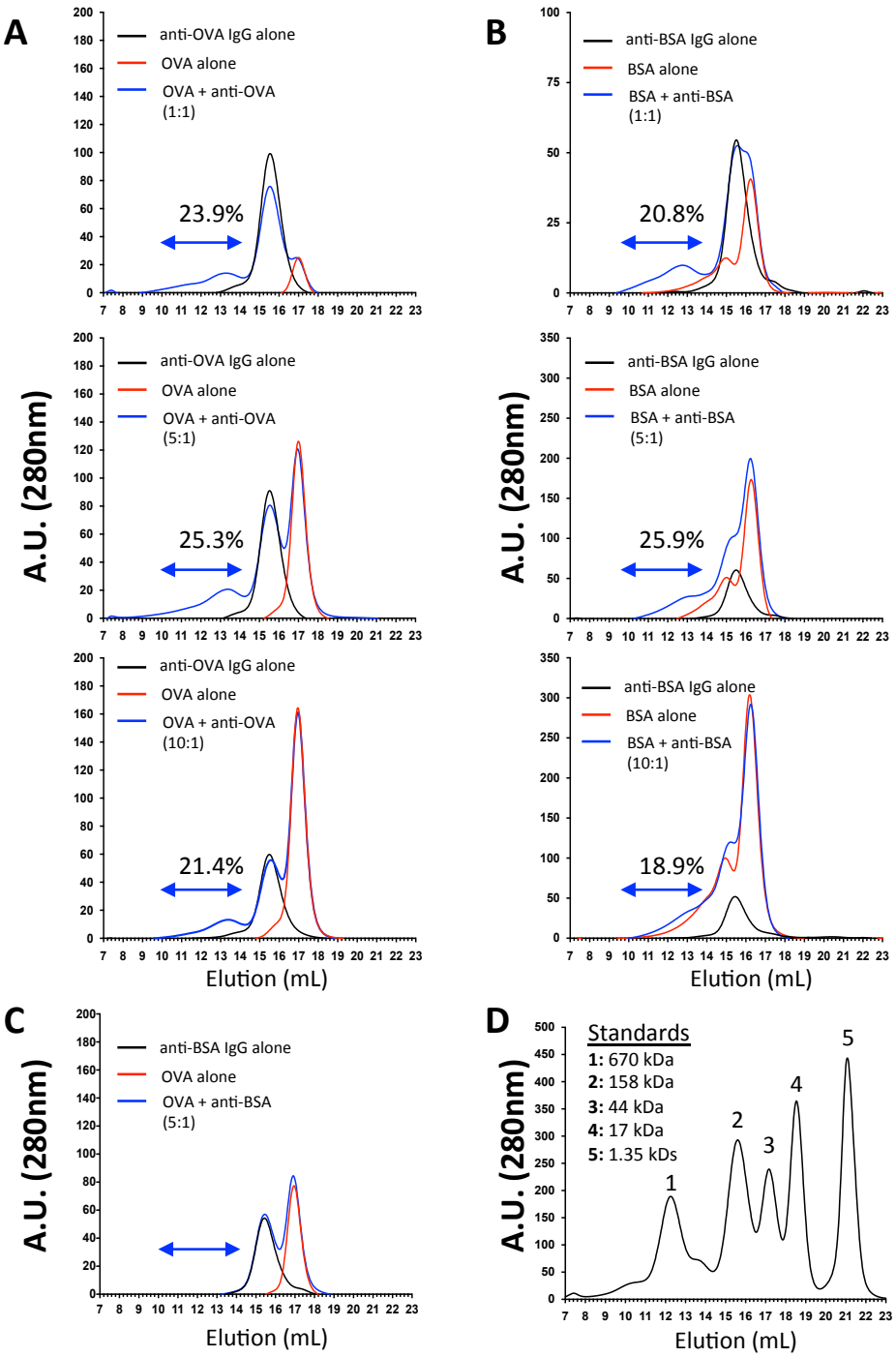

Figure 4.2. Characterisation of immune complexes generated in vitro at various Ag:Ab ratios. Two types of albumin (OVA and BSA) were mixed with polyclonal antibodies directed against them at various Ag:Ab molar ratios for 1h at 4ºC, and were acquired in an FPLC column to measure the amount of immune complexes formed *in vitro* with this method. **(A)** Chromatography of OVA+anti-OVA mixture at Ag:Ab molar ratios of 1:1 (top), 5:1 (middle) or 10:1 (bottom) shown as blue curves, and the corresponding amounts of OVA alone (red) or anti-OVA alone (black). The resulting ICs form a peak around 13.3mL elution (blue double arrow). **(B)** Similar runs of chromatography for BSA+anti-BSA or each separately. Percentages of immune complexes are shown for each molar ratio (see Materials and Methods for calculation). **(C)** Specificity test **(D)** A mixture of proteins with known weights was run on the cromatography column as standards. Each line represents a single run on the machine.

The results show that mixing albumins with their respective antibodies results in the formation of immune complexes (**Figure 4.2-A**, **B**, *blue double arrow*), of about 700 kDa (~13.3mL elution). When integrating the area under the curve corresponding to the IgG peak in the 'IC' samples, and calculating the ratio with the area under the total curve, it was estimated that 19 to 25% of IgGs were engaged in immune complexes (percentages in **Figure 4.2-A**, **B**). This was found for all Ag : Ab molar ratios tested (1 : 1, 5 : 1 and 10 : 1). As a control for the specificity of the immune complex formation, OVA was mixed with anti-BSA IgGs at 5 :1 molar ratio (**Figure 4.2-C**). This resulted in no immune complex formation (**Figure 4.2-C**, *black curve*), which suggests a good specificity of the antibodies used to generate immune complexes. The opposite mix (BSA + anti-OVA) was tested as well, resulting in no immune complex formation either (data not shown).

Together, these results show that the method used to generate immune complexes *in vitro* is relatively efficient, and immune complexes at 1 : 1 molar ratios were used for the rest of this work.

4.2.3. Replication of results obtained in the laboratory : uptake by kidney macrophages of immune complexes in a FcγRIV-dependent manner results in the production of TNFα and recruitment of leukocytes

Replicating results previously obtained in the laboratory by Efstathios Stamataides (Stamatiades et al., 2016), mice were injected with either fluorescently labeled BSA-TRITC or immune complexes (ICs) of BSA-TRITC + anti-BSA IgG (BSA-ICs), prepared as described above at 1 :1 molar ratio. Measuring their uptake by flow cytometry 2h after injection confirmed that TRITC fluorescence was detected in F4/80$^{\mathbf{bright}}$ CD11b$^{\mathbf{low}}$ macrophages of the kidney, and that this uptake was more efficient

when BSA was in immune complexes (**Figure 4.3-A**, *left* and *middle*). Mice with a hematopoietic cell-specific deletion of the gene coding for FcγRIV (*Csf1r*$^{iCre+}$ *Fcgr4*$^{\Delta/\Delta}$) and littermate controls (*Csf1r*$^{iCre-}$ *Fcgr4*$^{f/f}$) were injected with either BSA or BSA-ICs. Control mice showed a more efficient uptake of BSA-TRITC when BSA was in immune complexes, consistent with results from the C57BL/6 wild-type mice. However, conditional knock-out mice did not show increased uptake of BSA-ICs, which shows uptake of immune complexes by kidney macrophages is *Fcgr4*-dependent (**Figure 4.3-A**, *right*).

Next, C57BL/6 adult mice were injected with immune complexes (BSA-ICs), and sacrificed 1h after injection. Their kidney cells were placed in culture at 37ºC for 5 hours in a culture medium containing Brefeldin A, which inhibits the activity of the Golgi apparatus, hence prevents protein release from the cell. Then TNFα production was measured by intracellular staining and flow cytometry (see **Materials and Methods**, *section 2.2.1.4*). The results show TNFα production by kidney macrophages following BSA-ICs uptake (**Figure 4.3-B**), with >40% of F4/80^{bright} macrophages on average showing positivity for TNFα.

Finally, results from the laboratory generated by flow cytometry or intravital micrscopy showed injection of immune complexes resulted in the recruitment of monocytes and neutrophils in the kidney (Stamatiades et al., 2016). Experiments were carried out by intravital microscopy in *Cx3cr1*$^{gfp/+}$ *Rag2*$^{-/-}$ *Il2rg*$^{-/-}$ mice. Mice were injected *i.v.* with either BSA or BSA-ICs, and 2h later were prepared for intravital microscopy of the superficial cortex. These experiments showed that injection of immune complexes resulted in recruitment of monocytes (**Figure 4.3-C**, *left*), as well as neutrophils (**Figure 4.3-C**, *right*), as measured at the end of the imaging sessions with injection of anti-Gr-1 APC (neutrophils were identified as GFP^{-} Gr-1^{+}).

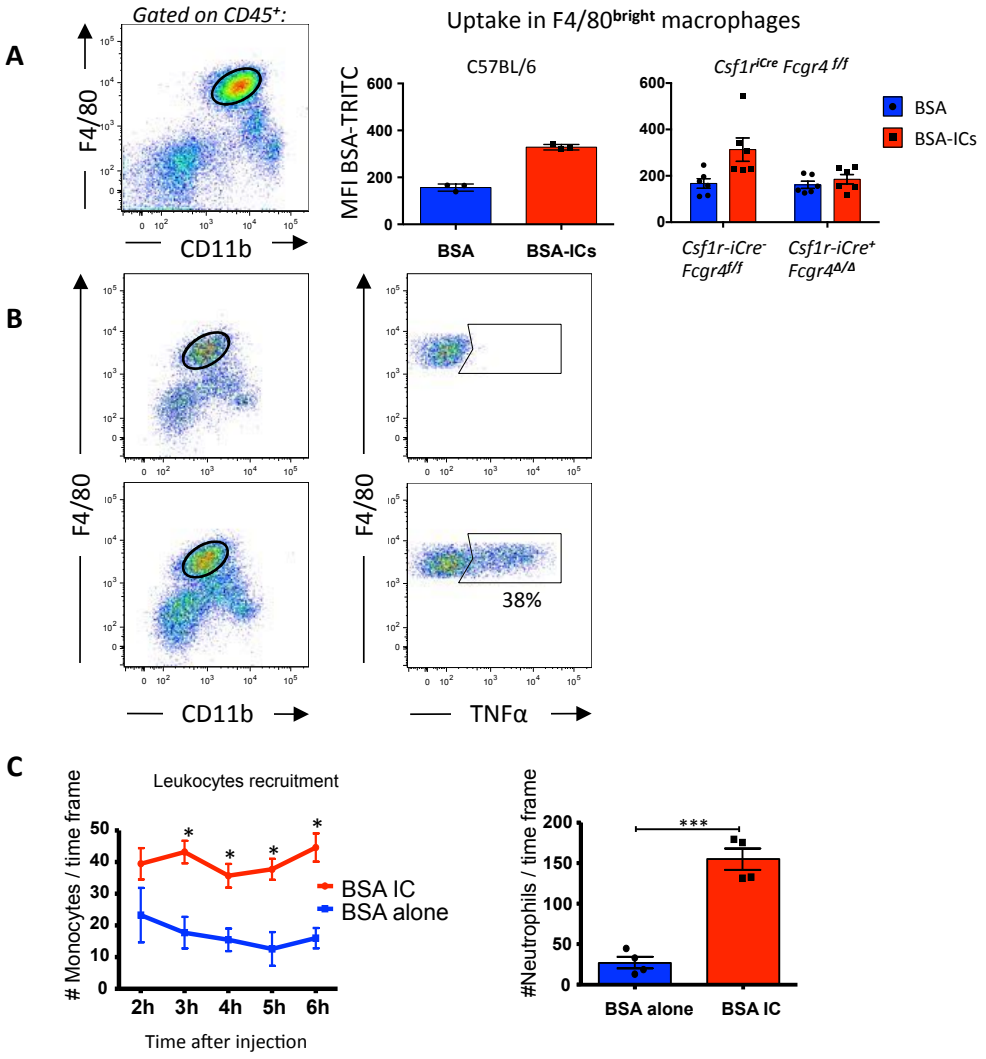

Figure 4.3. Uptake of immune complexes by macrophages results in TNFα and leukocyte recruitment, as previously shown in the lab. Repeating experiments performed previously, mice were injected with either PBS, 50µg of BSA, or 50µg BSA-ICs (see Methods), and measurements of uptake, cytokine production and leukocyte recruitment were performed. **(A)** FcγR-IV-dependent uptake of BSA-ICs by macrophages. After injection of either BSA or BSA-ICs, mice were sacrificed and their kidney processed for flow cytometry. BSA fluorescence in F4/80$^{\mathbf{bright}}$ macrophages (*left*) is higher when BSA is in immune complexes (*middle*), which is dependent on FcγR-IV as shown by the absence of uptake increase in the conditional KO for *Fcgr4* (*right*). Each dot corresponds to a single mouse. Bars represent mean ± SEM. n=3-6 mice per condition. **(B)** TNFα production was measured after injection of 50µg BSA-ICs by flow cytometry (percentage of TNFα^{+} macrophages is shown). Top panels represents staining of TNFα with isotype control, bottom panel with anti-TNFα antibody. Representative of 3 mice, %TNFα^{+} macrophages is 42.7%±4.82. **(C)** Leukocyte recruitment after BSA or BSA-ICs. 2h after injection, *Cx3cr1*$^{\mathbf{gfp/+}}$ *Rag2*$^{\mathbf{-/-}}$ *Il2rg*$^{\mathbf{-/-}}$ mice were prepared for intravital microscopy and their kidney imaged for 4h. At the end of this imaging session, 10µg of Gr-1 – APC antibody was injected and neutrophils (GFP^{-} Gr-1^{+}) were quantified. n=4-5 mice per condition. * represent p<0.01 in two-way ANOVA, *** represents p=0.0001 in Student t-test. Each dot on the right panel represents a single mouse.

Together, these data recapitulate some of the results obtained in the laboratory by Efstathios Stamatiades and published last year (Stamatiades et al., 2016), showing that F4/80$^{\mathbf{bright}}$ macrophages in the kidney uptake immune complexes in a FcγRIV-dependent manner, which leads to their production of TNFα, and results in the recruitment of leukocytes to the kidney.

4.2.4. Uptake of immune complexes in other organs

In order to investigate whether uptake of circulating immune complexes is a unique property of kidney macrophages, C57BL/6 mice were injected with either PBS, BSA or BSA-ICs, and populations of macrophages were analysed for BSA uptake in kidney macrophages, lung alveolar macrophages, brain microglia, epidermis Langerhans cells, dermis F4/80$^{\mathbf{bright}}$ macrophages, spleen red pulp macrophages (RPMΦ), and liver Kupffer cells. Uptake of BSA and BSA-ICs was observed only for kidney, spleen and liver macrophages, but not in lungs, brain, epidermis nor dermis (**Figure 4.4**). Similar to kidney macrophages, Kupffer cells and red pulp macrophages took up BSA-ICs more efficiently than BSA alone (**Figure 4.4**).

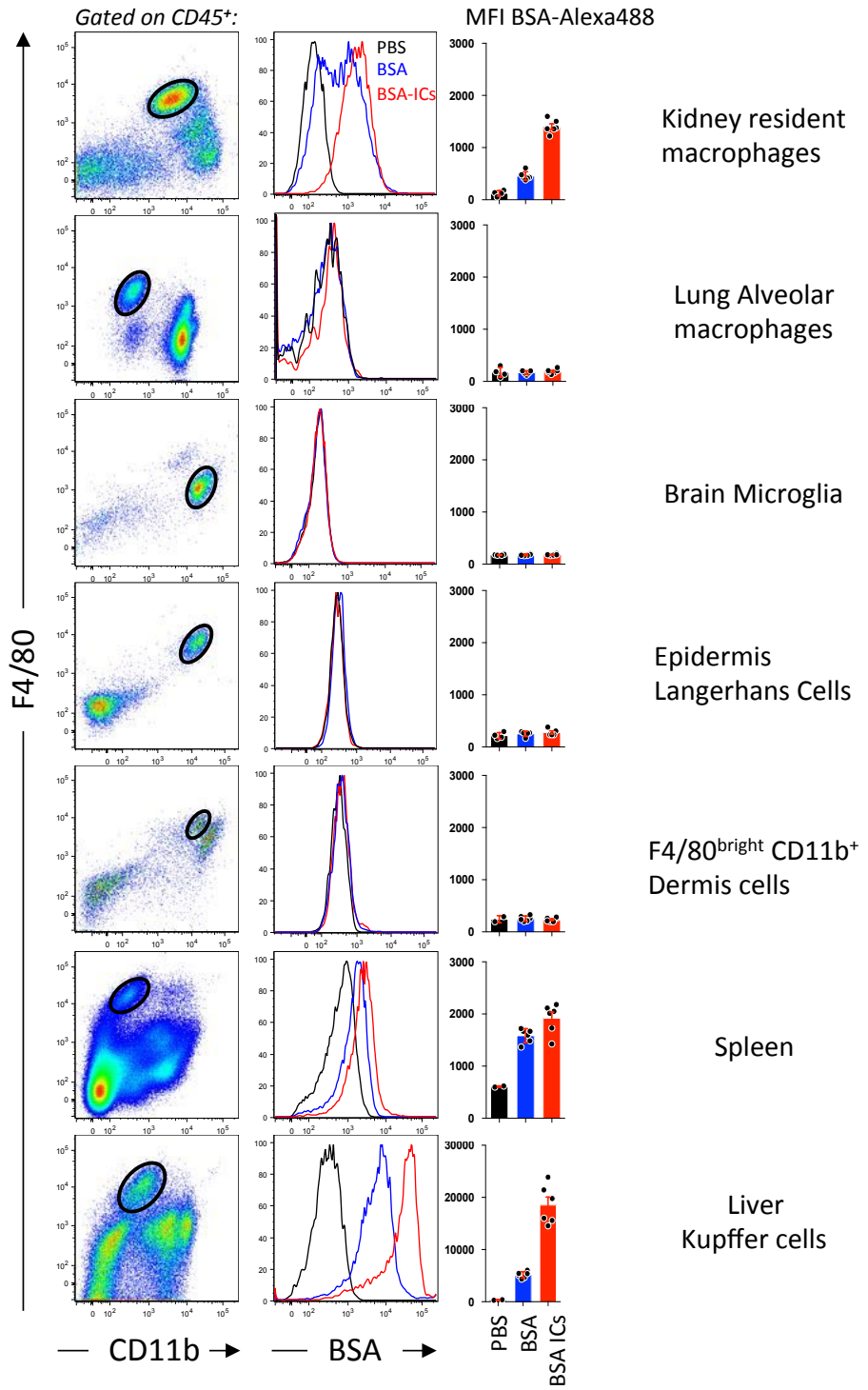

Figure 4.4. Uptake of immune complexes in various organs. C57BL/6 male mice were injected *i.v.* with either PBS, BSA-Alexa488, or BSA-ICs, and their kidney, lungs, brain, epidermis, dermis, spleen and liver were analysed by flow cytometry. The left panel shows the F4/80 vs CD11b profile of $CD45^{+}$ cells, and resident macrophages populations are gated as shown by the black oval. The middle panel show the BSA-Alexa488 content of the cells gated in the left panel, and PBS (black line), BSA (blue line) and BSA-ICs (red line) injected mice are shown, representative of 3 -6 mice per condition. The right panel showns the quantification of BSA-Alexa488 content as measured by the Mean Fluorescence Intensity (MFI) in the Alexa488 channel. Each dot represents a single mouse, bars represent mean ± SEM.

This prompted the question of the means of access of circulating proteins (such as albumin or immune complexes) to the resident macrophages of the kidney. Indeed, the structure of the sinusoid endothelial cells of the spleen and liver allow the RPMΦ and Kupffer cells, respectively, to be in direct contact with the circulating blood (Aird, 2007; Florey, 1966; Mebius and Kraal, 2005). However, this is not the case for the kidney (Stamatiades etal., 2016). Therefore, the last experiment presented in this thesis was designed to investigate this issue.

4.2.5. No vascular permeability observed after immune complex injection

The next experiment aimed at understanding how small circulating proteins such as albumins and immune complexes may access kidney resident macrophages despite their position behind the endothelium of capillaries. A study by Binstadt and colleagues showed that autoantibodies from arthitis-prone transgenic mice induced important and fast vascular leakage (Binstadt et al., 2006). The hypothesis that immune complexes may induce vascular leakage in our model was tested as follows. C57BL/6 were anesthesized, and their superficial renal cortex imaged by confocal microscopy in live animals. To visualse blood vessels, 70 kDa Dextran-TRITC was injected intravenously while imaging the kidney (**Figure 4.5-A**, *left panels*). Then, PBS, BSA or BSA-ICs were injected (all at a fixed volume) *i.v.* while continuously imaging (**Figure 4.5-A**, *second panels*), and the kidney was imaged for 30 more minutes.

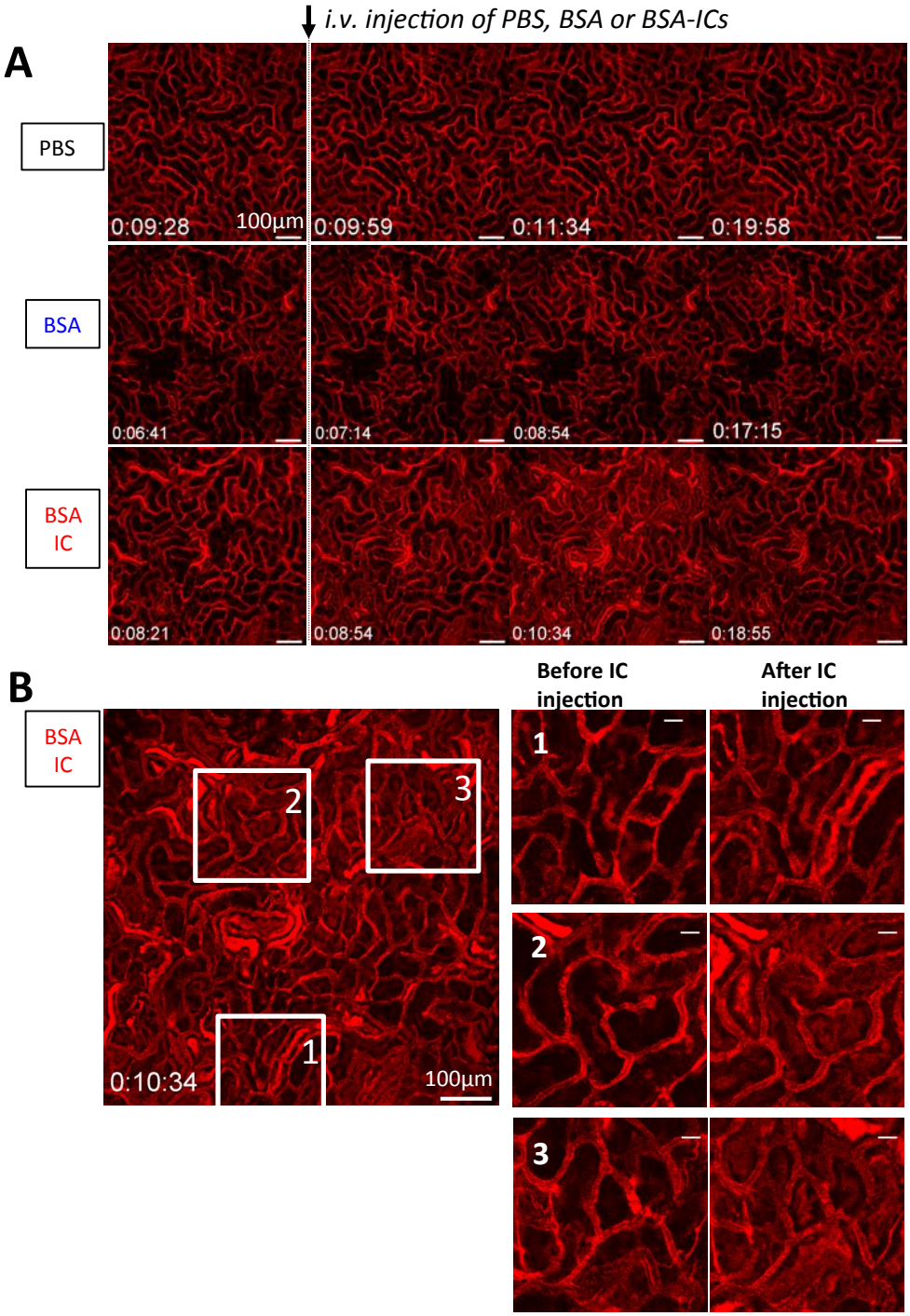

Figure 4.5. Vascular permeability assay. Kidney of C57BL/6 mice were imaged for a few minutes to measure background fluorescence. Then 70kDa Dextran-TRITC was injected *i.v.* in order to visualise the blood vessels. 5min after, either PBS, BSA or BSA-ICs was injected *i.v.* and the kidney was imaged for a further 30min. **(A)** Representative still frames of kidney volumes of PBS, BSA or BSA-ICs –injected mice. From left to right, the images show the vessels just before injection, just after injection, and two representative time points until 10min after injection. Bars represent 100µm. **(B)** Representative image of when tubule staining is maximal for BSA-ICs injected mice. left shows the whole field of view while right shows the inserts areas before injection (8min21) and at 10min34. bars represent 100µm (left) or 20µm (right). Time is shown as hh:mm:ss after the start of imaging. Representative of three mice per condition

Analysis of the capillaries of the kidney cortex showed no observable vascular leak throughout the imaging time (**Figure 4.5-A**). An apparent increase in tubular fluorescence in BSA-ICs-injected mice was observed (**Figure 4.5-B**), but no vascular leakage. This increased fluorescence was observed in the three mice injected with BSA-ICs (data not shown), but may represent an experimental artefact. Fluorescence of the tubules following injection of Dextran-TRITC of various sizes (including 70kDa as used here) was observed on many occasions in the laboratory (data not shown), therefore no conclusion may be drawn from this observation.

These data rule out the hypothesis that immune complexes gain access to the macrophages underlining the endothelial cells. Intravital confocal microscopy and electron microscopy revealed another mechanism, as will be discussed in the next section.

4.3. Discussion and further work

The results presented in this chapter helped uncovering some aspects of Ly6C^{low} monocyte and resident macrophage functions in the kidney.

Platelets have a well-characterised role in hemostasis, as the key players during the process of coagulation. However, work from many groups over the last two decades or so, has allowed the emergence of platelets as crucial actors of inflammation as well (Schulz et al., 2013; Semple et al., 2011; Weyrich et al., 2003). An active crosstalk between platelets and cells of the innate arm of immunity has been found, notably between platelets and monocytes and neutrophils (Schulz et al., 2013). In the case of Deep Vein Thrombosis (DVT), a major cause of morbidity and mortality worldwide, the intravascular thrombus contains large numbers of leukocytes, 30% of which are

monocytes, and 70% of which are neutrophils, where they are found in association with platelets (von Bruhl et al., 2012). Platelets also play a critical role in infections, such as *Staphylococcus aureus* and HIV (Youssefian et al., 2002). In the liver, Kupffer cells constitutively express von Willebrand factor at their surface, and platelets have dynamic interactions with this vWF during steady state (termed 'touch-and-go' interactions, Wong et al., 2013). In the context of bacterial infection, the capture of microbes by the Kupffer cells involves platelets that accumulate at the focal site of capture, and platelet depletion leads to a worsen bacterial load (Wong et al., 2013).

Given the increasingly recognized role of platelets in inflammation, it was relevant to assess their role in the patrolling monocyte activity in the kidney. The results presented in this thesis (**Figure 4.1**) indicate that platelets are necessary for the retention of monocytes upon TLR7 signals, notably consistent with *in vitro* results showing increased adherence of monocyte to Human Umbilical Vein Endothelial Cells (HUVEC) when engaged in aggregates with platelets via P-selectins (Da Costa Martins et al., 2004). The absence of neutrophil recruitment observed after platelet depletion in the context of TLR7 agonist topical application on the kidney is consistent with the absence of retention of monocytes, are patrolling Ly6C^{low} CX$_3$CR1^{hi} monocytes have been shown to be responsible for neutrophil recruitment in this model (Carlin et al., 2013). Because platelets also express a wide range of pattern recognition receptors at their surface (Takeuchi and Akira, 2010), investigating whether platelets engage them in our model would be interesting (Koupenova et al., 2014). Recently, a study has used similar models to the ones presented in **Figure 4.1**, though in the mesenteric vessels, to show very elegant results on the interactions between Ly6C^{low} monocytes patrolling the endothelium and recruiting neutrophils upon R848 treatment, all through close interactions with platelets (Imhof et al., 2016).

Of note, the staining performed on platelets as shown in **Figure 4.1-D**, and suggesting monocyte-platelets-aggregates, is to be considered with care. First, the use of CD49b is not optimal, as other cells are known to express this marker, and cells of a size too large to be platelets were observed in that staining (data not shown). Such aggregates have been observed, notably when using fluorescently labeled antibodies directed at another platelet surface glycoprotein, GPIIbIIIa (CD41, Hidalgo et al., 2009). Second, monocytes express all FcγR (Biburger et al., 2011), and have been shown to be major actors of antibody-mediated platelet depletion. Therefore, it is also possible that the snapshot shown in **Figure 4.1-D** represents a monocyte in the process of phagocytosing platelets. This is also the reason why it was important to analyse the effects of the platelet depletion antibody used for **Figure 4.1-B**. in order to make sure that monocytes were not actively involved in platelet depletion. Fortunately, the platelet depletion mediated by the anti-GPIbα (Emfret analytics, Cat#R300, see **Methods**) used for this study was shown by the group that generated them (Nieswandt et al., 2000) to be FcR-independent, which is consistent with our results (**Figure 4.1-B**).

The next portion of results presented in this chapter shed light on certain aspects of another inflammatory setting, the circulation of immune complexes. The first step undertaken was to make sure that immune complexes were formed in a specific and reproducible fashion using a simple *in vitro* method, which was shown to be the case in **Figure 4.2**. The specificity of the polyclonal antibodies to the two types of albumin was shown by mixing OVA to anti-BSA IgGs. Interestingly, this confirms the great specificity of anitbody production, showing that when producing an antibody in rabbits (our polyclonal IgG are from rabbits), the IgGs are generated aginst the portion of albumin that is specific to the other species. The immune complexes formed were of 700kDa, which suggests that several IgGs are involved for each molecule of albumin. Around 20 to 25% of the immunoglobulins were involved in immune complexes

according to a semi-quantitative analysis. This posed the question of the impact of the free IgGs still present in the injected solution, on uptake, activation of macrophages and production of inflammatory cytokines. Experiments were performed in the laboratory by Efstathios Stamatiades to elucidate this, and injection of IgGs alone had no effect in terms of TNFα production or macrophage activation (Stamatiades et al., 2016, *Figure 5H and S5H*). This suggested that IgGs have to be involved in immune complexes, engaging sevral Fc receptors, for there to be sufficient intracellular signaling downstream of FcγRIV, and inducing macrophage activation and cytokine production.

Some of the results regarding FcγRIV-mediated uptake, leukocyte recruitment and TNFα production were successfully reproduced in this thesis (**Figure 4.3**) ; reproducibility of results is always important, and sometimes underrated aspect of research, when the pressure for publication relegates this type of work to a 'less urgent' category of planned experiments. Regarding the TNFα results presented in this thesis, they do not constitute in themselves a well controlled experiment, as only control for APC fluorescence is shown with the isotype staining. However, TNFα production was established by better controlled experiments in the laboratory, as shown in Stamatiades et al., 2016 (see the *Figure 5E*, *F*). Injection of BSA alone does not induce cytokine production by F4/80$^{\mathbf{bright}}$ macrophages of the kidney, showing that constant uptake of circulating particules is not inflammatory in itself.

The uptake of circulating immune complexes in several organs was investigated, and found only in liver Kupffer cells and spleen RPMΦ, in addition to kidney resident macrophages (**Figure 4.4**). This phenomenon in the liver and spleen was consistent with the structure of the sinuisoidal endothelium of these tissues, where the macrophages lie in direct contact with the bloodstream. However, intravital microscopy studies suggested that kidney, although sitting close to the capillary vessels of the kidney cortex, may not be in direct contact with the circulating blood. The resolution of this

technique was however not quite sufficient to indicate whether processes of the macrophages cells could go through the vessel wall to contact the bloodstream. Experiments performed as shown in **Figure 4.5** ruled out the possibility that access of circulating immune complexes may be mediated by an induced vascular leakage, as observed in other conditions (Binstadt et al., 2006). Transmission electron microscopy experiments performed by Marie-Eve Tremblay (University of Laval, Canada) very elegantly showed that macrophages lie directly between the basement membranes of kidney tubules and the endothelial cells. Furthermore, in accordance with seminal work performed notably by Palade and colleagues in the 1960s to 1990s (Bruns and Palade, 1968; Milici et al., 1985; Predescu and Palade, 1993), endothelial cells of the kidney were found to be rich in caveolae, clathrin-coated vesicles and trans-endothelial channels (Stamatiades et al., 2016, *figure 3*). Experiments with immunogold-labeled BSA indicated the presence of immunogold staining in the caveolae and endosomal compartments of kidney macrophages, consistent with (i) trans-endothelial transport of circulating proteins, and (ii) with intravital experiments using BSA labeled with pH-sensitive dyes showing the uptaken BSA was ingested and processed in endocytic compartments.

Altogether, the work presented in this chapter participated to the characterisation of the function of kidney resident macrophages, which constitute a functional unit with endothelial cells, through the caleolae of which circulating particles are pumped and being delivered to the underlying macrophages. Therefore these cells perform an immune monitoring of the circulation in the kidney, while Ly6C$^{\mathbf{low}}$ monocytes patrol the capillaries of the kidney, requesting the help of platelets in the context of TLR7-mediated inflammation. These results may carry some relevance for disease models of autoimmune disorders, which will be discussed in the next chapter.

5 – Discussion and general conclusion

5.1. A multidisciplinary approach to tackle the question of monocyte dynamics

Previous work in the laboratory carried out by Hannah Garner has prompted a re-examination of monocyte dynamics in relation to their progenitors in the bone marrow. Genetic data showing that one subset of monocytes could be strongly decreased without a major influence on the other in terms of number, as well as a description of a potential precursor cell for Ly6C^{low} monocytes, seemed to be away from the current model for Ly6C^{low} monocyte generation *in vivo*, supported by several publications (Yona et al., 2013 ; Varol et al., 2007 ; Hettinger et al., 2013, notably), and which suggests that Ly6C^{+} monocytes convert into Ly6C^{low} monocytes in the blood circulation. However, quantitative data to support any other hypothesis was missing. Therefore, the approach presented in **Chapter 3** was followed.

An examination of this issue with a mathematical, computer-assisted model was performed. Experimentally parameterized models have yielded new results in several areas of research in biology as discussed in the introduction chapter of this thesis. A similar approach has been adopted recently to decipher monocyte subsets relationship in human (Patel et al., 2017), as will be discussed below.

As described in the **Materials and Methods**, the model generated by our collaborators Grégoire Altan-Bonnet and Amir Erez regards populations of the various organs considered (BM, Blood and Spleen) as a closed, dynamic system. Therefore, specific cell populations had to be chosen to be analysed as a group; this prompted the consideration of the known progenitors for monocytes: MDP (Fogg et al., 2006), cMoP (Hettinger et al., 2013), as well as monocytes of blood and spleen, and monocyte-like populations of the bone marrow (**Figure 3.1**). Determining their size was of critical importance, as this is one of the parameters the model takes into account. Indeed, let us consider a pair of cell populations, with is a potential lineage relationship between them.

Then if the upstream population is small compared to the second one, it will need to proliferate very actively, in order to generate the second one. Conversely, a large population that would be giving rise to a small population of cells would not need to dedicate much of its proliferative capacity to generate its downstream population. Time is also of the essence, as the kinetics of EdU increase and decrease within the different populations dictates the speed at which differentiation needs to occur. This is why the calculations and estimates were perfomed for **Figure 3.2**.

Subsequently, identification of the main proliferating populations was needed in order to establish where the EdU uptake would take place (**Figure 3.2**), and this also guided the analysis of the next set of experiments (**Figures 3.3** to **3.5**), designed to characterise the early events of proliferation and differentiation. Our data show that a single injection of EdU provides a very short time window for cells in S-phase to uptake (~15min). The bioavilability of EdU following *i.p.* injection was shown previously to be as efficient as the *i.v.* route (Sun et al., 2016). This means a restricted wave of progenitor/precursor cells were labelled with EdU, and that all the EdU detected subsequently would have to come from these early uptake events. Analysis of the intensity of the EdU signal was also performed in order to inform on what 'generation' of cells were analysed at any given time point, since each cell division will decrease the EdU content by half in the daughter cells. Unfortunately, the precision of the measurement of EdU content was not high enough in our hands, to provide specific information about the number of divisions, consistent with previous reports indicating the difficulty of such measurements (Pereira et al., 2017). However, it was estimated that the EdU levels would fall below detection threshold after around 5 divisions.

The various analysis presented from **Figure 3.6** to **3.10** describe attempts to analyse a data set of EdU kinetics over 10 days, in three organs, in three mice per time point. Indeed, less 'biased' gating was attempted through the use of the algorithm t-SNE. This

tool allows the clustering of cells solely based on the intensity of staining for the cell markers used in cytometry, whether it is fluorescence based or mass cytometry (CyTOF). Using this technique, potential 'missing link' were identified in the sequence of differentiation from the proliferating late progenitors/precursor cells (MDP, cMoP, BM Ly6C^{+}) to the mature, non-proliferating Ly6C$^{\mathbf{low}}$ populations (BM CD115$^{\mathbf{low}}$ and BM Ly6C$^{\mathbf{low}}$ cells). However, a more solid mathematical analysis was finally obtained when the preparation of the cells was optimised, allowing to recover more Ly6C$^{\mathbf{low}}$ monocytes in the bone marrow. This dismissed the need for a 'missing link', as Ly6C$^{\mathbf{low}}$ monocytes of the BM constituted a viable 'destination' population.

This latest analysis, presented in **Figure 3.11**, is consistent with a transition from Ly6C$^{\mathbf{high}}$ monocytes to the Ly6C$^{\mathbf{low}}$ populations occurring in parallel in bone marrow, blood and spleen. However, the quantification of the 'flow' of cells from high to low expression of Ly6C seems to indicate this transition is most prevalent in the bone marrow, while less intense flow occurs in the blood, and a very small one in the spleen (**Figure 3.11-E**). This is consistent with previous adoptive transfer experiments performed by Hannah Garner in the laboratory (data not shown) : when injecting sorted BM Ly6C^{+} cells into a non irradiated host, Ly6C$^{\mathbf{low}}$ *Nr4a1*$^{\mathbf{bright}}$ monocytes were recovered in the circulation of the hosts. However, this could not be achieved by transferring Ly6C^{+} monocytes sorted from the circulating blood. This suggested that the precursor to Ly6C$^{\mathbf{low}}$ monocytes resides within the BM Ly6C^{+} cells. In addition, careful analysis of *Irf8*$^{-/-}$ mice, which lack most Ly6C^{+} monocytes in blood and bone marrow, show that a relatively small number of Ly6C^{+} cells remains in the bone marrow. These cells, being *Irf8*-independent, might represent the fraction that gives rise to Ly6C$^{\mathbf{low}}$ monocytes; however, more investigation will be needed to determine this.

This latest analysis suggesting a transition from Ly6C$^{\mathbf{high}}$ to Ly6C$^{\mathbf{low}}$ is not fully in line with the current model of monocyte development, which states a conversion from

one subset to the other in the circulation. However, more work will be necessary to confirm it. Moreover, the discussion in **Chapter 3** (see **section 3.3**) provides an overview of the limits associated with these latest result, and points to directions that future investigations could take in order to more firmly establish a strong model. Should the hypothesis of a differentiation from Ly6C^{high} to Ly6C^{low} monocytes in the bone marrow be confirmed, it will be very interesting to look at the published corpus of work that points to a conversion in the blood, in light of this new hypothesis. Adoptive transfer experiments of BM Ly6C^{+} cells, or of cMoP (Hettinger et al., 2013) have been published, and the sequential generation of Ly6C^{+} followed by Ly6C^{low} monocytes has so far been interpreted as the manifestation of the fact that Ly6C^{+} monocytes give rise to Ly6C^{low} monocytes. An alternative interpretation, in light of our results, could be that within heterogeneous BM Ly6C^{+} cells (Chong et al., 2016), rapidly differentiating cells give rise to Ly6C^{+} monocytes in the blood, while a fraction differentiates slower in the bone marrow to give rise to Ly6C^{low} monocytes. This is also the case for the interpretation of EdU or BrdU kinetic data, showing successive peaks of EdU (or BrdU) appearing for Ly6C^{+} cells and then Ly6C^{low} cells (Yona et al., 2013). However, more work will be needed to confirm or infirm the validity of this latest analysis, in order to decipher the molecular control that dictate monocyte differentiation.

Interestingly, a modeling approach has been adopted and published recently, for the investigation of human monocyte subsets differentiation (Patel et al., 2017), where the authors have analysed the kinetics of uptake and distribution throughout time of Deuterium at various time points following a single injection. Mathematical modelisation of the monocyte compartment supports a transition from CD14^{+} CD16^{-} to CD14^{dim} CD16^{+} monocytes, through an intermediate CD14^{+} CD16^{+} stage. These kinetic analyses were also supported with experiments of inflammatory challenges leading to monocytopenia and repopulation of the monocyte compartment (Patel et al., 2017),

where sequential generation of the three subpopulations were observed, consistent with the modeling analysis. This is consistent with results published for mouse monocytes, which as mentioned above are believed to convert from Ly6C^{high} monocytes (homologues of human CD14^{+} CD16^{-}) to Ly6C^{low} (homologues of human CD14^{dim} CD16^{+}). The sequence of differentiation through an intermediate stage is also consistent with mouse data showing transition form Ly6C^{high} to Ly6C^{low} through a Ly6C^{int} intermediate stage (Mildner et al., 2017). This study implements a multidisciplinary approach like our own, where mathematics are used as an unbiased, 'blind' tool to put hypothesis to the test of experimental data. It is also an interesting by-pass to the difficulty of experimenting on humans, where approaches such as adoptive transfer are impossible.

Overall, the work presented in this thesis regarding monocyte dynamics participates to the growing body of work in biology, as nicely exemplified with the work of Patel and colleagues, which attempts to bring together experimental data, with its impredictible set of unknowns, and its necessarily present lack of exactitude, with the most exact of sciences, mathematics. The work shown here presents a multidisciplinary effort from various investigators of different backgrounds, which hopefully will continue to progress.

5.2. Description of a tissue-specific function for kidney resident macrophages, with potential relevance in disease

The results presented in chapter 4 participated to the uncovering of platelet-monocyte cooperation, and to the identification of a functional unit formed by the endothelial cells and resident macrophages in the kidney.

Monocyte-platelet cooperation for good or ill has been increasingly well characterised over the last couple of decades (Semple et al., 2011; Schulz et al., 2013), although the specific interactions of platelets with the patrolling Ly6C^{low} monocyte subset remained to be examined. Here it was shown that although GPIbα engagement is not crucial, platelet depletion prevents normal Ly6C^{low} monocyte retention and subsequent recruitment of neutrophils (**Figure 4.1**). The specific receptor/ligand interactions between the two cell types would be interesting to investigate, as there has been show to be several potential molecular bridges between them, such as through P-Selectin (Higashiyama et al., 2008), or tissue factor produced by monocytes and neutrophils during deep vein thrombosis (von Bruhl et al., 2012). Platelet-neutrophil aggregates have also been observed *in vivo* when injecting anti-CD49b *i.v.* to mice while imaging (data not shown), so it would also be an interesting topic of investigation to uncover the specific interactions between platelets and neutrophils in the context of TLR7 signals. The recruitment of neutrophils by patrolling monocytes following topical application of the TLR7 agonist R848 has been shown to induce necrosis of endothelial cells (Carlin et al., 2013). Therefore, using transmission electron microscopy to analyse endothelium structure following platelet depletion would inform on whether it also prevents these later events. The results presented here are consistent with a recent study showing similar results and characterising the system in larger vessels (Quintar et al., 2017).

The rest of the results presented in **Chapter 4** of this thesis focus on another inflammatory stimulus: the presence of small immune complexes in the circulation, and the way kidney resident macrophages respond to them. Characterising the products of the *in vitro* preparation method (**Figure 4.2**) was important, in combination with the various injections of immunoglobulin performed by Efstathios Stamatiades (Stamatiades et al., 2016), to discard the hypothesis that the components (albumin, IgGs) alone were responsible for the inflammatory response. Indeed, it was shown *in*

vitro that macrophages can produce iNOS in response to endotoxin-free albumin, and notably BSA (Poteser and Wakabayashi, 2004).

Investigating uptake of albumin and immune complexes in organs other than the kidney demonstrated that only two others harbor macrophages that have the ability to do so: liver and spleen. These two organs have fenestrations of endothelium that allow direct contact of the macrophages (Kupffer cells and RPMΦ) with the blood flow; however, intravital microscopy and transmission electron microscopy studies showed no such contact between kidney resident macrophagesand the circulation (Stamatiades et al., 2016). Therefore, the access of macrophages to the circulating proteins was investigated and found that it was not due to vascular leakage in the kidney (Figure 4.5), but allowed by a caveolae system which performs a sampling of the circulation by the endolthelial cells, which transport circulation content to the underlying macrophages, which extend long (up to ~100μm) processes and receive the endocytosed particles. Discarding the vascular leakage hypothesis was interesting, as it has been shown to occur in the context of a mouse model of Rheumatoid Arthritis (Binstadt et al., 2006). Moreover, these data, and more generally the work of Stamatiades and colleagues (Stamatiades et al., 2016), shed light on a broader question regarding type III hypersensitivity. This group of autoimmune disorders is characteried by the circulation of immune complexes due to autoimmune reaction to nucleic acid antigens. Kidney inflammation and damage follow, and it was unclear whether the deposit of immune complexes on the interstitium was a cause for inflammation, or following kidney damage induced through another mechanism. The data provided by Stamatiades and colleagues provides a mechanism for early inflammation in the kidney due to immune complexes, showing that the immune complexes are taken up by kidney resident macrophages via FcγRIV, which in turn produce inflammatory cytokines. Monocytes and neutrophils also express FcγRIV (Nimmerjahn et al., 2005), while endothelial cells

do not, as seen by qPCR analysis of sorted $CD45^-$ $CD31^+$ cells from the kidney (Stamatiades et al., 2016). However, the engagement of FcγRIV on the surface of circulating leukocytes does not impact the inflammatory process in this model of study (Stamatiades et al., 2016).

Together, these results shed light on the functional unit formed by kidney resident macrophages and endothelial cells of the kidney, which monitors the content of circulation and triggers an inflammatory reaction. This may have interesting relevance in the context of deseases of type III hypersensitivity; the mechanism uncovered is distinct form the Arthus reaction (Hazenbos et al., 1996; Nimmerjahn et al., 2010), or immune complex-mediated peritonitis (Hasenberg et al., 2015). It may also participate to the understanding of SLE.

5.3. General conclusion

The work presented in this thesis provided some insight into the biology of myeloid populations, both regarding development and function. A multidisciplinary approach to data analysis allowed the production of a new hypothesis for the development of $Ly6C^{low}$ monocytes, which may occur in the bone marrow rather than the circulation. A collaborative effort has allowed the identification of a tissue-specific function of kidney resident macrophages, in line with the hypothesis that Metchnikoff formulated in the late 18th century, that macropahges participate to the homeostasis of their tissue of residence.

References

Abramson, S.L., and Gallin, J.I. (1990). IL-4 inhibits superoxide production by human mononuclear phagocytes. J. Immunol. *144*, 625–630.

Adolfsson, J., Månsson, R., Buza-Vidas, N., Hultquist, A., Liuba, K., Jensen, C.T., Bryder, D., Yang, L., Borge, O.J., Thoren, L.A.M., et al. (2005). Identification of Flt3+ lympho-myeloid stem cells lacking erythro-megakaryocytic potential: A revised road map for adult blood lineage commitment. Cell *121*, 295–306.

Aird, W.C. (2007). Phenotypic heterogeneity of the endothelium: I. Structure, function, and mechanisms. Circ. Res. *100*, 158–173.

Ajami, B., Bennett, J.L., Krieger, C., Tetzlaff, W., and Rossi, F.M. V (2007). Local self-renewal can sustain CNS microglia maintenance and function throughout adult life. Nat. Neurosci. *10*, 1538–1543.

Akashi, K., Traver, D., Miyamoto, T., and Weissman, I.L. (2000). A clonogenic common myeloid progenitor that gives rise to all myeloid lineages. Nature *404*, 193–197.

Alder, J.K., Georgantas, R.W., Hildreth, R.L., Kaplan, I.M., Morisot, S., Yu, X., McDevitt, M., and Civin, C.I. (2008). Kruppel-Like Factor 4 Is Essential for Inflammatory Monocyte Differentiation In Vivo. J. Immunol. *180*, 5645–5652.

Aldridge, J.R., Moseley, C.E., Boltz, D.A., Negovetich, N.J., Reynolds, C., Franks, J., Brown, S.A., Doherty, P.C., Webster, R.G., and Thomas, P.G. (2009). TNF/iNOS-producing dendritic cells are the necessary evil of lethal influenza virus infection. Proc. Natl. Acad. Sci. *106*, 5306–5311.

Altan-Bonnet, G., and Germain, R.N. (2005). Modeling T cell antigen discrimination based on feedback control of digital ERK responses. PLoS Biol. *3*, 1925–1938.

Amano, H., Amano, E., Santiago-Raber, M.L., Moll, T., Martinez-Soria, E., Fossati-Jimack, L., Iwamoto, M., Rozzo, S.J., Kotzin, B.L., and Izui, S. (2005). Selective expansion of a monocyte subset expressing the CD11c dendritic cell marker in the Yaa model of systemic lupus erythematosus. Arthritis Rheum. *52*, 2790–2798.

Ambrose, C.T. (2006). The Osler slide, a demonstration of phagocytosis from 1876: Reports of phagocytosis before Metchnikoff's 1880 paper. Cell. Immunol. *240*, 1–4.

Ancuta, P., Autissier, P., Wurcel, A., Zaman, T., Stone, D., and Gabuzda, D. (2006). CD16+ Monocyte-Derived Macrophages Activate Resting T Cells for HIV Infection by Producing CCR3 and CCR4 Ligands. J. Immunol. *176*, 5760–5771.

Antonelli, L.R. V, Gigliotti Rothfuchs, A., Gonçalves, R., Roffê, E., Cheever, A.W., Bafica, A., Salazar, A.M., Feng, C.G., and Sher, A. (2010). Intranasal Poly-IC treatment exacerbates tuberculosis in mice through the pulmonary recruitment of a pathogen-permissive monocyte/macrophage population. J. Clin. Invest. *120*, 1674–1682.

Arnold-Schrauf, C., Dudek, M., Dielmann, A., Pace, L., Swallow, M., Kruse, F., Kühl,

A.A., Holzmann, B., Berod, L., and Sparwasser, T. (2014). Dendritic Cells Coordinate Innate Immunity via MyD88 Signaling to Control Listeria monocytogenes Infection. Cell Rep. *6*, 698–708.

Atkins, R.C., Glasgow, E.F., Holdsworth, S.R., and Matthews, F.E. (1976). The macrophagen in human rapidly progressive glomerulonephritis. Lancet *1*, 830–832.

Auffray, C., Fogg, D., Garfa, M., Elain, G., Join-Lambert, O., Kayal, S., Sarnacki, S., Cumano, A., Lauvau, G., and Geissmann, F. (2007a). Monitoring of blood vessels and tissues by a population of monocytes with patrolling behavior. Science *317*, 666–670.

Auffray, C., Fogg, D.K., Narni-Mancinelli, E., Senechal, B., Trouillet, C., Saederup, N., Leemput, J., Bigot, K., Campisi, L., Abitbol, M., et al. (2009). CX_3CR1^+ $CD115^+$ $CD135^+$ common macrophage/DC precursors and the role of CX_3CR1 in their response to inflammation. J. Exp. Med. *206*, 595–606.

Austyn, J.M., Hankins, D.F., Larsen, C.P., Morris, P.J., Rao, A.S., and Roake, J.A. (1994). Isolation and characterization of dendritic cells from mouse heart and kidney. J Immunol *152*, 2401–2410.

Bain, C.C., Scott, C.L., Uronen-Hansson, H., Gudjonsson, S., Jansson, O., Grip, O., Guilliams, M., Malissen, B., Agace, W.W., and Mowat, A.M. (2013). Resident and pro-inflammatory macrophages in the colon represent alternative context-dependent fates of the same Ly6Chi monocyte precursors. Mucosal Immunol. *6*, 498–510.

Bain, C.C., Bravo-Blas, A., Scott, C.L., Gomez Perdiguero, E., Geissmann, F., Henri, S., Malissen, B., Osborne, L.C., Artis, D., and Mowat, A.M. (2014). Constant replenishment from circulating monocytes maintains the macrophage pool in the intestine of adult mice. Nat. Immunol. *15*, 929–937.

Bain, C.C., Hawley, C.A., Garner, H., Scott, C.L., Schridde, A., Steers, N.J., Mack, M., Joshi, A., Guilliams, M., Mowat, A.M.I., et al. (2016). Long-lived self-renewing bone marrow-derived macrophages displace embryo-derived cells to inhabit adult serous cavities. Nat. Commun. *7*, ncomms11852.

Baratin, M., Simon, L., Jorquera, A., Ghigo, C., Dembele, D., Nowak, J., Gentek, R., Wienert, S., Klauschen, F., Malissen, B., et al. (2017). T Cell Zone Resident Macrophages Silently Dispose of Apoptotic Cells in the Lymph Node. Immunity *47*, 349–362.e5.

Becker, A.M., Michael, D.G., Satpathy, A.T., Sciammas, R., Singh, H., and Bhattacharya, D. (2012). IRF-8 extinguishes neutrophil production and promotes dendritic cell lineage commitment in both myeloid and lymphoid mouse progenitors. Blood *119*, 2003–2012.

Bergmeier, W., Rackebrandt, K., Schröder, W., Zirngibl, H., and Nieswandt, B. (2000). Structural and functional characterization of the mouse von Willebrand factor receptor GPIb-IX with novel monoclonal antibodies. Blood *95*, 886–893.

Bertrand, J.Y., Giroux, S., Golub, R., Klaine, M., Jalil, A., Boucontet, L., Godin, I., and Cumano, A. (2005). Characterization of purified intraembryonic hematopoietic stem cells as a tool to define their site of origin. Proc. Natl. Acad. Sci. *102*, 134–139.

Bertrand, J.Y., Chi, N.C., Santoso, B., Teng, S., Stainier, D.Y.R., and Traver, D. (2010).

Haematopoietic stem cells derive directly from aortic endothelium during development. Nature *464*, 108–111.

Bertrand, J.Y., Jalil, A., Klaine, M., Jung, S., Cumano, A., Godin, I., and Dc, W. (2013). Three pathways to mature macrophages in the early mouse yolk sac Three pathways to mature macrophages in the early mouse yolk sac. Blood *106*, 3004–3011.

Biburger, M., Aschermann, S., Schwab, I., Lux, A., Albert, H., Danzer, H., Woigk, M., Dudziak, D., and Nimmerjahn, F. (2011). Monocyte Subsets Responsible for Immunoglobulin G-Dependent Effector Functions In Vivo. Immunity *35*, 932–944.

Binstadt, B.A., Patel, P.R., Alencar, H., Nigrovic, P.A., Lee, D.M., Mahmood, U., Weissleder, R., Mathis, D., and Benoist, C. (2006). Particularities of the vasculature can promote the organ specificity of autoimmune attack. Nat. Immunol. *7*, 284–292.

Blander, J.M. (2016). Death in the intestinal epithelium???basic biology and implications for inflammatory bowel disease. FEBS J. *283*, 2720–2730.

Bliss, S.K., Butcher, B.A., and Denkers, E.Y. (2000). Rapid Recruitment of Neutrophils Containing Prestored IL-12 During Microbial Infection. J. Immunol. *165*, 4515–4521.

Bocharov, G., Argilaguet, J., and Meyerhans, A. (2015). Understanding Experimental LCMV Infection of Mice: The Role of Mathematical Models. J. Immunol. Res. *2015*.

Boisset, J.-C., van Cappellen, W., Andrieu-Soler, C., Galjart, N., Dzierzak, E., and Robin, C. (2010). In vivo imaging of haematopoietic cells emerging from the mouse aortic endothelium. Nature *464*, 116–120.

Bonnett, C.R., Cornish, E.J., Harmsen, A.G., and Burritt, J.B. (2006). Early neutrophil recruitment and aggregation in the murine lung inhibit germination of Aspergillus fumigatus conidia. Infect. Immun. *74*, 6528–6539.

Boring, L., Gosling, J., Chensue, S.W., Kunkel, S.L., Farese, R. V., Broxmeyer, H.E., and Charo, I.F. (1997). Impaired monocyte migration and reduced type 1 (Th1) cytokine responses in C-C chemokine receptor 2 knockout mice. J. Clin. Invest. *100*, 2552–2561.

Boyce, B.F., Yao, Z., and Xing, L. (2009). Osteoclasts have multiple roles in bone in addition to bone resorption. Crit. Rev. Eukaryot. Gene Expr. *19*, 171–180.

Boyce, N.W., Tipping, P.G., and Holdsworth, S.R. (1989). Glomerular macrophages produce reactive oxygen species in experimental glomerulonephritis. Kidney Int *35*, 778–782.

Brown, A.S., Yang, C., Fung, K.Y., Bachem, A., Bourges, D., Bedoui, S., Hartland, E.L., and van Driel, I.R. (2016). Cooperation between Monocyte-Derived Cells and Lymphoid Cells in the Acute Response to a Bacterial Lung Pathogen. PLoS Pathog. *12*.

von Bruhl, M.-L., Stark, K., Steinhart, a., Chandraratne, S., Konrad, I., Lorenz, M., Khandoga, a., Tirniceriu, a., Coletti, R., Kollnberger, M., et al. (2012). Monocytes, neutrophils, and platelets cooperate to initiate and propagate venous thrombosis in mice in vivo. J. Exp. Med. *209*, 819–835.

Brunet, A., LeBel, M., Egarnes, B., Paquet-Bouchard, C., Lessard, A.J., Brown, J.P.,

and Gosselin, J. (2016). NR4A1-dependent Ly6Clow monocytes contribute to reducing joint inflammation in arthritic mice through Treg cells. Eur. J. Immunol. *46*, 2789–2800.

Bruns, R.R., and Palade, G.E. (1968). Studies on blood capillaries. II. Transport of ferritin molecules across the wall of muscle capillaries. J. Cell Biol. *37*, 277–299.

Bruttger, J., Karram, K., Wörtge, S., Regen, T., Marini, F., Hoppmann, N., Klein, M., Blank, T., Yona, S., Wolf, Y., et al. (2015). Genetic Cell Ablation Reveals Clusters of Local Self-Renewing Microglia in the Mammalian Central Nervous System. Immunity *43*, 92–107.

Busch, K., Klapproth, K., Barile, M., Flossdorf, M., Holland-Letz, T., Schlenner, S.M., Reth, M., Höfer, T., and Rodewald, H.-R. (2015). Fundamental properties of unperturbed haematopoiesis from stem cells in vivo. Nature *518*, 542–546.

Carlin, L.M., Stamatiades, E.G., Auffray, C., Hanna, R.N., Glover, L., Vizcay-Barrena, G., Hedrick, C.C., Cook, H.T., Diebold, S., and Geissmann, F. (2013). Nr4a1-dependent Ly6C(low) monocytes monitor endothelial cells and orchestrate their disposal. Cell *153*, 362–375.

Carrel, A., and Ebeling, A.H. (1926). THE FUNDAMENTAL PROPERTIES OF THE FIBROBLAST AND THE MACROPHAGE : II. THE MACROPHAGE. J. Exp. Med. *44*, 285–305.

Carrer, A., Moimas, S., Zacchigna, S., Pattarini, L., Zentilin, L., Ruozi, G., Mano, M., Sinigaglia, M., Maione, F., Serini, G., et al. (2012). Neuropilin-1 identifies a subset of bone marrow Gr1-monocytes that can induce tumor vessel normalization and inhibit tumor growth. Cancer Res. *72*, 6371–6381.

Casson, C.N., Doerner, J.L., Copenhaver, A.M., Ramirez, J., Holmgren, A.M., Boyer, M.A., Siddarthan, I.J., Rouhanifard, S.H., Raj, A., and Shin, S. (2017). Neutrophils and Ly6Chimonocytes collaborate in generating an optimal cytokine response that protects against pulmonary Legionella pneumophila infection. PLoS Pathog. *13*, 1–26.

Cattell, V., Largen, P., de Heer, E., and Cook, T. (1991). Glomeruli synthesize nitrite in active Heymann nephritis; the source is infiltrating macrophages. Kidney Int *40*, 847–851.

Cecchini, M.G., Dominguez, M.G., Mocci, S., Wetterwald, A., Felix, R., Fleisch, H., Chisholm, O., Hofstetter, W., Pollard, J.W., and Stanley, E.R. (1994). Role of colony stimulating factor-1 in the establishment and regulation of tissue macrophages during postnatal development of the mouse. Development *120*, 1357–1372.

Champhekar, A., Damle, S.S., Freedman, G., Carotta, S., Nutt, S.L., and Rothenberg, E. V. (2015). Regulation of early T-lineage gene expression and developmental progression by the progenitor cell transcription factor PU.1. Genes Dev. *29*, 832–848.

Chao, L.C., Soto, E., Hong, C., Ito, A., Pei, L., Chawla, A., Conneely, O.M., Tangirala, R.K., Evans, R.M., and Tontonoz, P. (2013). Bone marrow NR4A expression is not a dominant factor in the development of atherosclerosis or macrophage polarization in mice. J. Lipid Res. *54*, 806–815.

Chen, M.J., Li, Y., De Obaldia, M.E., Yang, Q., Yzaguirre, A.D., Yamada-Inagawa, T.,

Vink, C.S., Bhandoola, A., Dzierzak, E., and Speck, N.A. (2011). Erythroid/myeloid progenitors and hematopoietic stem cells originate from distinct populations of endothelial cells. Cell Stem Cell *9*, 541–552.

Cho, C.H., Koh, Y.J., Han, J., Sung, H.K., Lee, H.J., Morisada, T., Schwendener, R.A., Brekken, R.A., Kang, G., Oike, Y., et al. (2007). Angiogenic role of LYVE-1-positive macrophages in adipose tissue. Circ. Res. *100*.

Chong, S.Z., Evrard, M., Devi, S., Chen, J., Lim, J.Y., See, P., Zhang, Y., Adrover, J.M., Lee, B., Tan, L., et al. (2016). CXCR4 identifies transitional bone marrow premonocytes that replenish the mature monocyte pool for peripheral responses. J Exp Med jem.20160800-.

Chorro, L., Sarde, A., Li, M., Woollard, K.J., Chambon, P., Malissen, B., Kissenpfennig, A., Barbaroux, J.-B., Groves, R., and Geissmann, F. (2009). Langerhans cell (LC) proliferation mediates neonatal development, homeostasis, and inflammation-associated expansion of the epidermal LC network. J. Exp. Med. *206*, 3089–3100.

Chua, C.L.L., Brown, G., Hamilton, J.A., Rogerson, S., and Boeuf, P. (2013). Monocytes and macrophages in malaria: protection or pathology? Trends Parasitol. *29*, 26–34.

Chun, J., Hla, T., Lynch, K.R., Spiegel, S., and Moolenaar, W.H. (2010). International Union of Basic and Clinical Pharmacology . LXXVIII . Lysophospholipid. Pharmacol. Rev. *62*, 579–587.

Coffman, R.L., and Weissman, I.L. (1981). B220: a B cell-specific member of the T200 glycoprotein family. Nature *289*, 681–683.

Colvin, G.A., Lambert, J.-F., Abedi, M., Hsieh, C.-C., Carlson, J.E., Stewart, F.M., and Quesenberry, P.J. (2004). Murine marrow cellularity and the concept of stem cell competition: geographic and quantitative determinants in stem cell biology. Leukemia *18*, 575–583.

Combadière, C., Potteaux, S., Rodero, M., Simon, T., Pezard, A., Esposito, B., Merval, R., Proudfoot, A., Tedgui, A., and Mallat, Z. (2008). Combined inhibition of CCL2, CX3CR1, and CCR5 abrogates Ly6Chi and Ly6Clo monocytosis and almost abolishes atherosclerosis in hypercholesterolemic mice. Circulation *117*, 1649–1657.

Cook, H.T., Smith, J., Salmon, J.A., and Cattell, V. (1989). Functional characteristics of macrophages in glomerulonephritis in the rat. O2- generation, MHC class II expression, and eicosanoid synthesis. Am J Pathol *134*, 431–437.

Copin, R., de Baetselier, P., Carlier, Y., Letesson, J.-J., and Muraille, E. (2007). MyD88-dependent activation of B220- CD11b+ LY-6C+ dendritic cells during Brucella melitensis infection. J. Immunol. (Baltimore, Md 1950) *178*, 5182–5191.

Copley, M.R., Babovic, S., Benz, C., Knapp, D.J.H.F., Beer, P.A., Kent, D.G., Wohrer, S., Treloar, D.Q., Day, C., Rowe, K., et al. (2013). The Lin28b–let-7–Hmga2 axis determines the higher self-renewal potential of fetal haematopoietic stem cells. Nat. Cell Biol. *15*, 916–925.

Cortez-Retamozo, V., Etzrodt, M., Newton, A., Rauch, P.J., Chudnovskiy, A., Berger, C., Ryan, R.J.H., Iwamoto, Y., Marinelli, B., Gorbatov, R., et al. (2012). Origins of

tumor-associated macrophages and neutrophils. Proc. Natl. Acad. Sci. *109*, 2491–2496.

Da Costa Martins, P., Van Den Berk, N., Ulfman, L.H., Koenderman, L., Hordijk, P.L., and Zwaginga, J.J. (2004). Platelet-Monocyte Complexes Support Monocyte Adhesion to Endothelium by Enhancing Secondary Tethering and Cluster Formation. Arterioscler. Thromb. Vasc. Biol. *24*, 193–199.

Cros, J., Cagnard, N., Woollard, K., Patey, N., Zhang, S.-Y., Senechal, B., Puel, A., Biswas, S.K., Moshous, D., Picard, C., et al. (2010). Human CD14dim monocytes patrol and sense nucleic acids and viruses via TLR7 and TLR8 receptors. Immunity *33*, 375–386.

Cross, M.A., and Enver, T. (1997). The lineage commitment of haemopoietic progenitor cells. Curr. Opin. Genet. Dev. *7*, 609–613.

Cumano, A., Dieterlen-Lievre, F., and Godin, I. (1996). Lymphoid potential, probed before circulation in mouse, is restricted to caudal intraembryonic splanchnopleura. Cell *86*, 907–916.

Cumano, A., Ferraz, J.C., Klaine, M., Di Santo, J.P., and Godin, I. (2001). Intraembryonic, but not yolk sac hematopoietic precursors, isolated before circulation, provide long-term multilineage reconstitution. Immunity *15*, 477–485.

Cummings, R.J., Barbet, G., Bongers, G., Hartmann, B.M., Gettler, K., Muniz, L., Furtado, G.C., Cho, J., Lira, S.A., and Blander, J.M. (2016). Different tissue phagocytes sample apoptotic cells to direct distinct homeostasis programs. Nature *539*, 565–569.

Cyster, J.G., and Schwab, S.R. (2012). Sphingosine-1-Phosphate and Lymphocyte Egress from Lymphoid Organs. Annu. Rev. Immunol. *30*, 69–94.

Dai, X., Ryan, G.R., Hapel, a J., Dominguez, M.G., Russell, R.G., Kapp, S., Sylvestre, V., and Stanley, E.R. (2002). Targeted disruption of the mouse CSF-1 receptor gene results in osteopetrosis, mononuclear phagocyte deficiency, increased primititive progenitor cell frequencies and reproductive defects. Blood *99*, 111–120.

Dakic, A., Metcalf, D., Di Rago, L., Mifsud, S., Wu, L., and Nutt, S.L. (2005). PU.1 regulates the commitment of adult hematopoietic progenitors and restricts granulopoiesis. J. Exp. Med. *201*, 1487–1502.

Dal-Secco, D., Wang, J., Zeng, Z., Kolaczkowska, E., Wong, C.H.Y., Petri, B., Ransohoff, R.M., Charo, I.F., Jenne, C.N., and Kubes, P. (2015). A dynamic spectrum of monocytes arising from the in situ reprogramming of CCR2 $^{+}$ monocytes at a site of sterile injury. J. Exp. Med. *212*, 447–456.

Daley-Bauer, L.P., Roback, L.J., Wynn, G.M., and Mocarski, E.S. (2014). Cytomegalovirus hijacks CX3CR1(hi) patrolling monocytes as immune-privileged vehicles for dissemination in mice. Cell Host Microbe *15*, 351–362.

Davalos, D., Grutzendler, J., Yang, G., Kim, J. V, Zuo, Y., Jung, S., Littman, D.R., Dustin, M.L., and Gan, W.-B. (2005). ATP mediates rapid microglial response to local brain injury in vivo. Nat. Neurosci. *8*, 752–758.

Davies, L.C., Rosas, M., Smith, P.J., Fraser, D.J., Jones, S.A., and Taylor, P.R. (2011). A quantifiable proliferative burst of tissue macrophages restores homeostatic

macrophage populations after acute inflammation. Eur. J. Immunol. *41*, 2155–2164.

Dawson, T.C., Beck, M.A., Kuziel, W.A., Henderson, F., and Maeda, N. (2000). Contrasting Effects of CCR5 and CCR2 Deficiency in the Pulmonary Inflammatory Response to Influenza A Virus. Am. J. Pathol. *156*, 1951–1959.

Day, Y.-J., Huang, L., Ye, H., Linden, J., and Okusa, M.D. (2005). Renal ischemia-reperfusion injury and adenosine 2A receptor-mediated tissue protection: role of macrophages. Am. J. Physiol. Renal Physiol. *288*, F722-31.

Debien, E., Mayol, K., Biajoux, V., Daussy, C., De Aguero, M.G., Taillardet, M., Dagany, N., Brinza, L., Henry, T., Dubois, B., et al. (2013). S1PR5 is pivotal for the homeostasis of patrolling monocytes. Eur. J. Immunol. *43*, 1667–1675.

DeKoter, R.P., Walsh, J.C., and Singh, H. (1998). PU.1 regulates both cytokine-dependent proliferation and differentiation of granulocyte/macrophage progenitors. EMBO J. *17*, 4456–4468.

Deng, L., Zhou, J.-F., Sellers, R.S., Li, J.-F., Nguyen, A. V., Wang, Y., Orlofsky, A., Liu, Q., Hume, D.A., Pollard, J.W., et al. (2010). A Novel Mouse Model of Inflammatory Bowel Disease Links Mammalian Target of Rapamycin-Dependent Hyperproliferation of Colonic Epithelium to Inflammation-Associated Tumorigenesis. Am. J. Pathol. *176*, 952–967.

Dieterlen-Lievre, F. (1975). On the origin of haemopoietic stem cells in the avian embryo: an experimental approach. J Embryol Exp Morphol *33*, 607–619.

Doherty, P.C., Topham, D.J., Tripp, R. a, Cardin, R.D., Brooks, J.W., and Stevenson, P.G. (1997). Effector CD4+ and CD8+ T-cell mechanisms in the control of respiratory virus infections. Immunol. Rev. *159*, 105–117.

Domínguez-Andrés, J., Feo-Lucas, L., Minguito de la Escalera, M., González, L., López-Bravo, M., and Ardavín, C. (2017). Inflammatory Ly6C high Monocytes Protect against Candidiasis through IL-15-Driven NK Cell/Neutrophil Activation. Immunity *46*, 1059–1072.e4.

Driggers, P.H., Ennist, D.L., Gleason, S.L., Mak, W.H., Marks, M.S., Levi, B.Z., Flanagan, J.R., Appella, E., and Ozato, K. (1990). An interferon gamma-regulated protein that binds the interferon-inducible enhancer element of major histocompatibility complex class I genes. Proc. Natl. Acad. Sci. U. S. A. *87*, 3743–3747.

Duffield, J.S., Forbes, S.J., Constandinou, C.M., Clay, S., Partolina, M., Vuthoori, S., Wu, S., Lang, R., and Iredale, J.P. (2005a). Selective depletion of macrophages reveals distinct, opposing roles during liver injury and repair. J. Clin. Invest. *115*, 56–65.

Duffield, J.S., Tipping, P.G., Kipari, T., Cailhier, J.-F., Clay, S., Lang, R., Bonventre, J. V, and Hughes, J. (2005b). Conditional ablation of macrophages halts progression of crescentic glomerulonephritis. Am. J. Pathol. *167*, 1207–1219.

Dunay, I.R., Fuchs, A., and David Sibley, L. (2010). Inflammatory monocytes but not neutrophils are necessary to control infection with Toxoplasma gondii in mice. Infect. Immun. *78*, 1564–1570.

Ebert, R.H., and Florey, H.W. (1939). The Extravascular Development of the Monocyte

Observed In vivo. Br. J. Exp. Pathol. *20*, 342.

Economou, A.D., and Green, J.B.A. (2014). Modelling from the experimental developmental biologists viewpoint. Semin. Cell Dev. Biol. *35*, 58–65.

Endele, M., Etzrodt, M., and Schroeder, T. (2014). Instruction of hematopoietic lineage choice by cytokine signaling. Exp. Cell Res. *329*, 207–213.

Enver, T., Heyworth, C.M., and Dexter, T.M. (1998). Do stem cells play dice? Blood *92*, 348–51; discussion 352.

Erwig, L.-P., Stewart, K., and Rees, A.J. (2000). Macrophages from Inflamed but Not Normal Glomeruli Are Unresponsive to Anti-Inflammatory Cytokines. Am. J. Pathol. *156*, 295–301.

Espinosa, V., Jhingran, A., Dutta, O., Kasahara, S., Donnelly, R., Du, P., Rosenfeld, J., Leiner, I., Chen, C.C., Ron, Y., et al. (2014). Inflammatory Monocytes Orchestrate Innate Antifungal Immunity in the Lung. PLoS Pathog. *10*.

Fairbairn, L., Kapetanovic, R., Beraldi, D., Sester, D.P., Tuggle, C.K., Archibald, A.L., and Hume, D. a (2013). Comparative analysis of monocyte subsets in the pig. J. Immunol. *190*, 6389–6396.

Ferenbach, D.A., Sheldrake, T.A., Dhaliwal, K., Kipari, T.M.J., Marson, L.P., Kluth, D.C., and Hughes, J. (2012). Macrophage/monocyte depletion by clodronate, but not diphtheria toxin, improves renal ischemia/reperfusion injury in mice. Kidney Int. *82*, 928–933.

Florey, Lord (1966). The Endothelial Cell. Br. Med. J. *2*, 487–490.

Fogg, D.K., Sibon, C., Miled, C., Jung, S., Aucouturier, P., Littman, D.R., Cumano, A., and Geissmann, F. (2006). A clonogenic bone marrow progenitor specific for macrophages and dendritic cells. Science *311*, 83–87.

Frame, J.M., Fegan, K.H., Conway, S.J., McGrath, K.E., and Palis, J. (2016). Definitive Hematopoiesis in the Yolk Sac Emerges from Wnt-Responsive Hemogenic Endothelium Independently of Circulation and Arterial Identity. Stem Cells *34*, 431–444.

François, P., Voisinne, G., Siggia, E.D., Altan-bonnet, G., and Vergassola, M. (2013). Phenotypic model for early T-cell activation displaying sensitivity , speci fi city , and antagonism. Proc. Natl. Acad. Sci. U. S. A. *110*, E888–E897.

Franklin, R. a, Liao, W., Sarkar, A., Kim, M. V, Bivona, M.R., Liu, K., Pamer, E.G., and Li, M.O. (2014). The cellular and molecular origin of tumor-associated macrophages. Science *344*, 921–925.

De Frutos, M., Cifuentes, A., Díez-Masa, J.C., Camafeita, E., and Méndez, E. (1998). Multiple peaks in HPLC of proteins: Bovine serum albumin eluted in a reversed-phase system. HRC J. High Resolut. Chromatogr. *21*, 18–24.

van Furth, R., Cohn, Z.A., Hirsch, J.G., Humphrey, J.H., Spector, W.G., and Langevoort, H.L. (1972). The mononuclear phagocyte system: a new classification of macrophages, monocytes, and their precursor cells. Bull. World Health Organ. *46*, 845–

852.

Gallily, R. (1971). In vitro and in vivo studies of the properties and effects of antimacrophage sera (AMS). Clin. Exp. Immunol. *9*, 381–391.

Geissmann, F., and Mass, E. (2015). A stratified myeloid system, the challenge of understanding macrophage diversity. Semin. Immunol. *27*, 353–356.

Geissmann, F., Jung, S., and Littman, D.R. (2003). Blood monocytes consist of two principal subsets with distinct migratory properties. Immunity *19*, 71–82.

Gekas, C., Dieterlen-Lièvre, F., Orkin, S.H., and Mikkola, H.K.A. (2005). The placenta is a niche for hematopoietic stem cells. Dev. Cell *8*, 365–375.

Gerrity, R.G., Naito, H.K., Richardson, M., and Schwartz, C.J. (1979). Dietary induced atherogenesis in swine. Morphology of the intima in prelesion stages. Am. J. Pathol. *95*, 775–792.

Getts, D.R., Terry, R.L., Getts, M.T., Müller, M., Rana, S., Shrestha, B., Radford, J., Van Rooijen, N., Campbell, I.L., and King, N.J.C. (2008). Ly6C + "inflammatory monocytes" are microglial precursors recruited in a pathogenic manner in West Nile virus encephalitis. J. Exp. Med. *205*, 2319–2337.

Ginhoux, F., Greter, M., Leboeuf, M., Nandi, S., See, P., Gokhan, S., Mehler, M.F., Conway, S.J., Ng, L.G., Stanley, E.R., et al. (2010). Fate mapping analysis reveals that adult microglia derive from primitive macrophages. Science (841-845) *330*.

Girgis, N.M., Gundra, U.M., Ward, L.N., Cabrera, M., Frevert, U., and Loke, P. (2014). Ly6Chigh Monocytes Become Alternatively Activated Macrophages in Schistosome Granulomas with Help from CD4+ Cells. PLoS Pathog. *10*.

Girlanda, R., Kleiner, D.E., Duan, Z., Ford, E.A.S., Wright, E.C., Mannon, R.B., and Kirk, A.D. (2008). Monocyte infiltration and kidney allograft dysfunction during acute rejection. Am. J. Transplant. *8*, 600–607.

Godin, I.E., Garcia-Porrero, J.A., Coutinho, A., Dieterlen-Lièvre, F., and Marcos, M.A.R. (1993). Para-aortic splanchnopleura from early mouse embryos contains B1a cell progenitors. Nature *364*, 67–70.

Golub, R., and Cumano, A. (2013). Embryonic hematopoiesis. Blood Cells, Mol. Dis. *51*, 226–231.

Gomez Perdiguero, E., Klapproth, K., Schulz, C., Busch, K., Azzoni, E., Crozet, L., Garner, H., Trouillet, C., de Bruijn, M.F., Geissmann, F., et al. (2014). Tissue-resident macrophages originate from yolk-sac-derived erythro-myeloid progenitors. Nature *518*, 547–551.

Gordon, S. (2003). Alternative activation of macrophages. Nat. Rev. Immunol. *3*, 23–35.

Gosselin, D., Link, V.M., Romanoski, C.E., Fonseca, G.J., Eichenfield, D.Z., Spann, N.J., Stender, J.D., Chun, H.B., Garner, H., Geissmann, F., et al. (2014). Environment drives selection and function of enhancers controlling tissue-specific macrophage identities. Cell *159*, 1327–1340.

Gottschalk, C., and Kurts, C. (2015). The debate about dendritic cells and macrophages in the kidney. Front. Immunol. *6*, 1–7.

Grage-Griebenow, E., Flad, H.D., and Ernst, M. (2001a). Heterogeneity of human peripheral blood monocyte subsets. J. Leukoc. Biol. *69*, 11–20.

Grage-Griebenow, E., Zawatzky, R., Kahlert, H., Brade, L., Flad, H., and Ernst, M. (2001b). Identification of a novel dendritic cell-like subset of CD64(+) / CD16(+) blood monocytes. Eur. J. Immunol. *31*, 48–56.

Gross, M., Salame, T.M., and Jung, S. (2015). Guardians of the gut - murine intestinal macrophages and dendritic cells. Front. Immunol. *6*, 1–10.

Guilliams, M., Ginhoux, F., Jakubzick, C., Naik, S.H., Onai, N., Schraml, B.U., Segura, E., Tussiwand, R., and Yona, S. (2014). Dendritic cells, monocytes and macrophages: a unified nomenclature based on ontogeny. Nat. Rev. Immunol. *14*, 571–578.

Guy, C.T., Cardiff, R.D., and Muller, W.J. (1992). Induction of mammary tumors by expression of polyomavirus middle T oncogene: a transgenic mouse model for metastatic disease. Mol. Cell. Biol. *12*, 954–961.

Hackness, and Wagner (2005). Biology and Medicine of Rabbits and Rodents.

Halpern, B.N. (1959). The Role and Function of the Reticulo???Endothelial System in Immunological Processes. J. Pharm. Pharmacol. *11*, 321–338.

Hambleton, S., Salem, S., Bustamante, J., Bigley, V., Boisson-Dupuis, S., Azevedo, J., Fortin, A., Haniffa, M., Ceron-Gutierrez, L., Bacon, C.M., et al. (2011). *IRF8* Mutations and Human Dendritic-Cell Immunodeficiency. N. Engl. J. Med. *365*, 127–138.

Hamers, A. a J., Vos, M., Rassam, F., Marinković, G., Marincovic, G., Kurakula, K., van Gorp, P.J., de Winther, M.P.J., Gijbels, M.J.J., de Waard, V., et al. (2012). Bone marrow-specific deficiency of nuclear receptor Nur77 enhances atherosclerosis. Circ. Res. *110*, 428–438.

Hanahan, D., and Weinberg, R.A. (2011). Hallmarks of cancer: The next generation. Cell *144*, 646–674.

Hancock, W., Thomson, N.M., and Atkins, R.C. (1983). COMPOSITION OF INTERSTITIAL CELLULAR INFILTRATE BY MONOCLONAL ANTIBODIES IN RENAL CANCER BIOPSIES OF REJECTING HUMAN RENAL ALLOGRAFTS. Transplantation *35*, 458–463.

Hanna, R.N., Carlin, L.M., Hubbeling, H.G., Nackiewicz, D., Green, A.M., Punt, J. a, Geissmann, F., and Hedrick, C.C. (2011). The transcription factor NR4A1 (Nur77) controls bone marrow differentiation and the survival of Ly6C- monocytes. Nat. Immunol. *12*, 778–785.

Hanna, R.N., Shaked, I., Hubbeling, H.G., Punt, J. a, Wu, R., Herrley, E., Zaugg, C., Pei, H., Geissmann, F., Ley, K., et al. (2012). NR4A1 (Nur77) deletion polarizes macrophages toward an inflammatory phenotype and increases atherosclerosis. Circ. Res. *110*, 416–427.

Hanna, R.N., Cekic, C., Sag, D., Tacke, R., Thomas, G.D., Nowyhed, H., Herrley, E.,

Rasquinha, N., McArdle, S., Wu, R., et al. (2015). Patrolling monocytes control tumor metastasis to the lung. Science (80-.). *350*, 985–990.

Hardy, R.R., and Hayakawa, K. (1991). A developmental switch in B lymphopoiesis. Proc. Natl. Acad. Sci. U. S. A. *88*, 11550–11554.

Hasenberg, A., Hasenberg, M., Männ, L., Neumann, F., Borkenstein, L., Stecher, M., Kraus, A., Engel, D.R., Klingberg, A., Seddigh, P., et al. (2015). Catchup: a mouse model for imaging-based tracking and modulation of neutrophil granulocytes. Nat. Methods *12*, 445–452.

Hashimoto, D., Chow, A., Noizat, C., Teo, P., Beasley, M.B., Leboeuf, M., Becker, C.D., See, P., Price, J., Lucas, D., et al. (2013). Tissue-resident macrophages self-maintain locally throughout adult life with minimal contribution from circulating monocytes. Immunity *38*, 792–804.

Hazenbos, W.L., Gessner, J.E., Hofhuis, F.M., Kuipers, H., Meyer, D., Heijnen, I.A., Schmidt, R.E., Sandor, M., Capel, P.J., Daëron, M., et al. (1996). Impaired IgG-dependent anaphylaxis and Arthus reaction in Fc gamma RIII (CD16) deficient mice. Immunity *5*, 181–188.

Helmick, C.G., Felson, D.T., Lawrence, R.C., Gabriel, S., Hirsch, R., Kwoh, C.K., Liang, M.H., Kremers, H.M., Mayes, M.D., Merkel, P.A., et al. (2008). Estimates of the prevalence of arthritis and other rheumatic conditions in the United States. Part I. Arthritis Rheum. *58*, 15–25.

Henderson, R.B., Hobbs, J.A.R., Mathies, M., and Hogg, N. (2003). Rapid recruitment of inflammatory monocytes is independent of neutrophil migration. Blood *102*, 328–335.

Herbomel, P., Thisse, B., and Thisse, C. (1999). Ontogeny and behaviour of early macrophages in the zebrafish embryo. Development *126*, 3735–3745.

Heron, M., Grutters, J.C., Van Velzen-Blad, H., Veltkamp, M., Claessen, A.M.E., and Van Den Bosch, J.M.M. (2008). Increased expression of CD16, CD69, and very late antigen-1 on blood monocytes in active sarcoidosis. Chest *134*, 1001–1008.

Hettinger, J., Richards, D.M., Hansson, J., Barra, M.M., Joschko, A.-C., Krijgsveld, J., and Feuerer, M. (2013). Origin of monocytes and macrophages in a committed progenitor. Nat. Immunol. *14*, 821–830.

Hidalgo, A., Chang, J., Jang, J.-E., Peired, A.J., Chiang, E.Y., and Frenette, P.S. (2009). Heterotypic interactions enabled by polarized neutrophil microdomains mediate thromboinflammatory injury. Nat. Med. *15*, 384–391.

Higashiyama, M., Hokari, R., Matsunaga, H., Takebayashi, K., Watanabe, C., Komoto, S., Okada, Y., Kurihara, C., Kawaguchi, A., Nagao, S., et al. (2008). P-selectin-dependent monocyte recruitment through platelet interaction in intestinal microvessels of LPS-treated mice. Microcirculation *15*, 441–450.

Hilgendorf, I., Gerhardt, L.M.S., Tan, T.C., Winter, C., Holderried, T. a W., Chousterman, B.G., Iwamoto, Y., Liao, R., Zirlik, A., Scherer-Crosbie, M., et al. (2014). Ly-6Chigh monocytes depend on Nr4a1 to balance both inflammatory and reparative phases in the infarcted myocardium. Circ. Res. *114*, 1611–1622.

Hill, G.S., Delahousse, M., Nochy, D., R??my, P., Mignon, F., M??ry, J.P., and Bari??ty, J. (2001). Predictive power of the second renal biopsy in lupus nephritis: Significance of macrophages. Kidney Int. *59*, 304–316.

Hirsch, M.S., Gary, G.W., and Murphy, F.A. (1969). In vitro and in vivo properties of antimacrophage sera. J. Immunol. *102*, 656.

Hochheiser, K., Heuser, C., Krause, T.A., Teteris, S., Ilias, A., Weisheit, C., Hoss, F., Tittel, A.P., Knolle, P.A., Panzer, U., et al. (2013). Exclusive CX3CR1 dependence of kidney DCs impacts glomerulonephritis progression. J. Clin. Invest. *123*, 4242–4254.

Holdsworth, S.R., Neale, T.J., and Wilson, C.B. (1981). Abrogation of macrophage-dependent injury in experimental glomerulonephritis in the rabbit. Use of an antimacrophage serum. J. Clin. Invest. *68*, 686–698.

Holtschke, T., Löhler, J., Kanno, Y., Fehr, T., Giese, N., Rosenbauer, F., Lou, J., Knobeloch, K.P., Gabriele, L., Waring, J.F., et al. (1996). Immunodeficiency and chronic myelogenous leukemia-like syndrome in mice with a targeted mutation of the ICSBP gene. Cell *87*, 307–317.

Hoppe, P.S., Schwarzfischer, M., Loeffler, D., Kokkaliaris, K.D., Hilsenbeck, O., Moritz, N., Endele, M., Filipczyk, A., Gambardella, A., Ahmed, N., et al. (2016). Early myeloid lineage choice is not initiated by random PU.1 to GATA1 protein ratios. Nature *535*, 299–302.

Houssaint, E. (1981). Differentiation of the mouse hepatic primordium. II. Extrinsic origin of the haemopoietic cell line. Cell Differ. *10*, 243–252.

Howard, J.G., Boak, J.L., and Christie, G.H. (1965). FURTHER STUDIES ON THE TRANSFORMATION OF THORACIC DUCT CELLS INTO LIVER MACROPHAGES. Ann. N. Y. Acad. Sci. *129*, 327–339.

Huber, R.G., Marzinek, J.K., Holdbrook, D.A., and Bond, P.J. (2017). Multiscale molecular dynamics simulation approaches to the structure and dynamics of viruses. Prog. Biophys. Mol. Biol. *128*, 121–132.

Hume, D.A., and Gordon, S. (1983). Mononuclear phagocyte system of the mouse defined by immunohistochemical localization of antigen F4/80. Identification of resident macrophages in renal medullary and cortical interstitium and the juxtaglomerular complex. J. Exp. Med. *157*, 1704–1709.

Hume, D.A., Perry, V.H., and Gordon, S. (1983). Immunohistochemical localization of a macrophage-specific antigen in developing mouse retina: Phagocytosis of dying neurons and differentiation in microglial cells to form a regular array in the plexiform layers. J. Cell Biol. *97*, 253–257.

Hume, D.A., Loutit, J.F., and Gordon, S. (1984a). The mononuclear phagocyte system of the mouse defined by immunohistochemical localization of antigen F4/80: macrophages of bone and associated connective tissue. J. Cell Sci. *66*, 189–194.

Hume, D.A., Perry, V.H., and Gordon, S. (1984b). The mononuclear phagocyte system of the mouse defined by immunohistochemical localisation of antigen F4/80: Macrophages associated with epithelia. Anat. Rec. *210*, 503–512.

Hume, D.A., Monkley, S.J., and Wainwright, B.J. (1995). Detection of c-fms protooncogene in early mouse embryos by whole mount in situ hybridization indicates roles for macrophages in tissue remodelling. Br. J. Haematol. *90*, 939–942.

Hussen, J., Düvel, A., Sandra, O., Smith, D., Sheldon, I.M., Zieger, P., and Schuberth, H.J. (2013). Phenotypic and Functional Heterogeneity of Bovine Blood Monocytes. PLoS One *8*, 1–11.

Ikuta, K., and Weissman, I.L. (1992). Evidence that hematopoietic stem cells express mouse c-kit but do not depend on steel factor for their generation. Proc. Natl. Acad. Sci. U. S. A. *89*, 1502–1506.

Ikuta, K., Kina, T., MacNeil, I., Uchida, N., Peault, B., Chien, Y. hsiu, and Weissman, I.L. (1990). A developmental switch in thymic lymphocyte maturation potential occurs at the level of hematopoietic stem cells. Cell *62*, 863–874.

Imhof, B.A., Jemelin, S., Ballet, R., Vesin, C., Schapira, M., Karaca, M., and Emre, Y. (2016). CCN1/CYR61-mediated meticulous patrolling by Ly6C ^{low} monocytes fuels vascular inflammation. Proc. Natl. Acad. Sci. *113*, E4847–E4856.

Inaba, K., Inaba, M., Deguchi, M., Hagi, K., Yasumizuf, R., Ikeharat, S., Muramatsu, S., and Steinman, R.M. (1993). Granulocytes, macrophages, and dendritic cells arise from a common major histocompatibility complex class II-negative progenitor in mouse bone marrow. Immunology *90*, 3038–3042.

Ingersoll, M., Spanbroek, R., Lottaz, C., Gautier, E., Frankenberger, M., Hoffmann, R., Lang, R., Haniffa, M., Collin, M., Tacke, F., et al. (2010). Comparison of gene expression profiles between human and mouse monocyte subsets. Blood *115*, 10–20.

Inoue, A., Hasegawa, H., Kohno, M., Ito, M.R., Terada, M., Imai, T., Yoshie, O., Nose, M., and Fujita, S. (2005). Antagonist of fractalkine (CX3CL1) delays the initiation and ameliorates the progression of lupus nephritis in MRL/lpr mice. Arthritis Rheum. *52*, 1522–1533.

Jacome-Galarza, C.E., Lee, S.K., Lorenzo, J.A., and Aguila, H.L. (2013). Identification, characterization, and isolation of a common progenitor for osteoclasts, macrophages, and dendritic cells from murine bone marrow and periphery. J. Bone Miner. Res. *28*, 1203–1213.

Jacquin, C., Gran, D.E., Lee, S.K., Lorenzo, J.A., and Aguila, H.L. (2006). Identification of multiple osteoclast precursor populations in murine bone marrow. J. Bone Miner. Res. *21*, 67–77.

Jaworowski, A., Ellery, P., Maslin, C.L., Naim, E., Heinlein, A.C., Ryan, C.E., Paukovics, G., Hocking, J., Sonza, S., and Crowe, S.M. (2006). Normal CD16 expression and phagocytosis of Mycobacterium avium complex by monocytes from a current cohort of HIV-1-infected patients. J. Infect. Dis. *193*, 693–697.

Jenne, C.N., Enders, A., Rivera, R., Watson, S.R., Bankovich, A.J., Pereira, J.P., Xu, Y., Roots, C.M., Beilke, J.N., Banerjee, A., et al. (2009). T-bet–dependent S1P $_5$ expression in NK cells promotes egress from lymph nodes and bone marrow. J. Exp. Med. *206*, 2469–2481.

Jhingran, A., Mar, K.B., Kumasaka, D.K., Knoblaugh, S.E., Ngo, L.Y., Segal, B.H.,

Iwakura, Y., Lowell, C.A., Hamerman, J.A., Lin, X., et al. (2012). Tracing Conidial Fate and Measuring Host Cell Antifungal Activity Using a Reporter of Microbial Viability in the Lung. Cell Rep. *2*, 1762–1773.

Ji, R.P., Phoon, C.K.L., Aristizábal, O., McGrath, K.E., Palis, J., and Turnbull, D.H. (2003). Onset of cardiac function during early mouse embryogenesis coincides with entry of primitive erythroblasts into the embryo proper. Circ. Res. *92*, 133–135.

Jia, T., Serbina, N. V., Brandl, K., Zhong, M.X., Leiner, I.M., Charo, I.F., and Pamer, E.G. (2008). Additive Roles for MCP-1 and MCP-3 in CCR2-Mediated Recruitment of Inflammatory Monocytes during Listeria monocytogenes Infection. J. Immunol. *180*, 6846–6853.

Jo, S.K., Sung, S.A., Cho, W.Y., Go, K.J., and Kim, H.K. (2006). Macrophages contribute to the initiation of ischaemic acute renal failure in rats. Nephrol. Dial. Transplant. *21*, 1231–1239.

Jung, K., Kim, P., Leuschner, F., Gorbatov, R., Kim, J.K., Ueno, T., Nahrendorf, M., and Yun, S.H. (2013). Endoscopic time-lapse imaging of immune cells in infarcted mouse hearts. Circ. Res. *112*, 891–899.

Jung, S., Aliberti, J., Graemmel, P., Sunshine, M.J., Kreutzberg, G.W., Sher, A., and Littman, D.R. (2000). Analysis of Fractalkine Receptor CX3CR1 Function by Targeted Deletion and Green Fluorescent Protein Reporter Gene Insertion. Mol. Cell. Biol. *20*, 4106–4114.

Kabithe, E., Hillegas, J., Stokol, T., Moore, J., and Wagner, B. (2010). Monoclonal antibodies to equine CD14. Vet. Immunol. Immunopathol. *138*, 149–153.

Kaissling, B., and Le Hir, M. (1994). Characterization and distribution of interstitial cell types in the renal cortex of rats. Kidney Int. *45*, 709–720.

Kanno, Y., Levi, B.-Z., Tamura, T., and Ozato, K. (2005). Immune cell-specific amplification of interferon signaling by the IRF-4/8-PU.1 complex. J. Interferon Cytokine Res. *25*, 770–779.

Kantakamalakul, W., Politis, A.D., Marecki, S., Sullivan, T., Ozato, K., Fenton, M.J., and Vogel, S.N. (1999). Regulation of IFN consensus sequence binding protein expression in murine macrophages. J. Immunol. *162*, 7417–7425.

Karkar, a M., Smith, J., and Pusey, C.D. (2001). Prevention and treatment of experimental crescentic glomerulonephritis by blocking tumour necrosis factor-alpha. Nephrol. Dial. Transplant *16*, 518–524.

Karsunky, H., Inlay, M.A., Serwold, T., Bhattacharya, D., and Weissman, I.L. (2008). Flk2 + common lymphoid progenitors possess equivalent differentiation potential for the B and T lineages. Blood *111*, 5562–5570.

Kawamura, S., Onai, N., Miya, F., Sato, T., Tsunoda, T., Kurabayashi, K., Yotsumoto, S., Kuroda, S., Takenaka, K., Akashi, K., et al. (2017). Identification of a Human Clonogenic Progenitor with Strict Monocyte Differentiation Potential: A Counterpart of Mouse cMoPs. Immunity *46*, 835–848.e4.

Keller, N.M., Gentek, R., Gimenez, G., Bigot, S., Mailfert, S., and Sieweke, M.H.

(2017). Developmental origin and maintenance of distinct testicular macrophage populations. Jem 1–14.

Keurentjes, J.J.B., Molenaar, J., and Zwaan, B.J. (2013). Predictive modelling of complex agronomic and biological systems. Plant, Cell Environ. *36*, 1700–1710.

Kiel, M.J., Yilmaz, Ö.H., Iwashita, T., Yilmaz, O.H., Terhorst, C., and Morrison, S.J. (2005). SLAM family receptors distinguish hematopoietic stem and progenitor cells and reveal endothelial niches for stem cells. Cell *121*, 1109–1121.

Kierdorf, K., Erny, D., Goldmann, T., Sander, V., Schulz, C., Perdiguero, E.G., Wieghofer, P., Heinrich, A., Riemke, P., Hölscher, C., et al. (2013). Microglia emerge from erythromyeloid precursors via Pu.1- and Irf8-dependent pathways. Nat. Neurosci. *16*, 273–280.

Kieusseian, A., de la Grange, P.B., Burlen-Defranoux, O., Godin, I., and Cumano, A. (2012). Immature hematopoietic stem cells undergo maturation in the fetal liver. Development *139*, 3521–3530.

Kim, W.-K., Sun, Y., Do, H., Autissier, P., Halpern, E.F., Piatak, M., Lifson, J.D., Burdo, T.H., McGrath, M.S., and Williams, K. (2010). Monocyte heterogeneity underlying phenotypic changes in monocytes according to SIV disease stage. J. Leukoc. Biol. *87*, 557–567.

Kingsley, P.D., Malik, J., Fantauzzo, K.A., and Palis, J. (2004). Yolk sac-derived primitive erythroblasts enucleate during mammalian embryogenesis. Blood *104*, 19–25.

Kingsley, P.D., Malik, J., Emerson, R.L., Bushnell, T.P., McGrath, K.E., Bloedorn, L.A., Bulger, M., and Palis, J. (2006). "Maturational" globin switching in primary primitive erythroid cells. Blood *107*, 1665–1672.

Kissa, K., and Herbomel, P. (2010). Blood stem cells emerge from aortic endothelium by a novel type of cell transition. Nature *464*, 112–115.

Kluth, D.C., Erwig, L.P., and Rees, A.J. (2004). Multiple facets of macrophages in renal injury. Kidney Int. *66*, 542–557.

Kondo, M., Weissman, I.L., Akashi, K., Akashi, K., Weissman, I.L., Akashi, K., Harada, M., Shibuya, T., Fukagawa, K., Kimura, N., et al. (1997). Identification of clonogenic common lymphoid progenitors in mouse bone marrow. Cell *91*, 661–672.

Koupenova, M., Vitseva, O., MacKay, C.R., Beaulieu, L.M., Benjamin, E.J., Mick, E., Kurt-Jones, E.A., Ravid, K., and Freedman, J.E. (2014). Platelet-TLR7 mediates host survival and platelet count during viral infection in the absence of platelet-dependent thrombosis. Blood *124*, 791–802.

Kruger, T. (2004). Identification and Functional Characterization of Dendritic Cells in the Healthy Murine Kidney and in Experimental Glomerulonephritis. J. Am. Soc. Nephrol. *15*, 613–621.

Kurotaki, D., Osato, N., Nishiyama, A., Yamamoto, M., Ban, T., Sato, H., Nakabayashi, J., Umehara, M., Miyake, N., Matsumoto, N., et al. (2013). Essential role of the IRF8-KLF4 transcription factor cascade in murine monocyte differentiation. Blood *121*, 1839–1849.

Kurotaki, D., Yamamoto, M., Nishiyama, A., Uno, K., Ban, T., Ichino, M., Sasaki, H., Matsunaga, S., Yoshinari, M., Ryo, A., et al. (2014). IRF8 inhibits C/EBPα activity to restrain mononuclear phagocyte progenitors from differentiating into neutrophils. Nat. Commun. *5*, 4978.

Lam, E.Y.N., Hall, C.J., Crosier, P.S., Crosier, K.E., and Flores, M.V. (2010). Live imaging of Runx1 expression in the dorsal aorta tracks the emergence of blood progenitors from endothelial cells. Blood *116*, 909–914.

Lan, H.Y., Nikolic-Paterson, D.J., Zarama, M., Vannice, J.L., and Atkins, R.C. (1993). Suppression of experimental crescentic glomerulonephritis by the interleukin-1 receptor antagonist. Kidney Int. *43*, 479–485.

Lan, H.Y., Nikolic-Paterson, D.J., Mu, W., Vannice, J.L., and Atkins, R.C. (1995). Interleukin-1 receptor antagonist halts the progression of established crescentic glomerulonephritis in the rat. Kidney Int. *47*, 1303–1309.

Lan, H.Y., Yang, N., Metz, C., Mu, W., Song, Q., Nikolic-Paterson, D.J., Bacher, M., Bucala, R., and Atkins, R.C. (1997). TNF-alpha up-regulates renal MIF expression in rat crescentic glomerulonephritis. Mol Med *3*, 136–144.

Lavin, Y., Winter, D., Blecher-Gonen, R., David, E., Keren-Shaul, H., Merad, M., Jung, S., and Amit, I. (2014). Tissue-resident macrophage enhancer landscapes are shaped by the local microenvironment. Cell *159*, 1312–1326.

Lawson, L.J., Perry, V.H., and Gordon, S. (1992). Turnover of resident microglia in the normal adult mouse brain. Neuroscience *48*, 405–415.

Lee, J., Breton, G., Aljoufi, A., Zhou, Y.J., Puhr, S., Nussenzweig, M.C., and Liu, K. (2015a). Clonal analysis of human dendritic cell progenitor using a stromal cell culture. J. Immunol. Methods *425*, 21–26.

Lee, J., Breton, G., Oliveira, T.Y.K., Zhou, Y.J., Aljoufi, A., Puhr, S., Cameron, M.J., Sékaly, R.-P., Nussenzweig, M.C., and Liu, K. (2015b). Restricted dendritic cell and monocyte progenitors in human cord blood and bone marrow. J. Exp. Med. *212*, 385–399.

Lee, S.L., Wesselschmidt, R.L., Linette, G.P., Kanagawa, O., Russell, J.H., and Milbrandt, J. (1995). Unimpaired thymic and peripheral T cell death in mice lacking the nuclear receptor NGFI-B (Nur77). Science *269*, 532–535.

Li, H., Kolluri, S.K., Gu, J., Dawson, M.I., Cao, X., Hobbs, P.D., Lin, B., Chen, G., Lu, J., Lin, F., et al. (2000). Cytochrome c release and apoptosis induced by mitochondrial targeting of nuclear orphan receptor TR3. Science *289*, 1159–1164.

Li, W., Nava, R.G., Bribriesco, A.C., Zinselmeyer, B.H., Spahn, J.H., Gelman, A.E., Krupnick, A.S., Miller, M.J., and Kreisel, D. (2012a). Intravital 2-photon imaging of leukocyte trafficking in beating heart. J. Clin. Invest. *122*, 2499–2508.

Li, Y., Du, X.F., Liu, C.S., Wen, Z.L., and Du, J.L. (2012b). Reciprocal Regulation between Resting Microglial Dynamics and Neuronal Activity In Vivo. Dev. Cell *23*, 1189–1202.

Li, Z., Lan, Y., He, W., Chen, D., Wang, J., Zhou, F., Wang, Y., Sun, H., Chen, X., Xu,

C., et al. (2012c). Mouse embryonic head as a site for hematopoietic stem cell development. Cell Stem Cell *11*, 663–675.

Lim, J.K., Obara, C.J., Rivollier, A., Pletnev, A.G., Kelsall, B.L., and Murphy, P.M. (2011). Chemokine Receptor Ccr2 Is Critical for Monocyte Accumulation and Survival in West Nile Virus Encephalitis. J. Immunol. *186*, 471–478.

Limsirichaikul, S., Niimi, A., Fawcett, H., Lehmann, A., Yamashita, S., and Ogi, T. (2009). A rapid non-radioactive technique for measurement of repair synthesis in primary human fibroblasts by incorporation of ethynyl deoxyuridine (EdU). Nucleic Acids Res. *37*, 1–10.

Lin, K.L., Suzuki, Y., Nakano, H., Ramsburg, E., and Gunn, M.D. (2008). CCR2+ Monocyte-Derived Dendritic Cells and Exudate Macrophages Produce Influenza-Induced Pulmonary Immune Pathology and Mortality. J. Immunol. *180*, 2562–2572.

Lionakis, M.S., Lim, J.K., Lee, C.-C.R., and Murphy, P.M. (2011). Organ-Specific Innate Immune Responses in a Mouse Model of Invasive Candidiasis. J. Innate Immun. *3*, 180–199.

Lopez, B.G., Tsai, M.S., Baratta, J.L., Longmuir, K.J., and Robertson, R.T. (2011). Characterization of Kupffer cells in livers of developing mice. Comp. Hepatol. *10*, 2.

Lu, B., Rutledge, B.J., Gu, L., Fiorillo, J., Lukacs, N.W., Kunkel, S.L., North, R., Gerard, C., and Rollins, B.J. (1998). Abnormalities in monocyte recruitment and cytokine expression in monocyte chemoattractant protein 1-deficient mice. J. Exp. Med. *187*, 601–608.

Lux, C.T., Yoshimoto, M., Mcgrath, K., Conway, S.J., Palis, J., and Yoder, M.C. (2008). All primitive and definitive hematopoietic progenitor cells emerging before E10 in the mouse embryo are products of the yolk sac Brief report All primitive and definitive hematopoietic progenitor cells emerging before E10 in the mouse embryo are products . Blood *111*, 3435–3438.

Van Der Maaten, L.J.P., and Hinton, G.E. (2008). Visualizing high-dimensional data using t-sne. J. Mach. Learn. Res. *9*, 2579–2605.

Månsson, R., Hultquist, A., Luc, S., Yang, L., Anderson, K., Kharazi, S., Al-Hashmi, S., Liuba, K., Thorén, L., Adolfsson, J., et al. (2007). Molecular Evidence for Hierarchical Transcriptional Lineage Priming in Fetal and Adult Stem Cells and Multipotent Progenitors. Immunity *26*, 407–419.

Mantovani, A., Sica, A., Sozzani, S., Allavena, P., Vecchi, A., and Locati, M. (2004). The chemokine system in diverse forms of macrophage activation and polarization. Trends Immunol. *25*, 677–686.

Marks, S.C., and Lane, P.W. (1976). Osteopetrosis, a new recessive skeletal mutation on chromosome 12 of the mouse. J. Hered. *67*, 11–18.

Martinez, F.O., Helming, L., and Gordon, S. (2009). Alternative Activation of Macrophages: An Immunologic Functional Perspective. Annu. Rev. Immunol. *27*, 451–483.

Martínez-González, J., and Badimon, L. (2005). The NR4A subfamily of nuclear

receptors: New early genes regulated by growth factors in vascular cells. Cardiovasc. Res. *65*, 609–618.

Mass, E., Ballesteros, I., Farlik, M., Halbritter, F., Gunther, P., Crozet, L., Jacome-Galarza, C.E., Handler, K., Klughammer, J., Kobayashi, Y., et al. (2016). Specification of tissue-resident macrophages during organogenesis. Science (80-.). *353*, aaf4238-aaf4238.

McElrath, M.J., Steinman, R.M., and Cohn, Z.A. (1991). Latent HIV-1 infection in enriched populations of blood monocytes and T cells from seropositive patients. J. Clin. Invest. *87*, 27–30.

McGrath, K.E., Koniski, A.D., Malik, J., and Palis, J. (2003). Circulation is established in a stepwise pattern in the mammalian embryo. Blood *101*, 1669–1676.

McGrath, K.E., Frame, J.M., Fromm, G.J., Koniski, A.D., Kingsley, P.D., Little, J., Bulger, M., and Palis, J. (2011). A transient definitive erythroid lineage with unique regulation of the β-globin locus in the mammalian embryo. Blood *117*, 4600–4608.

McGrath, K.E., Frame, J.M., Fegan, K.H., Bowen, J.R., Conway, S.J., Catherman, S.C., Kingsley, P.D., Koniski, A.D., and Palis, J. (2015). Distinct Sources of Hematopoietic Progenitors Emerge before HSCs and Provide Functional Blood Cells in the Mammalian Embryo. Cell Rep. *11*, 1892–1904.

McKenna, H.J., Stocking, K.L., Miller, R.E., Brasel, K., De Smedt, T., Maraskovsky, E., Maliszewski, C.R., Lynch, D.H., Smith, J., Pulendran, B., et al. (2000). Mice lacking flt3 ligand have deficient hematopoiesis affecting hematopoietic progenitor cells, dendritic cells, and natural killer cells. Blood *95*, 3489–3497.

McKercher, S.R., Torbett, B.E., Anderson, K.L., Henkel, G.W., Vestal, D.J., Baribault, H., Klemsz, M., Feeney, A.J., Wu, G.E., Paige, C.J., et al. (1996). Targeted disruption of the PU.1 gene results in multiple hematopoietic abnormalities. EMBO J. *15*, 5647–5658.

Mebius, R.E., and Kraal, G. (2005). Structure and function of the spleen. Nat Rev Immunol *5*, 606–616.

Medvinsky, A., Rybtsov, S., and Taoudi, S. (2011). Embryonic origin of the adult hematopoietic system: advances and questions. Development *138*, 1017–1031.

Medvinsky, A.L., Samoylina, N.L., Müller, A.M., and Dzierzak, E.A. (1993). An early pre-liver intraembryonic source of CFU-S in the developing mouse. Nature *364*, 64–67.

Menezes, S., Melandri, D., Anselmi, G., Perchet, T., Loschko, J., Dubrot, J., Patel, R., Gautier, E.L., Hugues, S., Longhi, M.P., et al. (2016). The Heterogeneity of Ly6Chi Monocytes Controls Their Differentiation into iNOS+ Macrophages or Monocyte-Derived Dendritic Cells. Immunity *45*, 1205–1218.

Merad, M., Manz, M.G., Karsunky, H., Wagers, A., Peters, W., Charo, I., Weissman, I.L., Cyster, J.G., and Engleman, E.G. (2002). Langerhans cells renew in the skin throughout life under steady-state conditions. Nat. Immunol. *3*, 1135–1141.

Metchnikoff, E. (1883). The Ancestral History of the Inflammatory. Mesodermic Phagocytes Certain Vertebr. Biol. Cent. 112–117.

Michaud, J.-P., Bellavance, M.-A., Préfontaine, P., and Rivest, S. (2013). Real-time in vivo imaging reveals the ability of monocytes to clear vascular amyloid beta. Cell Rep. *5*, 646–653.

Milbrandt, J. (1988). Nerve growth factor induces a gene homologous to the glucocorticoid receptor gene. Neuron *1*, 183–188.

Mildner, A., Schönheit, J., Giladi, A., David, E., Lara-Astiaso, D., Lorenzo-Vivas, E., Paul, F., Chappell-Maor, L., Priller, J., Leutz, A., et al. (2017). Genomic Characterization of Murine Monocytes Reveals C/EBPβ Transcription Factor Dependence of Ly6C− Cells. Immunity *46*, 849–862.e7.

Milici, a J., L'Hernault, N., and Palade, G.E. (1985). Surface densities of diaphragmed fenestrae and transendothelial channels in different murine capillary beds. Circ. Res. *56*, 709–717.

Miller, J., Horner, A., Stacy, T., Lowrey, C., Lian, J.B., Stein, G., Nuckolls, G.H., and Speck, N. a (2002). The core-binding factor beta subunit is required for bone formation and hematopoietic maturation. Nat. Genet. *32*, 645–649.

Misharin, A. V, Morales-Nebreda, L., Reyfman, P.A., Cuda, C.M., Walter, J.M., McQuattie-Pimentel, A.C., Chen, C.-I., Anekalla, K.R., Joshi, N., Williams, K.J.N., et al. (2017). Monocyte-derived alveolar macrophages drive lung fibrosis and persist in the lung over the life span. J. Exp. Med. 1–18.

Misharin, A. V., Cuda, C.M., Saber, R., Turner, J.D., Gierut, A.K., Kenneth Haines, G.K., Berdnikovs, S., Filer, A., Clark, A.R., Buckley, C.D., et al. (2014). Nonclassical Ly6C- monocytes drive the development of inflammatory arthritis in mice. Cell Rep. *9*, 591–604.

Miyamoto, T., Iwasaki, H., Reizis, B., Ye, M., Graf, T., Weissman, I.L., and Akashi, K. (2002). Myeloid or lymphoid promiscuity as a critical step in hematopoietic lineage commitment. Dev. Cell *3*, 137–147.

Molawi, K., Wolf, Y., Kandalla, P.K., Favret, J., Hagemeyer, N., Frenzel, K., Pinto, A.R., Klapproth, K., Henri, S., Malissen, B., et al. (2014). Progressive replacement of embryo-derived cardiac macrophages with age. J. Exp. Med. *211*, 2151–2158.

Molitoris, J.M., Paliwal, S., Sekar, R.B., Blake, R., Park, J., Trayanova, N.A., Tung, L., and Levchenko, A. (2016). Precisely parameterized experimental and computational models of tissue organization. Integr. Biol. *8*, 230–242.

Moniuszko, M., Bodzenta-Lukaszyk, A., Kowal, K., Lenczewska, D., and Dabrowska, M. (2009). Enhanced frequencies of CD14++CD16+, but not CD14+CD16+, peripheral blood monocytes in severe asthmatic patients. Clin. Immunol. *130*, 338–346.

Moore, M.A., and Metcalf, D. (1970). Ontogeny of the haemopoietic system: yolk sac origin of in vivo and in vitro colony forming cells in the developing mouse embryo. Br. J. Haematol. *18*, 279–296.

Morahan, P.S., Dempsey, W.L., Volkman, A., and Connor, J. (1986). Antimicrobial activity of various immunomodulators: independence from normal levels of circulating monocytes and natural killer cells. Infect Immun *51*, 87–93.

Moran, A.E., Holzapfel, K.L., Xing, Y., Cunningham, N.R., Maltzman, J.S., Punt, J., and Hogquist, K.A. (2011). T cell receptor signal strength in T_{reg} and iNKT cell development demonstrated by a novel fluorescent reporter mouse. J. Exp. Med. *208*, 1279–1289.

Moreau-Gachelin, F., Tavitian, A., and Tambourin, P. (1988). Spi-1 is a putative oncogene in virally induced murine erythroleukaemias. Nature *331*, 277–280.

Morris, L., Graham, C.F., and Gordon, S. (1991). Macrophages in haemopoietic and other tissues of the developing mouse detected by the monoclonal antibody F4/80. Development *112*, 517–526.

Morrison, S.J., Weissman, I.L., Athens, J.W., Haab, O.P., Raab, S.O., Mauer, A.M., Ashenbrucker, H., Cartwright, G.E., Wintrobe, M.M., Baum, C.M., et al. (1994). The long-term repopulating subset of hematopoietic stem cells is deterministic and isolatable by phenotype. Immunity *1*, 661–673.

Morrison, S.J., Wandycz, a M., Hemmati, H.D., Wright, D.E., and Weissman, I.L. (1997). Identification of a lineage of multipotent hematopoietic progenitors. Development *124*, 1929–1939.

Mosmann, T., and Coffman, R. (1989). TH1 AND TH2 CELLS : Different Patterns of Lymphokine Functional Properties. Ann Rev Immunol *7*, 145–173.

Mossadegh-Keller, N., Sarrazin, S., Kandalla, P.K., Espinosa, L., Stanley, E.R., Nutt, S.L., Moore, J., and Sieweke, M.H. (2013). M-CSF instructs myeloid lineage fate in single haematopoietic stem cells. Nature *497*, 239–243.

Mucenski, M.L., McLain, K., Kier, A.B., Swerdlow, S.H., Schreiner, C.M., Miller, T.A., Pietryga, D.W., Scott, W.J., and Potter, S.S. (1991). A functional c-myb gene is required for normal murine fetal hepatic hematopoiesis. Cell *65*, 677–689.

Mukouyama, Y., Chiba, N., Mucenski, M.L., and July, C.B. (1999). Supplementary material Hematopoietic cells in cultures of the murine embryonic aorta – gonad – mesonephros region are induced by c-Myb. Curr. Biol.

Muller, P.A., Koscsó, B., Rajani, G.M., Stevanovic, K., Berres, M.L., Hashimoto, D., Mortha, A., Leboeuf, M., Li, X.M., Mucida, D., et al. (2014). Crosstalk between muscularis macrophages and enteric neurons regulates gastrointestinal motility. Cell *158*, 300–313.

Müller, A.M., Medvinsky, A., Strouboulis, J., Grosveld, F., and Dzierzakt, E. (1994). Development of hematopoietic stem cell activity in the mouse embryo. Immunity *1*, 291–301.

Muller-Sieburg, C.E., Whitlock, C.A., and Weissman, I.L. (1986). Isolation of two early B lymphocyte progenitors from mouse marrow: A committed Pre-Pre-B cell and a clonogenic Thy-1lo hematopoietic stem cell. Cell *44*, 653–662.

Munn, D.H., Garnick, M.B., and Cheung, N.K. (1990). Effects of parenteral recombinant human macrophage colony-stimulating factor on monocyte number, phenotype, and antitumor cytotoxicity in nonhuman primates. Blood *75*, 2042–2048.

Munn, D.H., Bree, a G., Beall, a C., Kaviani, M.D., Sabio, H., Schaub, R.G., Alpaugh,

R.K., Weiner, L.M., and Goldman, S.J. (1996). Recombinant human macrophage colony-stimulating factor in nonhuman primates: selective expansion of a CD16+ monocyte subset with phenotypic similarity to primate natural killer cells. Blood *88*, 1215–1224.

Murdoch, C., Tazzyman, S., Webster, S., and Lewis, C.E. (2007). Expression of Tie-2 by Human Monocytes and Their Responses to Angiopoietin-2. J. Immunol. *178*, 7405–7411.

Nahrendorf, M., Swirski, F.K., Aikawa, E., Stangenberg, L., Wurdinger, T., Figueiredo, J.-L., Libby, P., Weissleder, R., and Pittet, M.J. (2007). The healing myocardium sequentially mobilizes two monocyte subsets with divergent and complementary functions. J. Exp. Med. *204*, 3037–3047.

Naito, M., Yamamura, F., Nishikawa, S., and Takahashi, K. (1989). Development, Differentiation, and Maturation of Fetal Mouse Yolk Sac Macrophages in Culture. J. Leukoc. Biol. *46*, 1–10.

Nakashima, Y., Plump, A.S., Raines, E.W., Breslow, J.L., and Ross, R. (1994). ApoE-deficient mice develop lesions of all phases of atherosclerosis throughout the arterial tree. Arterioscler. Thromb. a J. Vasc. Biol. *14*, 133–140.

Nakatani, K., Yoshimoto, S., Iwano, M., Asai, O., Samejima, K., Sakan, H., Terada, M., Hasegawa, H., Nose, M., and Saito, Y. (2010). Fractalkine expression and CD16+ monocyte accumulation in glomerular lesions: association with their severity and diversity in lupus models. Am. J. Physiol. Renal Physiol. *299*, F207-16.

Nakorn, T.N., Miyamoto, T., and Weissman, I.L. (2003). Characterization of mouse clonogenic megakaryocyte progenitors. Proc. Natl. Acad. Sci. U. S. A. *100*, 205–210.

Narni-Mancinelli, E., Campisi, L., Bassand, D., Cazareth, J., Gounon, P., Glaichenhaus, N., and Lauvau, G. (2007). Memory CD8 $^{+}$ T cells mediate antibacterial immunity via CCL3 activation of TNF/ROI $^{+}$ phagocytes. J. Exp. Med. *204*, 2075–2087.

Narni-Mancinelli, E., Soudja, S.M.H., Crozat, K., Dalod, M., Gounon, P., Geissmann, F., and Lauvau, G. (2011). Inflammatory monocytes and neutrophils are licensed to kill during memory responses in vivo. PLoS Pathog. *7*.

Nascimento, M., Huang, S.C., Smith, A., Everts, B., Lam, W., Bassity, E., Gautier, E.L., Randolph, G.J., and Pearce, E.J. (2014). Ly6Chi Monocyte Recruitment Is Responsible for Th2 Associated Host-Protective Macrophage Accumulation in Liver Inflammation due to Schistosomiasis. PLoS Pathog. *10*.

Nathan, C.F., Murray, H.W., Wiebe, M.E., and Rubin, B.Y. (1983). Identification of interferon-gamma as the lymphokine that activates human macrophage oxidative metabolism and antimicrobial activity. J. Exp. Med. *158*, 670–689.

Neal, L.M., and Knoll, L.J. (2014). Toxoplasma gondii Profilin Promotes Recruitment of Ly6Chi CCR2+ Inflammatory Monocytes That Can Confer Resistance to Bacterial Infection. PLoS Pathog. *10*.

Nelson, N., Kanno, Y., Hong, C., Contursi, C., Fujita, T., Fowlkes, B.J., O'Connell, E., Hu-Li, J., Paul, W.E., Jankovic, D., et al. (1996). Expression of IFN regulatory factor family proteins in lymphocytes. Induction of Stat-1 and IFN consensus sequence

binding protein expression by T cell activation. J. Immunol. *156*, 3711–3720.

Nerlov, C., Querfurth, E., Kulessa, H., and Graf, T. (2000). GATA-1 interacts with the myeloid PU. 1 transcription factor and represses PU. 1-dependent transcription. Blood *95*, 2543–2551.

Ngo, L.Y., Kasahara, S., Kumasaka, D.K., Knoblaugh, S.E., Jhingran, A., and Hohl, T.M. (2014). Inflammatory monocytes mediate early and organ-specific innate defense during systemic candidiasis. J. Infect. Dis. *209*, 109–119.

Nguyen, K.D., Qiu, Y., Cui, X., Goh, Y.P.S., Mwangi, J., David, T., Mukundan, L., Brombacher, F., Locksley, R.M., and Chawla, A. (2011). Alternatively activated macrophages produce catecholamines to sustain adaptive thermogenesis. Nature *480*, 104–108.

Nimmerjahn, F., and Ravetch, J. V (2011). FcγRs in health and disease. Curr. Top. Microbiol. Immunol. *350*, 105–125.

Nimmerjahn, F., Bruhns, P., Horiuchi, K., and Ravetch, J. V. (2005). FcgammaRIV: a novel FcR with distinct IgG subclass specificity. Immunity *23*, 41–51.

Nimmerjahn, F., Lux, A., Albert, H., Woigk, M., Lehmann, C., Dudziak, D., Smith, P., and Ravetch, J. V. (2010). Fc RIV deletion reveals its central role for IgG2a and IgG2b activity in vivo. Proc. Natl. Acad. Sci. *107*, 19396–19401.

Noronha, L.E., Harman, R.M., Wagner, B., and Antczak, D.F. (2012). Generation and characterization of monoclonal antibodies to equine CD16. Vet. Immunol. Immunopathol. *146*, 135–142.

North, T., Gu, T.L., Stacy, T., Wang, Q., Howard, L., Binder, M., Marín-Padilla, M., and Speck, N.A. (1999). Cbfa2 is required for the formation of intra-aortic hematopoietic clusters. Development *126*, 2563–2575.

Nussenzweig, M.C., and Steinman, R.M. (1980). Contribution of dendritic cells to stimulation of the murine syngeneic mixed leukocyte reaction. J. Exp. Med. *151*, 1196–1212.

Ogawa, D., Shikata, K., Matsuda, M., Okada, S., Usui, H., Wada, J., Taniguchi, N., and Makino, H. (2002). Protective effect of a novel and selective inhibitor of inducible nitric oxide synthase on experimental crescentic glomerulonephritis in WKY rats. Nephrol. Dial. Transplant *17*, 2117–2121.

Oguro, H., Ding, L., and Morrison, S.J. (2013). SLAM family markers resolve functionally distinct subpopulations of hematopoietic stem cells and multipotent progenitors. Cell Stem Cell *13*, 102–116.

Onai, N., Obata-Onai, A., Schmid, M.A., Ohteki, T., Jarrossay, D., and Manz, M.G. (2007). Identification of clonogenic common Flt3+M-CSFR+ plasmacytoid and conventional dendritic cell progenitors in mouse bone marrow. Nat. Immunol. *8*, 1207–1216.

Palframan, R.T., Jung, S., Cheng, G., Weninger, W., Luo, Y., Dorf, M., Littman, D.R., Rollins, B.J., Zweerink, H., Rot, A., et al. (2001). Inflammatory chemokine transport and presentation in HEV: a remote control mechanism for monocyte recruitment to

lymph nodes in inflamed tissues. J. Exp. Med. *194*, 1361–1373.

Palis, J. (2016). Hematopoietic stem cell-independent hematopoiesis: emergence of erythroid, megakaryocyte, and myeloid potential in the mammalian embryo. FEBS Lett. *590*, 3965–3974.

Palis, J., Robertson, S., Kennedy, M., Wall, C., and Keller, G. (1999). Development of erythroid and myeloid progenitors in the yolk sac and embryo proper of the mouse. Development *126*, 5073–5084.

Palis, J., Chan, R.J., Koniski, A., Patel, R., Starr, M., and Yoder, M.C. (2001). Spatial and temporal emergence of high proliferative potential hematopoietic precursors during murine embryogenesis. Proc. Natl. Acad. Sci. *98*, 4528–4533.

De Palma, M., Venneri, M.A., Galli, R., Sergi, L.S., Politi, L.S., Sampaolesi, M., and Naldini, L. (2005). Tie2 identifies a hematopoietic lineage of proangiogenic monocytes required for tumor vessel formation and a mesenchymal population of pericyte progenitors. Cancer Cell *8*, 211–226.

Paolicelli, R.C., Bisht, K., and Tremblay, M.-Ã. (2014). Fractalkine regulation of microglial physiology and consequences on the brain and behavior. Front. Cell. Neurosci. *8*, 1–10.

Pappalardo, F., Flower, D., Russo, G., Pennisi, M., and Motta, S. (2015). Computational modelling approaches to vaccinology. Pharmacol. Res. *92*, 40–45.

Park, S.J., Hughes, M.A., Burdick, M., Strieter, R.M., and Mehrad, B. (2009). Early NK Cell-Derived IFN-y Is Essential to Host Defense in. J. Immunol.

Passlick, B., Flieger, D., and Ziegler-Heitbrock, H.W. (1989). Identification and characterization of a novel monocyte subpopulation in human peripheral blood. Blood *74*, 2527–2534.

Patel, A.A., Zhang, Y., Fullerton, J.N., Boelen, L., Rongvaux, A., Maini, A.A., Bigley, V., Flavell, R.A., Gilroy, D.W., Asquith, B., et al. (2017). The fate and lifespan of human monocyte subsets in steady state and systemic inflammation. J. Exp. Med. 1–11.

Paul, F., Arkin, Y., Giladi, A., Jaitin, D.A., Kenigsberg, E., Keren-Shaul, H., Winter, D., Lara-Astiaso, D., Gury, M., Weiner, A., et al. (2015). Transcriptional Heterogeneity and Lineage Commitment in Myeloid Progenitors. Cell *163*, 1663–1677.

Paulson, K.E., Zhu, S.N., Chen, M., Nurmohamed, S., Jongstra-Bilen, J., and Cybulsky, M.I. (2010). Resident intimal dendritic cells accumulate lipid and contribute to the initiation of atherosclerosis. Circ. Res. *106*, 383–390.

Pei, L., Castrillo, A., Chen, M., Hoffmann, A., and Tontonoz, P. (2005). Induction of NR4A orphan nuclear receptor expression in macrophages in response to inflammatory stimuli. J. Biol. Chem. *280*, 29256–29262.

Perdiguero, E.G., and Geissmann, F. (2014). Identifying the infiltrators. Science (80-.). *344*, 801–802.

Perdiguero, E.G., and Geissmann, F. (2015). The development and maintenance of resident macrophages. Nat. Immunol. *17*, 2–8.

Pereira, P.D., Serra-Caetano, A., Cabrita, M., Bekman, E., Braga, J., Rino, J., Santus, R., Filipe, P.L., Sousa, A.E., Ferreira, J.A., et al. (2017). Quantification of cell cycle kinetics by EdU (5-ethynyl-2′-deoxyuridine)-coupled-fluorescence-intensity analysis. Oncotarget *8*, 40514–40532.

Perié, L., Duffy, K.R., Kok, L., De Boer, R.J., and Schumacher, T.N. (2015). The Branching Point in Erythro-Myeloid Differentiation. Cell *163*, 1655–1662.

Perry, V.H., Hume, D.A., and Gordon, S. (1985). Immunohistochemical localization of macrophages and microglia in the adult and developing mouse brain. Neuroscience *15*, 313–326.

Peters, W., Scott, H.M., Chambers, H.F., Flynn, J.L., Charo, I.F., and Ernst, J.D. (2001). Chemokine receptor 2 serves an early and essential role in resistance to Mycobacterium tuberculosis. Proc.Natl.Acad.Sci.U.S.A *98*, 7958–7963.

Petritus, P.M., Manzoni-de-Almeida, D., Gimblet, C., Gonzalez Lombana, C., and Scott, P. (2012). Leishmania mexicana Induces Limited Recruitment and Activation of Monocytes and Monocyte-Derived Dendritic Cells Early during Infection. PLoS Negl. Trop. Dis. *6*.

Pietras, E.M., Reynaud, D., Kang, Y.A., Carlin, D., Calero-Nieto, F.J., Leavitt, A.D., Stuart, J.A., G??ttgens, B., and Passegu??, E. (2015). Functionally Distinct Subsets of Lineage-Biased Multipotent Progenitors Control Blood Production in Normal and Regenerative Conditions. Cell Stem Cell *17*, 35–46.

Pinkett, M.O., Cowdrey, C.R., and Nowell, P.C. (1966). Mixed hematopoietic and pulmonary origin of “alveolar macrophages” as demonstrated by chromosome markers. Am. J. Pathol. *48*, 859–867.

Plump, A.S., and Breslow, J.L. (1995). Apolipoprotein E and the apolipoprotein E-deficient mouse. Annu. Rev. Nutr. *15*, 495–518.

Poteser, M., and Wakabayashi, I. (2004). Serum albumin induces iNOS expression and NO production in RAW 267.4 macrophages. Br. J. Pharmacol. *143*, 143–151.

Powathil, G.G., Swat, M., and Chaplain, M.A.J. (2015). Systems oncology: Towards patient-specific treatment regimes informed by multiscale mathematical modelling. Semin. Cancer Biol. *30*, 13–20.

Predescu, D., and Palade, G.E. (1993). Plasmalemmal vesicles represent the large pore system of continuous microvascular endothelium. Am. J. Physiol. *265*, H725-33.

Prigogine, I., Nicolis, G., and Babloyantz, A. (1974). Nonequilibrium problems in biological phenomena. Ann. N. Y. Acad. Sci. *231*, 99–105.

Quintar, A., McArdle, S., Wolf, D., Marki, A., Ehinger, E., Vassallo, M., Miller, J., Mikulski, Z., Ley, K., and Buscher, K. (2017). Endothelial Protective Monocyte Patrolling in Large Arteries Intensified by Western Diet and Atherosclerosis. Circ. Res. *120*, 1789–1799.

Quiros, E., Garcia, F., Maroto, M.C., Bernal, M.C., Cabezas, T., and Piedrola, G. (1995). Human immunodeficiency virus type-1 can be detected in monocytes by polymerase chain reaction. J Med Microbiol *42*, 411–414.

Rahman, A., and Isenberg, D.A. (2008). Systemic Lupus Erythematosus. N. Engl. J. Med. *358*, 929–939.

Rajpal, A., Cho, Y.A., Yelent, B., Koza-Taylor, P.H., Li, D., Chen, E., Whang, M., Kang, C., Turi, T.G., and Winoto, A. (2003). Transcriptional activation of known and novel apoptotic pathways by Nur77 orphan steroid receptor. EMBO J. *22*, 6526–6536.

Ramirez-Ortiz, Z.G., Lee, C.K., Wang, J.P., Boon, L., Specht, C.A., and Levitz, S.M. (2011). A nonredundant role for plasmacytoid dendritic cells in host defense against the human fungal pathogen Aspergillus fumigatus. Cell Host Microbe *9*, 415–424.

Ramond, C., Berthault, C., Burlen-Defranoux, O., de Sousa, A.P., Guy-Grand, D., Vieira, P., Pereira, P., and Cumano, A. (2014). Two waves of distinct hematopoietic progenitor cells colonize the fetal thymus. Nat. Immunol. *15*, 27–35.

Rezaie, P., and Male, D. (2002). {MESOGLIA} & {MICROGLIA} – A Historical Review of the Concept of Mononuclear Phagocytes Within the Central Nervous System. J Hist Neurosci *11*, 325–374.

Rieger, M. a, Hoppe, P.S., Smejkal, B.M., Eitelhuber, A.C., and Schroeder, T. (2009). Hematopoietic cytokines can instruct lineage choice. Science *325*, 217–218.

Risdon, R.A., Sloper, J.C., and De Wardener, H.E. (1968). Relationship Between Renal Function and Histological Changes Found in Renal-Biopsy Specimens From Patients With Persistent Glomerular Nephritis. Lancet *292*, 363–366.

Robben, P.M., LaRegina, M., Kuziel, W.A., and Sibley, L.D. (2005). Recruitment of Gr-1+ monocytes is essential for control of acute toxoplasmosis. J. Exp. Med. *201*, 1761–1769.

Robin, C., Bollerot, K., Mendes, S., Haak, E., Crisan, M., Cerisoli, F., Lauw, I., Kaimakis, P., Jorna, R., Vermeulen, M., et al. (2009). Human Placenta Is a Potent Hematopoietic Niche Containing Hematopoietic Stem and Progenitor Cells throughout Development. Cell Stem Cell *5*, 385–395.

Rodríguez-Iturbe, B., Pons, H., Herrera-Acosta, J., and Johnson, R.J. (2001). Role of immunocompetent cells in nonimmune renal diseases. Kidney Int. *59*, 1626–1640.

Romo, G.M., Dong, J.F., Schade, A.J., Gardiner, E.E., Kansas, G.S., Li, C.Q., McIntire, L. V, Berndt, M.C., and López, J.A. (1999). The glycoprotein Ib-IX-V complex is a platelet counterreceptor for P-selectin. J. Exp. Med. *190*, 803–814.

Van Rooijen, N., and Sanders, A. (1997). Elimination, blocking, and activation of macrophages: three of a kind? J. Leukoc. Biol. *62*, 702–709.

Rosen, H., Gordon, S., and North, R.J. (1989). Exacerbation of murine listeriosis by a monoclonal antibody specific for the type 3 complement receptor of myelomonocytic cells. Absence of monocytes at infective foci allows Listeria to multiply in nonphagocytic cells. J. Exp. Med. *170*, 27–37.

Ross, R. (1999). Inflammation or Atherogenesis. N. Engl. J. Med. *340*, 115–126.

Sabin, F.R. (1917). Preliminary Note on the Differentiation of Angioblasts and the Method by Which They Produce Blood-Vessels. Anat. Rec. *13*, 5–7.

Samokhvalov, I.M., Samokhvalova, N.I., and Nishikawa, S. (2007). Cell tracing shows the contribution of the yolk sac to adult haematopoiesis. Nature *446*, 1056–1061.

Samstein, M., Schreiber, H.A., Leiner, I.M., Sušac, B., Glickman, M.S., and Pamer, E.G. (2013). Essential yet limited role for CCR2 $^{+}$ inflammatory monocytes during *Mycobacterium tuberculosis* -specific T cell priming. Elife *2*, 1–10.

Santiago-Raber, M.L., Amano, H., Amano, E., Baudino, L., Otani, M., Lin, Q., Nimmerjahn, F., Sjef Verbeek, J., Ravetch, J. V., Takasaki, Y., et al. (2009). Fc-gamma receptor-dependent expansion of a hyperactive monocyte subset in lupus-prone mice. Arthritis Rheum. *60*, 2408–2417.

Sasmono, R.T., Oceandy, D., Pollard, J.W., Tong, W., Pavli, P., Wainwright, B.J., Ostrowski, M.C., Himes, S.R., and Hume, D. a (2003). PHAGOCYTES A macrophage colony-stimulating factor receptor – green fluorescent protein transgene is expressed throughout the mononuclear phagocyte system of the mouse. Gene *101*, 1155–1163.

Sawyer, R.T. (1986). The cytokinetic behavior of pulmonary alveolar macrophages in monocytopenic mice. J. Leukoc. Biol. *39*, 89–99.

Schittler, D., Allgöwer, F., and De Boer, R.J. (2013). A new model to simulate and analyze proliferating cell populations in BrdU labeling experiments. BMC Syst Biol *7 Suppl 1*, S4.

Schönheit, J., Kuhl, C., Gebhardt, M.L., Klett, F.F., Riemke, P., Scheller, M., Huang, G., Naumann, R., Leutz, A., Stocking, C., et al. (2013). PU.1 level-directed chromatin structure remodeling at the Irf8 gene drives dendritic cell commitment. Cell Rep. *3*, 1617–1628.

Schulz, C., Perdiguero, E.G., Chorro, L., Szabo-Rogers, H., Cagnard, N., Kierdorf, K., Prinz, M., Wu, B., Jacobsen, S.E.W., Pollard, J.W., et al. (2012). A Lineage of Myeloid Cells Independent of Myb and Hematopoietic Stem Cells. Science (80-.). *336*, 86–90.

Schulz, C., Engelmann, B., and Massberg, S. (2013). Crossroads of coagulation and innate immunity: The case of deep vein thrombosis. J. Thromb. Haemost. *11*, 233–241.

Scott, E., Simon, M., Anastasi, J., and Singh, H. (1994). Requirement of transcription factor PU.1 in the development of multiple hematopoietic lineages. Science (80-.). *265*, 1573–1577.

Scriba A, Schneider M, Grau V, van der Meide PH, S.B. (1997). macrophages of mouse splenic and thymic T cells Cell lines and culturing Assays of -endorphin hydrolysis AND Isolation of bone marrow cells and in vitro maturation of macrophages (LDH) assay Morphology of macrophages e : e ’ lls F-derived mouse isolatio. J Leukoc Biol *62*, 741–752.

Semple, J.W., Italiano, J.E., and Freedman, J. (2011). Platelets and the immune continuum. Nat. Rev. Immunol. *11*, 264–274.

Serbina, N. V, and Pamer, E.G. (2006). Monocyte emigration from bone marrow during bacterial infection requires signals mediated by chemokine receptor CCR2. Nat. Immunol. *7*, 311–317.

Serbina, N. V, Kuziel, W., Flavell, R., Akira, S., Rollins, B., and Pamer, E.G. (2003a).

Sequential MyD88-independent and -dependent activation of innate immune responses to intracellular bacterial infection. Immunity *19*, 891–901.

Serbina, N. V., Salazar-Mather, T.P., Biron, C.A., Kuziel, W.A., and Pamer, E.G. (2003b). TNF/iNOS-producing dendritic cells mediate innate immune defense against bacterial infection. Immunity *19*, 59–70.

Serbina, N. V., Hohl, T.M., Cherny, M., and Pamer, E.G. (2009). Selective Expansion of the Monocytic Lineage Directed by Bacterial Infection. J. Immunol. *183*, 1900–1910.

Shand, F.H.W., Ueha, S., Otsuji, M., Koid, S.S., Shichino, S., Tsukui, T., Kosugi-Kanaya, M., Abe, J., Tomura, M., Ziogas, J., et al. (2014). Tracking of intertissue migration reveals the origins of tumor-infiltrating monocytes. Proc. Natl. Acad. Sci. *111*, 7771–7776.

Shi, C., Velazquez, P., Hohl, T.M., Leiner, I., Dustin, M.L., and Pamer, E.G. (2010). Monocyte Trafficking to Hepatic Sites of Bacterial Infection Is Chemokine Independent and Directed by Focal Intercellular Adhesion Molecule-1 Expression. J. Immunol. *184*, 6266–6274.

Skrzeczynska-Moncznik, J., Bzowska, M., Loseke, S., Grage-Griebenow, E., Zembala, M., and Pryjma, J. (2008). Peripheral blood CD14high CD16+ monocytes are main producers of IL-10. Scand. J. Immunol. *67*, 152–159.

Sluss, P.M., Ph, D., and Lewandrowski, K.B. (2004). case records of the massachusetts general hospital,Laboratory Reference Values. N. Engl. J. Med. *351*, 2461–2461.

Sorokin, S.P., Hoyt, R.F., Blunt, D.G., and McNelly, N.A. (1992). Macrophage development: II. Early ontogeny of macrophage populations in brain, liver, and lungs of rat embryos as revealed by a lectin marker. Anat. Rec. *232*, 527–550.

Soucie, E.L., Weng, Z., Geirsdottir, L., Molawi, K., Maurizio, J., Fenouil, R., Mossadegh-Keller, N., Gimenez, G., VanHille, L., Beniazza, M., et al. (2016). Lineage-specific enhancers activate self-renewal genes in macrophages and embryonic stem cells. Science (80-.). *351*, aad5510-aad5510.

Spangrude, G.J., Heimfeld, S., and Weissman, I.L. (1988). Purification and characterization of mouse hematopoietic stem cells. Science *241*, 58–62.

Spellberg, B., Ibrahim, A.S., Edwards, J.E., and Filler, S.G. (2005). Mice with disseminated candidiasis die of progressive sepsis. J. Infect. Dis. *192*, 336–343.

Sponaas, A., Paula, A., Voisine, C., Mastelic, B., Koernig, S., Jarra, W., Renia, L., Mauduit, M., Potocnik, A.J., Langhorne, J., et al. (2009). Migrating monocytes recruited to the spleen play an important role in control of blood stage malaria. Blood *114*, 5522–5531.

Springer, T.A. (1994). Traffic signals for lymphocyte recirculation and leukocyte emigration: The multistep paradigm. Cell *76*, 301–314.

Stamatiades, E.G., Tremblay, M.E., Bohm, M., Crozet, L., Bisht, K., Kao, D., Coelho, C., Fan, X., Yewdell, W.T., Davidson, A., et al. (2016). Immune Monitoring of Trans-endothelial Transport by Kidney-Resident Macrophages. Cell *166*, 991–1003.

Steinman, R., and Cohn, Z. (1974). Identification of a novel cell type in peripheral lymphoid organs of mice. II. Functional properties in vitro. J. Exp. Med. *139*, 380–397.

Steinman, R.M., and Cohn, Z.A. (1973). Identification of a novel cell type in peripheral lymphoid organs of mice. I. Morphology, quantitation, tissue distribution. J. Exp. Med. *137*, 1142–1162.

Steinman, B.R.M., Adams, J.C., and Cohn, Z.A. (1975). IDENTIFICATION OF A NOVEL CELL TYPE IN PERIPHERAL LYMPHOID ORGANS OF MICE IV. Identification and Distribution in Mouse Spleen. J Exp Med *141*, 804–820.

Steinman, R.M., Lustig, D.S., and Cohn, Z.A. (1974). Identification of a novel cell type in peripheral lymphoid organs of mice. 3. Functional properties in vivo. J. Exp. Med. *139*, 1431–1445.

Steinman, R.M., Kaplan, G., Witmer, M.D., and Cohn, Z.A. (1979). Identification of a novel cell type in peripheral lymphoid organs of mice. V. Purification of spleen dendritic cells, new surface markers, and maintenance in vitro. J. Exp. Med. *149*, 1–16.

Steinman, R.M., Gutchinov, B., Witmer, M.D., and Nussenzweig, M.C. (1983). Dendritic cells are the principal stimulators of the primary mixed leukocyte reaction in mice. J. Exp. Med. *157*, 613–627.

Stevens, D. a., and Melikian, G.L. (2011). Aspergillosis in the "Nonimmunocompromised" Host. Immunol. Invest. *40*, 751–766.

Sumagin, R., Prizant, H., Lomakina, E., Waugh, R.E., and Sarelius, I.H. (2010). LFA-1 and Mac-1 define characteristically different intralumenal crawling and emigration patterns for monocytes and neutrophils in situ. J. Immunol. *185*, 7057–7066.

Sumner, R., Crawford, A., Mucenski, M., and Frampton, J. (2000). Initiation of adult myelopoiesis can occur in the absence of c-Myb whereas subsequent development is strictly dependent on the transcription factor. Oncogene *19*, 3335–3342.

Sun, X., Zhang, C., Jin, H., Sun, G., Tian, Y., Shi, W., and Zhang, D. (2016). Flow cytometric analysis of T lymphocyte proliferation in vivo by EdU incorporation. Int. Immunopharmacol. *41*, 56–65.

Sunderkotter C, Nikolic T, Dillon MJ, Van Rooijen N, Stehling M, Drevets DA, et al. Subpopulations of mouse blood monocytes differ in maturation stage and inflammatory response. *J Immunol* (2004) **172**:4410–7. doi:10.4049/jimmunol.172.7.4410

Swirski, F.K., Libby, P., Aikawa, E., Alcaide, P., Luscinskas, F.W., Weissleder, R., and Pittet, M.J. (2007). Ly-6Chi monocytes dominate hypercholesterolemia-associated monocytosis and give rise to macrophages in atheromata. J. Clin. Invest. *117*, 195–205.

Swirski, F.K., Wildgruber, M., Ueno, T., Figueiredo, J.L., Panizzi, P., Iwamoto, Y., Zhang, E., Stone, J.R., Rodriguez, E., Chen, J.W., et al. (2010). Myeloperoxidase-rich Ly-6C+ myeloid cells infiltrate allografts and contribute to an imaging signature of organ rejection in mice. J. Clin. Invest. *120*, 2627–2634.

Tacke, F., Alvarez, D., Kaplan, T.J., Jakubzick, C., Spanbroek, R., Llodra, J., Garin, A., Liu, J., Mack, M., van Rooijen, N., et al. (2007). Monocyte subsets differentially employ CCR2, CCR5, and CX3CR1 to accumulate within atherosclerotic plaques. J.

Clin. Invest. *117*, 185–194.

Tacke, R., Hilgendorf, I., Garner, H., Waterborg, C., Park, K., Nowyhed, H., Hanna, R.N., Wu, R., Swirski, F.K., Geissmann, F., et al. (2015). The transcription factor NR4A1 is essential for the development of a novel macrophage subset in the thymus. Sci. Rep. *5*, 10055.

Takahashi, K. (1989). Differentiation , Maturation , and Proliferation Macrophages in the Mouse Yolk Sac : of and Ultrastructural Study. J. Leukoc. Biol. *96*, 87–96.

Takeuchi, O., and Akira, S. (2010). Pattern recognition receptors and inflammation. Cell *140*, 805–820.

Tamura, T., and Ozato, K. (2002). ICSBP/IRF-8: its regulatory roles in the development of myeloid cells. J.Interferon Cytokine Res. *22*, 145–152.

Tamura, A., Hirai, H., Yokota, A., Sato, A., Shoji, T., Kashiwagi, T., Iwasa, M., Fujishiro, A., Miura, Y., and Maekawa, T. (2015). Accelerated apoptosis of peripheral blood monocytes in Cebpb-deficient mice. Biochem. Biophys. Res. Commun. *464*, 654–658.

Tamura, A., Hirai, H., Yokota, A., Kamio, N., Sato, A., Shoji, T., Kashiwagi, T., Torikoshi, Y., Miura, Y., Tenen, D.G., et al. (2017). C/EBPβ is required for survival of Ly6C ¯ monocytes.

Tamura, T., Nagamura-Inoue, T., Shmeltzer, Z., Kuwata, T., and Ozato, K. (2000). ICSBP directs bipotential myeloid progenitor cells to differentiate into mature macrophages. Immunity *13*, 155–165.

Tamura, T., Yanai, H., Savitsky, D., and Taniguchi, T. (2008). The IRF family transcription factors in immunity and oncogenesis. Annu. Rev. Immunol. *26*, 535–584.

Terry, R.L., Deffrasnes, C., Getts, D.R., Minten, C., Van Vreden, C., Ashhurst, T.M., Getts, M.T., Xie, R.D.V., Campbell, I.L., and King, N.J.C. (2015). Defective inflammatory monocyte development in IRF8-deficient mice abrogates migration to the West Nile virus-infected brain. J. Innate Immun. *7*, 102–112.

Theurl, M., Theurl, I., Hochegger, K., Obrist, P., Subramaniam, N., van Rooijen, N., Schuemann, K., and Weiss, G. (2008). Kupffer cells modulate iron homeostasis in mice via regulation of hepcidin expression. J. Mol. Med. *86*, 825.

Till, J.E., and McCulloch, E.A. (1961). A Direct Measurement of the Radiation Sensitivity of Normal Mouse Bone Marrow Cells 1. Radiat. Res. *178*, AV3-AV7.

Till, J.E., McCulloch, E. a., and Siminovitch, L. (1964). a Stochastic Model of Stem Cell Proliferation, Based on the Growth of Spleen Colony-Forming Cells*. Proc. Natl. Acad. Sci. U. S. A. *51*, 29–36.

Tipping, P.G., Lowe, M.G., and Holdsworth, S.R. (1991). Glomerular interleukin 1 production is dependent on macrophage infiltration in anti-GBM glomerulonephritis. Kidney Int. *39*, 103–110.

Tober, J., Koniski, A., McGrath, K.E., Vemishetti, R., Emerson, R., De Mesy-Bentley, K.K.L., Waugh, R., and Palis, J. (2007). The megakaryocyte lineage originates from

hemangioblast precursors and is an integral component both of primitive and of definitive hematopoiesis. Blood *109*, 1433–1441.

Trautwein-Weidner, K., Gladiator, A., Kirchner, F.R., Becattini, S., Rülicke, T., Sallusto, F., and LeibundGut-Landmann, S. (2015). Antigen-Specific Th17 Cells Are Primed by Distinct and Complementary Dendritic Cell Subsets in Oropharyngeal Candidiasis. PLoS Pathog. *11*, 1–23.

Tremblay, M.-È. (2011). The role of microglia at synapses in the healthy CNS: novel insights from recent imaging studies. Neuron Glia Biol. *7*, 67–76.

Tremblay, M.-E., Stevens, B., Sierra, A., Wake, H., Bessis, A., and Nimmerjahn, A. (2011). The Role of Microglia in the Healthy Brain. J. Neurosci. *31*, 16064–16069.

Tremblay, M.Ě., Lowery, R.L., and Majewska, A.K. (2010). Microglial interactions with synapses are modulated by visual experience. PLoS Biol. *8*.

Tsou, C.L., Peters, W., Si, Y., Slaymaker, S., Aslanian, A.M., Weisberg, S.P., Mack, M., and Charo, I.F. (2007). Critical roles for CCR2 and MCP-3 in monocyte mobilization from bone marrow and recruitment to inflammatory sites. J. Clin. Invest. *117*, 902–909.

Tsujimura, H., Nagamura-Inoue, T., Tamura, T., and Ozato, K. (2002). IFN Consensus Sequence Binding Protein/IFN Regulatory Factor-8 Guides Bone Marrow Progenitor Cells Toward the Macrophage Lineage. J. Immunol. *169*, 1261–1269.

Usman, A., Ribatti, D., Sadat, U., and Gillard, J.H. (2015). From Lipid Retention to Immune-Mediate Inflammation and Associated Angiogenesis in the Pathogenesis of Atherosclerosis. J. Atheroscler. Thromb. *22*, 739–749.

VandenBergh, M.F.Q., Verweij, P.E., and Voss, A. (1999). Epidemiology of nosocomial fungal infections: invasive aspergillosis and the environment. Diagn. Microbiol. Infect. Dis. *34*, 221–227.

Varol, C., Landsman, L., Fogg, D.K., Greenshtein, L., Gildor, B., Margalit, R., Kalchenko, V., Geissmann, F., and Jung, S. (2007). Monocytes give rise to mucosal, but not splenic, conventional dendritic cells. J. Exp. Med. *204*, 171–180.

Venneri, M.A., De Palma, M., Ponzoni, M., Pucci, F., Scielzo, C., Zonari, E., Mazzieri, R., Doglioni, C., and Naldini, L. (2007). Identification of proangiogenic TIE2-expressing monocytes (TEMs) in human peripheral blood and cancer. Blood *109*, 5276–5285.

Vieira-de-Abreu, A., Campbell, R.A., Weyrich, A.S., and Zimmerman, G.A. (2012). Platelets: Versatile effector cells in hemostasis, inflammation, and the immune continuum. Semin. Immunopathol. *34*, 5–30.

Villani, A.-C., Satija, R., Reynolds, G., Sarkizova, S., Shekhar, K., Fletcher, J., Griesbeck, M., Butler, A., Zheng, S., Lazo, S., et al. (2017). Single-cell RNA-seq reveals new types of human blood dendritic cells, monocytes, and progenitors. Science (80-.). *356*, eaah4573.

Voisinne, G., Nixon, B.G., Melbinger, A., Gasteiger, G., Vergassola, M., and Altan-Bonnet, G. (2015). T Cells Integrate Local and Global Cues to Discriminate between

Structurally Similar Antigens. Cell Rep. *11*, 1208–1219.

VOLKMAN, A., and GOWANS, J.L. (1965). THE PRODUCTION OF MACROPHAGES IN THE RAT. Br. J. Exp. Pathol. *46*, 50–61.

Waddington, S., Cook, H.T., Reaveley, D., Jansen, a, and Cattell, V. (1996). L-arginine depletion inhibits glomerular nitric oxide synthesis and exacerbates rat nephrotoxic nephritis. Kidney Int. *49*, 1090–1096.

Wake, H., Moorhouse, A.J., Jinno, S., Kohsaka, S., and Nabekura, J. (2009). Resting Microglia Directly Monitor the Functional State of Synapses In Vivo and Determine the Fate of Ischemic Terminals. J. Neurosci. *29*, 3974–3980.

Walzer, T., Chiossone, L., Chaix, J., Calver, A., Carozzo, C., Garrigue-Antar, L., Jacques, Y., Baratin, M., Tomasello, E., and Vivier, E. (2007). Natural killer cell trafficking in vivo requires a dedicated sphingosine 1-phosphate receptor. Nat. Immunol. *8*, 1337–1344.

Wang, Z., Benoit, G., Liu, J., Prasad, S., Aarnisalo, P., Liu, X., Xu, H., Walker, N.P., and Perlmann, T. (2003). Structure and function of Nurr1 identifies a class of ligand-independent nuclear receptors. Nature *423*, 555–560.

Weissman, I.L., and Shizuru, J.A. (2008). The origins of the identification and isolation of hematopoietic stem cells, and their capability to induce donor-specific transplantation tolerance and treat autoimmune diseases. Blood *112*, 3543–3553.

Weyrich, A.S., Lindeaaann, S., and Zimmerman, G.A. (2003). The evolving role of platelets in inflammation. J. Thromb. Haemost. *1*, 1897–1905.

Wigner, E. (1960). the Unreasonable Effectivenss of Mathematics in the Natural. Commun. Pure Appl. Math. *13*, 1–9.

Wiktor-Jedrzejczak, W., Bartocci, A., Ferrante, A.W., Ahmed-Ansari, A., Sell, K.W., Pollard, J.W., and Stanley, E.R. (1990). Total absence of colony-stimulating factor 1 in the macrophage-deficient osteopetrotic (op/op) mouse. Proc. Natl. Acad. Sci. U. S. A. *87*, 4828–4832.

Wiktor-Jedrzejczak, W.W., Ahmed, A., Szczylik, C., and Skelly, R.R. (1982). Hematological characterization of congenital osteopetrosis in op/op mouse. Possible mechanism for abnormal macrophage differentiation. J. Exp. Med. *156*, 1516–1527.

Willekens, F.L.A., Werre, J.M., Kruijt, J.K., Roerdinkholder-Stoelwinder, B., Groenen-Döpp, Y.A.M., van den Bos, A.G., Bosman, G.J.C.G.M., and van Berkel, T.J.C. (2005). Liver Kupffer cells rapidly remove red blood cell-derived vesicles from the circulation by scavenger receptors. Blood *105*, 2141–2145.

Witmer-Pack, M.D., Hughes, D. a, Schuler, G., Lawson, L., McWilliam, a, Inaba, K., Steinman, R.M., and Gordon, S. (1993). Identification of macrophages and dendritic cells in the osteopetrotic (op/op) mouse. J. Cell Sci. *104 (Pt 4*, 1021–1029.

Wofsy, D., Kerger, C.E., and Seaman, W.E. (1984). Monocytosis in the BXSB model for systemic lupus erythematosus. J. Exp. Med. *159*, 629–634.

Wong, C.H.Y., Jenne, C.N., Petri, B., Chrobok, N.L., and Kubes, P. (2013). Nucleation

of platelets with blood-borne pathogens on Kupffer cells precedes other innate immunity and contributes to bacterial clearance. Nat. Immunol. *14*, 785–792.

Wong, P.M., Chung, S.W., Reicheld, S.M., and Chui, D.H. (1986). Hemoglobin switching during murine embryonic development: evidence for two populations of embryonic erythropoietic progenitor cells. Blood *67*, 716–721.

Woollard, K.J., and Geissmann, F. (2010). Monocytes in atherosclerosis: subsets and functions. Nat. Rev. Cardiol. *7*, 77–86.

Worton, R.G., McCulloch, E.A., and Till, J.E. (1969). Physical separation of hemopoietic stem cells differing in their capacity for self-renewal. J. Exp. Med. *130*, 91–103.

Wu, A.M., Till, J.E., Siminovitch, L., and McCulloch, E.A. (1968). Cytological evidence for a relationship between normal hemotopoietic colony-forming cells and cells of the lymphoid system. J. Exp. Med. *127*, 455–464.

Xiong, H., Carter, R.A., Leiner, I.M., Tang, Y.W., Chen, L., Kreiswirth, B.N., and Pamer, E.G. (2015). Distinct contributions of neutrophils and $CCR2^{+}$ monocytes to pulmonary clearance of different Klebsiella pneumoniae strains. Infect. Immun. *83*, 3418–3427.

Xu M, J., Matsuoka, S., Yang, F.C., Ebihara, Y., Manabe, a, Tanaka, R., Eguchi, M., Asano, S., Nakahata, T., and Tsuji, K. (2001). Evidence for the presence of murine primitive megakaryocytopoiesis in the early yolk sac. Blood *97*, 2016–2022.

Yamada, M., Naito, M., and Takahashi, K. (1990). Kupffer cell proliferation and glucan-induced granuloma formation in mice depleted of blood monocytes by strontium-89. J. Leukoc. Biol. *47*, 195–205.

Yamamoto, R., Morita, Y., Ooehara, J., Hamanaka, S., Onodera, M., Rudolph, K.L., Ema, H., and Nakauchi, H. (2013). Clonal analysis unveils self-renewing lineage-restricted progenitors generated directly from hematopoietic stem cells. Cell *154*, 1112–1126.

Yona, S., and Gordon, S. (2015). From the reticuloendothelial to mononuclear phagocyte system - The unaccounted years. Front. Immunol. *6*, 1–7.

Yona, S., Kim, K.-W., Wolf, Y., Mildner, A., Varol, D., Breker, M., Strauss-Ayali, D., Viukov, S., Guilliams, M., Misharin, A., et al. (2013). Fate mapping reveals origins and dynamics of monocytes and tissue macrophages under homeostasis. Immunity *38*, 79–91.

Yoshida, H., Hayashi, S., Kunisada, T., Ogawa, M., Nishikawa, S., Okamura, H., Sudo, T., and Shultz, L.D. (1990). The murine mutation osteopetrosis is in the coding region of the macrophage colony stimulating factor gene. Nature *345*, 442–444.

Youssefian, T., Drouin, A., Massé, J.M., Guichard, J., and Cramer, E.M. (2002). Host defense role of platelets: engulfment of HIV and Staphylococcus aureus ocurs in a specific subcellular compoartmente and is enhanced by platelet activation. Blood *99*, 4021–4029.

Yu, J.C., and Fernandez-Gonzalez, R. (2016). Quantitative modelling of epithelial

morphogenesis: Integrating cell mechanics and molecular dynamics. Semin. Cell Dev. Biol.

Yuan, J., Nguyen, C.K., Liu, X., Kanellopoulou, C., and Muljo, S. a (2012). Lin28b reprograms adult bone marrow hematopoietic progenitors to mediate fetal-like lymphopoiesis. Science *335*, 1195–1200.

Zhang, P., Zhang, X., Iwama, A., Yu, C., Smith, K.A., Mueller, B.U., Narravula, S., Torbett, B.E., Orkin, S.H., and Tenen, D.G. (2000). PU.1 inhibits GATA-1 function and erythroid differentiation by blocking GATA-1 DNA binding. Blood *96*, 2641–2648.

Zhou, T., Cheng, J., Yang, P., Wang, Z., Liu, C., Su, X., Bluethmann, H., and Mountz, J.D. (1996). Inhibition of Nur77/Nurr1 leads to inefficient clonal deletion of self-reactive T cells. J. Exp. Med. *183*, 1879–1892.

Zhu, T., Muthui, D., Holte, S., Nickle, D., Feng, F., Brodie, S., Hwangbo, Y., Mullins, J.I., and Corey, L. (2002). Evidence for human immunodeficiency virus type 1 replication in vivo in CD14(+) monocytes and its potential role as a source of virus in patients on highly active antiretroviral therapy. J. Virol. *76*, 707–716.

Zhu, Y., Herndon, J.M., Sojka, D.K., Kim, K.W., Knolhoff, B.L., Zuo, C., Cullinan, D.R., Luo, J., Bearden, A.R., Lavine, K.J., et al. (2017). Tissue-Resident Macrophages in Pancreatic Ductal Adenocarcinoma Originate from Embryonic Hematopoiesis and Promote Tumor Progression. Immunity *47*, 323–338.e6.

Ziegler-Heitbrock, L. (2014). Reprint of: Monocyte subsets in man and other species. Cell. Immunol. *291*, 11–15.

Ziegler-Heitbrock, H.W., Passlick, B., and Flieger, D. (1988). The monoclonal antimonocyte antibody My4 stains B lymphocytes and two distinct monocyte subsets in human peripheral blood. Hybridoma *7*, 521–527.

Ziegler-Heitbrock, L., Ancuta, P., Crowe, S., Dalod, M., Grau, V., Hart, D.N., Leenen, P.J.M., Liu, Y., MacPherson, G., Randolph, G.J., et al. (2010). Nomenclature of monocytes and dendritic cells in blood. Blood *116*, e74-80.

ZIEGLER‐HEITBROCK, H.W.L., APPL, B., KÄFFERLEIN, E., LÖFFLER, T., JAHN‐HENNINGER, H., GUTENSOHN, W., NORES, J.R., MCCULLOUGH, K., PASSLICK, B., LABETA, M.O., et al. (1994). The Antibody MY4 Recognizes CD14 on Porcine Monocytes and Macrophages. Scand. J. Immunol. *40*, 509–514.

Zovein, A.C., Hofmann, J.J., Lynch, M., French, W.J., Turlo, K.A., Yang, Y., Becker, M.S., Zanetta, L., Dejana, E., Gasson, J.C., et al. (2008). Fate Tracing Reveals the Endothelial Origin of Hematopoietic Stem Cells. Cell Stem Cell *3*, 625–636.

Supplemental Figures

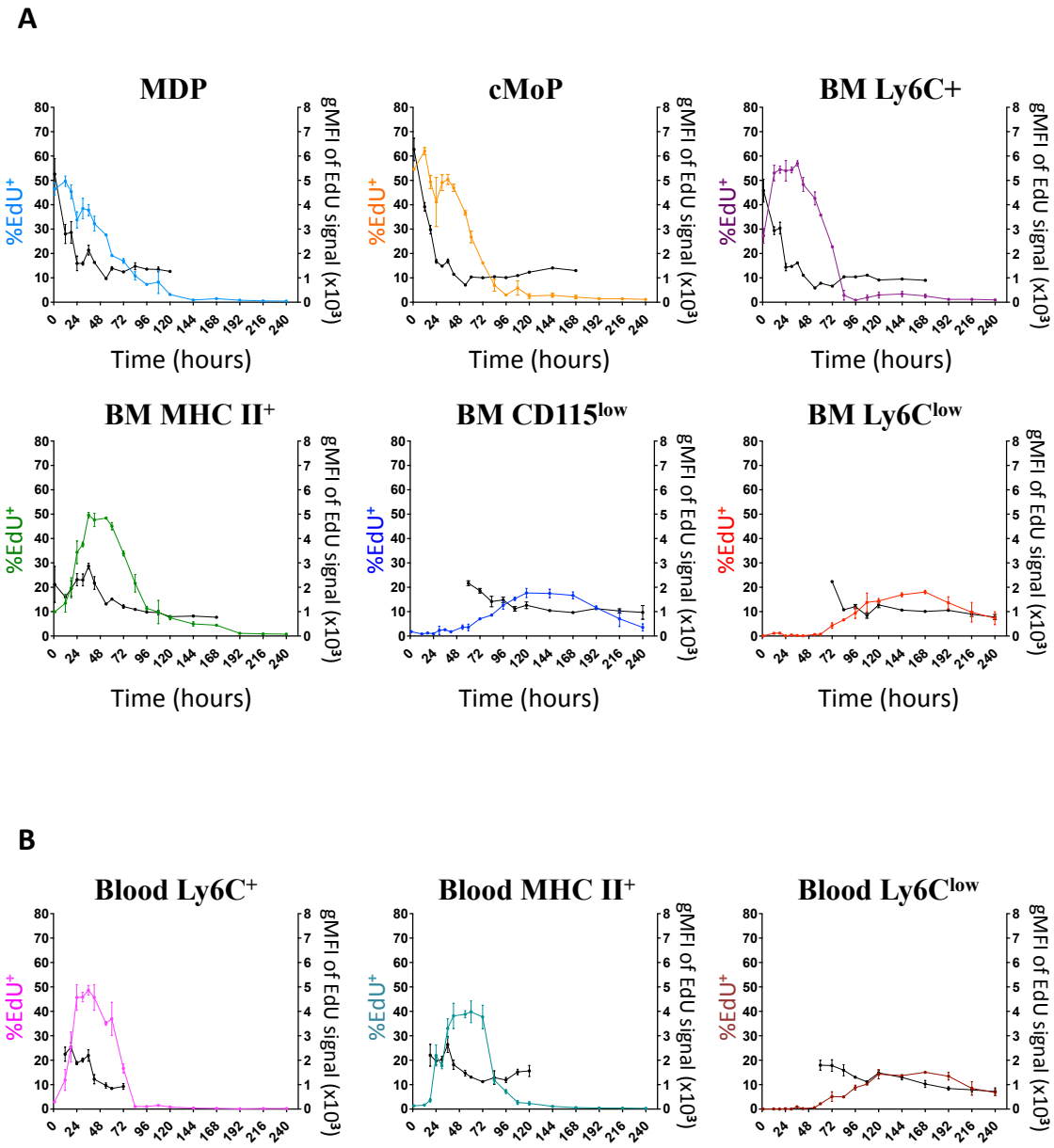

Supplemental Figure 3.1. Kinetics of EdU signal intensity over 10 days
C57BL/6 mice were injected with a single dose of 0.5mg of EdU intraperitoneally, and sacrificed at the indicated time points after injection for analysis of their BM **(A)**, Blood **(B)** for EdU content in the indicated populations. Coloured lines represent %EdU$^+$ cells (same data as **Figure 3.6**), while black lines represent the gMFI of the EdU signal in EdU$^+$ cells. gMFI was only measured when at least ~2% of EdU$^+$ cells were present. Data from Spleen was also analysed, but not shown here. n=3 mice per time point. Bars represent mean ± SD

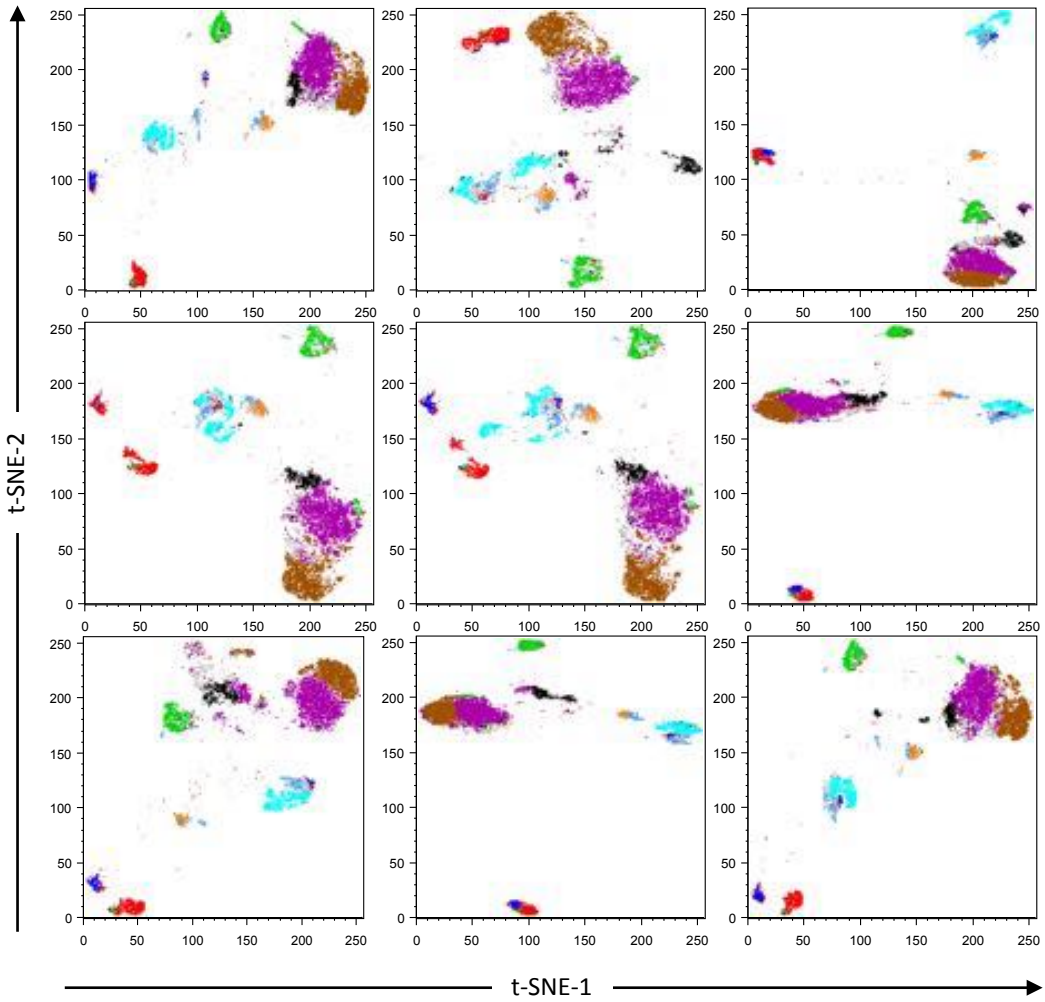

Supplemental Figure 3.2. Multiple t-SNE performed on *Cx3cr1-gfp*$^{+}$ cells. All dot plots show 2-dimensional plots of GFP^{+} cells, with classical populations gated separately and overlayed as in **Figure 3.7**.

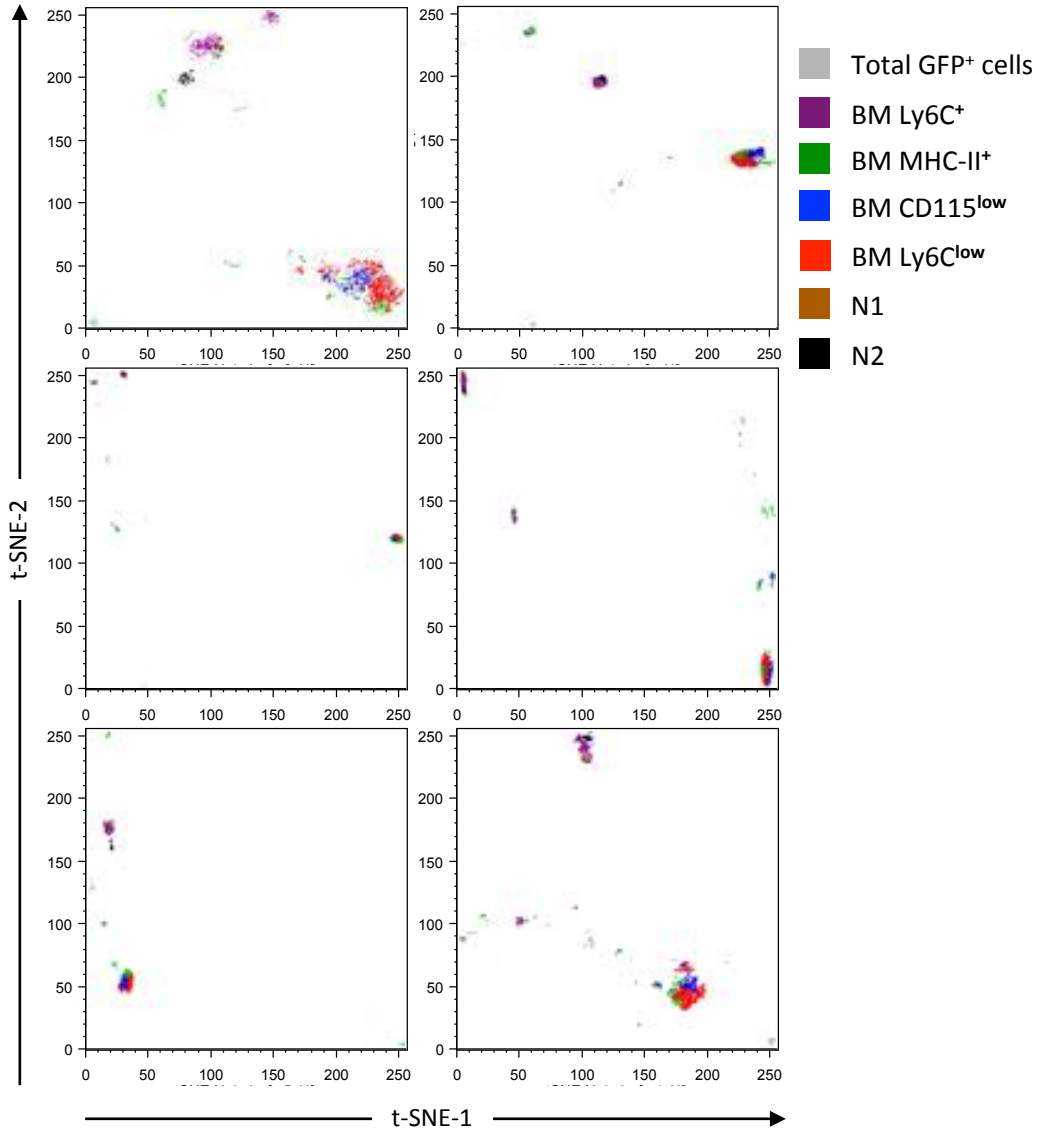

Supplemental Figure 3.3. Multiple t-SNE performed on *Nr4a1-gfp*$^{+}$ cells. All dot plots show 2-dimensional plots of GFP^{+} cells, with classical populations gated separately and overlayed as in **Figure 3.8**.